Development of Balanced Mixture Design Index Parameters and the Flex Suite of Performance Analysis Tools for Asphalt Pavements—Volume II

PUBLICATION NO. FHWA-HRT-24-111

JULY 2024

U.S. Department of Transportation
Federal Highway Administration

Research, Development, and Technology
Turner-Fairbank Highway Research Center
6300 Georgetown Pike
McLean, VA 22101-2296

FOREWORD

Highway agencies need to construct durable, long-lasting pavements that maximize highway investments and satisfy user expectations. These needs drive highway owners to investigate and improve the way they test and evaluate pavement materials. Owner agencies want to move beyond the traditional quality assurance specification focus on the as-constructed product quality toward specifications that evaluate long-term durability and performance across the asset's life. This report describes Federal Highway Administration research efforts to develop mechanistic-based performance testing and analysis tools for the purpose of understanding fundamental pavement performance and easing deployment of performance tests and associated analysis and evaluation tools to understand long-term performance. The research team developed two performance test indexes to support balanced mixture design concepts and provide agencies information and tools to evaluate their mixtures and pavements: S_{app}, the cyclic fatigue index parameter, for cracking, and the Rutting Strain Index for rutting. This report presents a framework for the asphalt mixture performance tester-based performance tests and indexes for balanced mix design. The Maine Department of Transportation, Missouri Department of Transportation, and Western Federal Land Highway Division also conducted three shadow projects. Three Microsoft® Excel®-based analysis tools were developed to aid equipment data transfer and the analysis of the test results, indexes, and pavement structure.

Jean A. Nehme, Ph.D., P.E.
Director, Office of Infrastructure
Research and Development

Notice

This document is disseminated under the sponsorship of the U.S. Department of Transportation in the interest of information exchange. The U.S. Government assumes no liability for the use of the information contained in this document.

Non-Binding Contents

Except for the statutes and regulations cited, the contents of this document do not have the force and effect of law and are not meant to bind the States or the public in any way. This document is intended only to provide information regarding existing requirements under the law or agency policies.

Quality Assurance Statement

The Federal Highway Administration (FHWA) provides high-quality information to serve Government, industry, and the public in a manner that promotes public understanding. Standards and policies are used to ensure and maximize the quality, objectivity, utility, and integrity of its information. FHWA periodically reviews quality issues and adjusts its programs and processes to ensure continuous quality improvement.

Disclaimer for Product Names and Manufacturers

The U.S. Government does not endorse products or manufacturers. Trademarks or manufacturers' names appear in this document only because they are considered essential to the objective of the document. They are included for informational purposes only and are not intended to reflect a preference, approval, or endorsement of any one product or entity.

TECHNICAL REPORT DOCUMENTATION PAGE

1. Report No. FHWA-HRT-24-111	2. Government Accession No.	3. Recipient's Catalog No.
4. Title and Subtitle Development of Balanced Mixture Design Index Parameters and the Flex Suite of Performance Analysis Tools for Asphalt Pavements—Volume II		5. Report Date July 2024 6. Performing Organization Code:
7. Author(s) Y. Richard Kim (0000-0003-3295-977X), B. Shane Underwood (0000-0002-7223-3968), Murthy N. Guddati (0000-0002-4134-3435), Amir Ghanbari (0000-0003-3828-8065), Behrooz Keshavarzi, Yizhuang David Wang (0000-0002-5149-9898), Jaehoon Jeong (0000-0001-8692-4965), Douglas Mocelin (0000-0002-7670-6136), Felipe Do Canto Pivetta, and Noor Al Hoda Saleh (0000-0003-2847-4999)		8. Performing Organization Report No.
9. Performing Organization Name and Address North Carolina State University Department of Civil, Construction, and Environmental Engineering Campus Box 7908 Raleigh, NC 27695		10. Work Unit No. 11. Contract or Grant No. DTFH61-13-C-00025
12. Sponsoring Agency Name and Address Federal Highway Administration Office of Infrastructure Research and Development 6300 Georgetown Pike McLean, VA 22101-2296		13. Type of Report and Period Covered Final Report; September 2013–August 2021 14. Sponsoring Agency Code HRDI-20
15. Supplementary Notes The contracting officer's representative was Matthew Corrigan (HRDI-20; ORCID: 0000-0002-1230-8462).		

16. Abstract

This report documents research efforts to advance mechanistic models, performance analysis and evaluation, and design methodologies to aid agency efforts to understand asphalt pavement performance. The research team developed FlexMAT™ version 2.1 and FlexPAVE™ version 2.0 as the material-level and pavement-level analysis tools, respectively. FlexPAVE 2.0 includes the simplified viscoelastic continuum damage model for fatigue and thermal cracking, the permanent strain shift model for rutting, and the NCHRP 09-54 aging models. FlexMAT 2.1 is designed to develop the input material properties for FlexPAVE 2.0 in a seamless manner. The team developed S_{app} and the Rutting Strain Index as the cracking and rutting indexes, respectively, to aid balanced mixture design (BMD) and facilitate improved performance analysis. The threshold values for these two indexes were determined as a function of traffic level using more than 100 different asphalt mixtures. The team also developed a performance-volumetrics relationship and index-volumetrics relationship using the four corners concept and used these relationships as the foundation for BMD and performance-related specifications. The developed BMD methods optimize the mixture for both aggregate gradation and binder content for a given set of aggregate stockpiles and binder. The team employed uncertainty analysis based on the Bayesian inference-based Markov Chain Monte Carlo technique to develop a reliability framework for distress predictions using FlexPAVE 2.0. The team also developed PASSFlex™ to support the user in the different steps of a performance evaluation on a project. One of the performance protocols recommended by the TFRS-01 project is implemented into PASSFlex. All the analysis tools developed in this research are based on Microsoft® Excel® and are seamlessly integrated. Finally, the research team performed three shadow projects in concert with the Western Federal Lands Highway Division, Maine Department of Transportation, and Missouri Department of Transportation to introduce the asphalt mixture performance tester suite of performance tests and performance models to State departments of transportation.

17. Key Words	18. Distribution Statement
FlexMAT, FlexPAVE, PASSFlex, thermal cracking, S-VECD, shift model, S_{app}, RSI, PVR, IVR, balanced mix design, shadow project, reliability, performance specification, PRS	No restrictions. This document is available to the public through the National Technical Information Service, Springfield, VA 22161. http://www.ntis.gov

19. Security Classif. (of this report)	20. Security Classif. (of this page)	21. No. of Pages	22. Price
Unclassified	Unclassified	270	N/A

Form DOT F 1700.7 (8-72) Reproduction of completed page authorized.

SI* (MODERN METRIC) CONVERSION FACTORS

APPROXIMATE CONVERSIONS TO SI UNITS

Symbol	When You Know	Multiply By	To Find	Symbol
		LENGTH		
in	inches	25.4	millimeters	mm
ft	feet	0.305	meters	m
yd	yards	0.914	meters	m
mi	miles	1.61	kilometers	km
		AREA		
in^2	square inches	645.2	square millimeters	mm^2
ft^2	square feet	0.093	square meters	m^2
yd^2	square yard	0.836	square meters	m^2
ac	acres	0.405	hectares	ha
mi^2	square miles	2.59	square kilometers	km^2
		VOLUME		
fl oz	fluid ounces	29.57	milliliters	mL
gal	gallons	3.785	liters	L
ft^3	cubic feet	0.028	cubic meters	m^3
yd^3	cubic yards	0.765	cubic meters	m^3
	NOTE: volumes greater than 1,000 L shall be shown in m^3			
		MASS		
oz	ounces	28.35	grams	g
lb	pounds	0.454	kilograms	kg
T	short tons (2,000 lb)	0.907	megagrams (or "metric ton")	Mg (or "t")
		TEMPERATURE (exact degrees)		
°F	Fahrenheit	5 (F-32)/9 or (F-32)/1.8	Celsius	°C
		ILLUMINATION		
fc	foot-candles	10.76	lux	lx
fl	foot-Lamberts	3.426	$candela/m^2$	cd/m^2
		FORCE and PRESSURE or STRESS		
lbf	poundforce	4.45	newtons	N
lbf/in^2	poundforce per square inch	6.89	kilopascals	kPa

APPROXIMATE CONVERSIONS FROM SI UNITS

Symbol	When You Know	Multiply By	To Find	Symbol
		LENGTH		
mm	millimeters	0.039	inches	in
m	meters	3.28	feet	ft
m	meters	1.09	yards	yd
km	kilometers	0.621	miles	mi
		AREA		
mm^2	square millimeters	0.0016	square inches	in^2
m^2	square meters	10.764	square feet	ft^2
m^2	square meters	1.195	square yards	yd^2
ha	hectares	2.47	acres	ac
km^2	square kilometers	0.386	square miles	mi^2
		VOLUME		
mL	milliliters	0.034	fluid ounces	fl oz
L	liters	0.264	gallons	gal
m^3	cubic meters	35.314	cubic feet	ft^3
m^3	cubic meters	1.307	cubic yards	yd^3
		MASS		
g	grams	0.035	ounces	oz
kg	kilograms	2.202	pounds	lb
Mg (or "t")	megagrams (or "metric ton")	1.103	short tons (2,000 lb)	T
		TEMPERATURE (exact degrees)		
°C	Celsius	1.8C+32	Fahrenheit	°F
		ILLUMINATION		
lx	lux	0.0929	foot-candles	fc
cd/m^2	candela/m2	0.2919	foot-Lamberts	fl
		FORCE and PRESSURE or STRESS		
N	newtons	2.225	poundforce	lbf
kPa	kilopascals	0.145	poundforce per square inch	lbf/in^2

*SI is the symbol for International System of Units. Appropriate rounding should be made to comply with Section 4 of ASTM E380. (Revised March 2003)

TABLE OF CONTENTS

LIST OF FIGURES

LIST OF TABLES

LIST OF ABBREVIATIONS

AASHTO	American Association of State Highway and Transportation Officials
ABC	aggregate base course
AC	asphalt content
AC-AV	binder content-air void content
ADSE	actuator deformation standard error
ALF	Accelerated Loading Facility
AMAC	asphalt mixture aging-cracking
AMPT	asphalt mixture performance tester
APS	average permanent strain
AQC	acceptance quality characteristics
BMD	balanced mix design
CALUW	coarse aggregate loose unit weight
COV	coefficients of variance
CPU	central processing unit
CTC	coefficient of thermal contraction
CUW	coarse unit weight
DCT	disc-shaped compact tension
DMR	dynamic modulus ratio
DPSE	dissipated pseudostrain energy
EICM	Enhanced Integrated Climatic Model
ESAL	equivalent single-axle load
FHWA	Federal Highway Administration
GB	gigabyte
GUI	graphical user interface
HMA	hot-mix asphalt
HT	high temperature
HWT	Hamburg wheel-tracking
IP-VFA	in-place VFA
IP-VMA	in-place VMA
IPO	index-based BMD performance optimum
IVR	index-volumetrics relationship
K-S test	Kolmogorov-Smirnov test
LMLC	laboratory-mixed laboratory-compacted
LOE	line of equality
LT	low temperature
LTPP	long-term pavement performance program
LVE	linear viscoelastic
MaineDOT	Maine Department of Transportation
MCMC	Markov Chain Monte Carlo
MERRA-2	National Aeronautics and Space Administration Modern-Era Retrospective Analysis for Research and Applications, Version 2
MESAL	1,000,000 equivalent single-axle load
MnROAD	Minnesota Cold Weather Pavement Testing Facility
MoDOT	Missouri Department of Transportation

NCDOT	North Carolina Department of Transportation
NCHRP	National Cooperative Highway Research Program
NCSU	North Carolina State University
NMAS	nominal maximum aggregate size
PAM	pavement aging model
PEMD	performance-engineered mix design
PG	performance grade
PGAB	performance graded asphalt binder
PID	proportional integral derivative
PLD	predicted life difference
PMLC	plant-mixed laboratory-compacted
PPO	predictive BMD performance optimum
PRS	performance-related specifications
PVR	performance-volumetrics relationship
QA	quality assurance
RAM	random-access memory
RAP	reclaimed asphalt pavement
RSI	rutting strain index
SHRP	Strategic Highway Research Program
SMA	stone matrix asphalt
SSE	standard squared error
SSR	stress sweep rutting (test method)
S-VECD	simplified viscoelastic continuum damage
SVO	Superpave™ volumetric optimum
TFHRC	Turner-Fairbank Highway Research Center
TSRST	thermal stress restrained specimen test
VBA	Microsoft® Visual Basic for Applications®
VFA	voids filled with asphalt
VMA	voids in mineral aggregate
WFLHD	Western Federal Lands Highway Division
WMA	warm-mix asphalt
2S2P1D	two springs, two parabolic elements, one dashpot

CHAPTER 1. PERFORMANCE AND INDEX-VOLUMETRICS RELATIONSHIPS

This chapter describes research efforts to develop a performance-volumetrics relationship (PVR) and index-volumetrics relationship (IVR). These relationships are important elements in the asphalt mixture performance tester (AMPT) balanced mix design (BMD) and performance-related specifications (PRS).[1]

DEVELOPMENT OF PERFORMANCE-VOLUMETRICS RELATIONSHIPS FOR ASPHALT MIXTURES

This section aims to establish the relationships between the volumetric properties of asphalt mixtures and their performance in terms of pavement fatigue cracking and rutting. A good PVR can dramatically improve the working efficiency of mixtures and can be used in AMPT-based BMD and PRS. (See references 1–7.) For this study, three asphalt mixtures were first designed to incorporate systematic changes in volumetric conditions. Then, fatigue cracking and rutting performance tests were conducted at each condition. Statistical analyses of the results suggest that a first-order (linear) model and power model would be an appropriate form of the PVR function. Also, the number of volumetric conditions required to calibrate the PVR function is investigated. Finally, a rule of thumb for selecting the volumetric conditions for the model calibrations is provided. The verification results show that the developed PVR function can capture the mixtures' performance responses that result from changes in volumetric conditions.

The focus of recent research in the asphalt pavement industry has been changing from empirical concepts to mechanistic concepts. Applications of this new focus include BMD, mechanistic-empirical pavement design, and PRS. (See references 1–7.) In these applications, the key is to predict the performance of asphalt pavements using mechanistic models. However, mechanistic models typically require detailed material property information, which can be time-consuming to measure. This time becomes even more critical when considering how often the properties need to be measured for some applications. For instance, in PRS, construction variability must be evaluated on a lot-by-lot basis, which requires that performance tests and simulations must be conducted for each lot using the asphalt mixture samples collected during production. To complete the full testing and analysis of each lot, the agency may spend several workdays on laboratory tests to determine the material properties. Similarly, for BMD, multiple sets of performance tests are required to ensure that the asphalt mixture is engineered to the optimal combination of the components. Owing to these challenges, the state-of-the-practice technologies primarily utilize volumetric methods for asphalt mixture design and quality control and assurance specifications.

These methods have a great advantage over those based on mechanistic properties because the volumetric properties can be measured quickly, and the results can be used to make production adjustments if necessary. The disadvantage, however, is that although volumetric-based methods are related to performance, the specific relationship for a given mixture is not known. If the relationship between performance and volumetric properties is known, then the following advantages can be recognized:

- Allow engineers to continue to use current test methods and equipment for quality assurance (QA) purposes.
- Allow material characterization to be completed in a short period during the mixture design and QA processes.
- Bridge the gap between the volumetric properties and performance of asphalt mixtures and allow engineering judgment in mix design and QA to be based on performance.

Numerous studies have been carried out to correlate mix volumetric properties with engineering properties. (See references 8–11.) However, the relationship established here is intended to correlate the volumetric properties or the changes in volumetrics directly to the mixture performance in pavements, i.e., fatigue damage and permanent deformation. The PVR developed in this study is based on a series of performance tests and analyses of three different asphalt mixtures. Performance tests of each study mixture were conducted using mixture samples at different volumetric conditions. The performance of the samples then was correlated with the corresponding volumetric conditions. The volumetric conditions were formulated according to different combinations of gradation, binder content, compaction level, etc. The performance characteristics used in this study include the amount of fatigue damage and permanent deformation in the wheel paths that was predicted by the mechanistic models. The models used for fatigue and rutting analyses at the material level are the simplified viscoelastic continuum damage (S-VECD) model and the shift model, respectively.[12–14] The cyclic fatigue test and stress sweep rutting (SSR) test were used to calibrate the S-VECD and shift models, respectively.[15,16] At the structural level, analysis was conducted using FlexPAVE™ (details in chapter 5 in volume I of this report).[17,18]

The objective of this study is to develop a performance-volumetrics relationship that can be used in BMD and PRS. In this study, the modeling work for the volumetric properties and performance characterization is presented in the first two sections, respectively. The third section presents the experimental design and test results. The fourth section establishes the PVR, required number of volumetric conditions for PVR calibration, and the rule that can be used to select the required number of volumetric conditions. Conclusions and recommendations for future work are provided at the end of this section.

Understanding Volumetric Properties of Asphalt Mixtures

In most States, volumetric theory is applied in current design specifications and for QA of asphalt mixtures and pavements. The assumption is that volumetric properties are related to the performance of asphalt mixtures and that, as such, criteria for volumetric parameters must be satisfied. Typical critical volumetric parameters include the voids in mineral aggregate (VMA) and voids filled with asphalt (VFA) at the design compaction level (N_{des}) in the laboratory. Other parameters, such as the air void content (V_a) at the N_{des} can be derived from the VMA and VFA. These volumetric parameters are used because they change with changes in mixture composition (aggregate gradation and binder content) and production (mixing time, storage time, temperatures, etc.). These volumetric parameters function as indicators of the performance of the mixture in the field if the as-constructed compaction level and the design compaction level are the same.

Mixture consistency is one aspect of quality materials and another is the density of that material once it is transported, placed, and compacted at the job site. This density usually differs from that targeted in the laboratory at N_{des}, i.e., 95 to 97 percent of the maximum specific gravity (G_{mm}). By contrast, the in-place percentage of G_{mm} (%G_{mm}) that is targeted for QA processes is often between 91 percent G_{mm} to 98 percent G_{mm} (i.e., 9 to 2 percent air void content). For QA purposes, the VMA and VFA at the N_{des} and as-constructed $\%G_{mm}$ are almost always included as the acceptance quality characteristics (AQCs). As for the actual performance in the field, the in-place volumetric parameters, i.e., the in-place VMA (IP-VMA) and the in-place VFA (IP-VFA), may better represent the performance of the as-constructed mixtures. Fortunately, these in-place volumetric parameters can be calculated if the VMA and VFA at the N_{des} value and the in-place %G_{mm} are known. Figure 1-A and Figure 1-B present diagrams that show the relationships among the volumetric parameters at the designed compaction level and the as-constructed (in-place) compaction level, respectively. For clarity and consistency, the volumetric parameters at the as-constructed compaction level are designated as in-place or using the subscript "IP." The exception is that whenever %G_{mm} is used, it refers to the as-constructed compaction level. The parameters without "in-place" or subscript IP are at the designed compaction level.

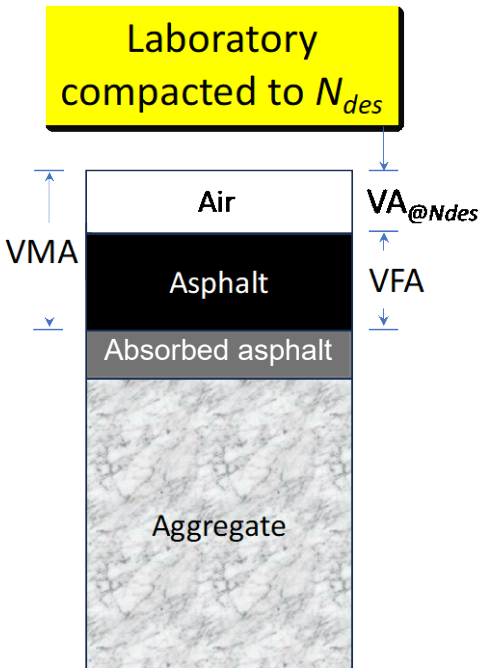

A. At design compaction level (N_{des}).

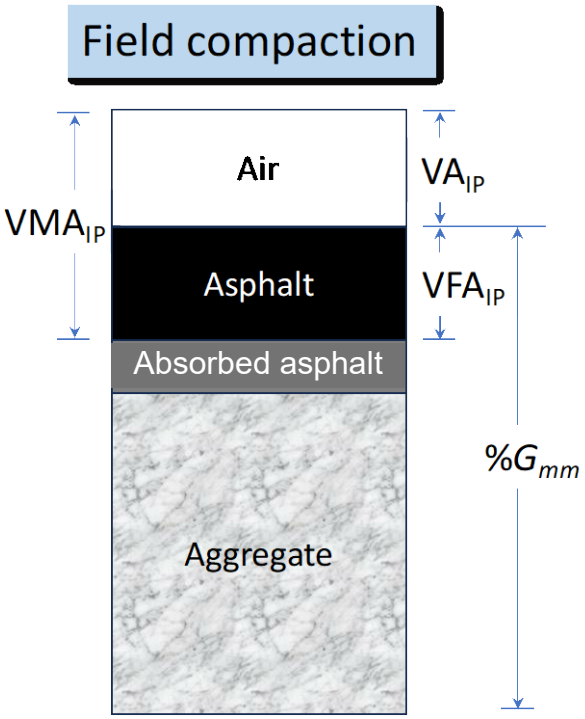

B. As-constructed (in-place) compaction level.

Figure 1. Illustrations. Volumetric diagrams.[19]

Although the laboratory- and field-constructed volumetric parameters differ, the in-place parameters can be calculated from the volumetric conditions at the design compaction level as long as the as-constructed %G_{mm} is also measured. This calculation is feasible because the gradation and binder content of the mixture are assumed to be the same under both conditions, and the only changing variable is the air void content. Equations 1 and 2 describe the VMA at the design compaction level and as-constructed compaction level, respectively.

$$VMA = 100 - \frac{(100 - V_a) \times G_{mm} \times P_s}{G_{sb}} \tag{1}$$

$$VMA_{IP} = 100 - \frac{\%G_{mm} \times G_{mm} \times P_s}{G_{sb}} \tag{2}$$

Where:

VMA = voids in mineral aggregate at the design compaction level (N_{des}).
VMA_{IP} = voids in mineral aggregate as constructed.
V_a = percentage of air void content at N_{des}.
G_{mm} = theoretical maximum specific gravity at N_{des}.
%G_{mm} = G_{mm} of a paving mixture at the in-place compacted density, percentage by the G_{mm} at N_{des}.
P_s = aggregate content, percentage by total mass of the mixture.
G_{sb} = bulk specific gravity of aggregate.

Because P_s and G_{sb} are the same for both the laboratory and field conditions, equations 1 and 2 can be rearranged to relate the VMA at N_{des} and the IP-VMA, as shown in equation 3 or equation 4.

$$\frac{100 - VMA_{IP}}{\%G_{mm}} = \frac{100 - VMA}{100 - V_a} \quad \text{or} \tag{3}$$

$$VMA_{IP} = 100 - \frac{\%G_{mm}}{100 - V_a} \times (100 - VMA) \quad \text{or} \tag{4}$$

using the in-place air void content of $V_{a,IP}$:

$$VMA_{IP} = 100 - \frac{(100 - V_{a,IP})}{100 - V_a} \times (100 - VMA) \tag{5}$$

Equation 5 explains that the VMA values at the two volumetric conditions are proportional to the air void contents because the proportion of binder to aggregate remains the same. The IP-VFA then can be computed as shown in equation 6.

$$VFA_{IP} = 100 - \frac{100 - \%G_{mm}}{VMA_{IP}} \times 100 \quad \text{or} \tag{6}$$

Using the in-place air void content of $V_{a,IP}$,

$$VFA_{IP} = 100 - \frac{V_{a,IP}}{VMA_{IP}} \times 100 \tag{7}$$

Figure 2 shows specific directional patterns in the VMA_{IP} versus VFA_{IP} space when the in-place density (or test specimen air void content for laboratory testing), binder content, and aggregate gradation are varied in the same mixture. When the in-place density value becomes higher (the air void content becomes lower), the volumetric coordinates move in the top-left direction, as shown by the dashed lines in figure 2. When the binder content is increased for the same aggregate gradation, the volumetric coordinates move to the right, as shown by the solid lines. The directional pattern for aggregate gradation is different for different gradation types. The volumetric coordinates move to the right, as shown by the dotted lines, as fine gradations become finer or coarse gradations become coarser.

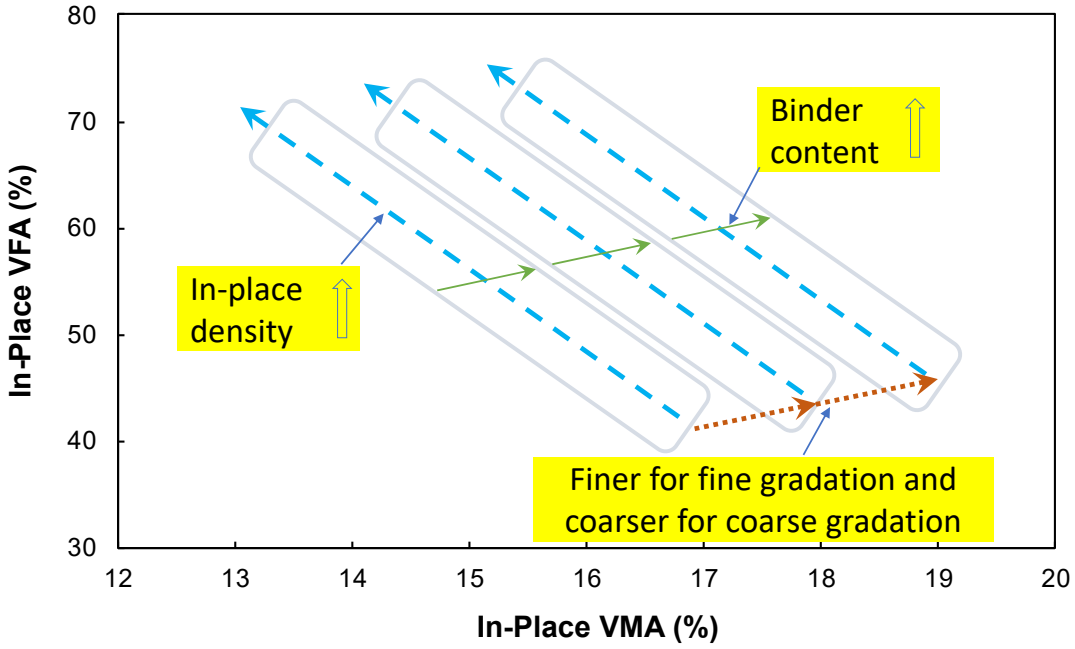

Figure 2. Illustration. Changes in VMA_{IP} and VFA_{IP} as a function of mixture characteristics.[19]

The two variables, IP-VMA and IP-VFA, are used in this study mainly to model the performance of the asphalt mixtures. The advantages of using these two parameters include the following:

- The two variables represent the true volumetric conditions in the field, i.e., the as-constructed volumes of the binder, aggregate, and air voids.
- Multiple AQC parameters, such as the VMA, VFA, V_a at N_{des}, and $\%G_{mm}$, are implicitly taken into account, and the number of variables needed for the PVR function is successfully reduced to two.

Therefore, the PVR function is incorporated in such formulae, as shown in equations 8 and 9.

$$\%Damage = f\left(VMA_{IP}, VFA_{IP}\right) \tag{8}$$

$$Rut\ Depth = g\left(VMA_{IP}, VFA_{IP}\right) \tag{9}$$

Where:

$\%Damage$ = percentage of fatigue damage in a specific pavement.
$Rut\ Depth$ = rut depth (mm) in a specific pavement.

Once equations 8 and 9 have been calibrated for a specific mixture in a specific pavement structure, the change in fatigue damage and rut depth can be related to the changes in volumetric parameters and vice versa. Because the IP-VMA and IP-VFA are functions of the design VMA, VFA, V_a, and $\%G_{mm}$, the performance of the mixture, or the resultant %Damage and rut depth, are essentially functions of those AQC parameters as well, as presented in equations 10 and 11.

$$\%Damage = f_1\left(VMA, VFA, V_a, \%G_{mm}\right) \tag{10}$$

$$Rut\ Depth = g_1\left(VMA, VFA, V_a, \%G_{mm}\right) \tag{11}$$

Mechanistic Models for Performance Characterization

This study characterized the performance of the asphalt mixtures by using mechanistic models. The models used at the material level and structural level are presented briefly in this section.

Mechanistic Models for the Material Level

At the material level, the mechanical properties of asphalt mixtures are characterized based on three aspects: the linear viscoelastic (LVE) property (dynamic modulus), fatigue cracking properties, and permanent deformation properties. The dynamic modulus can be used to calculate the LVE responses of the mixture, i.e., the strain and stress, under a specific loading history, with the time and temperature effects taken into account. Details regarding the dynamic modulus can be found in the literature.[20] The fatigue model used here is the S-VECD model (discussed in detail in chapter 3 in Volume I of this report; see also Underwood et al. for details about the theoretical background of the S-VECD model).[12,13,18] The permanent deformation (rutting) model used for this work is the shift model (discussed in detail in chapter 3 in Volume I of this report, along with the related SSR test; see also Kim and Kim for details).[18,21]

Performance Predictions for Asphalt Pavement Structures

The performance of asphalt mixtures can be evaluated and compared using pavement performance analyses if the pavement structure, traffic load, and climate conditions are fixed and only the asphalt mixture in the pavement structure is varied. In this study, pavement performance was simulated using FlexPAVE. The fatigue damage is calculated using the S-VECD model, and the shift model is applied for rutting analysis.[12] The output of the FlexPAVE analysis includes the percentage of the fatigue damage (%Damage) in the pavement cross section and permanent deformation in each layer during the entire design life. This study uses the %Damage and rut depth results at the end of the design life. Regarding rutting, this study uses only the rut depth attributed to the target asphalt layer. According to previous studies, the results of the performance simulations yielded excellent agreement with observations in the field under various climate conditions.[1]

The researchers chose pavement performance instead of index parameters to evaluate the asphalt mixtures for the following reasons:

- Pavement performance can fully represent mixture performance when only the asphalt mixture is varied in the analysis.

- Pavement performance simulations can reflect mixture performance more accurately than index parameters because they consider the structural effects and the effects of realistic climate conditions and traffic loads.

- The %Damage output and rut depth data can be utilized directly to develop PRS based on changes in pavement life due to changes in mixture performance when actual pavement structures are used in the analysis.

Experimental Design and Test Results

Two laboratory-mixed laboratory-compacted (LMLC) mixtures and one plant-mixed laboratory-compacted (PMLC) mixture were used for this study. The two LMLC mixtures, SM12.5 from Virginia and RS9.5B from North Carolina, were designed systematically with different gradations, binder contents, and compaction levels. In total, 21 volumetric conditions were included for the SM12.5 mixture and nine volumetric conditions were included for the RS9.5B mixture. Details regarding each mixture are presented in the next sections. The mechanical properties at each volumetric condition were characterized in a set of performance tests using an AMPT.[(1)] After the mechanistic models were calibrated using the performance test results, pavement performance simulations were performed using FlexPAVE. For those simulations, the pavement structures were fixed to be 4-inch single-layer asphalt pavements on top of an 8-inch aggregate base with 10 million equivalent single-axle loads (MESALs) over a 20-yr design life. The climate data were obtained from the Enhanced Integrated Climatic Model (EICM) database using data from climate stations in Washington, D.C. and Raleigh, NC.[(22)] The results of the performance simulations were used to establish the PVR functions.

The compaction levels in the field also were simulated in this study. The parameters of the volumetric conditions, i.e., VMA, VFA, and V_a, were measured from gyratory-compacted samples that were compacted to the N_{des}. The dimensions of the samples were 150 mm in diameter and 115 mm ±5 mm at the N_{des}. The specimens for the performance tests were extracted from 180-mm tall gyratory-compacted samples. The air void contents of the test specimens were designed to be varied and not necessarily the same as the V_a at N_{des} to simulate the different $\%G_{mm}$ values in the field. The air void contents of the test specimens were designated as in-place air voids, or VA_{IP}, and the value of (100-VA_{IP}) is equal to the $\%G_{mm}$. The term in-place is used, even though the mixtures with these volumetric conditions were never actually paved in the field, to represent the volumetric properties of performance test specimens. The relationships among the volumetric parameters, i.e., VMA, VFA, V_a, VMA_{IP}, VFA_{IP}, $\%G_{mm}$ (or VA_{IP}), follow equations 1 through 6.

As for the PMLC mixture, the samples were acquired during QA checks from an actual paving project in Maine. Ten samples were collected on 10 d. The volumetric properties of the

10 samples differed due to construction-related variability. Performance tests were carried out for each sample, and then performance simulations were conducted. The samples were collected as part of one of the three shadow projects undertaken in this study, which are described in detail in chapter 3.[23] The PMLC mixture discussed in this section is referred to as the Maine mixture.

SM12.5 Mixture

The SM12.5 mixture was previously used in the reclaimed asphalt pavement (RAP) and warm-mix asphalt (WMA) study at the Federal Highway Administration (FHWA) Accelerated Loading Facility (ALF) in McLean, Virginia in 2013; it was used to pave ALF Lane 6.[24] The mixture is a coarse-graded 12.5-mm nominal maximum aggregate size (NMAS) mixture that contains performance grade (PG) 64-22 binder and 22 percent RAP. For this study, the original job mix formula was modified to yield different volumetric conditions at the N_{des} and in-place conditions, but the RAP content was kept constant at 22 percent. The job mix modifications included two additional gradations so that three different VMA percentages at the N_{des} (13, 14, and 15 percent) could be included in the tests. The gradations were designed using the Bailey method to ensure that the final VMA percentages were close to the targets.[25] For each gradation, three binder contents were applied to yield different VFA percentages and air void contents at the N_{des}. In total, nine different combinations of the components were created.

Test specimens were then fabricated for performance testing. To mimic different compaction levels in the field, the test specimens were compacted with three different in-place air void contents (VA_{IP}). This experimental design should have yielded 27 conditions, but due to the limited compactability for some combinations, only 21 conditions were actually evaluated. Table 1 presents the volumetric properties and test results for the SM12.5 mixture. The IP-VMA and IP-VFA values were calculated and are presented in figure 3. The performance tests were conducted in the laboratory at FHWA's Turner-Fairbank Highway Research Center (TFHRC). Detailed information can be found in Lee and Gibson's study.[24] The terminology used for the Bailey method is used in this study.[25] The gradation is represented by its percentage of coarse aggregate loose unit weight (%CALUW), or simply coarse unit weight (CUW). Different CUW percentages yield different VMA percentages according to the Bailey method packing theory.[25,26]

Table 1. Volumetric properties and test results of SM12.5 mixture.

Gradation	No.	ID	VMA at N_{des}	%AC at N_{des}	VFA at N_{des}	V_a at N_{des}	VA_{IP}	VMA_{IP}	VFA_{IP}	%Damage	Rut Depth (mm)
CUW 110	1	A	15	4.2	64.7	5.3	7	16.5	57.6	31.9	2.0
CUW 110	2	B	15	4.2	64.7	5.3	9	18.3	50.9	33.1	3.6
CUW 110	3	C	14.5	4.5	73.8	3.8	5	15.6	67.9	28.4	2.1
CUW 110	4	D	14.5	4.5	73.8	3.8	7	17.3	59.6	29.8	3.3
CUW 110	5	E	14.5	4.5	73.8	3.8	9	19.1	52.9	30.2	3.6
CUW 110	6	F	14.7	4.9	79.6	3	5	16.5	69.6	26.6	3.7
CUW 110	7	G	14.7	4.9	79.6	3	7	18.2	61.6	26.6	3.7
CUW 100	8	H	14.1	3.8	65.2	4.9	7	16.0	56.2	40.3	1.8
CUW 100	9	I	14.1	3.8	65.2	4.9	9	17.8	49.4	38.0	2.1

Gradation	No.	ID	VMA at N_{des}	%AC at N_{des}	VFA at N_{des}	V_a at N_{des}	VA_{IP}	VMA_{IP}	VFA_{IP}	%Damage	Rut Depth (mm)
CUW 100	10	J	13.5	4.1	72.6	3.7	5	14.7	65.9	41.5	1.5
CUW 100	11	K	13.5	4.1	72.6	3.7	7	16.5	57.5	34.2	2.1
CUW 100	12	L	13.5	4.1	72.6	3.7	9	18.3	50.7	37.2	2.5
CUW 100	13	M	13.7	4.4	78.7	2.9	5	15.6	67.9	31.9	2.7
CUW 100	14	N	13.7	4.4	78.7	2.9	7	17.3	59.6	31.2	2.8
CUW 95	15	O	12.9	3.2	60.5	5.1	7	14.6	52.2	62.4	1.0
CUW 95	16	P	12.9	3.2	60.5	5.1	9	16.5	45.4	51.2	1.9
CUW 95	17	Q	12.5	3.6	68.8	3.9	5	13.5	63.0	45.4	1.3
CUW 95	18	R	12.5	3.6	68.8	3.9	7	15.3	54.3	45.4	1.4
CUW 95	19	S	12.5	3.6	68.8	3.9	9	17.1	47.5	39.3	2.8
CUW 95	20	T	12.8	3.9	75.8	3.1	5	14.5	65.5	47.0	1.8
CUW 95	21	U	12.8	3.9	75.8	3.1	7	16.3	57.1	39.5	1.8

AC = asphalt content; VMA_{IP} = in-place voids in mineral aggregate; and VFA_{IP} = in place voids filled with asphalt.

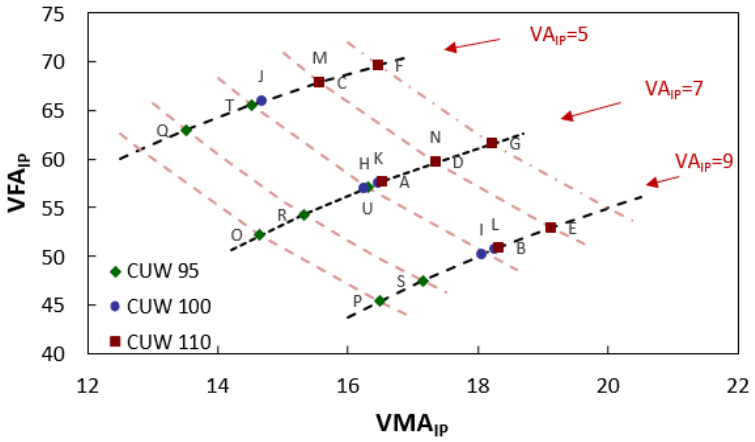

Figure 3. Graph. Distribution of volumetric conditions for SM12.5 mixture.[19]

RS9.5B Mixture

The RS9.5B mix is a typical fine-graded 9.5-mm NMAS North Carolina surface mixture. It contains 30 percent RAP and the virgin binder grade is PG 58-28. Similar to the SM12.5 mixture tests, the tests of this mixture were designed to have different volumetric conditions. Three gradations were selected using the Bailey method to yield different VMAs.[25] The three gradations from fine to coarse are designated as CUW 50, CUW 60, and CUW 70, respectively. Two binder contents and three in-place air void contents were tested at the conditions used for gradations CUW 50 and CUW 70. One volumetric condition for CUW 60 was generated and tested. The RS9.5B mixtures are all designated with a preceding C, two numbers that designate the CUW of the gradation (50, 60, or 70), one number that designates the target V_a at the N_{des}, and a final number that indicates the target in-place air void content, VA_{IP}. The CUW number is

separated from the target V_a at the N_{des} number with a dash. Table 2 presents the measured volumetric properties and test results. Figure 4 presents the volumetric conditions. This work was completed at North Carolina State University (NCSU).[27]

Table 2. Volumetric properties and test results of RS9.5B mixture.

Gradation	ID	VMA at N_{des}	%AC at N_{des}	VFA at N_{des}	Va at N_{des}	VA_{IP}	VMA_{IP}	VFA_{IP}	%Damage	Rut Depth (mm)
CUW 70	C70-33	15.3	6.0	80.4	3.0	2.9	15.2	80.9	11.5	3.2
CUW 70	C70-53	15.7	5.3	68.1	5.0	3.2	14.1	77.0	11.2	1.7
CUW 70	C70-55	15.7	5.3	68.1	5.0	4.7	15.4	69.6	14.1	2.1
CUW 70	C70-57	15.7	5.3	68.1	5.0	6.8	17.2	60.7	14.7	3.5
CUW 60	C60-44	16.3	5.8	71.2	4.7	4.2	15.9	73.3	11.6	2.8
CUW 50	C50-33	17.4	7.0	82.8	3.0	3.3	17.6	81.6	9.3	5.2
CUW 50	C50-54	17.2	6.1	70.9	5.0	3.9	16.2	76.0	10.1	2.7
CUW 50	C50-55	17.2	6.1	70.9	5.0	5.4	17.6	69.1	11.3	3.8
CUW 50	C50-57	17.2	6.1	70.9	5.0	7.3	19.2	61.8	11.4	4.6

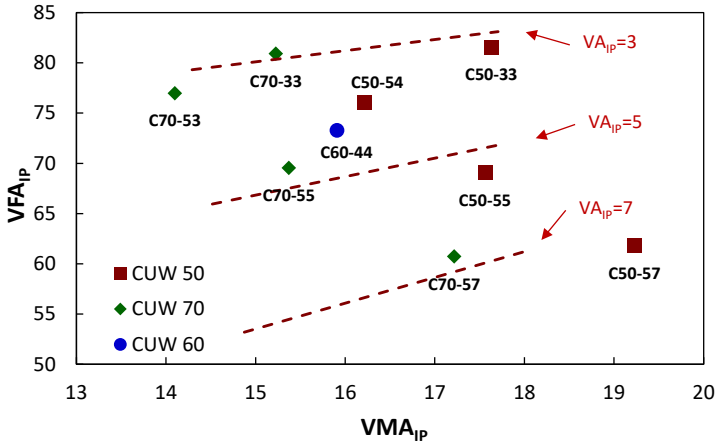

Figure 4. Graph. Distribution of volumetric conditions for RS9.5B mixture.[19]

Maine Mixture

The Maine mixture is a 12.5-mm coarse-graded asphalt mixture with PG 64-28 binder and 20 percent RAP.[23] Even though this mix testing utilized a single target gradation and binder content, the measured gradations and volumetric properties varied from sample to sample due to construction variability. In addition, for some samples, the performance tests were carried out at multiple in-place air void contents. Therefore,10 volumetric properties were included in the tests. Some of these performance tests were conducted at the Maine Department of Transportation (MaineDOT) and some at NCSU.[27] The sample ID follows the naming convention used by MaineDOT. Table 3 presents the measured volumetric properties and test results. Figure 5 presents the volumetric conditions.

Table 3. Volumetric properties and test results of Maine mixture.

Tester	ID	VMA at N_{des}	%AC at N_{des}	VFA at N_{des}	Va at N_{des}	VA_{IP}	VMA_{IP}	VFA_{IP}	%Damage	Rut Depth (mm)
Maine DOT	159352	15.5	5.3	70	4.7	7.2	17.7	59.4	12.9	2.1
Maine DOT	159355	15.9	5.2	72	4.4	2.2	14.2	82.4	9.9	1.2
Maine DOT	159360	16.8	5.9	77	3.9	2.4	15.6	84.0	9.7	1.2
Maine DOT	159361	17.3	5.9	73	4.7	7.6	19.7	61.9	12.7	2.2
Maine DOT	159352B	15.5	5.3	70	4.7	3.1	14.3	76.9	9.0	1.3
Maine DOT	159354A	16.2	5.7	78	3.5	4.9	17.4	72.1	12.5	1.5
Maine DOT	159354B	16.2	5.7	78	3.5	5.8	18.4	67.3	12.0	1.8
NCSU	159362	17.0	5.8	73	4.4	5.8	18.1	68.6	11.0	2.0
NCSU	159358	16.4	5.3	72	4.6	4.6	16.4	71.9	9.6	1.6
NCSU	159353	16.4	5.5	73	4.5	4.4	15.7	72.3	11.4	1.5

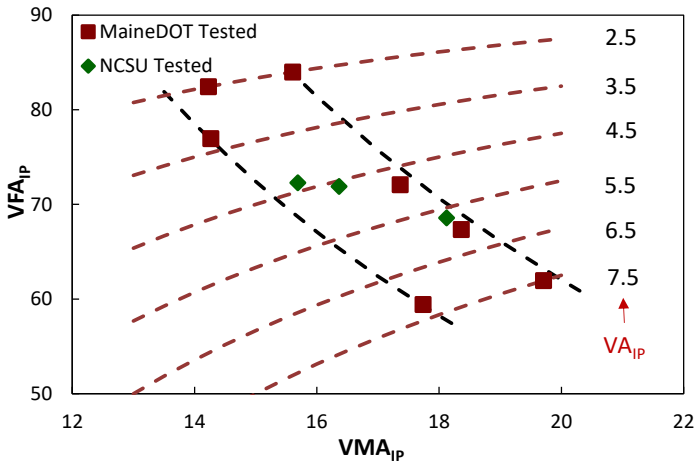

Figure 5. Graph. Distribution of volumetric conditions for Maine mixture.[19]

Development of Performance-Volumetrics Relationship Function

This section presents the development and establishment of the relationship between the volumetric parameters and the performance of the asphalt mixtures. Equations 8 and 9 show the basic forms of the PVR function. Statistical analyses were applied in this study to find the relationship between the predictors and response variables. In statistics, such relationships are defined via a response surface model.

Response Surface Model

Wang et al. investigated the response surface model by plotting contours of pavement performance (%Damage and rut depth) in the VFA_{IP} and VMA_{IP} domain for the SM12.5 mixture, RS9.5B mixture, and Maine mixture.[19,28] The contours showed that the shape of the contour lines might have been affected by testing variability; however, within the scope of interest, the contour lines could be approximated to some straight lines for simplicity or some lines with minor curvature.

To complete the regression analysis for the response surface model, the form of the function had to be determined first. Because the contour lines show some linearity, the first-order model could be examined by checking the linearity between the response variable and the predictors. Figure 6 presents the relationship between %Damage and the individual volumetric parameters in the SM12.5 mixture as an example. Figure 6 shows a strong linear relationship between the %Damage and the VFA_{IP} when the VMA_{IP} is kept constant. The same observation can be made between %Damage and the VMA_{IP}. In addition, the similarity in the slopes of the fitted trend lines also indicates that an interaction term may not be necessary. For asphalt mixtures, the physical meaning of the interaction term, which is the product of VMA_{IP} and VFA_{IP}, is the in-place volume of the effective binder, V_{beff}. This finding means that the effect of V_{beff} has already been considered in VMA_{IP} and VFA_{IP}. Based on the observations, the first-order model appears to be a good candidate for the regression analysis.

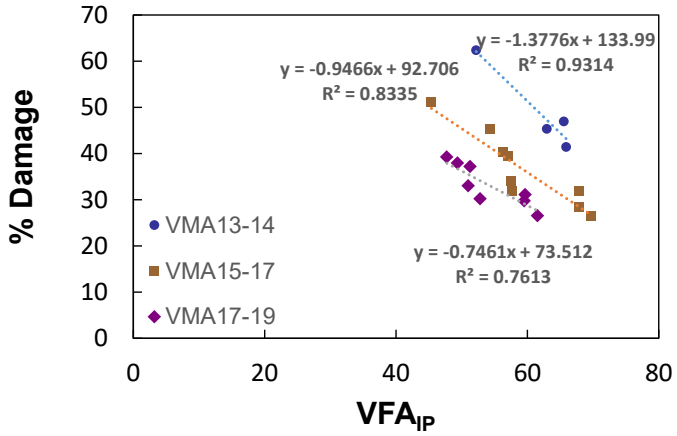

A. %Damage versus IP-VFA.

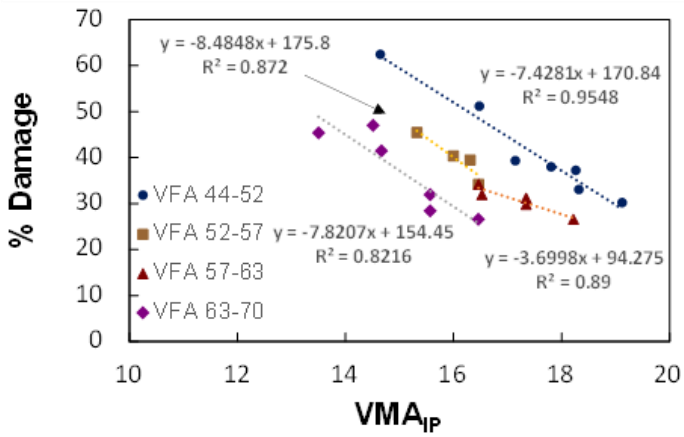

B. %Damage versus IP-VMA.

Figure 6. Graphs. Linearity in performance-volumetric relationship.[19]

Other typical models also were evaluated and compared in this study using statistical methods. These models are presented as equations 12 through 16.

First-order model:

$$\%Damage = \beta_0 + \beta_1 \times VMA_{IP} + \beta_2 \times VFA_{IP} + \varepsilon \quad (12)$$

First-order model with interaction:

$$\%Damage = \beta_0 + \beta_1 \times VMA_{IP} + \beta_2 \times VFA_{IP} + \beta_{12} \times V_{beff,IP} + \varepsilon \quad (13)$$

Second-order model:

$$\%Damage = \beta_0 + \beta_1 \times VMA_{IP} + \beta_2 \times VFA_{IP} + \beta_{12} \times V_{beff,IP} + \beta_{11} \times VMA_{IP}^{\ 2} + \beta_{22} \times VFA_{IP}^{\ 2} + \varepsilon \quad (14)$$

Exponential function:

$$\%Damage = \ln\left(\beta_0 + \beta_1 \times VMA_{IP} + \beta_2 \times VFA_{IP} + \varepsilon\right) \quad (15)$$

Power function:

$$\%Damage = \beta_0 \times VMA_{IP}^{\beta_1} \times VFA_{IP}^{\beta_2} \quad (16)$$

Where:

$V_{beff,IP}$ = in-place volume of effective binder.
$\beta_0, \beta_1, \beta_2, \beta_{12}, \beta_{11}, \beta_{22}$ = fitting coefficients.
ε = residual of the regression.

The exponential equation and power function are essentially linear functions in log-log scale.

These typical models were evaluated and compared statistically using the following parameters: adjusted R^2 values, *p*-values from analysis of variance tests, and *p*-values of each term from student's t-tests. Table 4 presents the parameters used in the three sets of tests. According to the statistics, the regression with the linear function shows significance in all cases, whereas the first-order model with interaction and the second-order model seem to be unable to model the relationship.

Table 4. Statistical parameters in regression analysis.

Mixture	Parameter	First-Order Model	First-Order Model with Interaction	Second-Order Model	Exponential	Power
SM12.5	R^2	0.84	0.85	0.88	0.88	0.89
SM12.5	Adjusted R^2	0.83	0.82	0.84	0.87	0.87
SM12.5	*p*-value	5.18E-08	0.00	0.01	5.16E-09	3.37E-09
SM12.5	*p-value* β_0	3.37E-10	0.04	0.01	1.91E-14	1.25E-11
SM12.5	*p-value* β_1	4.42E-08	0.21	0.03	5.32E-09	3.57E-09
SM12.5	*p-value* β_2	3.58E-07	0.34	0.07	3.32E-08	2.35E-08
SM12.5	*p-value* β_{12}	—	0.69	0.11	—	—
SM12.5	*p-value* β_{11}	—	—	0.05	—	—
SM12.5	*p-value* β_{22}	—	—	0.27	—	—
RS9.5B	*p-value* R^2	0.76	0.80	0.90	0.79	0.79
RS9.5B	Adjusted R^2	0.68	0.68	0.73	0.72	0.72
RS9.5B	*p* -value	0.01	0.03	0.10	0.01	0.01
RS9.5B	*p-value* β_0	1.29E-03	0.12	0.45	1.18E-04	1.16E-03
RS9.5B	*p-value* β_1	2.93E-02	0.25	0.96	1.95E-02	2.00E-02
RS9.5B	*p-value* β_2	4.95E-03	0.23	0.23	3.29E-03	3.49E-03
RS9.5B	*p-value* β_{12}	—	0.36	0.62	—	—
RS9.5B	*p-value* β_{11}	—	—	0.62	—	—
RS9.5B	*p-value* β_{22}	—	—	0.22	—	—
Maine	R^2	0.70	0.70	0.73	0.69	0.70
Maine	Adjusted R^2	0.61	0.55	0.39	0.60	0.61

Mixture	Parameter	First-Order Model	First-Order Model with Interaction	Second-Order Model	Exponential	Power
Maine	*P-value*	0.02	0.05	0.24	0.02	0.01
Maine	*p-value* β_0	0.00	0.81	0.79	0.03	0.36
Maine	*p-value* β_1	0.02	0.85	0.74	0.24	0.23
Maine	*p-value* β_2	0.01	0.91	0.83	0.31	0.30
Maine	*p-value* β_{12}	—	0.97	0.78	—	—
Maine	*p-value* β_{11}	—	—	0.72	—	—
Maine	*p-value* β_{22}	—	—	0.89	—	—

—No data.

This evaluation also used other variables in the regression. Figure 7 presents the residuals, normal probability, and model predictions from the linear regression using the first-order model; only the data from the SM12.5 mixture are shown as an example. The figure shows that the residuals are normally distributed along the x-axis, the normal probabilities are linearly distributed, and the comparison between the predicted %Damage and observed %Damage shows good agreement. The research team used the same process to evaluate the regression using other models. In summary, the team found the first-order model and power model to be the most promising.

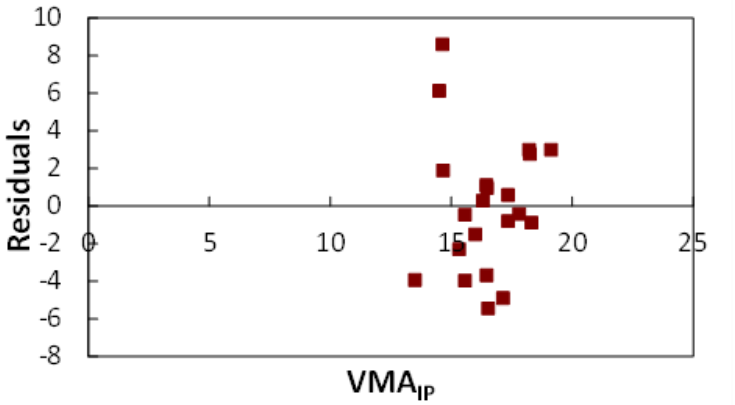

A. Residual plots for VMAIP.

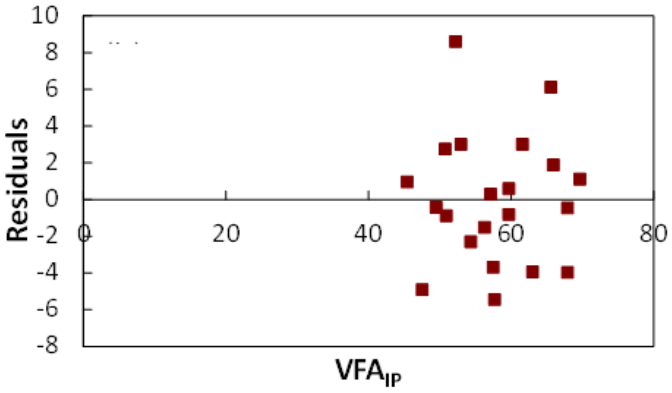

B. Residual plots for VFA_{IP}.

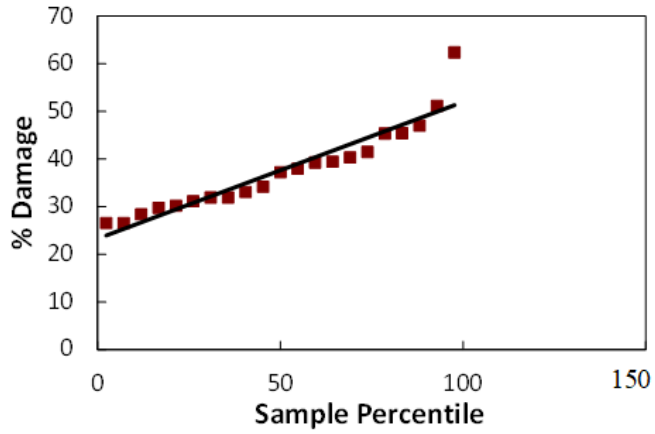

C. Normal probability plot.

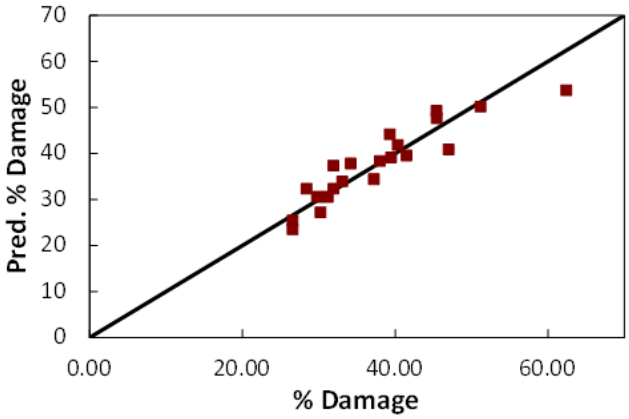

D. Comparison between predictions and observations.

Figure 7. Graphs. Regression analysis results.[19]

The following observations can be made on the two models:

- Both the models have only three coefficients to calibrate; thus, their simplicity allows much less work for model calibration.
- The first-order model provides reasonable fit and predictions; however, the power function can represent nonlinearity better than the first-order model in some scenarios.

In addition, the developed PVR function may be used in situations where extrapolation is necessary and in these cases the sensitivity of the model affects the prediction accuracy. The research team conducted an indepth investigation and found that the linear model shows less sensitivity to the variability in the experimental data than the power model. Laboratory-to-field transfer functions had not yet been implemented in FlexPAVE when this study was performed. The transfer functions are expected to be nonlinear, and therefore, the linear PVR function would result in nonlinear change in the pavement performance as a function of the volumetric parameters when the transfer functions are applied.

Finally, the PVR functions chosen from this study are:

$$\%Damage = \beta_{f0} + \beta_{f1} \times VMA_{IP} + \beta_{f2} \times VFA_{IP} \quad (17)$$

$$Rut\ Depth = \beta_{r0} + \beta_{r1} \times VMA_{IP} + \beta_{r2} \times VFA_{IP} \quad (18)$$

Where β_{f0}, β_{f1}, β_{f2}, β_{r0}, β_{r1}, β_{r2} is fitting coefficients.

Characterization of Performance-Volumetrics Surface

According to the results presented in the previous section, the first-order model and the power form model are sufficient to represent the PVR function. However, when the function is implemented in the industry, agencies or contractors cannot afford to conduct the 10 sets of performance tests needed to calibrate the function for one asphalt mixture. Therefore, agencies and contractors need a method that reduces the amount of work required for model calibration.

Both the first-order function and the power function have three model coefficients to calibrate, which means that at least three sets of data should be provided for calibration. However, due to the inevitable random errors in performance tests, selecting three volumetric conditions may not be sufficient to calibrate the entire surface. Thus, the research team evaluated the number of necessary volumetric conditions. This study recommends a rule of thumb to select the effective volumetric conditions needed for model calibration. The evaluation shown in this study is based on the first-order model, but the same approach philosophy can be applied to the power model as well.

Rule of Thumb for Detecting Volumetric Conditions for Model Calibration

A brute force approach was adopted to develop the rule of thumb selection process. First, all possible combinations of three conditions were chosen and used to fit the coefficients of the linear model. For example, the SM12.5 mixture had a total of 21 conditions, which results in 1,330 possible unique combinations with three conditions, each of which must be evaluated. Then, the same process was repeated using combinations of four and five conditions. The fitted coefficients then were used to predict the %Damage and rut depths for all the volumetric conditions that had been tested. Next, the errors between the predictions and observations were calculated. The combinations were then ranked by the normalized R^2 value defined in equation 19, considering the sum of squared error in both the fatigue and rutting performance predictions. The normalized R^2 value, being different from traditional R^2 values, varies from 2 to minus infinity. Higher values indicate less error in regression.

$$R_n^2 = \left(1 - \frac{\sum_{i=1}^{n}\left(\hat{f}_i - f_0\right)^2}{\sum_{i=1}^{n}\left(f_i - f_0\right)^2}\right) + \left(1 - \frac{\sum_{i=1}^{n}\left(\hat{r}_i - r_0\right)^2}{\sum_{i=1}^{n}\left(r_i - r_0\right)^2}\right) \quad (19)$$

Where:

R_n^2 = normalized R^2 value.
n = number of total volumetric conditions in each experiment, not limited to the number of conditions used in the calibration.
f_i = value of individual observation for fatigue damage.
f_i = value of individual observation for rut depth.
f_0 = mean value of observation for fatigue damage.
r_0 = mean value of observation for rut depth.

$\hat{f}_i$ = predicted value at each volumetric condition for fatigue damage.

$\hat{r}_i$ = predicted value at each volumetric condition for rut depth.

The combinations that yielded high normalized R^2 values were evaluated. Regardless of the number of conditions used in the calibration, the best 10 or 20 combinations in each scenario were selected for further investigation. The selected combinations were almost always the ones where the selected conditions were spread out and located at the edge of the IP-VMA and IP-VFA space. This finding is expected because the wider the range the calibration conditions can cover, the more representative of the performance surface the calibrated functions can become. For example, to calibrate the performance surface of the SM12.5 mixture, the combination of conditions Q, P, and G and the combination of conditions A, E, Q, and P both yield high-quality regression results (see table 1 and figure 3 for these conditions). In summary, the rule of thumb for the condition selection used in the model calibration is to spread out the conditions in the volumetric space to ensure that a wide range of conditions is covered.

The amount of time that is required for conducting performance tests for model calibration is an important factor regarding efficiency. To implement the PVR function in the industry, the testing time should not exceed a certain limit. The concept of PVR is introduced so that the performance tests do not have to be performed during mixture production and paving. The performance tests at the required volumetric conditions need be performed during BMD or during PRS development. Three to five different volumetric conditions should be sufficient to characterize the response surface if the conditions are determined based on the developed rule of thumb. All the scenarios with three, four, and five combinations were evaluated. To understand the criterion that is used to examine the combinations, the combinations are ranked by average absolute error, which can be computed using equation 20.

$$\bar{e} = \frac{\sum_{i=1}^{n} \left| \frac{\hat{y}_i - y_i}{y_i} \times 100 \right|}{n} \tag{20}$$

Where:

$\bar{e}$ = average absolute percentage of error (%Error).

$\hat{y}_i$ = predicted percentage of damage (%Damage) or rut depth for each individual condition.

y_i = %Damage or rut depth for each individual condition.

Figure 8 presents the averaged absolute percentages of error ($\bar{e}$) for all the combinations for the SM12.5 mixture. As shown in figure 8-A and figure 8-B, when three, four, or five conditions are chosen for calibration, the average error starts at 6 percent with the best combination. The rule of thumb serves as guidance to select the best or suitable combinations. Also, in all cases, the best few hundred combinations can yield less than 10 percent average error when they are used in the model calibration. Figure 8-C and figure 8-D show the number and probability of finding combinations that yield less than 10 percent error when using three, four, or five conditions. Figure 8-D shows that, if three conditions are used in the model calibration for the SM12.5

mixture, among all the combinations, 30 percent can provide predictions with less than 10 percent average error. The percentages for four and five combinations are higher. Thus, using four or five conditions in the PVR model calibration can reduce the likelihood of low-quality predictions. The increase in the acceptable percentage from four conditions to five conditions is less than that from three to four conditions.

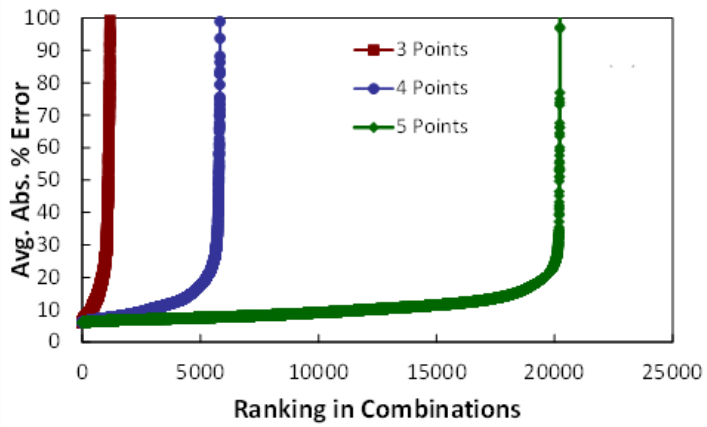

A. Average absolute percentage error versus ranking in combinations.

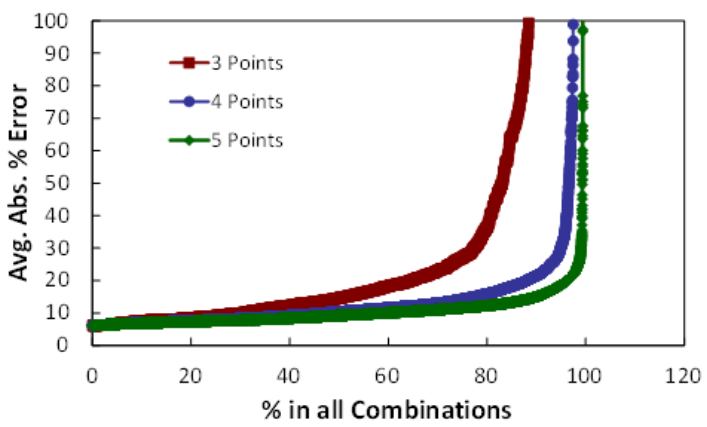

B. Average absolute percentage error versus percentage in all combinations.

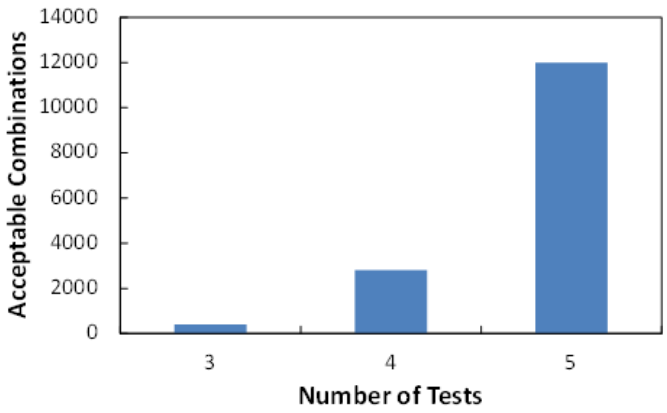

C. Number of acceptable combinations versus number of tests.

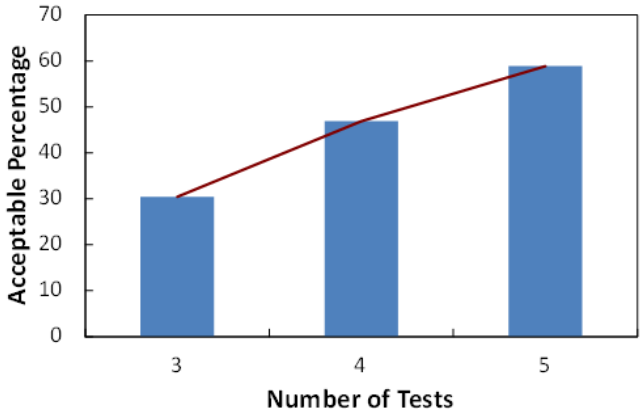

D. Acceptable percentage versus number of tests.

Figure 8. Graphs. Evaluation results for combinations of volumetric conditions in model regression.[19]

Based on these observations, the research team selected four conditions as the optimal number of volumetric conditions needed to calibrate the PVR function. The best way to select the four volumetric conditions is to spread out the conditions in the volumetric space to ensure that a wide range of conditions is covered. This report refers to the four volumetric conditions that are used to calibrate the PVR function as four corners, to describe the four representative volumetric conditions that are located furthest from each other to form a quadrangular shape but within the limit for mixture acceptance. Figure 9 presents the suggested four corners locations in the VMA_{IP} versus VFA_{IP} volumetric space.

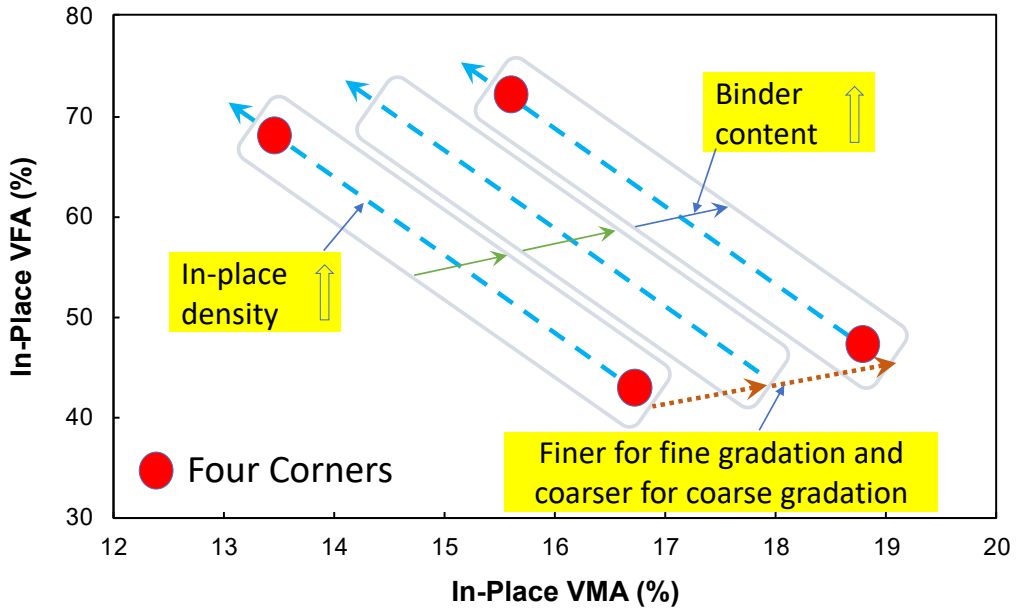

Figure 9. Illustration. Four corners in the volumetric space.[19]

Figure 10 presents the prediction results for the three mixtures. The research team applied the first-order model and calibrated the PVR function using four corners for each of the three mixtures. The team selected the volumetric conditions for each mix based on the four corners concept. Specifically, the four corners for the SM12.5 mixture are conditions E, F, P, and Q, those for the NC RS9.5B mixture are conditions C70-53, C70-57, C50-33, and C50-57, and those for the Maine mix are 159352, 159360, 159361, and 159352B. The predictions obtained from the PVR function in these scenarios yielded good agreement with the measurements obtained from the tests. The PVR function the research team calibrated using the performance data from the four corners can capture the effects of the changes in volumetrics on mixture performance.

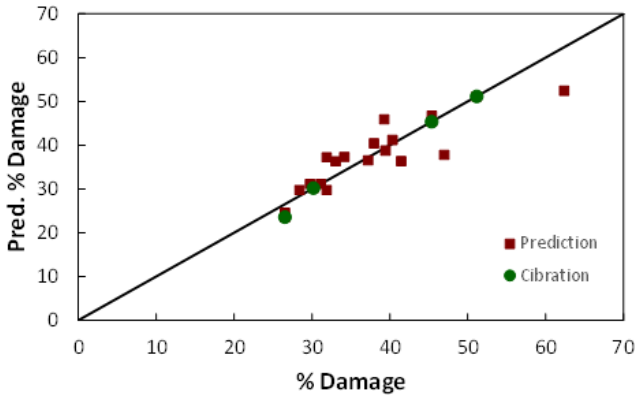

A. SM12.5 mixture (%Damage).

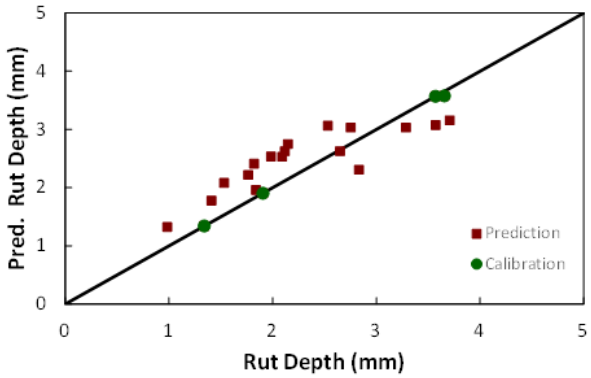

1 mm = 0.04 inches.

B. SM12.5 mixture (rut depth).

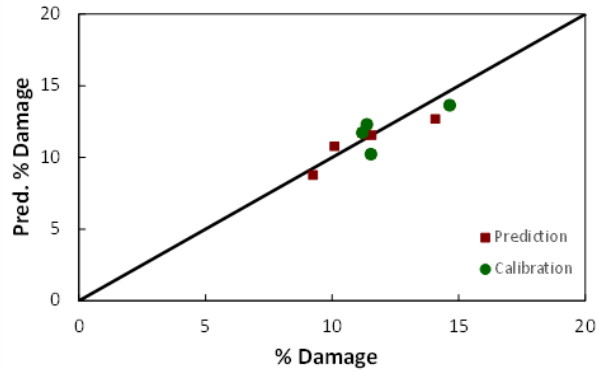

C. RS9.5B mixture (%Damage).

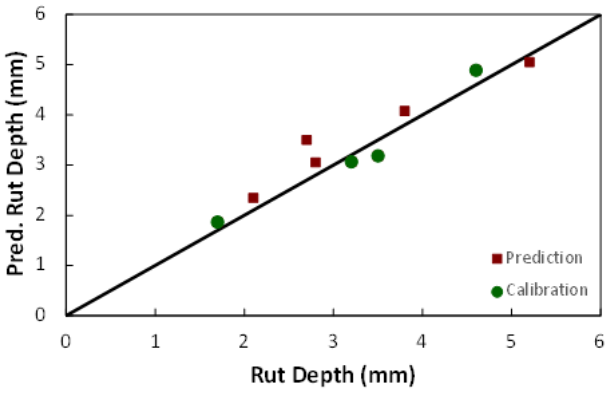

1 mm = 0.04 inches.

D. RS9.5B mixture (rut depth).

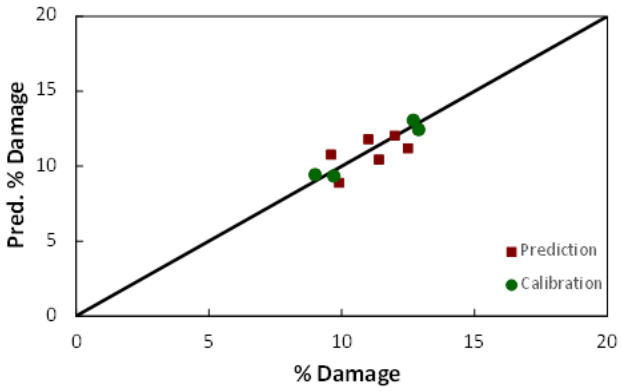

E. Maine mixture (%Damage).

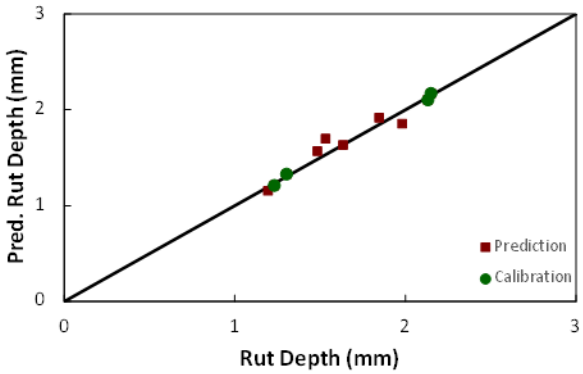

1 mm = 0.04 inches.

F. Maine mixture (rut depth).

Figure 10. Graphs. Prediction results obtained from calibrated PVR function.[19]

Summary

This section proposes a function that describes the PVR. Experimental data are presented, and the PVR model is established. The following conclusions can be drawn:

- The volumetric properties or traditional AQC parameters can be articulated as two parameters, IP-VMA and IP-VFA.
- Statistical analysis results indicate that the first-order model and the power model can be used in the PVR function.

- The optimal number of volumetric conditions needed to calibrate the PVR for a mixture is four. The four volumetric conditions, the four corners, should be located furthest from each other to form a quadrangular shape in the VMA_{IP} versus VFA_{IP} space but within the limit for mixture acceptance.

- The performance predictions from the calibrated PVR function show good agreement with the measurements from other volumetric conditions that are not used in the PVR calibration.

- The PVR function can be used in BMD and PRS by conducting AMPT performance tests at the four volumetric conditions.[1] Once the PVR is calibrated, engineers can evaluate the performance of the mixture for any volumetric condition.

DEVELOPMENT OF AN INDEX-VOLUMETRICS RELATIONSHIP FOR ASPHALT MIXTURES

As mentioned in previous chapters, the current Superpave™ mix design focuses on volumetric properties; however, volumetric properties alone cannot reflect the quality of the binder or mixture that directly relates to pavement performance. Therefore, an additional mixture performance test is needed to supplement the volumetric mix design method.

Many index-based tests have been developed to address fatigue cracking. State highway agencies use such tests for their mix designs to improve the mixture's fatigue resistance. Survey responses from State agency personnel and asphalt contractors indicate that the direct tension cyclic fatigue test (referred to in this report simply as the cyclic fatigue test) is an effective test to investigate potential bottom-up and top-down fatigue cracking.[1] This cracking test uses the S_{app} index that can be applied for mix design and QA purposes and to characterize fatigue cracking performance.

In this section, the IVR is proposed as a method to predict the value for cracking and rutting indexes using the volumetric properties of asphalt mixtures. Because most State highway agencies and contractors conduct volumetric tests for their QA processes, an advantage of the proposed methodology is that, once IVRs are developed for the mixture in question, the performance of the QA samples can be predicted using the agency's conventional QA measurements without the need to conduct mixture performance tests.

This study's primary goal is to demonstrate the IVR's ability to predict cracking and rutting performance using PMLC mixtures obtained from field projects. The secondary goal is to evaluate the effects of in-place density on S_{app} and the rutting strain index (RSI) in a QA framework. Because plant-produced mixtures have a small range of binder content, the effect of binder content on the IVR is not considered here.

In the following sections, the IVR concept is described first. The calibration and verification of the fatigue and rutting IVRs are presented in separate sections to avoid confusion. Also included in these sections is the application of the developed IVRs to evaluate the effects of in-place density variability on pavement performance.

Index-Volumetrics Relationship

The underlying concept of the IVR is the same as that of the PVR; that is, the performance of an asphalt mixture under any volumetric conditions can be predicted by testing the asphalt mixture at four corners.[19] The volumetric conditions considered are the VMA_{IP} and VFA_{IP}. The same PVR development principle has been applied successfully to develop IVRs for rutting performance using PMLC mixtures.[29]

The IVR is developed using linear regression based on the relationships between the four corners volumetric conditions and the performance index values. Equations 21 and 22 present the IVR function for fatigue and rutting performance, respectively.

$$Fatigue\ Index = a_f \times VMA_{IP} + b_f \times VFA_{IP} + d_f \quad (21)$$

$$Rutting\ Index = a_r \times VMA_{IP} + b_r \times VFA_{IP} + d_r \quad (22)$$

Where a_f, b_f, d_f, a_r, b_r, d_r is fitting coefficients.

Fatigue IVR

This section presents the calibration, verification, and application of fatigue IVRs using PMLC mixtures.

Mixture Information

This study used two North Carolina PMLC mixtures, RS9.5C and RI19.0C obtained from a field project, to introduce the methodology and utilize the IVR concept to predict the cracking index values. Table 5 summarizes the general information for each mixture. For the RS9.5C mixture, seven mixture samples were collected from seven different truck loads in the project. For the RI19.0C mixture, six mixture samples were obtained using the same procedure as for RS9.5C. The average production of each truck load was approximately 19 tons, and 270 kg (600 lb) of mixture samples were obtained per truck load. The first sample was acquired from the fifth truck load and the interval of the sampling was approximately 30 min for the RS9.5C mixture; there was no interval pattern for the RI19.0C mixture. The sampling process lasted 4 d, assigning 2 d for each mixture. The mixture samples were labeled sequentially. This sampling method is intended to generate natural sample-to-sample variations in typical paving projects.

Table 5. Mixture information.

Mixture	RS9.5C	RI19.0C
Layer	Surface	Intermediate
NMAS (mm)	9.5	19
Binder type	PG 64-22	PG 64-22
Total binder content (percent)	5.8	4.6
RAP content (percent)	40	30

Direct Tension Cyclic Fatigue Test

The cyclic fatigue test is an actuator displacement-controlled test that applies repeated cyclic loadings to a test specimen until the specimen fails. The test results include the applied stress value, on-specimen axial strain response, and the number of cycles to failure. These data are used to calibrate the coefficients in the S-VECD model.[12]

The cyclic fatigue test uses the S_{app} parameter as a test index. The S_{app} index values for this study were calculated using FlexMAT™ Cracking version 1.1.2 software that can be found on FHWA's website: https://www.fhwa.dot.gov/pavement/asphalt/analysis. Also, the dynamic modulus test—American Association of State Highway and Transportation Officials (AASHTO) TP 132—should be conducted at the same air void content as the cyclic fatigue test to derive the S_{app} values.[30] Table 6 summarizes the information for the cyclic fatigue test.

Table 6. General information for two cracking tests and indexes.

Test	Cyclic Fatigue Test
Test standard	AASHTO T 411[15]
Test temperature	Varies depending on the binder PG grades (18 °C for the study mixtures)
Test rate	10 Hz
Specimen geometry	Cylindrical diameter: 38 mm, height: 110 mm
Replicates	3
Index	S_{app}
Index calculation	$\frac{1}{1000}^{\frac{\alpha}{2}-1} \times \frac{a_T^{\frac{1}{\alpha+1}} \left(\frac{D^R}{C_{11}}\right)^{\frac{1}{C_{12}}}}{\left\|E^*\right\|^{\frac{\alpha}{4}}}$
Note	Calculated by FlexMAT Cracking

Experimental Plan

Volumetric Conditions Calculations

The research team used seven (numbers 1, 2, 3, 4, 5, 6, and 7) and six (numbers 1, 2, 3, 4, 5, and 6) mixture samples from different truck loads for the RS9.5C and RI19.0C mixtures, respectively. The team conducted volumetric tests for each mixture sample and calculated the volumetric conditions using equations 5 and 7. Table 7 presents the volumetric test results, in-place air void contents of the mixture samples, calculated volumetric conditions, the cracking tests that were used to test the mixture samples, and the coefficients of variance (COVs) for the measurements. For the COVs presented in table 7, the in-place air void content for the RS9.5C mixture shows the greatest variation within the seven samples and the V_a at N_{des} shows the second greatest variation. For the 19.0C mixture COVs, the V_a at N_{des} shows the greatest variation and the in-place air void content follows as the second greatest. The variation of the binder content within the samples is relatively small for both mixtures. Based on these results, the binder content appears to have been better controlled during the mixture production phase than the air void content during the construction phase. Figure 11 shows the volumetric conditions of the two mixtures in the VMA_{IP} and VFA_{IP} domain. The volumetric conditions are not spread too far apart in the diagonal direction from the bottom left to the top right of both graphs due to the small variation in the binder content for each mixture.

Table 7. Volumetric conditions of mixture samples.

Mix	Sample ID	Binder Content (Percent)	VMA (Percent)	V_a (N_{des}, Percent)	In-Place Air Void Content (Percent)	VMA_{IP} (Percent)	VFA_{IP} (Percent)
RS9.5C	1	5.8	15.5	2.6	6.8	19.1	64.5
RS9.5C	2	5.6	14.3	1.7	8.5	20.2	58.0
RS9.5C	3	6.1	15.9	2.3	6.5	19.5	66.7
RS9.5C	4	5.9	15.5	2.4	5.8	18.4	68.6
RS9.5C	5	5.8	15.8	2.9	8.8	20.9	57.9
RS9.5C	6	6.0	15.9	2.6	4.9	17.9	72.6
RS9.5C	7	6.1	16.1	2.5	5.2	18.4	71.8
RS9.5C	COV (percent)	3.1	3.9	15.4	23.0	5.6	9.1
RI19.0C	1	4.6	13.9	3.9	3.8	13.8	72.5
RI19.0C	2	4.8	13.6	3.1	4.9	15.2	67.8
RI19.0C	3	4.7	13.0	2.7	4.3	14.4	70.2
RI19.0C	4	4.6	13.7	3.8	6.3	15.9	60.5
RI19.0C	5	4.5	13.2	3.5	5.7	15.2	62.4
RI19.0C	6	4.1	13.5	4.7	5.7	14.4	60.4
RI19.0C	COV (percent)	5.3	2.5	19.2	18.6	5.1	7.9

V_a = air void content; N_{des} = design gyration level.

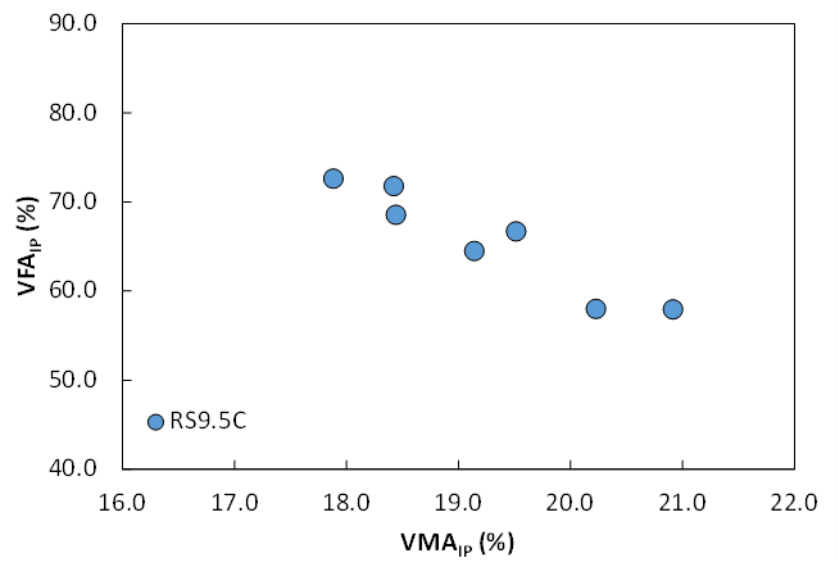

A. RS9.5C mixture.

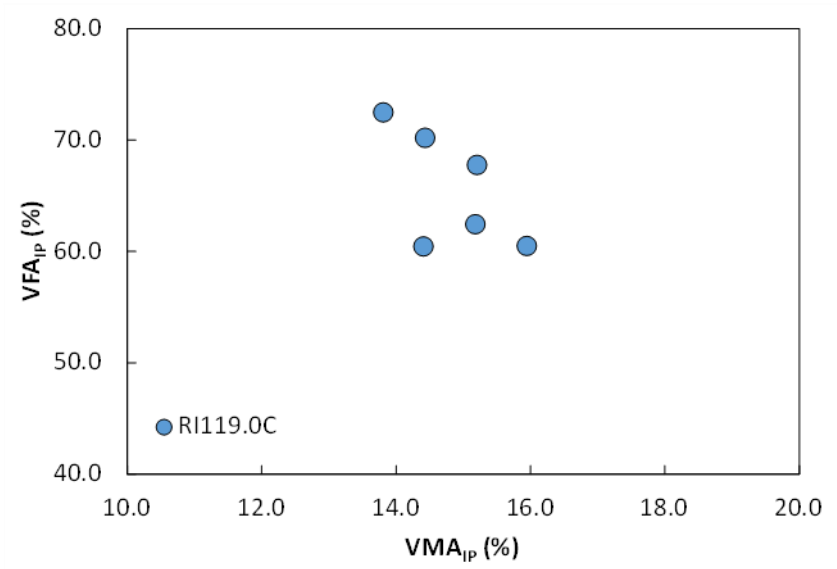

B. RI19.0C mixture.

Figure 11. Graphs. Calculated VMA_{IP} and VMA_{IP}.[31]

Mixture Sample Selection for Four Corners

For the next step, the research team selected the mixture samples that would make four corners based on the locations of the data points in the volumetric domain. To create a reasonable IVR or, in other words, to make a large area that can be covered by the four corners, the mixture

samples that are located far away from each other in terms of both VMA_{IP} and VFA_{IP} should be selected. Because PMLC mixtures were used in this study, the only way to make the four corners was to extend the current locations of the selected samples by changing the air void contents of the test specimens, as the binder content and aggregate gradation are unchangeable variables. Based on these factors, figure 12 shows the mixture samples the team selected for the four corners.

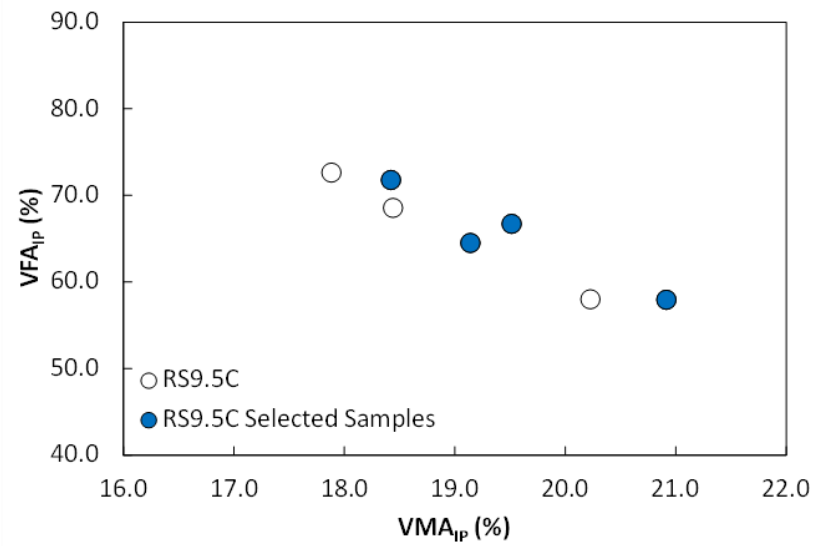

A. RS9.5C mixture.

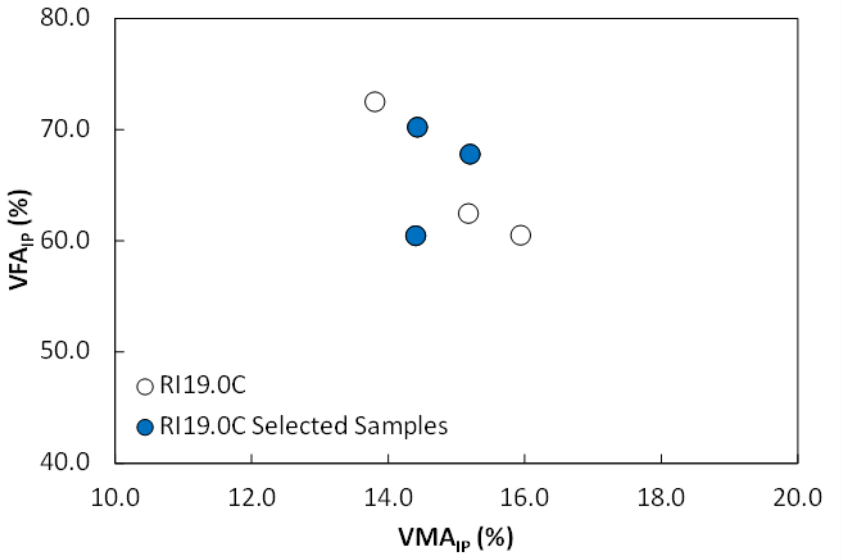

B. RI19.0C mixture.

Figure 12. Graphs. Mixture samples selected for the four corners.[31]

Index-Volumetrics Relationship Calibration and Verification Design

Once the mixture samples had been selected for four corners, the research team devised a test plan to develop the IVRs by targeting two low and two high target test specimen air void contents using the selected mixture samples to make a quadrangular shape in the volumetric domain. First, the team determined the target test specimen air void contents. Figure 13 shows the final positions for the four corners conditions and verification conditions in the volumetric space. The mixture samples that were not used for the IVR calibration, the verification samples, were later used to verify how well the IVR could predict the index values. These verification samples were fabricated at the same in-place air void contents shown in table 7. A verification sample was located outside the four corners range and thus was used to determine the extrapolation ability of the IVR. Table 8 provides a summary of the target test specimen air void contents that were used to calibrate and verify the IVRs.

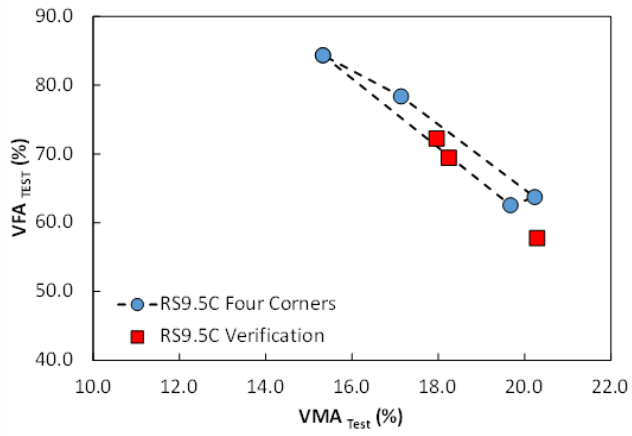

A. RS9.5C mixture.

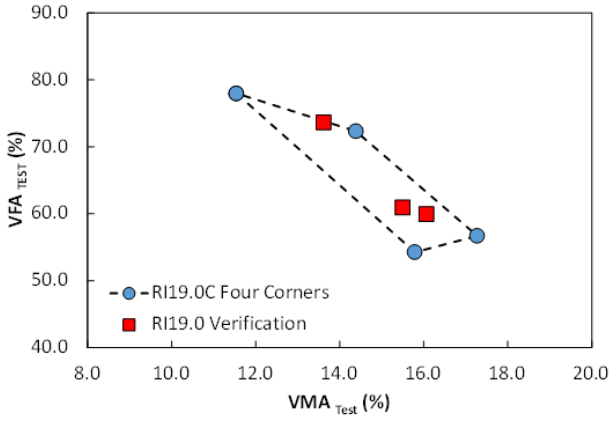

B. RI19.0C mixture.

Figure 13. Graphs. IVR calibration plan.[31]

Table 8. Test specimen target air void contents used to calibrate and verify the IVR.

Mix	Sample ID	Purpose	Test Specimen Target Air Voids (Percent)
RS9.5C	1	Four corners	2.5
RS9.5C	3	Four corners	7.5
RS9.5C	5	Four corners	7.5
RS9.5C	7	Four corners	4.0
RS9.5C	2	Verification	8.5
RS9.5C	4	Verification	5.8
RS9.5C	6	Verification	4.9
RI19.0C	2	Four corners	4.0
RI19.0C	3	Four corners	7.5
RI19.0C	6-1	Four corners	2.5
RI19.0C	6-2	Four corners	7.5
RI19.0C	1	Verification	3.8
RI19.0C	4	Verification	6.3
RI19.0C	5	Verification	5.7

Fatigue Test Results

Table 9 presents a summary of the test results based on the experimental plan. Figure 14 shows that the S_{app} index exhibits a reasonable trend in terms of the test specimen air void content because the higher air void in the asphalt mixture has more room to become fatigue distressed. Based on the results, the S_{app} index seems to be suitable for general QA processes that employ in-place density. Again, this study did not consider the binder effect because the binder content range is too narrow for the PMLC study mixtures.

Table 9. Fatigue test results.

Mix	Sample ID	Purpose	VMA_{IP} (Percent)	VFA_{IP} (Percent)	S_{app}
RS9.5C	1	Four corners	15.3	84.3	26.6
RS9.5C	3	Four corners	20.2	63.7	24.8
RS9.5C	5	Four corners	19.7	62.5	21.4
RS9.5C	7	Four corners	17.1	78.4	28.4
RS9.5C	2	Verification	20.3	57.8	20.6
RS9.5C	4	Verification	18.2	69.5	27.9
RS9.5C	6	Verification	18.0	72.2	25.9
RI19.0C	2	Four corners	14.4	72.3	10.0
RI19.0C	3	Four corners	17.3	56.7	6.2
RI19.0C	6-1	Four corners	11.5	78.0	13.6

Mix	Sample ID	Purpose	VMA_{IP} (Percent)	VFA_{IP} (Percent)	S_{app}
RI19.0C	6-2	Four corners	15.8	54.3	9.9
RI19.0C	1	Verification	13.6	73.6	9.3
RI19.0C	4	Verification	16.1	59.9	7.1
RI19.0C	5	Verification	15.5	60.9	10.0

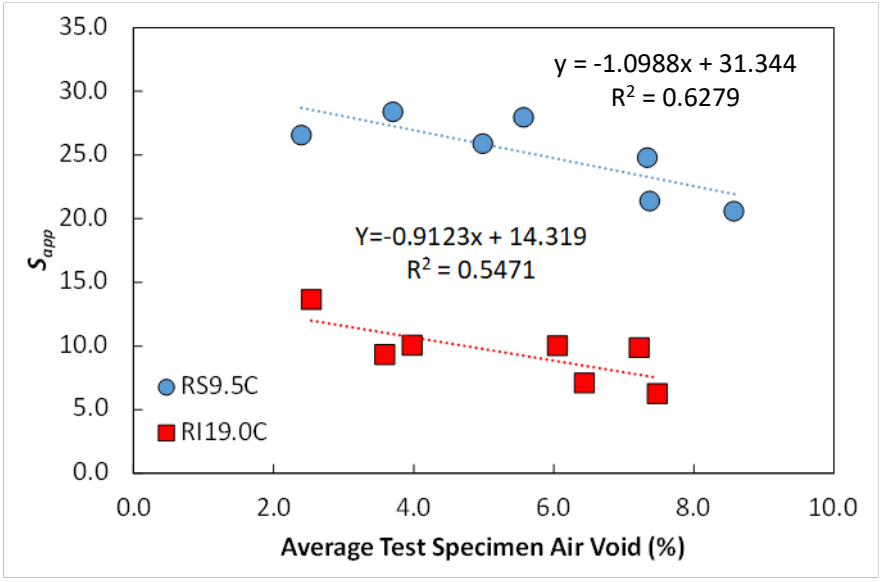

Figure 14. Graph. Fatigue index results as a function of average test specimen air void content.[31]

Index-Volumetrics Relationship Development and Verification

The research team developed IVRs using the S_{app} index values and the volumetric conditions of the four corners, as presented in table 9 and equation 21. Table 10 provides a summary of the coefficients of the developed IVRs for the individual mixtures. The signs for coefficients a_f, b_f, and d_f are not constant for both mixtures. The meaning of the signs for the IVR coefficients is not easy to decipher because the VMA_{IP} and VFA_{IP} are functions of several factors, as can be seen in equations 5 and 7. This discrepancy does not mean, however, that the S_{app} values predicted from IVRs show different trends for both mixtures with the change in air void content. Table 11 shows the changes in the VMA_{IP} and VFA_{IP} when the test specimens' air void contents are changed from 4 to 7 percent and shows the resultant predicted S_{app} index values when using sample 1 of each of the RS9.5C and RI19.0C mixtures as an example. The predicted S_{app} value decreased as the air void content was increased. This trend is the same as the actual test results in terms of the air void contents presented in figure 14. This outcome indicates that, in general, the developed IVRs can predict the cracking index trends as a function of air void content, similar to those trends observed from the actual tests. Specifically, the IVR is useful for predicting the effects of construction variability, such as in-place density, on pavement performance.

Table 10. Coefficients for fatigue index-volumetric relationship for two mixtures.

Mixture	a_f	b_f	d_f	R^2
RS9.5C	4.428	1.140	−137.189	0.99
RI19.0C	−1.780	−0.137	45.148	0.98

Table 11. Air void content sensitivity of index-volumetric relationship for two mixtures.

Mix	Sample ID	Test Specimen Air Voids (Percent)	VMA_{IP}	VFA_{IP}	Predicted S_{app} from IVR
RS9.5C	Sample 1	4	16.7	76.1	23.5
RS9.5C	Sample 1	5	17.6	71.6	22.2
RS9.5C	Sample 1	6	18.4	67.5	21.4
RS9.5C	Sample 1	7	19.3	63.8	21.0
RI19.0C	Sample 1	4	14.0	71.4	10.5
RI19.0C	Sample 1	5	14.9	66.4	9.6
RI19.0C	Sample 1	6	15.8	62.0	8.6
RI19.0C	Sample 1	7	16.7	58.0	7.5

Next, the research team verified the developed IVRs by comparing the measured index values to the index values predicted from the IVRs. The predicted index values are calculated by inputting the volumetric conditions of the tested mixture samples into the developed IVRs. Table 12 presents summary comparisons and the %Error between the measurements and the predictions of the S_{app} index, respectively, for both mixtures, and figure 15 presents these results schematically. Figure 15 shows that the verification data points are close to the line of equality (LOE), which indicates that the IVRs were able to predict the cracking index values reasonably well using the volumetric conditions. Numerically, the average %Error for the verification samples of the two mixtures do not exceed 15 percent. For the RS9.5C mixture, the %Error of the sample that is located outside the four corners is 10.1 percent, which indicates that the IVR could predict the data well by extrapolation.

Table 12. Summary of S_{app} index values obtained from tests and IVRs.

Mix	Sample ID	Purpose	Measured S_{app}	Predicted S_{app}	%Error
RS9.5C	1	Four corners	26.6	26.8	0.9
RS9.5C	3	Four corners	24.8	25.1	1.1
RS9.5C	5	Four corners	21.4	21.2	0.8
RS9.5C	7	Four corners	28.4	28.0	1.3
RS9.5C	2[a]	Verification	20.6	18.5	10.1
RS9.5C	4	Verification	27.9	22.8	18.5
RS9.5C	6	Verification	25.9	24.7	4.7
RS9.5C	Average	—	—	—	5.4
RS9.5C	%Error for verification samples	—	—	—	11.1

Mix	Sample ID	Purpose	Measured S_{app}	Predicted S_{app}	%Error
RS9.5C	%Error for verification samples within four corners	—	—	—	11.6
RI19.0C	2	Four corners	10.0	9.6	4.1
RI19.0C	3	Four corners	6.2	6.6	6.3
RI19.0C	6-1	Four corners	13.6	13.9	2.0
RI19.0C	6-2	Four corners	9.9	9.6	2.6
RI19.0C	1	Verification	9.3	10.8	16.0
RI19.0C	4	Verification	7.1	8.3	17.7
RI19.0C	5	Verification	10.0	9.2	8.0
RI19.0C	Average	—	—	—	3.7
RI19.0C	%Error for verification samples within four corners	—	—	—	13.9

—No data.

[a] Volumetric properties are not within the four corners range.

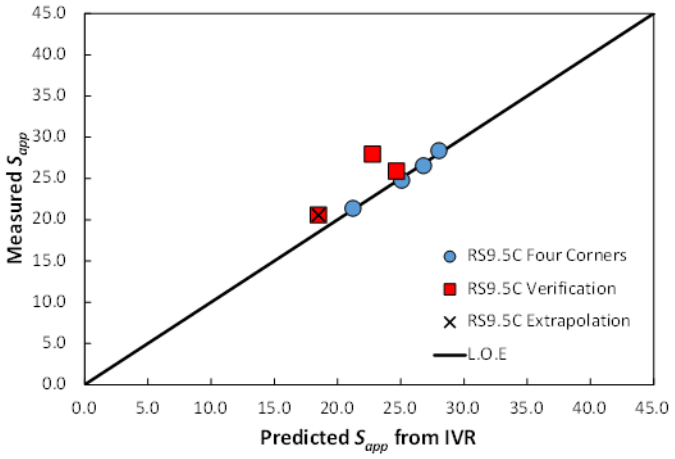

A. RS9.5C mixture.

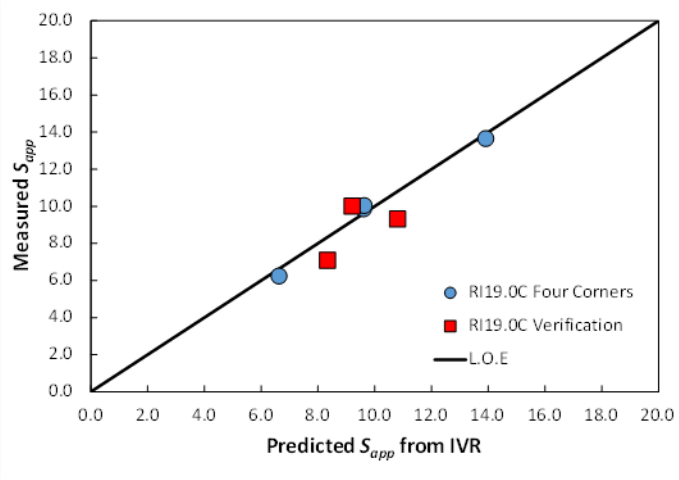

B. RI19.0C mixture.

Figure 15. Graphs. Comparison of measured and predicted S_{app} values obtained from IVRs.[31]

Effects of In-Place Density Variations on Index Value

The research team used the verified IVRs to predict the fatigue performance of the PMLC samples with varying in-place air void contents. The VMA_{IP} and VFA_{IP} values presented in Table 7 for different samples were input to the developed IVRs. Table 13 provides a summary of the predicted index values. The maximum differences between the maximum and minimum predicted pavement performance are 34.6 and 27.8 percent for the RS9.5C mixture and the RI19.0C mixture, respectively. These results indicate the impact of construction variability on pavement performance.

Table 13. Predicted index values for PMLC samples of two mixtures.

Mix	Sample ID	In-Place Air Void Content (Percent)	Predicted S_{app}
RS9.5C	1	6.8	21.1
RS9.5C	2	8.5	18.5
RS9.5C	3	6.5	25.2
RS9.5C	4	5.8	22.6
RS9.5C	5	8.8	21.4
RS9.5C	6	4.9	24.8
RS9.5C	7	5.2	26.2
RS9.5C	Average	6.6	22.8
RS9.5C	Maximum difference (percent)	—	34.6
RI19.0C	1	3.8	10.6
RI19.0C	2	4.9	8.8
RI19.0C	3	4.3	9.8

Mix	Sample ID	In-Place Air Void Content (Percent)	Predicted S_{app}
RI19.0C	4	6.3	8.5
RI19.0C	5	5.7	9.6
RI19.0C	6	5.7	11.2
RI19.0C	Average	5.1	9.8
RI19.0C	Maximum difference (percent)	—	27.8

—No data.

Figure 16 presents a plot of the changes in in-place air void content and index values as a function of sampling sequence. This figure could be used by QA engineers to monitor changes in material and construction quality as a paving project continues. In figure 16, the filled markers represent the in-place air void contents and the empty markers show the predicted S_{app} values. A reliable fatigue index should show the opposite slope to the slope of the in-place air void content from one sample to next. The correct trend can be observed for four of the six slopes of the RS9.5C samples and four of the five slopes of the RI19.0C samples. Based on these observations, the S_{app} index is shown to represent the mixture and construction performance.

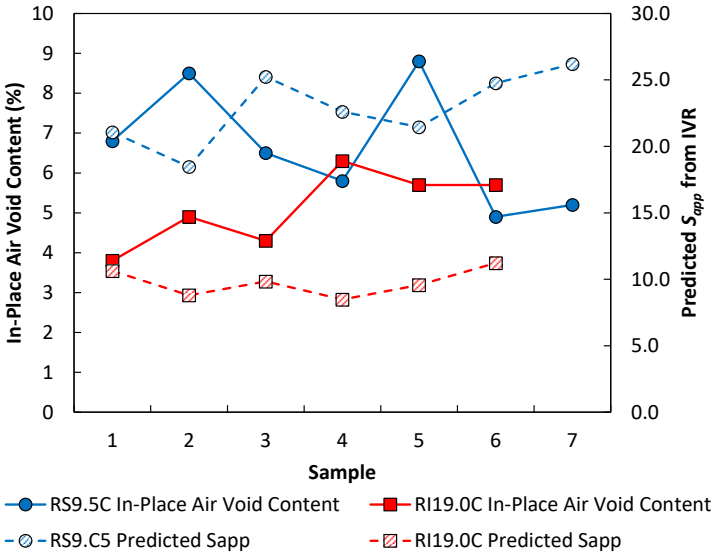

Figure 16. Graph. Predicted cracking performance of two field projects as a function of in-place air void content.[31]

Rutting IVR

This study's primary goal is to compare the results from SSR tests of plant-produced mixture samples obtained from two field projects and develop individual IVRs based on the SSR test results. This study's secondary goal is to use the developed IVRs to predict the effects of air void content and binder content on the rutting performance of the plant-produced mixture samples that have a range of AQCs.

The IVR is developed using linear regression based on the relationships between the four corners' volumetric properties and the index values. Equation 22 presents the IVR function for rutting performance. *Rutting Index* in equation 22 represents the RSI (percent) value for the SSR test.

Materials and Test

Two surface layer asphalt mixtures, stone matrix asphalt (SMA)12.5 from Ontario, Canada and RS9.5C from North Carolina, USA, were obtained from field projects for this rutting study. The SMA12.5 mixture is a 12.5-mm NMAS mixture that contains 5.7 percent PG 70-28 binder and no RAP. The RS9.5C mixture is a 9.5-mm NMAS mixture that contains 5.8 percent PG 64-22 binder and 40 percent RAP. During the field project construction, six SMA12.5 and seven RS9.5C mixture samples were acquired from different truck loads. The mixture samples of the SMA12.5 asphalt mixture are designated as 5-1, 5-2, 5-6, 5-7, 5-8, and 5-10 and the mixture samples of the RS9.5C asphalt mixture are designated as 1, 2, 3, 4, 7, 9, and 10. The relevant State highway agency provided the mixture information and measured sample variability in volumetrics using the agency's own method.

The SSR test was conducted on the two mixtures according to AASHTO TP 134.[(16)] The RSI values were calculated from the SSR test data by FlexMAT Rutting analysis tool. Figure 17 presents comparisons of the RSI values of the two mixtures used in this study to the asphalt concrete rut depths (mm) simulated by FlexPAVE under the environmental conditions for each field project. Figure 17 also shows that the RSI values obtained from the SSR tests and the asphalt concrete rut depths simulated by FlexPAVE have a strong linear relationship. Good correlations between the FlexPAVE simulations and field performance and the strong relationship between the FlexPAVE simulations and the RSI values together indicate the strength of the RSI as a rutting index parameter.

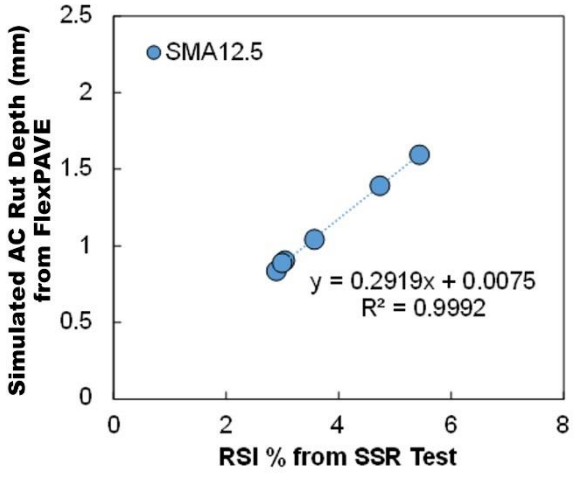

1 mm = 0.04 inches.

A. SMA12.5.

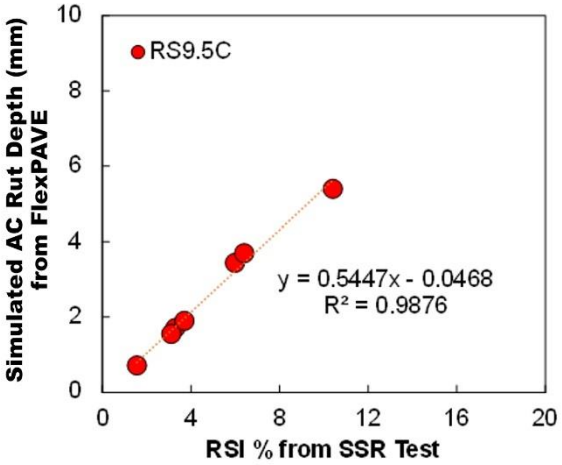

1 mm = 0.04 inches.

B. RS9.5C.

Figure 17. Graphs. Comparison of RSI values obtained from SSR test and asphalt concrete rut depths simulated by FlexPAVE.[29]

Rutting IVR Development

The volumetric tests of the obtained mixture samples were conducted by the relevant State highway agency using the relevant agency's own method to determine the AQCs, i.e., binder content, VMA, air void content at N_{des}, and in-place density. Because the AQCs show the sample-to-sample variability that occurs naturally during construction, the AQCs are key factors for determining the four corners to develop a mixture's IVR. Table 14 presents summaries of the measured AQCs of the SMA12.5 and RS9.5C mixture samples and the calculated volumetric conditions (VMA_{IP} and VFA_{IP}) obtained from equation 5 and equation 7. The variability of the AQCs is expressed by the COVs, which indicate that the variability of the air void content at N_{des} and the in-place air void content is significantly greater than the variability of the other factors.

Table 14. Measured AQC.

Mix	Sample ID	Binder Content (Percent)	VMA (Percent)	V_a (N_{des})	In-Place Air Void (Percent)	VMA_{IP} (Percent)	VFA_{IP} (Percent)
SMA12.5	5-1	5.9	16.2	1.6	3.9	18.1	78.5
SMA12.5	5-2	5.9	16.4	1.9	4.0	18.2	78.1
SMA12.5	5-6	5.8	16.2	1.5	4.7	18.9	75.2
SMA12.5	5-7	5.7	16.5	2.2	4.3	18.3	76.5
SMA12.5	5-8	5.8	17.2	2.9	4.3	18.4	76.6
SMA12.5	5-10	5.7	16.4	2.3	5.1	18.8	72.9
SMA12.5	COV (percent)	1.7	2.3	25.0	10.3	1.8	2.7
RS9.5C	1	5.8	15.5	2.6	6.8	19.2	64.5

Mix	Sample ID	Binder Content (Percent)	VMA (Percent)	V_a (N_{des})	In-Place Air Void (Percent)	VMA_{IP} (Percent)	VFA_{IP} (Percent)
RS9.5C	2	5.6	14.3	1.7	8.5	20.2	58.0
RS9.5C	3	6.1	15.9	2.3	6.5	19.5	66.7
RS9.5C	4	5.9	15.5	2.4	5.8	18.5	68.6
RS9.5C	7	5.8	15.8	2.9	8.8	20.9	58.0
RS9.5C	9	6.0	15.9	2.6	4.9	17.9	72.7
RS9.5C	10	6.1	16.1	2.5	5.2	18.4	71.7
RS9.5C	COV (percent)	3.1	3.9	15.4	23.0	5.6	9.1

Determination of Four Corners

Figure 18 presents plots of the in-place conditions of both sets of mixture samples in the volumetric domain. Because the variability of the in-place air voids is greater than that of the binder content for the plant-produced mixtures, the mixture samples in the volumetric domain show a relatively smaller range in the direction from the bottom-left corner to the top-right corner of the VMA_{IP}–VFA_{IP} space (represented by the binder content change) compared to the range in the direction from the top-left corner to the bottom-right corner of the volumetric space (represented by the change in the in-place air voids).

As discussed, samples for the four corners should be selected from the samples that are furthest apart in the VMA_{IP} - VFA_{IP} volumetric space. The gradations and binder contents for the plant-produced samples are fixed and therefore unchangeable. One way to change the VMA_{IP} and VFA_{IP} is to change the target air void contents of the test specimens. In this way, the samples for the four corners can be selected from the samples that are located furthest apart in the direction of the bottom-left corner to the top-right corner of the VMA_{IP} - VFA_{IP} space, which yields the largest range of binder content. Then, those samples are compacted at the lowest and highest air void contents within the acceptance limits to create the largest VMA_{IP} - VFA_{IP} space that can be generated using the plant-produced mixture samples. Based on this concept, figure 18 shows the four corners samples that were selected for each mixture and the movement of these samples when the target air void content is changed from 2.0 to 8.0 percent. Sample 5-1 of the SMA12.5 mixture and sample 2 of the RS9.5C mixture were not selected for the four corners even though they have the highest and lowest binder contents in each mixture, respectively, because their V_a at N_{des} is lower than the minimum V_a at N_{des} (2.0 percent) that is specified in the mixture specifications. Therefore, these samples were used instead to check the IVR's ability to predict the performance outside the calibration range.

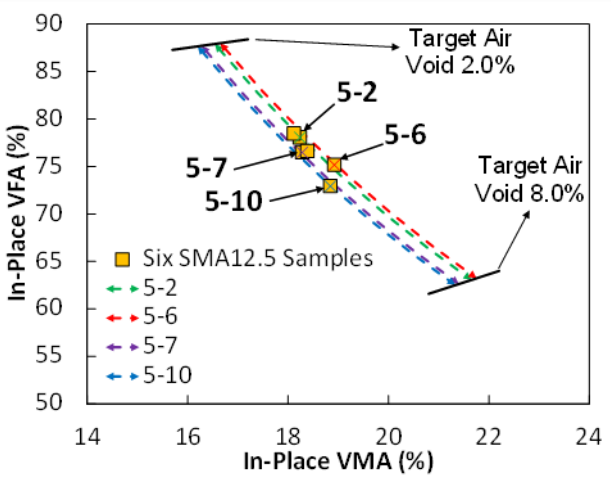

A. SMA12.5.

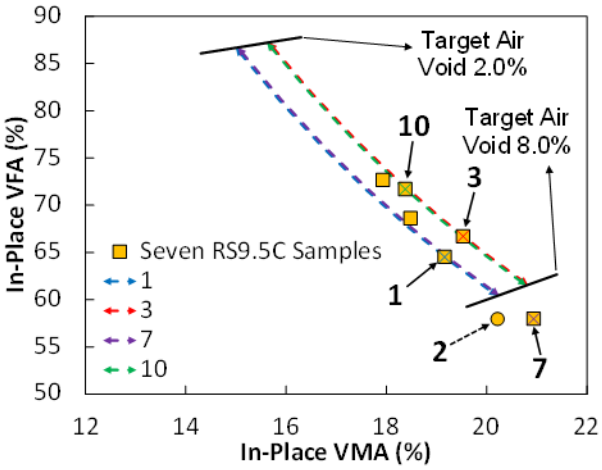

B. RS9.5C.

Figure 18. Graphs. Four corners samples selected for volumetric conditions of mixture samples.[29]

Performance Test Plans for Rutting Index-Volumetrics Relationship Development

Based on the selected four corners samples, table 15 presents a summary of the rutting performance testing plan to develop the IVRs. To determine the quadrangular range, the research team fabricated four corners samples at two low and two high air void contents that could be achieved using a gyratory compactor. The low and high air void contents should be determined based on the acceptance limits for the in-place air void contents that are recommended in each mixture's specifications, which normally range from 2 to 8 percent. The other samples that were not used for the four corners were fabricated at the same in-place air void contents to verify the

developed IVR. The tolerance for the air void measurements was set as ±0.5 percent. The tests were conducted at 22 ℃ and 42 ℃ for the SMA12.5 mixture and at 29 ℃ and 50 ℃ for the RS9.5C mixture based on AASHTO TP 134.[16]

Table 15. Target air void contents for IVR development.

Purpose	Sample ID (SMA12.5)	Target Air Void (Percent)	Sample ID (RS9.5C)	Target Air Void (Percent)
Four corners	5-2	6.5	1	2.5
Four corners	5-6	2.5	3	7.5
Four corners	5-7	2.5	7	7.5
Four corners	5-10-a	7.5	10	3.0
Verification	5-1	3.9	2	8.8
Verification	5-8	4.3	4	5.8
Verification	N/A	N/A	9	4.9

Selection of Four Corners and Rutting Performance Test Results

The research team conducted SSR tests according to the testing plan. Figure 19 presents the volumetric conditions of the tested specimens for SMA12.5 and RS9.5C, respectively, including four corners. The quadrangles defined by the selected four corners are narrow due to the wide range of air void content and narrow range of binder content in the plant-produced mixture samples. Also, the shapes of the area defined by the four corners are not quite ideal because fabricating the test specimens at exactly the same air void content as the target air void content was difficult (air void tolerance of ±0.5 percent was used in this study). Also, the narrow range of binder content in the plant-produced mixture samples made it difficult to fabricate the test specimens at the four corners that form the ideal quadrangle, similar to the one shown in figure 9. IVRs developed for BMD and PRS use asphalt mixtures that are fabricated using component materials. Therefore, the four corners volumetric conditions for those IVRs can cover a wider range of aggregate gradation, binder content, and air void content than the IVRs presented in this study, which were developed from plant-produced materials. Some verification mixture samples are slightly outside of the four corners range. Sample 2 of the RS9.5C mixture is significantly outside the range, which is intentional to determine whether the IVR could predict the sample's performance outside of the calibration range.

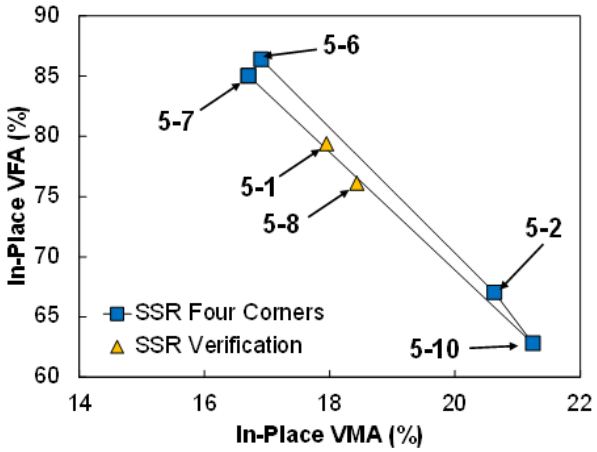

A. SMA12.5.

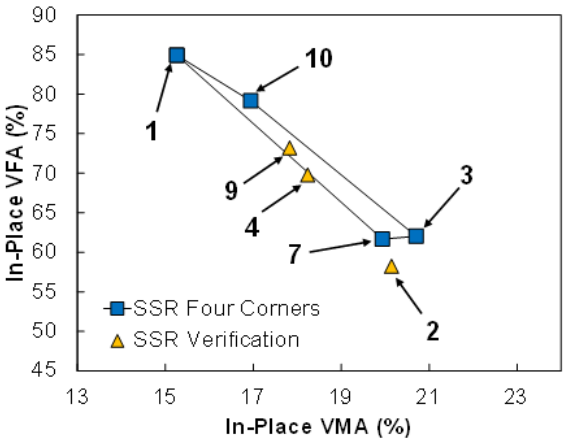

B. RS9.5C.

Figure 19. Graphs. Volumetric conditions of tested mixture samples.[29]

Table 16 presents the rutting test results for SMA12.5 and RS9.5C along with the volumetric conditions based on the measured test specimens' air void contents. The RSI values were determined from the SSR tests using FlexMAT version 2.0-ALPHA.

Table 16. Rutting performance test results.

Mix	Sample ID (SMA12.5)	Binder Content (Percent)	Specimen Air Void (Percent)	VMA_{IP}	VFA_{IP}	RSI (Percent)
SMA12.5	5-2[a]	5.9	6.8	20.6	67.0	4.73
SMA12.5	5-6[a]	5.8	2.3	16.9	86.4	3.04
SMA12.5	5-7[a]	5.7	2.5	16.7	85.0	2.89
SMA12.5	5-10-a[a]	5.7	7.9	21.2	62.8	5.44
SMA12.5	5-1[b]	5.9	3.7	17.9	79.4	3.57
SMA12.5	5-8[b]	5.8	4.4	18.4	76.1	3.00
RS9.5C	1[a]	5.8	2.3	15.3	84.9	1.56
RS9.5C	3[a]	6.1	7.9	20.7	62.0	5.99
RS9.5C	7[a]	5.8	7.6	19.9	61.7	6.40
RS9.5C	10[a]	6.1	3.5	16.9	79.1	3.29
RS9.5C	2[b]	5.6	8.4	20.1	58.2	10.4
RS9.5C	4[b]	5.9	5.5	18.2	69.8	3.7
RS9.5C	9[b]	6.0	4.8	17.8	73.2	3.11

[a] Samples at four corners tested for IVR development.
[b] Samples tested for IVR verification.

Figure 20 presents comparisons of both sets of test results plotted together in the volumetric domain in terms of VMA_{IP} and VFA_{IP}, respectively. The test results indicate that the rutting test results are strongly related to the volumetric conditions. The results show that the permanent deformation increases when the VMA_{IP} increases and decreases when the VFA_{IP} increases. The greater rut depths that are due to the increase in the VMA_{IP} make sense, whereas the lower rut depth values that are due to the increase in the VFA_{IP} do not seem as reasonable. This contradictory trend is due to the significant effect of air void content on the VMA_{IP} and VFA_{IP}, as shown in figure 21. Although the effect of binder content on the VMA_{IP} and VFA_{IP} is not clear, the effect of air void content on the VMA_{IP} and VFA_{IP} is obvious. As stated previously, the gradations, binder contents, and air void contents at N_{des} for plant-produced mixture samples cannot be changed, but the target air void contents could be changed to accommodate a wide range of air void content to establish the four corners volumetric conditions. The strong dependence of the VMA_{IP} and VFA_{IP} on the air void content suggests that the trends shown in figure 20 are due mostly to the changes in air void content. These observations are important when using the IVRs developed from the performance and volumetric properties of the four corners in this study to predict the rutting performance of the mixture samples. The developed IVRs would be strong functions of air void content but might not properly reflect the effect of binder content because of the narrow range of the binder content within the plant-produced mixture samples. This observation demonstrates the limitations of developing IVRs using plant-produced mixture samples and emphasizes the importance of using component materials to develop a large volumetric space within the four corners.

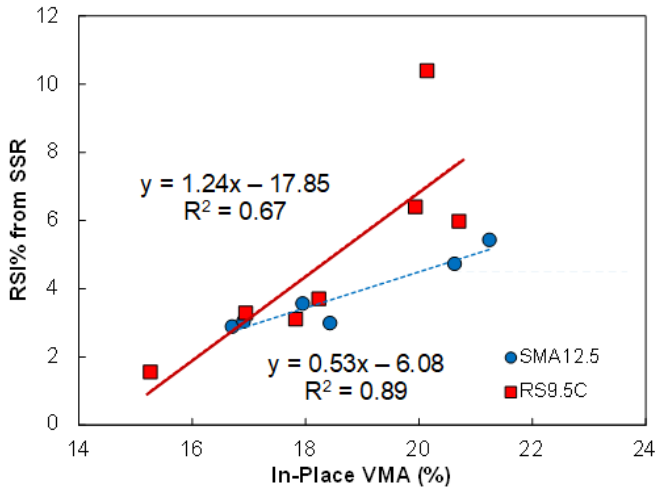

A. VMA_{IP}.

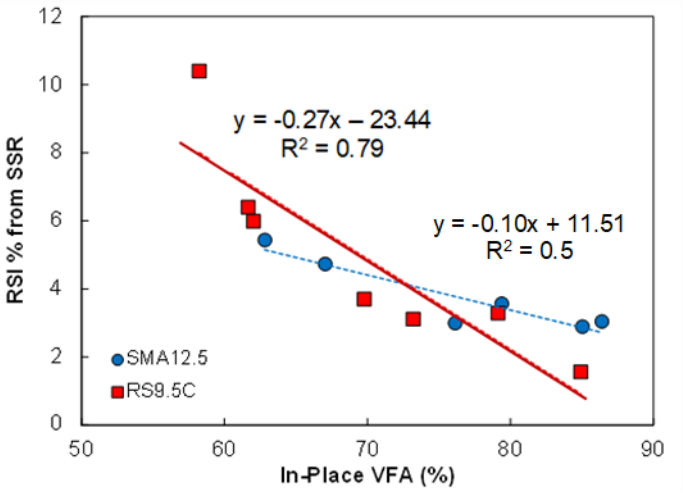

B. VFA_{IP}.

Figure 20. Graphs. Comparison of SSR test results in terms of volumetric parameter.[29]

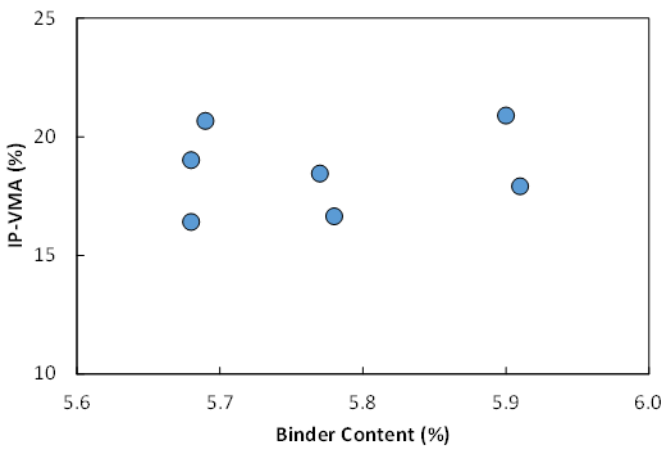

A. VMA_{IP} versus binder content.

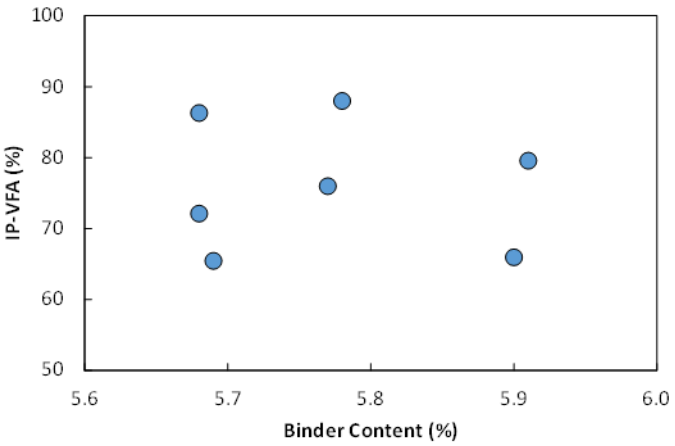

B. VFA_{IP} versus binder content.

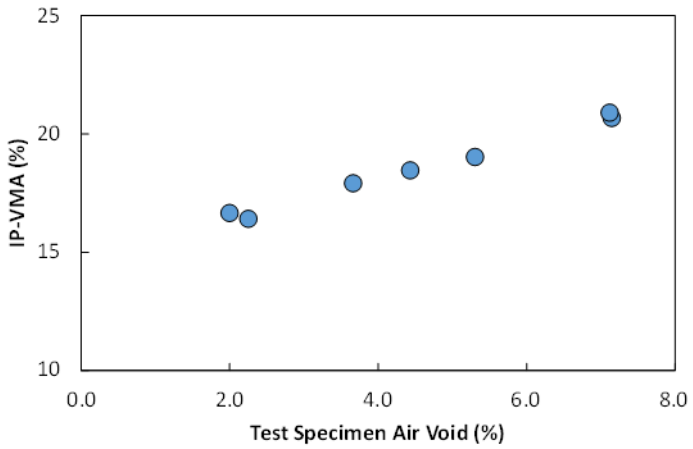

C. VMA_{IP} versus test specimen air void content.

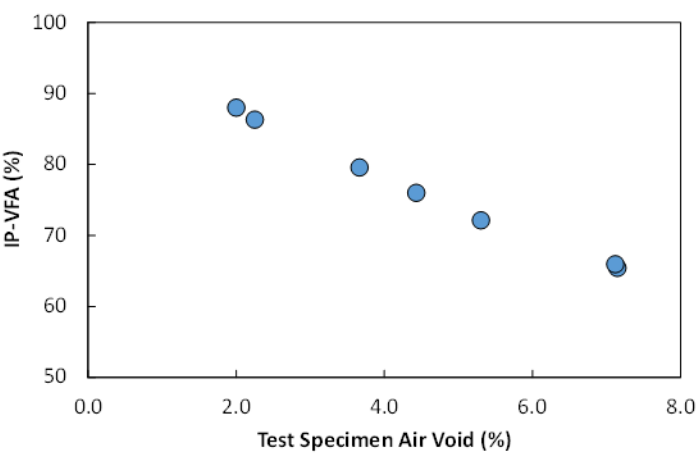

D. VFA_{IP} versus test specimen air void content.

Figure 21. Graphs. VFA_{IP} and VMA_{IP} as a function of binder content and test specimen air void content: SMA12.5 mixture.[29]

Verification of Rutting Index-Volumetrics Relationships

Based on the volumetric conditions and rutting performance test results, the IVRs were developed using Microsoft® Excel® and the Excel Data Analysis ToolPak add-in.[32] Table 17 presents the coefficients and intercepts needed for equation 22, which is the IVR equation for rutting performance. The two coefficients of the developed IVRs have different signs. The expected sign for VMA_{IP} is positive because the higher binder content (which will result in higher VMA_{IP}) and higher air void content (which will result in higher VMA_{IP}) will increase the RSI value. However, the sign for VFA_{IP} can be both positive and negative. The VFA_{IP} increases when the binder content increases, but VFA_{IP} decreases when the air void content increases.

Therefore, the sign of VFA_{IP} is determined by the more significant factor between binder content and the air void content. As previously discussed in the Selection of Four Corners and Rutting Performance Test Results section, the binder content shows less impact than the air void content due to its narrow range. Therefore, the VFA_{IP} coefficients for both mixtures show a negative sign.

Table 17. Coefficients for IVR for two mixtures.

Mixture	a_r	b_r	d_r	R^2
SMA12.5	0.285	−0.047	2.154	0.98
RS9.5C	0.002	−0.191	17.997	0.98

The research team verified the developed IVRs by comparing the RSI values determined from the SSR test to those predicted from the IVRs. The predicted values were calculated by inputting the volumetric conditions of the mixture samples (specified in table 16) to the developed IVRs. Table 18 presents summary comparisons of the measured and predicted rutting performance of the two mixtures. These comparisons also are shown schematically in figure 22 and show that the verification samples are located close to the LOE. The numerical results indicate that the averages of the %Difference between the measured and predicted index values for the SMA12.5 samples that fall within the four corners are 2.4 and 19.0 percent for the RS9.5C samples. These results show that the IVRs can reasonably capture the rutting performance of the verification samples when the samples are within or close to a reasonable IVR quadrangular range, but the IVR generated relatively greater differences for the samples that were located significantly outside the IVR quadrangular range, i.e., RS9.5C sample 2, and slightly outside the IVR quadrangular range, i.e., SMA12.5 sample 5–8 and RS9.5C sample 4 for the SSR test.

Table 18. Summary of rutting performance results obtained from tests and IVR.

Mix	Purpose	Sample ID (SMA12.5)	Measured RSI (Percent)	Predicted RSI (Percent) from IVR	%Difference
SMA12.5	Four corners	5-2	4.73	4.91	3.7
SMA12.5	Four corners	5-6	3.04	2.95	3.1
SMA12.5	Four corners	5-7	2.89	2.95	2.2
SMA12.5	Four corners	5-10-a	5.44	5.29	2.8
SMA12.5	Verification	5-1	3.57	3.57	0.1
SMA12.5	Verification	5-8[a]	3.00	3.86	25.3
SMA12.5	Average	—	—	—	2.4[b]
RS9.5C	Four corners	1	1.56	1.82	15.7
RS9.5C	Four corners	3	5.99	6.21	3.6
RS9.5C	Four corners	7	6.40	6.27	2.0
RS9.5C	Four corners	10	3.29	2.93	11.5
RS9.5C	Verification	2[a]	10.40	6.93	40.1
RS9.5C	Verification	4[a]	3.70	4.72	24.2

Mix	Purpose	Sample ID (SMA12.5)	Measured RSI (Percent)	Predicted RSI (Percent) from IVR	%Difference
RS9.5C	Verification	9	3.11	4.07	26.6
RS9.5C	Average	—	—	—	11.9[b]

—No data.
[a] Samples outside the quadrangle defined by the four corners.
[b] Average percentage difference for the samples within the quadrangle.

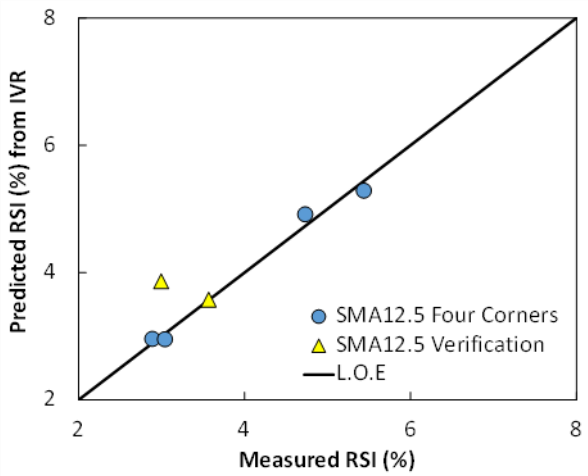

A. SMA12.5.

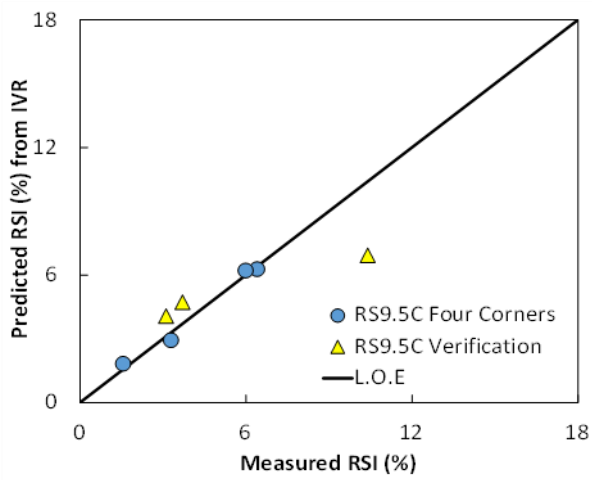

B. RS9.5C.

Figure 22. Graphs. Comparison of rutting performance obtained from test measurements and IVR.[(29)]

Prediction of Construction Variability Using the Developed Index-Volumetrics Relationships

The research team used the verified IVRs to predict the rutting performance of the field projects. The volumetric conditions of the field projects presented in table 14 were applied to the developed IVRs. Figure 23 presents the predicted rutting performance of the two field projects in terms of the two mixtures, respectively, and table 19 shows the numerical prediction results. The average RSI values for the two field projects were predicted to be 3.9 percent for the SMA12.5 mixture and 5.5 percent for the RS9.5C mixture. For the RS9.5C mixture, the maximum differences of the predicted RSI values and rut depths are 0.4 and 2.8 percent, respectively.

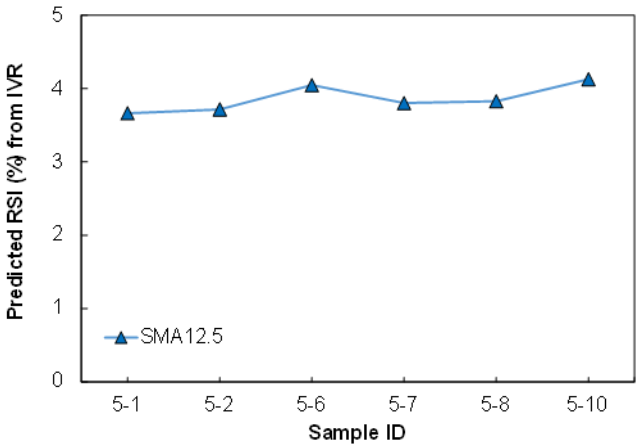

A. SMA12.5.

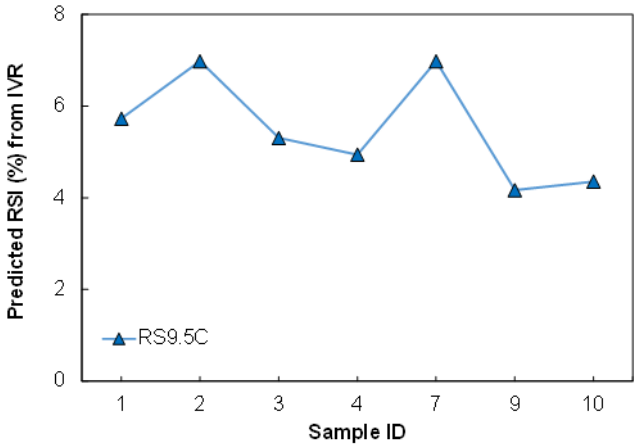

B. RS9.5C.

Figure 23. Graphs. Predicted rutting performance of field samples.[29]

Table 19. Predicted rutting performance of two field project mixtures.

Sample ID (SMA12.5)	Predicted RSI (Percent) from IVR	Sample ID (RS9.5C)	Predicted RSI (Percent) from IVR
5-1	3.7	1	5.7
5-2	3.7	2	7.0
5-6	4.0	3	5.3
5-7	3.8	4	4.9
5-8	3.8	7	7.0
5-10	4.1	9	4.2
—	—	10	4.4
Average	3.9	Average	5.5

—No data.

To understand the developed IVRs better, the predicted rutting index parameters of the field projects were plotted in terms of in-place air void content and binder content, as shown in figure 24 and figure 25, respectively. The mixtures are shown to become increasingly susceptible to rutting as the in-place air void content increases, which is a reasonable trend because the higher air void content allows more room for rutting by traffic loads. The figures also show that the SMA12.5 mixture has better rutting resistance than the RS9.5C mixture. The predicted rutting performance in terms of the binder content of the SMA12.5 mix does not show an explicit trend because the maximum binder content difference for the SMA12.5 four corners samples was 0.2 percent, which created a range too narrow to be captured adequately by the IVR. Also, the SMA12.5 mixture was designed specifically to be rut-resistant, so the performance test results could not easily capture this small range of the binder content's effect on rutting performance. For the RS9.5C mixture, however, the binder content's effect on rutting performance is clearer than for the SMA12.5 mixture, despite the narrow binder range of 0.5 percent. As was shown in figure 20, the effect of binder content on rutting performance is opposite to the commonly understood trend. Again, this contradictory trend occurs because the air void content has a stronger effect on rutting performance than the binder content because the air void contents in the tested samples have a much wider range compared to the range of the binder content tested in this study.

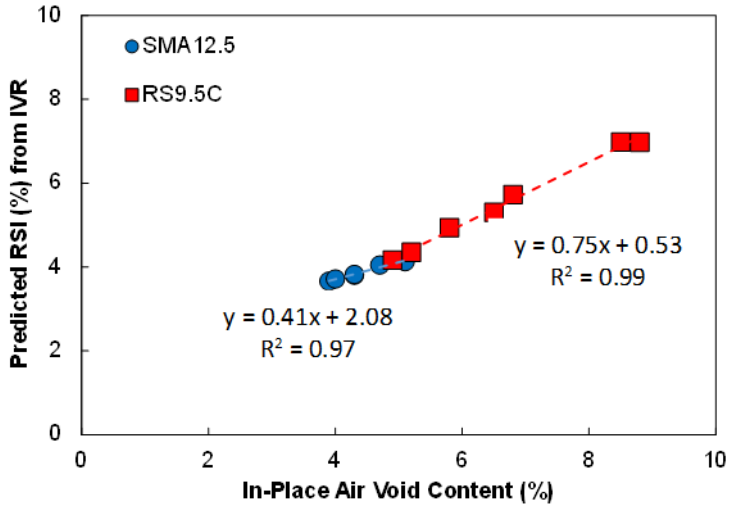

Figure 24. Graph. Comparison of predicted rutting performance versus in-place air void content.[29]

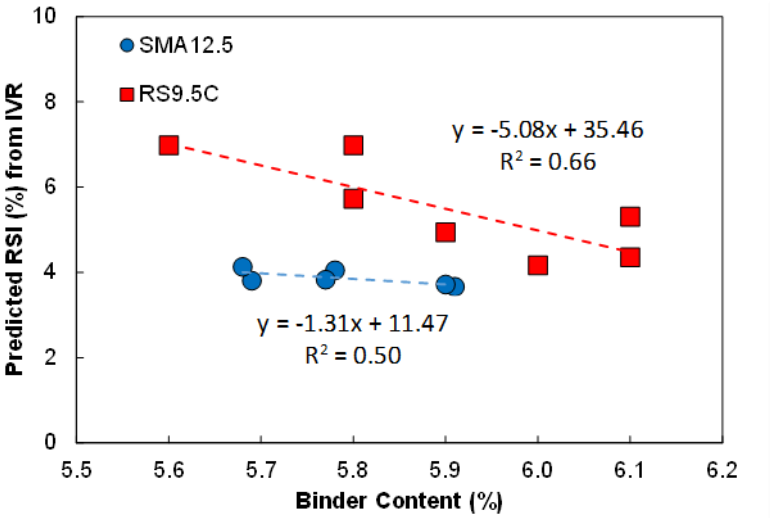

Figure 25. Graph. Comparison of predicted rutting performance versus binder content.[29]

Summary

This study used plant-produced samples from two mixtures (SMA12.5 and RS9.5C) obtained from two different field projects. The research team measured their AQCs and, based on the volumetric conditions calculated from these AQCs, determined the four corners to develop the IVRs for both mixtures. The team fabricated four corners mixture samples at two low and two high air void contents and conducted SSR tests using test specimens fabricated from the mixture samples. The data lead to the following conclusions:

- The SSR test results indicate a correlation in the similar rutting performance trends for both mixtures (SMA12.5 and RS9.5C) in terms of the volumetric conditions.

- The research team used FlexMAT version 2.0-ALPHA to process the SSR test results to determine the RSI values and to generate the input files for FlexPAVE software to simulate pavement rutting performance under field conditions. A strong linear relationship is evident between the RSI values and the rut depths predicted from FlexPAVE.

- The research team successfully developed IVRs for two mixtures using the volumetric conditions and RSI values from the SSR tests of the four corners samples. The developed IVRs were able to predict the respective rutting performance of the verification samples well. However, a more systematic study is needed to evaluate the effects of the volumetric properties at the four corners more thoroughly.

- The prediction accuracy is generally poorer for samples located outside the IVR quadrangular range compared to samples within the IVR quadrangular range.

- The developed IVRs were used to evaluate the two field projects. The average predicted RSI values of the SMA12.5 and RS9.5C mixtures were 3.9 and 5.5 percent, respectively.

- The developed IVRs showed reasonable correlations between the predicted rutting performance and the in-place air void contents. However, the binder content effect was not significant or opposite to the expected trend because the effect of the narrow range of the binder content in the plant-produced mixture samples on the rutting performance was difficult for the IVR to capture. This limitation demonstrates the need to use LMLC mixtures instead of PMLC mixtures to provide a wide volumetric space for IVR development. The SMA12.5 mixture showed less sensitivity to binder content than the RS9.5C mixture.

- The demonstrated prediction accuracy of the IVR will allow highway agencies and contractors to predict the performance of production samples using conventionally measured AQCs if the IVR is developed for the given mixture a priori, and thus will bring PRS one step closer to implementation.

CHAPTER 2. DEVELOPMENT OF ASPHALT MIXTURE PERFORMANCE TESTER BALANCED MIX DESIGN METHOD

Pavement engineers have been seeking improvements for asphalt mixture design since the Strategic Highway Research Program (SHRP) was completed.[33] Most State agencies in the United States still use the SHRP's Superpave volumetric mix design process.[34] According to the original SHRP contract, hierarchical levels of mixture design were initially planned. For example, when the design calls for mixtures to be loaded with more than 1 MESALs, then, in addition to meeting the volumetric criteria, pavement engineers should conduct performance tests and estimate pavement distress data as a function of time during the mixture design process. However, due to the limitations that are inherent in mechanistic models for asphalt mixtures and the test methods used in the 1990s, only volumetric mixture designs were ready for implementation at the end of the SHRP project.[35]

Over the past 25 yr, agencies have continued to seek ways to improve mixture design methods and the performance of asphalt mixtures. Approaches that researchers and practitioners have tried include changing the design criteria, e.g., increasing or decreasing the air void content at N_{des}, increasing the VMA. (See references 36–39.) However, such improved design methods fall within the framework of *empirical* volumetric design, so the performance component of the mixtures is still missing from the design methods. Another aspect for researchers and practitioners to consider is that, over the past two decades, technologies for asphalt mixtures have evolved dramatically. For instance, different binder modifiers are now commonly used to improve the performance of conventional hot-mix asphalt (HMA). Also, the use of recycled products in asphalt concrete has increased significantly. Therefore, providing contractors with more flexibility in mixture design that is based on sound engineering principles would benefit the pavement industry.

As more mechanistic models and practical test methods are being developed to improve mixture design, engineers have started to implement performance-related tests in the mixture design process. The integration of performance-related tests into mixture design is described as BMD. The FHWA Expert Task Group on Asphalt Mixtures and Construction set up a task force for BMD and introduced three BMD approaches to the asphalt paving community.[37] The first two approaches (approach 1 and approach 2) start with volumetric design and use performance-related tests to ensure adequate pavement and mixture performance in terms of resistance to critical distresses, i.e., rutting and fatigue cracking. In these two approaches, iterations may be needed if the trial mixture fails to pass the performance criteria.

Performance-related tests used in BMD typically include a fatigue test and a rutting test. The commonly used fatigue tests include the semi-circular beam test, indirect tension fracture energy test, Texas overlay test, Indirect Tensile Asphalt Cracking Test, and a few others. (See references 40–43.) The commonly used rutting tests are torture tests, such as the Hamburg wheel-tracking (HWT) test and the Asphalt Pavement Analyzer test.[1] BMD's third approach starts directly with performance design. Unfortunately, details about this design approach are lacking.

West et al. introduced a performance space diagram into a BMD framework.[1] The example in figure 26 is the product of cross-plotting fatigue and rutting index parameters. This example uses disc-shaped compact tension (DCT) and HWT tests to evaluate the fatigue and rutting properties of the asphalt mixture, respectively. This diagram is based on DCT fracture energy (the cracking index) and HWT rut depth (the rutting index) and shows that the four different regions are tied to preestablished thresholds. Based on the index parameters, the mixture will fall into one of these four defined regions. A further adjustment is then considered to move the mixture to the zone of interest.[1,44]

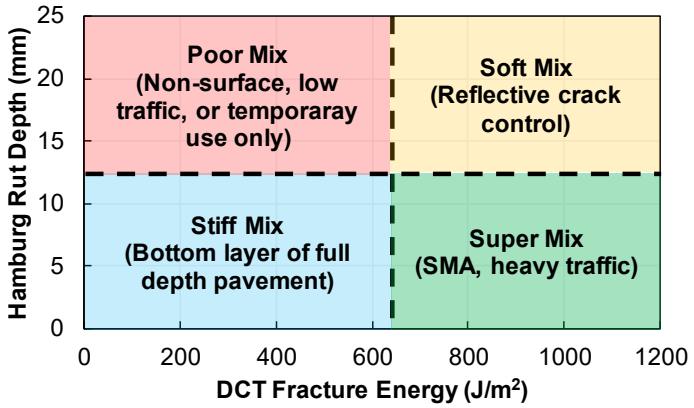

Source: FHWA.
1 mm = 0.04 inches.

Figure 26. Illustration. Example of a performance space diagram.[1]

Several State agencies and institutions have started to develop and implement their own BMD methods following the two main approaches used for BMD.[45,46] However, these design methods have a few inherent drawbacks. First, the performance-related tests are index-based pass or fail tests. These tests typically are performed at a limited number of temperatures (usually only one) and loading conditions and do not represent the material's performance under varying traffic loads and climate conditions. Second, the indexes provide only minimum requirements for mixture performance. Agencies cannot determine the performance deterioration over the service time frame and pavement life from those tests and analyses. Third, using performance criteria along with the existing volumetric requirements essentially applies more constraints on the mixture design process, which limits flexibility for pavement design engineers.

To address these shortcomings, this section presents a framework for newly developed AMPT BMD processes.[1] These approaches use fatigue cracking and rutting PVRs and IVRs to determine the optimal combination of aggregate gradation and asphalt content (AC). In contrast to the design methodology that is employed for other BMDs, the AMPT BMD allows users to predict the performance of all reasonable combinations of a given set of aggregate and binder instead of checking the performance of the candidate mixture that is selected using volumetric criteria.

Three tiers of the BMD method based on the AMPT suite of performance tests have been developed. Tiers 1 and 2 use the AMPT index parameters and in general follow approaches 1 and 2 suggested by West et al., respectively.[1] Tier 3 uses the pavement life

predicted by FlexPAVE. Tier 3 requires the most testing effort, followed by tier 2 and then tier 1. The major advantage of tier 2 compared to tier 3 is that tier 2 does not involve pavement performance predictions by FlexPAVE; material-level testing and analysis using FlexMAT are sufficient.

Figure 27 presents a comparative summary of the proposed frameworks for index-based (tier 2) and predictive (tier 3) BMD. In the following sections, the tier 2 and tier 3 BMD methods are described with examples.

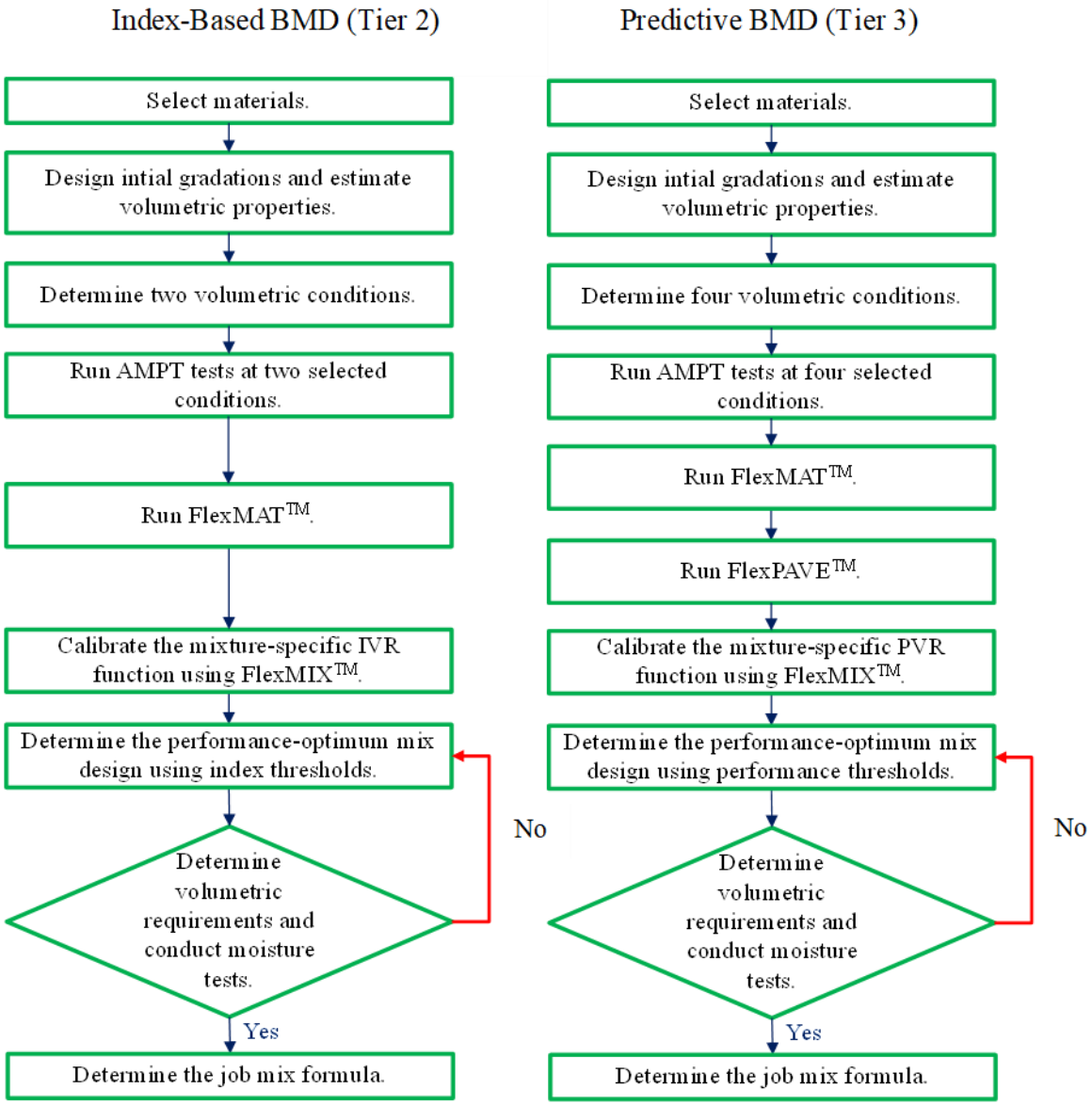

Source: FHWA.

Figure 27. Illustration. Proposed framework for index-based and predictive BMD.

DEVELOPMENT OF A FRAMEWORK FOR AN INDEX-BASED BALANCED MIX DESIGN PROCESS FOR ASPHALT MIXTURES (TIER 2)

This section presents a framework for index-based BMD using the cyclic fatigue test (AASHTO T 411) and SSR test (AASHTO TP 134).[15,16] The developed index parameters, i.e., the RSI and S_{app} for the SSR test and cyclic fatigue test, respectively, form the basis of the proposed methodology.

The basic concept of the tier 2 index-based BMD is similar to that of the tier 3 predictive BMD. The main difference is that this method uses the IVR concept and all the testing and analyses are performed at a fixed design air void (V_a) content (e.g., 4 percent). The procedure to develop the IVR is presented in chapter 1.

The PVR function can be applied to predict rut depth at different volumetric conditions. As discussed, the RSI is the average permanent strain (APS) at the end of 20 yr under specific structural and loading conditions. Thus, because the IVR for the RSI is similar to the PVR for rut depth under specific loading conditions, the IVR-RSI function can be used to predict the RSI. However, for the IVR-S_{app} function, the scenario is not the same as for the IVR-RSI function. Although S_{app} is a mechanics-based index parameter, it is not obtained through structural performance analysis. The NCSU research team is investigating the relationship between S_{app} and FlexPAVE predictions.

For purposes of tier 2 BMD, the IVR function is considered as the volumetric relationship for different gradations at the fixed design air void content (4.0 percent) at the design compaction level (N_{des}). For the general IVR function, three coefficients are considered as the fitting coefficients to calibrate the IVR. However, at the fixed design air void content, due to the intercorrelation of the VMA, VFA, and fixed design air void content (V_a), the IVR function can be calibrated using only two fitting coefficients.

A case study has validated the IVR function calibration. The case study uses a North Carolina 9.5-mm Superpave fine-graded surface mixture (RS9.5B) with 30 percent RAP, PG 58-22 binder, and 4.0 percent design air void content. For this case study, three different gradations were designed for the RS9.5B mixture; table 20 presents the volumetric data for these three gradations. Gradation 1 and gradation 2 were designed to cover a wide range of VMA and ACs. Therefore, these two mixtures can be used to calibrate the IVR.

Table 20. Volumetric properties for three different gradations of RS9.5B mix.

Mixture ID	P_b (Percent)	V_a (Percent)	VMA (Percent)	%CALUW
Gradation 1	5.6	4.0	17.3	50
Gradation 2	6.5	4.0	15.5	70
Gradation 3	6.1	4.0	16.3	60

P_b = volumetric optimum binder content; V_a = design air void content.

Figure 28 shows the RSI and S_{app} values for the conditions given in table 20. In figure 28, two variables change with each data point: AC (P_b) and gradation or %CALUW. The index values increase as the AC increases and the %CALUW decreases. The data from gradations 1 and 2

(two points) are fitted using the linear relationship shown in figure 28. The research team verified the linear relationship by identifying an intermediate gradation (gradation 3), finding the AC for that gradation to achieve 4.0 percent air void content, conducting AMPT tests, and plotting the results.[1] The intermediate condition that the research team selected is the current North Carolina Department of Transportation (NCDOT) mixture design for this RS9.5B mixture (the Superpave volumetric optimum (SVO)) and the results are denoted as verification in figure 28. These verification points are located close to the linear function. In this example, the measured RSI and S_{app} values for gradation 3 are 3.72 and 21.5, respectively. The RSI and S_{app} values predicted from the lines for the gradation 1 and gradation 3 data are 3.68 and 22.7, respectively. As a result, the errors in the prediction of the RSI and S_{app} values for gradation 3 are 1.1 and 5.1 percent, respectively. Therefore, the IVR function for this case study can be used to find the index parameter at 4.0 percent design air void for different gradations and ACs.

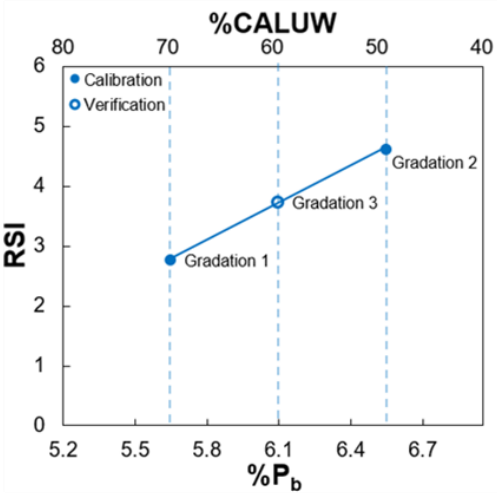

Source: FHWA.

A. RSI.

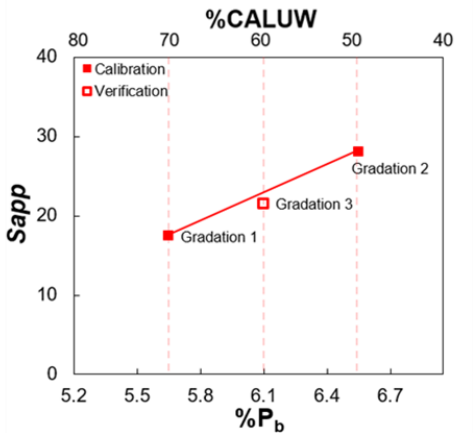

Source: FHWA.

B. S_{app}.

Figure 28. Graphs. Index parameters at fixed design air void (4.0 percent) for different gradations.

Equations 23 and 24 show the general form of the IVR-RSI and IVR-S_{app} functions at a fixed design air void content. As noted earlier, the IVR-RSI and IVR-S_{app} functions for the fixed air void content of 4.0 percent can be calibrated using two points.

$$\text{RSI} = \alpha_0 + \alpha_1 \times P_b \tag{23}$$

$$S_{app} = \beta_0 + \beta_1 \times P_b \tag{24}$$

Where:

α_0, α_1 = IVR-RSI fitting coefficients at fixed design air void (4 percent).
β_0, β_1 = IVR- S_{app} fitting coefficients at fixed design air void (4 percent).

Table 21 shows the IVR coefficients in equations 23 and 24 for the RS9.5B mixture. As noted earlier, these results were obtained from the data for gradation 1 and gradation 2.

Table 21. IVR mixture-specific coefficients.

IVR-RSI	IVR-S_{app}
α_0	B_0
2.04	11.83
α_1	β_1
−8.79	−49.48

Proposed Framework for Index-Based Balanced Mix Design

This section presents an example of the proposed index-based BMD procedure. Similar to the predictive BMD procedure, the research team produced gradation 1 and gradation 2 to achieve the largest VMA difference possible without changing the mixture classification from a fine-graded mixture to a coarse-graded mixture. Once the team established those gradations and determined the volumetric optimum binder content (P_b) at 4.0 percent design air void content (V_a) for each of the two gradations, the team took these two compositions as two points of the IVR function. Then the team performed AMPT performance tests using specimens fabricated under these two conditions.[1] In the next step, lines are drawn between the index values at the two points for the RSI and S_{app}. Finally, preestablished threshold values for S_{app} and the RSI are used to identify the range of allowable mixture designs (gradation and AC for those gradations that yield 4.0 percent design air void content).

In this example, the RS9.5B mixture is intended for roadways with traffic levels between 10 and 30 MESALS, so the threshold values are set at 24 for S_{app} and 4 for the RSI (table 18 and table 24 in volume I of this report).[18] Based on the IVR- S_{app} function, the S_{app} threshold will lead to the minimum AC of 6.21 percent. Based on the IVR-RSI function, the RSI threshold will lead to the maximum AC of 6.27 percent. Therefore, the potential optimum AC is in the range of 6.21 to 6.27 percent. Because the design air void content is fixed, the VMA can be calculated for

this range of AC. As a result, the optimum %CALUW is in the range of 56 to 58 percent. Figure 29 shows the results for the index-based BMD of the RS9.5B mixture.

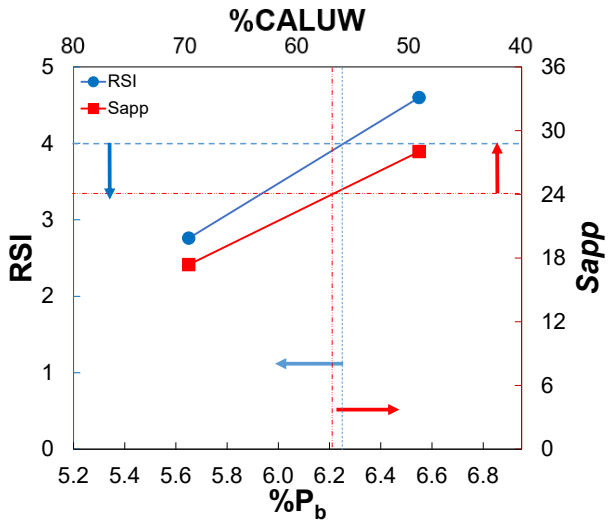

Source: FHWA.

Figure 29. Graph. Index-based BMD results for NC RS9.5B mixture: S_{app} and RSI as functions of AC and gradation.

Summary

In summary, the index-based tier 2 BMD optimum mix design lies between the mixture design with an AC of 6.21 percent and an aggregate gradation with %CALUW of 58 percent and the mixture design with an AC of 6.27 percent and an aggregate gradation with %CALUW of 56 percent. In this example, the optimum AC range happened to be narrow. If the range of the optimum AC is wider, State highway agency personnel can select the optimum AC based on factors such as engineering judgment and cost analysis.

This report describes two different proposed BMD approaches in which the RS9.5B mixture is used as an example to illustrate the two approaches. In this study, the optimum mix design obtained from each of these two approaches was compared. Table 22 presents a comparison of the BMD results for the RS9.5B mixture. Because the PVR function has been developed for this mixture, the performance life at any given volumetric condition can be determined. Several important observations can be made from table 22. First, the predictive BMD performance optimum (PPO) yields the longest life among all the designs, followed by the index-based BMD performance optimum (IPO) and the SVO mixture design. Second, both index-based and predictive BMD can balance fatigue and rutting much better than the Superpave volumetric mix design. Note too that the volumetric properties of the PPO and IPO mixtures meet all the Superpave volumetric requirements.

Table 22. Results from index-based and predictive BMD.

Optimum Type	%P_b	VMA (Percent)	VFA (Percent)	Dust to Binder	Fatigue Life (Years)	Rutting Life (Years)	Combined Life (Years)
PPO	6.3	17.8	77.6	0.90	15.4	14.7	14.7
IPO	6.2	17.2	76.8	1.10	12.6	19.0	12.6

The research team used limited data in the development of the index-based BMD and had to make some assumptions as a result. The team assumed the linearity of the IVR-S_{app} function and that assumption was verified by the case study mixture (RS9.5B); however, the validation of this assumption needs to be studied by testing more mixtures. Therefore, in future, researchers need to include more asphalt mixtures to verify the proposed framework.

DEVELOPMENT OF A FRAMEWORK FOR A PREDICTIVE BALANCED MIX DESIGN PROCESS FOR ASPHALT MIXTURES (TIER 3)

This section introduces the underlying concepts and framework for the proposed predictive BMD method (tier 3) and its application to the design of three different asphalt mixtures. Details regarding each step in the BMD process may vary depending on the agency's or contractor's current practice, but the presented framework does not change.

Materials

The research team used the three asphalt mixtures, RS9.5B, SM12.5, and RI19C, to develop the BMD method; the mixtures are presented here to demonstrate the BMD process. These mixtures contain aggregate materials from different sources, two different gradation types (fine-graded and coarse-graded), three different NMAS, two different binder PGs and three different RAP contents. Table 23 provides a summary of the information for the three study mixtures.

Table 23. Mixture information for AMPT BMD development.

Mixture	Base Binder Grade	NMAS (mm)	Gradation Type	RAP Content (Percent)	Design Traffic (MESALs)
RS9.5B	PG 58-28	9.5	Fine-graded	30	0.3–3
SM12.5	PG 64-22	12.5	Coarse-graded	22	0.3–3
RI19C	PG 64-22	19	Fine-graded	20	3–30

The research team used the RS9.5B mix as the primary mixture to develop the predictive BMD. It is a typical North Carolina fine-graded 9.5 mm NMAS surface mixture. The grade of the virgin binder in the RS9.5B mixture is PG 58-28 and the mixture contains 30 percent RAP. The design traffic level is 0.3 to 3 MESALs. The second mixture is the SM12.5 mixture from Virginia. Different from the RS9.5B mixture, the SM12.5 mixture is coarse-graded with 12.5 mm NMAS and contains PG 64-22 binder and 22 percent RAP. The SM12.5 mixture was used in the 2013 WMA and RAP study conducted at FHWA's ALF.[47] The SM12.5 mixture was used in ALF Lane 6 and served as the control mixture in that study. The third example mixture is RI19C,

a typical North Carolina fine-graded intermediate or base layer mixture with 19 mm NMAS. The virgin binder grade in the RI19C mixture is PG 64-22 and the mixture contains 20 percent RAP.

Performance-Volumetrics Relationship

Previous studies have found that, for asphalt mixtures that are composed of the same set of component materials and similar aggregate structures, a linear relationship exists between their performance and volumetric parameters, i.e., the VMA_{IP} and VFA_{IP}, as presented in equations 17 and 18. Equations 17 and 18 show the PVR for fatigue cracking and rutting, respectively. The PVR concept considers performance to be the performance of the asphalt mixture of interest in a pavement structure, represented by %Damage and the asphalt layer rut depth in the pavement cross section for fatigue cracking and rutting, respectively. The predictors in the PVR are the VMA_{IP} and VFA_{IP}, with performance being the response variable. The term in-place indicates that the volumetric properties are associated with the air voids in the AMPT test specimens or with the measured field density if field cores are tested. Equations 3 and 6 present the relationships for the VMA_{IP} and VFA_{IP} volumetric parameters, respectively.[19] These two equations demonstrate the relationship between the in-place volumetric parameters and the corresponding volumetric parameters as asphalt samples are compacted to the N_{des}. Essentially, these two equations show that the VMA_{IP} and VFA_{IP} are functions of typical design parameters (or AQCs), i.e., the VMA at N_{des}, VFA at N_{des}, air void content at N_{des}, AC, compaction density, and so forth. In other words, VMA_{IP} and VFA_{IP} can represent the various volumetric properties of a mixture in only two volumetric properties and can be used effectively for the PVR. In this study, the IP-VMA and IP-VFA are designated as VMA_{IP} and VFA_{IP}, but VMA and VFA without subscripts indicate the volumetric properties when asphalt samples are compacted to the N_{des}.

Predictive Balanced Mix Design Procedure and Results

This section presents the procedure for the predictive BMD. The RS9.5B mixture is the primary mixture and is used as to demonstrate each step. The results for the SM12.5 and RI19.0C mixtures are presented at the end of the section to provide supporting evidence for the predictive BMD.

Material Selection

The first step in the mixture design process is selecting the materials to be used in the mixture, such as the asphalt binder and aggregate. Any other components that will used, such as RAP and additives, should be determined as well. As is the case for current BMD practice, predictive BMD requires some relevant information, such as climate conditions and design traffic volume, to select the appropriate materials. In the predictive BMD method, the selection of the binder PG, NMAS, gradation type (fine-graded, coarse-graded, open-graded, or SMA), design number of gyrations (N_{des}), and other design parameters follow existing criteria and specifications. If the mixture is expected to contain RAP, the RAP content also can be predetermined in this step. The RAP contents by weight of aggregate in the RS9.5B, SM12.5, and RI19C mixtures used in this study are 30, 22, and 20 percent, respectively. These RAP contents were determined based on the desired asphalt binder replacement ratio, cost, etc. The following steps were taken to determine the performance-optimum mixture design using the selected materials.

Step 1. Design Gradations and Generate the Design Volumetric Space

In conventional mixture design, the candidate gradation is determined following the selection of the materials. However, in the predictive BMD method, a range of gradations within the given gradation type should be generated to find the optimal gradation for the given aggregate materials and gradation type (e.g., coarse versus fine). The range of gradations results in the various volumetric conditions in the design volumetric space, which can include almost all possible and reasonable combinations of the component materials.

In the predictive BMD, only four conditions (two boundary gradations and two binder contents at each gradation) are needed to build the volumetric space and calibrate the PVR function. These four volumetric conditions, i.e., the 'four corners', are recommended to be composed of two gradations that represent the boundary of the corresponding gradation type (fine-graded, coarse-graded, or SMA) and two binder contents that are recommended to be tested at each of the two gradations. As only four conditions are recommended for the proposed design method, more conditions were tested in the laboratory to further verify the effectiveness of the PVR function and fully evaluate the mixtures' performance. As a result, nine conditions were tested for the RS9.5B and RI19C mixtures, respectively, and 21 conditions were evaluated for the SM12.5 mixture. Table 1, Table 2table 2, and table 24 present the volumetric conditions of the four corners and verification points of the three mixtures used in this study, respectively. In the three tables, the gradations are designated in terms of the CUW, which is used in the Bailey method where gradations are quantified.[25] For the two North Carolina mixtures, RS9.5B and RI19C, the volumetric conditions are designated based on the gradation, air voids compacted to N_{des}, and the air void contents of the performance test specimens. For example, the designation C70-53 indicates that, at this condition, the gradation has 70 percent CUW and, using the design gradation and binder content, the gyratory-compacted specimen yields 5 percent air void content if it is compacted to N_{des}, and performance tests are conducted using specimens with this mixture design but controlled to 3 percent air void content after coring and cutting.

Table 24. Volumetric properties of RI19.0C mixture.

Gradation	ID	VMA at N_{des}	%AC at N_{des}	VFA at N_{des}	V_a at N_{des}	VA_{IP}	VMA_{IP}	VFA_{IP}
CUW 60	C60-33*	14.2	5.2	78.9	3.0	3.0	14.2	78.9
CUW 60	C60-55*	14.9	4.7	66.4	5.0	5.0	14.9	66.4
CUW 60	C60-57	14.9	4.7	66.4	5.0	7.0	16.7	58.0
CUW 67	C67-44	14.1	4.6	71.6	4.0	4.0	14.1	71.6
CUW 75	C75-33*	13.6	4.8	78.0	3.0	3.0	13.6	78.0
CUW 75	C75-44	13.7	4.4	70.8	4.0	4.0	13.7	70.8
CUW 75	C75-53	13.8	4.0	63.8	5.0	3.0	12.0	75.0
CUW 75	C75-55*	13.8	4.0	63.8	5.0	5.0	13.8	63.8
CUW 75	C75-57	13.8	4.0	63.8	5.0	7.0	15.6	55.2

*Four corners conditions that were used to calibrate the PVR function in the predictive BMD. Other conditions were tested for the PVR function verification. To illustrate the four corners conditions used in the predictive BMD, figure 30-A, figure 31-A, and figure 32-A present the two boundary gradations, and figure 30-B, figure 31-B, and figure 32-B show the binder contents used for the performance tests for each mixture. The methodology used to select the boundary gradations and binder contents for the performance tests is explained in the following paragraphs.

Based on experience from testing the RS9.5B, SM12.5, and RI19C mixtures in this study, the volumetric space can be large enough to cover various combinations of the component materials when the two gradations provide about 1 to 2 percent difference in VMA when compacted to the N_{des} at the corresponding Superpave initial binder content. Mixtures with large aggregate particles (greater than 12.5 mm NMAS) tend to be less sensitive to changes in gradation; therefore, a minimum of 1 percent difference in VMA is recommended for mixtures with 19 mm or larger NMAS as a preliminary criterion and a minimum of 2 percent difference in VMA for mixtures with NMAS smaller than 19 mm. The gradation type (i.e., fine-graded, coarse-graded, etc.) should remain consistent among the created gradations. To achieve the test boundary gradations and satisfy the requirements for the differences in VMA, the research team recommends the Bailey method.[25] Figure 30-A shows the created test boundary gradations for the RS9.5B mixture. The difference in VMA provided by the boundary gradations is approximately 2 percent.

For each of the boundary gradations, the research team used the Superpave mix design method to determine the initial binder content. In addition to the initial binder content at each gradation, two additional binder contents at the initial binder content ±0.5 percent are used for the volumetric tests. The team then measured volumetric properties from the three binder contents for each of the two boundary gradations for a total of six conditions. Figure 30-B, figure 31-B, and figure 32-B present the volumetric properties of the RS9.5, SM12.5, and RI19C mixtures at the six gradation-binder content combinations, respectively, for the binder content versus air void content space. Figure 30-C, figure 31-C, and figure 32-C present the same information for the VMA versus VFA space. The team calculated the VMA and VFA by assuming that the effective specific gravity (G_{se}) remains the same with the same gradation.

Figure 30-B, figure 31-B, and figure 32-B show a linear relationship between the binder content and the air void content at the N_{des}. The obtained relationships are used to determine the binder contents at 3 and 5 percent air void contents for each gradation. The research team used 3 and 5 percent air void contents as the boundary because the allowable air void percentage range in many design specifications is between 3 and 5 percent air void content at the N_{des}. Although many agencies adopt 4 percent as the design air void content, others modify the specifications and reduce the air void content to 3 percent to (hopefully) increase the binder content, and some agencies increase the air void content to 5 percent so that the compaction effort required in the field also is increased, and still others permit design to any value between 3 and 5 percent air void content.[39]

The volumetric properties at 3 and 5 percent air void contents for each gradation become the performance test conditions. These conditions are represented as empty circles in figure 30-B, figure 31-B, and figure 32-B and constitute the four corners for the PVR development shown in figure 30-D, figure 31-D, and figure 32-D. The specimens used in figure 30-B, figure 31-B, and figure 32-B are approximately 110 mm in height. The height of the gyratory sample that is used to produce the AMPT performance test specimens is 180 mm. The targeted mass of the 180 mm tall gyratory specimens for each target air void content is determined in accordance with AASHTO R 83.[48]

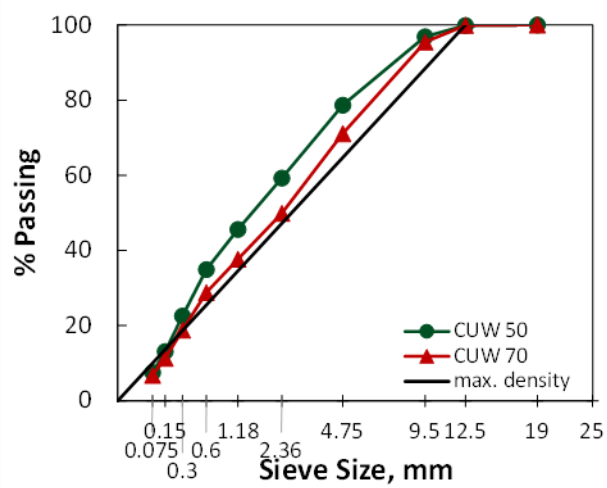

A. Created gradation.

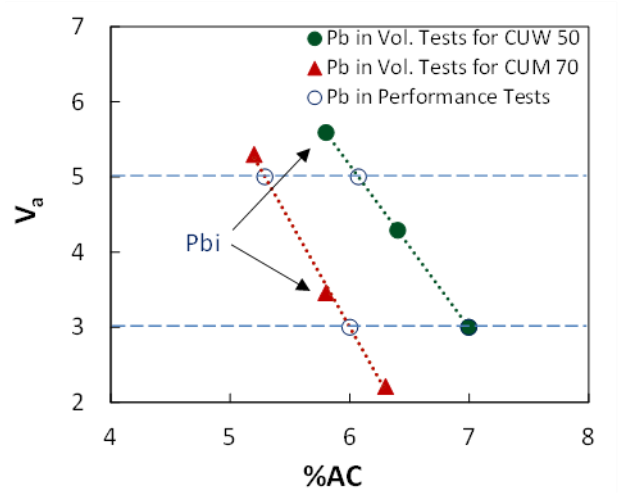

Pb = binder content; Pbi = optimum binder content at the corresponding gradation based on Superpave volumetric calculations.

B. Relationship between air void content at N_{des} and selected binder contents for performance testing (empty circles).

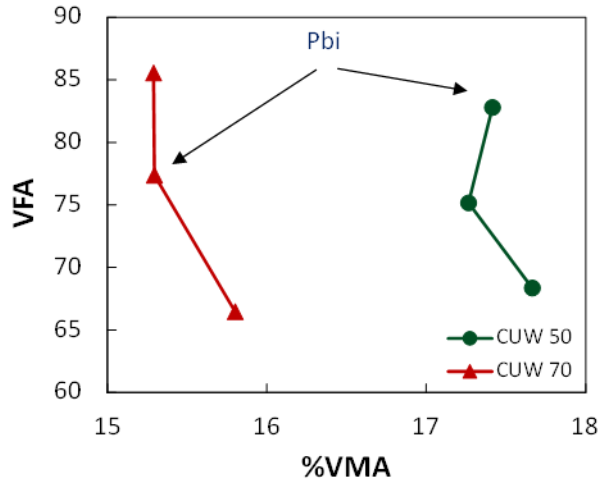

C. Measured volumetric data of the points in B.

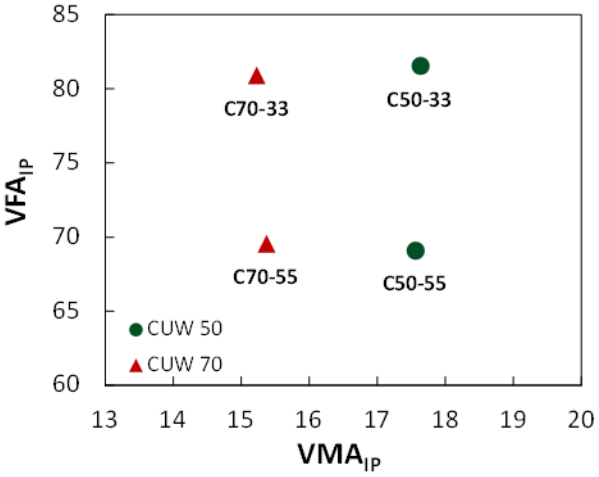

D. Selected design area and critical points in the volumetric space.

Figure 30. Graphs. RS9.5B mixture design information.[(26)]

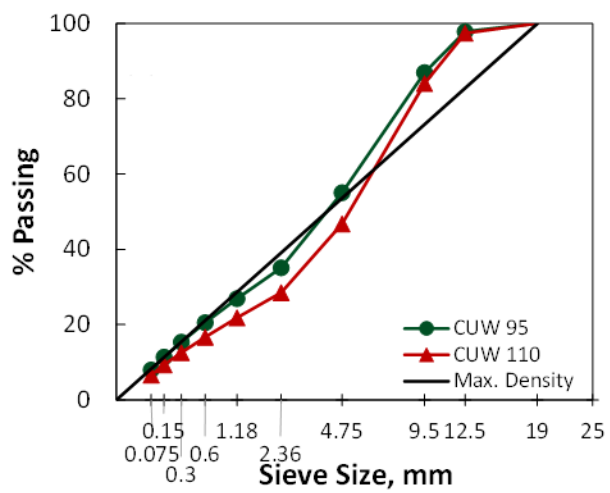

A. Created gradation.

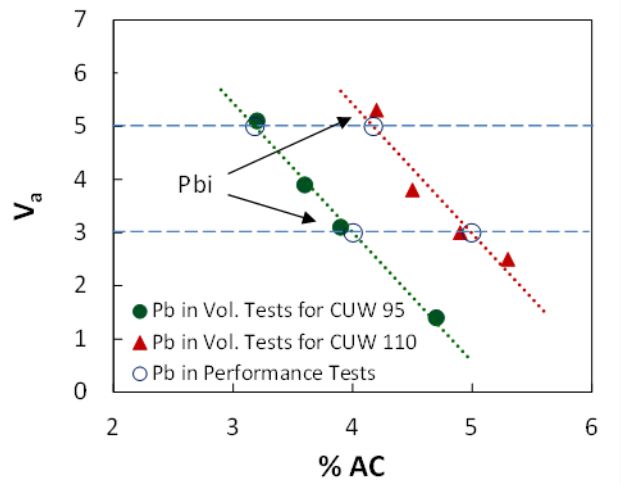

B. Relationship between air void content at N_{des} and selected binder contents for performance testing (empty circles).

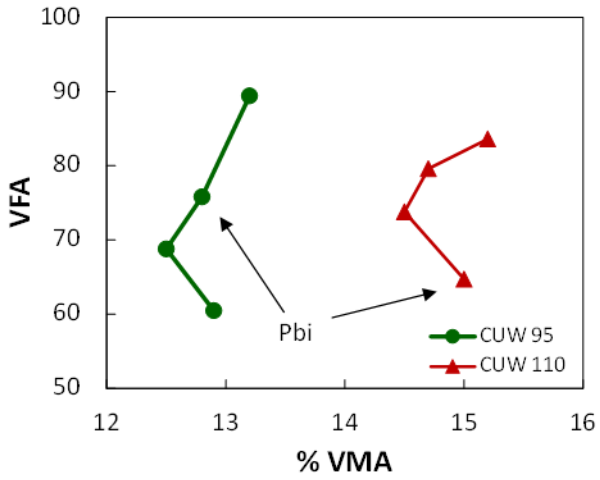

C. Measured volumetric data of the points in subfigure 32-B.

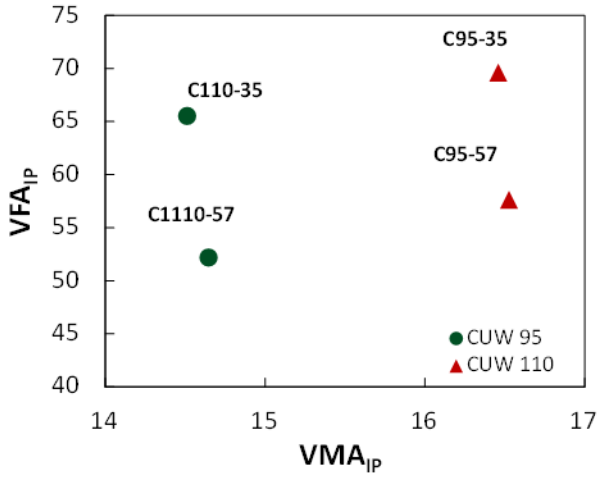

D. Selected design area and critical points in the volumetric space.

Figure 31. Graphs. SM12.5 mixture design information.[26]

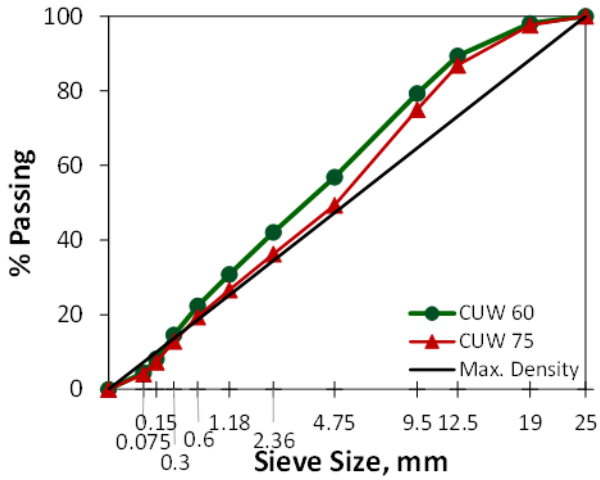

A. Created gradation.

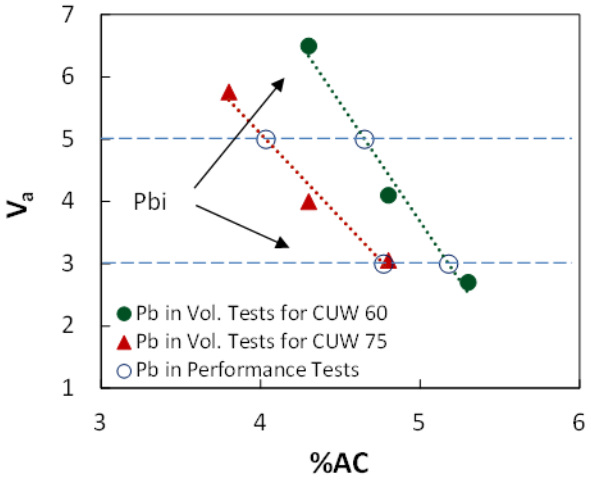

B. Relationship between air void content at N_{des} and selected binder contents for performance testing (empty circles).

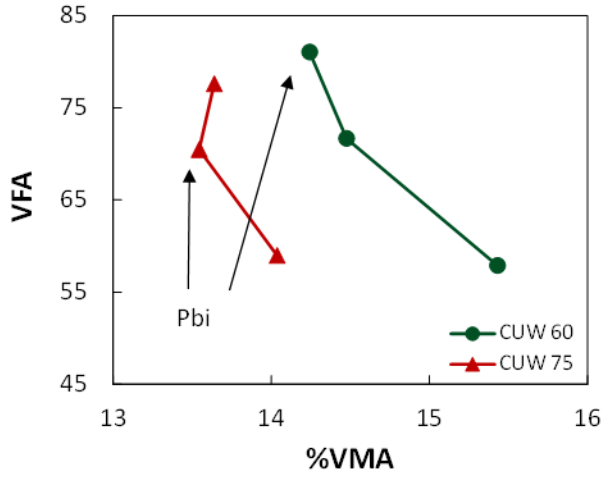

C. Measured volumetric data of the points in subfigure 33-B.

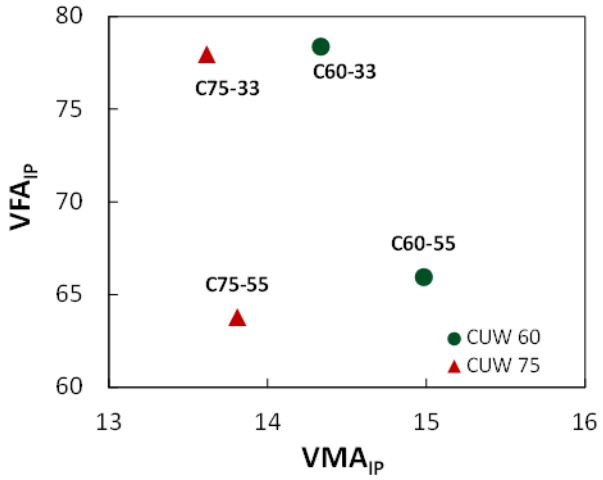

D. Selected design area and critical points in the volumetric space.

Figure 32. Graphs. RI19C mixture design information.[26]

The in-place air void contents of the performance test specimens are recommended to be the same as or to change consistently with a constant offset from the air void content at N_{des}. That is, for the 4 percent design air void content, the air void contents of the test specimens at N_{des} for the four corners conditions should be 3 and 5 percent. The air void contents of the performance test specimens that correspond to the volumetric conditions at N_{des} for 3 and 5 percent air void contents should be 3 and 5 percent or 5 and 7 percent, depending on the expected air void level in the pavement. When 5 and 7 percent air void contents are used for the test specimens, then clearly a 2 percent offset from the air void content at N_{des} has been applied. For the RS9.5B mixture, for example, one of the test conditions is C70-33. The naming convention indicates its volumetric conditions whereby the gradation is CUW 70, the air void content at N_{des}

is 3 percent, and the air void content of the performance test specimen is 3 percent. Using this naming convention, the four corners are designated as C70-33, C70-55, C50-33, and C50-55. The VMA_{IP} and VFA_{IP} (which are based on the in-place air void contents) of the three mixtures are calculated and cross-plotted in figure 30-D, figure 31-D, and figure 32. The two-dimensional space formed by the VMA_{IP} and VFA_{IP} is defined as the volumetric space. The area inside the four corners in the volumetric space is defined as the mix design volumetric region.

The main reason that the research team selected the in-place air void content to be the same as the air void content at N_{des} for the performance tests is that the compaction of the performance test specimens is guaranteed to not have any issues. If the in-place air void content is much higher than the air void content at N_{des}, e.g., C70-35, a potential problem can occur if the number of gyrations is too low for the performance test specimens, which would increase the test variability. If the in-place air void content is too low compared to the air void content at N_{des}, e.g., C70-53, a potential problem can cause difficulties in compacting the performance test specimens.

Step 2. Performance Test and Calibrate the Performance-Volumetrics Relationship Function

In this step, the AMPT performance tests (i.e., dynamic modulus, cyclic fatigue, and SSR tests) are conducted on the mixtures under the four corners volumetric conditions developed in step 1, and the results are used to build the PVR functions. Pavement engineers can use the PVR functions calibrated from the four corners volumetric conditions to predict the mixture performance for any volumetric condition in the volumetric space. The following steps use the developed PVRs to determine the performance-optimum design, and obtain the corresponding combination of component materials based on the known volumetric conditions.

Step 1 explains how to determine the volumetric properties of the test specimens. For example, for the RS9.5B mixture, the four corners conditions to be tested are designated as C70-33, C70-55, C50-33, and C50-55. The in-place air void contents are indicated by the last digit in the name designation. The actual in-place air void contents of the test specimens should be controlled within ±0.5 percent of the target air void content. The obtained model coefficients are then used in the performance simulation where the mixture performance is integrated with actual pavement structures. At this step, consider the following two scenarios:

- If the pavement structure is determined before the mixture is designed, or if the mixture and structure are designed simultaneously, then the mixture properties can be input into the available pavement structure.

- If the pavement structure is not yet determined, which is common for most State agencies in the United States, then typical pavement structures are considered for the design.

When mixtures are designed according to different traffic volume requirements, the pavement structures in which the mixtures will be used should likewise be in accordance with the traffic volume. Table 25 presents typical pavement structures recommended by the NCDOT for different traffic levels in the NCDOT Pavement Design Manual, which are used in this predictive BMD framework.[49] However, agencies and contractors can use typical structures based on their practice and experience. For structures with multiple asphalt layers, typical material properties

can be used in the pavement analysis of the mixtures that are not the mixture to be designed. For example, if the design mixture is a surface RS9.5B mixture, then for pavement performance analysis that uses 3 to 10 MESALs, typical material properties of an RI19C mixture can be used for the second layer.

Figure 33-A and figure 33-B present the damage evolution and APS growth, respectively, during the 20-yr design period for the RS9.5B mixture. The APS percentage, or %APS, is obtained by dividing the total permanent deformation of the target asphalt layer by the layer thickness. This analysis uses %APS instead of the predicted rut depth in the asphalt layer because a recent study found that %APS is a better indicator than rut depth to describe a material's rutting resistance.[14] The %Damage and %APS at the end of the design life are used to calibrate the PVR function. The PVR coefficients in equations 17 and 18 are obtained via curve fitting optimization. Table 26 presents the PVR coefficients for the three study mixtures.

Table 25. Typical structures recommended for different design traffic volumes by NCDOT.

Design Traffic Level 0.3–3 MESALs	Design Traffic Level 3–10 MESALs	Design Traffic Level 10–30 MESALs
7.62 cm (3 inches) asphalt 20.32 cm (8 inches) ABC (206 MPa) Subgrade (124 MPa)	7.62 cm (3 inches) asphalt 6.35 cm (2.5 inches) asphalt 20.32 cm (8 inches) ABC (206 MPa) Subgrade (124 MPa)	7.62 cm (3 inches) asphalt 10.16 cm (4 inches) asphalt 20.32 cm (8 inches) ABC (206 MPa) Subgrade (124 MPa)

ABC = aggregate base course.

Table 26. Coefficients of PVR functions for study asphalt mixtures.

Coefficient	RS9.5B	SM12.5	RI19C
β_{f0}	50.707	115.080	25.910
β_{f1}	−0.914	−3.910	−0.670
β_{f2}	−0.257	−0.505	−0.025
β_{r0}	−6.638	−0.870	−0.871
β_{r1}	0.303	0.401	0.097
β_{r2}	0.046	0.070	0.002

Figure 33-C and figure 33-D present the %Damage and %APS contours for the RS9.5B mixture in the two-dimensional volumetric space formed by the VMA_{IP} and VFA_{IP}, respectively. These contours are predicted by the PVR. The %Damage gradually increases in the diagonal direction from 12.9 percent at the top-right corner of the plot to approximately 19 percent at the bottom-left corner of the plot. The percent average permanent strain gradually changes in the diagonal direction from 2.7 percent at the top-right corner of the plot to approximately 12 percent at the bottom-left corner of the plot. Both VMA_{IP} and VFA_{IP} decrease as the position of mixture's volumetric condition in the volumetric space changes from the top-right corner to the bottom-left corner. As shown in figure 2, moving from the top-right corner of the volumetric space to the bottom-left corner indicates that the gradation becomes coarser because the mixture is fine-graded. When the gradation remains the same, this move means the decrease in binder

content. Therefore, the contour patterns shown in both figure 2 and figure 33 indicate that, as the gradation becomes coarser and the binder content decreases, the predicted %Damage increases while the predicted rut depth decreases. The predicted %Damage and rut depth obtained from the PVR are determined before the application of the transfer function in FlexPAVE. Applying the transfer function in the next step provides the predicted performance.

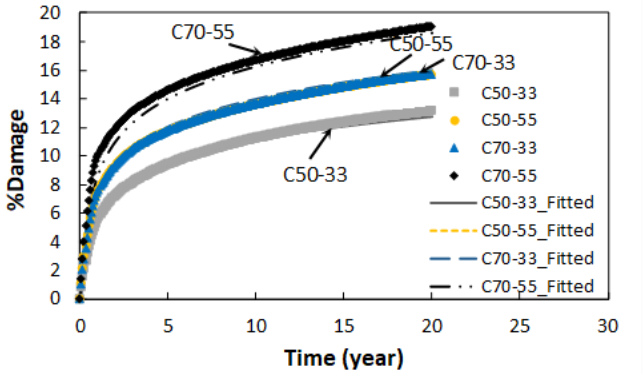

A. %Damage versus time at different volumetric conditions.

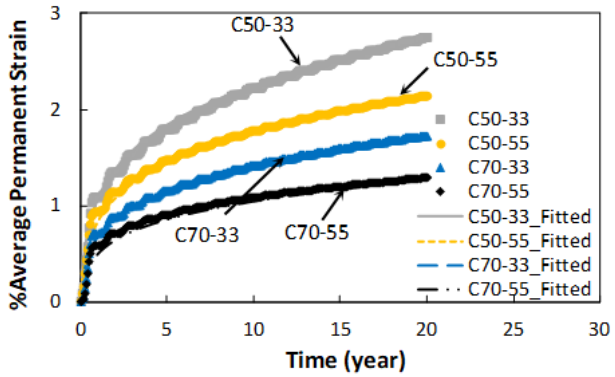

B. %APS versus time.

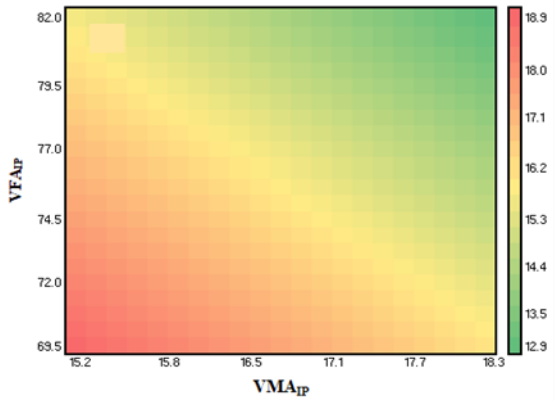

C. %Damage contours predicted by PVR.

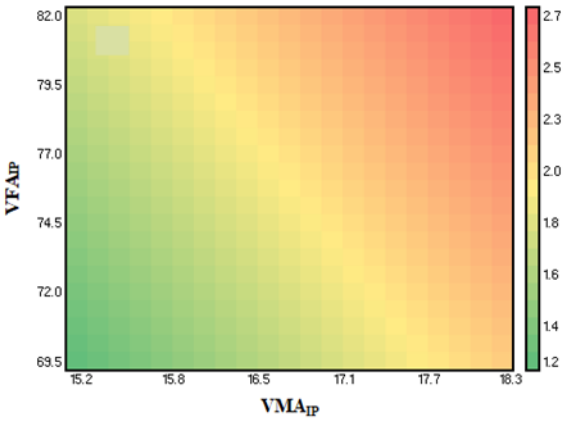

D. %APS contours predicted by PVR.

Figure 33. Illustrations. FlexPAVE simulation results for RS9.5B.[26]

Figure 34 and figure 35 present the FlexPAVE performance simulation results and PVR calibration results for the SM12.5 and RI19C mixtures, respectively. Similar trends can be found for these two mixtures as for the RS9.5B mixture in terms of performance predictions and PVR fitting. However, for the RI19C mixture, the predicted performance is not as sensitive to volumetric property changes as it is for the other two mixtures. The %Damage contour in figure 34 and figure 35 is similar to that in figure 33. To reduce redundancy, no detailed descriptions of the contour are given for figure 34 and figure 35. Instead, the similarity in %Damage contours in figure 33, figure 35, and figure 34 is noted.

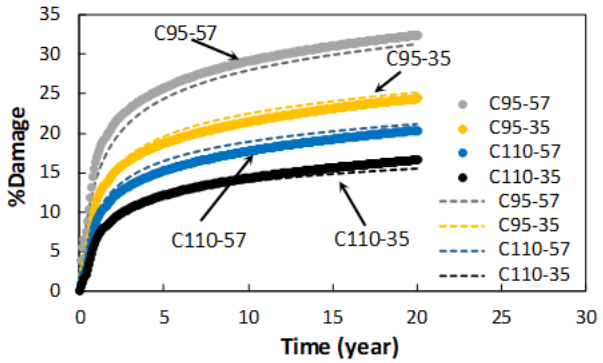

A. %Damage versus time at different volumetric conditions.

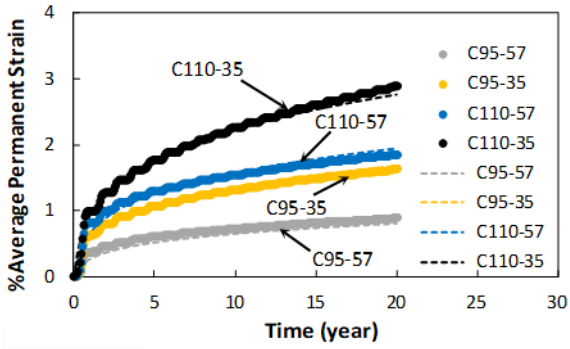

B. %APS versus time.

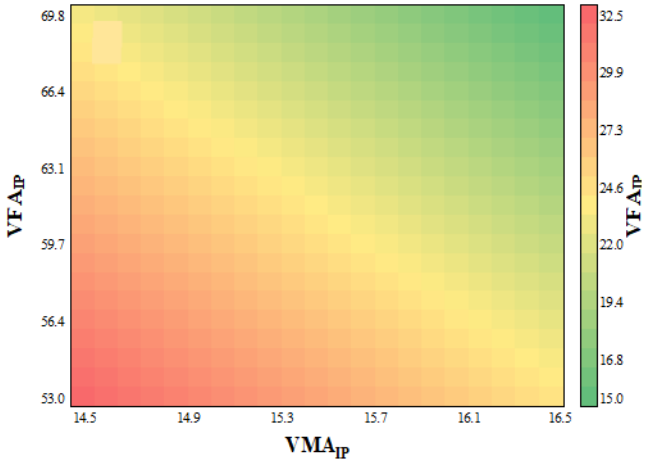

C. %Damage contours predicted by PVR.

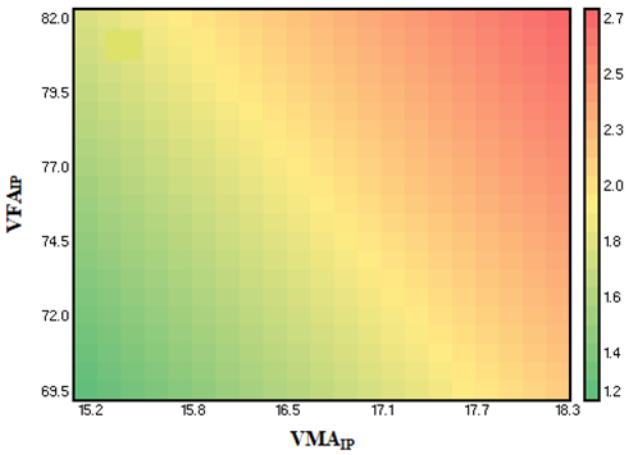

D. %APS contours predicted by PVR.

Figure 34. Illustrations. FlexPAVE simulation results for SM12.5.[26]

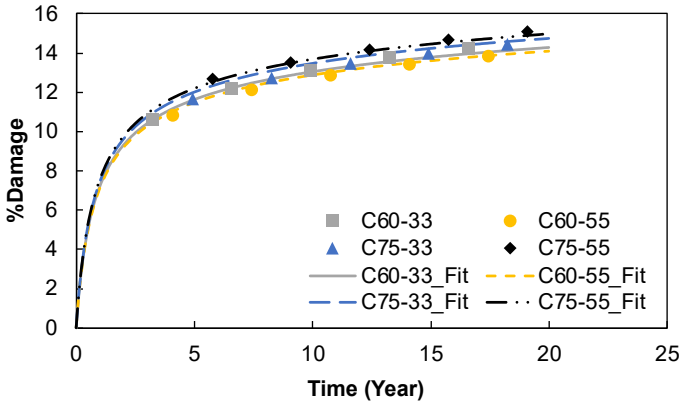

A. %Damage versus time at different volumetric conditions.

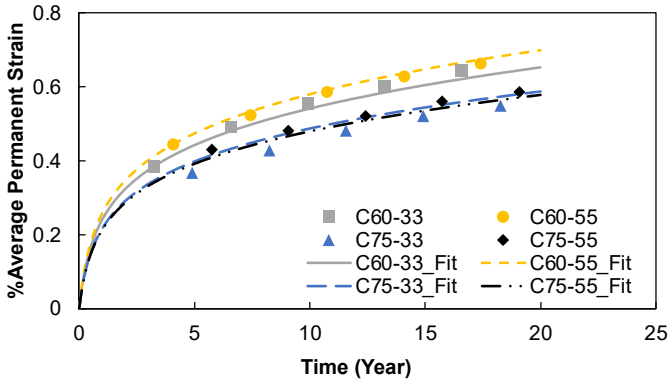

B. %APS versus time.

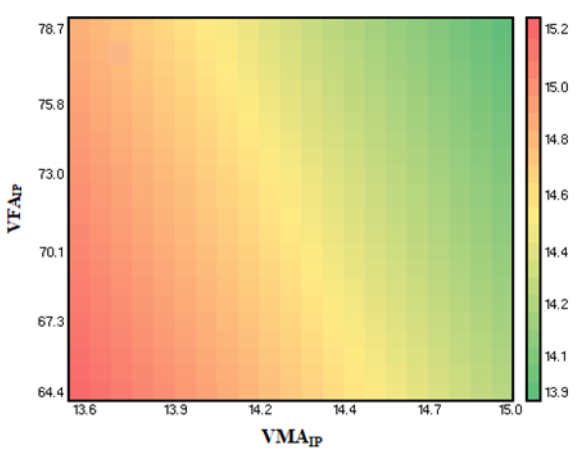

C. %Damage contours predicted by PVR.

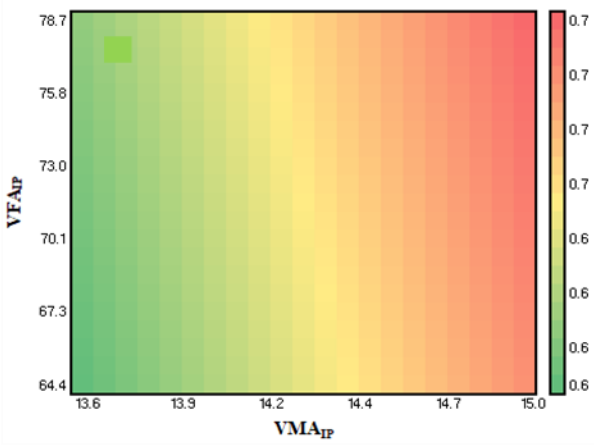

D. %APS contours predicted by PVR.

Figure 35. Illustrations. FlexPAVE simulation results for RI19C.[26]

Step 3. Determine the Pavement Life at Different Volumetric Conditions

The PVR functions that are calibrated in step 2 predict the mixture's performance at the end of the design life for a given mixture's volumetric conditions. To predict the damage evolution throughout the design life, another function, PVR with time (PVR-*t*) was developed in this study. PVR-*t* uses the performance at the end of the design life to predict pavement distress at any time before the end of the service time. When the failure criteria for pavement fatigue damage and rutting are given, the pavement life can be calculated based on the damage evolution predicted from the PVR-*t* function for the mixture at a given volumetric condition. The PVR-*t* function is expressed in equation 25.

$$Pf\left(t\right)=\frac{P_{20}\cdot p_0\cdot t}{\left(m+t\right)^n} \quad (25)$$

Where:

Pf(t) = predicted %Damage or %APS as a function of time.
P_{20} = predicted %Damage or %APS at the end of design life obtained from PVR.
t = time in months.
p_0, *m*, *n* = fitting coefficients.

The PVR-*t* function should be calibrated using the known performance evolution curves obtained from the four corners volumetric conditions first. Figure 34-A and figure 34-B present the calibrated PVR-*t* curves using dashed lines. After the model coefficients (p_0, *m*, and *n*) are obtained using the predicted %Damage or %APS at the design life (P_{20}) predicted from the PVR, the performance evolution curves for different volumetric conditions can be predicted from the PVR-*t* function. Table 27 presents the fitting coefficients and the calibrated PVR-*t* functions for the SM12.5 and RI19C mixtures.

Table 27. Coefficients of PVR-t functions for the study asphalt mixtures.

Coefficient	RS9.5B	SM12.5	RI19C
$p_{0\text{-}fatigue}$	0.606	0.707	0.774
$m_{\text{-}fatigue}$	0.376	0.644	0.620
$n_{\text{-}fatigue}$	0.829	0.877	0.908
$p_{0\text{-}rutting}$	0.455	0.439	0.482
$m_{\text{-}rutting}$	0.256	0.413	0.439
$n_{\text{-}rutting}$	0.736	0.719	0.753

The transfer functions for FlexPAVE are applied to the predicted %Damage and %APS results to obtain the final predicted performance.[36] The fatigue transfer function converts the predicted %Damage to the %Cracking on the pavement surface, and the rutting transfer function applies the calibration factor to the predicted values. The transfer function for cracking is presented in Volume I of this report in equation 150.[18]

By simplifying equation 150 from Volume I of this report, equation 26 is obtained.[18]

$$\%Cracking = \frac{50}{1 + \frac{7{,}970.327}{\%Damage^{6.0672}}} \tag{26}$$

The transfer function for rutting is shown in equation 27.

$$RD = C_r \cdot RD_{AC} \tag{27}$$

Where:

RD = percentage of permanent strain after calibration.
RD_{AC} = predicted percentage of permanent strain in the asphalt layers.
C_r = 0.929.

After the transfer functions are applied, the pavement life then can be determined by the calibrated performance evolution curve with given threshold values. In this study, 25 percent cracking and 2.5 percent permanent strain were considered the failure thresholds. Figure 36-A and Figure 36-B present the pavement life contours of the RS9.5B mixture determined by fatigue cracking and rutting failures, respectively. Similar to the %Damage and %APS contours in figure 33-C and figure 33-D respectively, the pavement life due to fatigue cracking decreases and the pavement life due to rutting increases as the volumetric properties change from the top-right corner to the bottom-left corner of the volumetric space. These trends indicate that the pavement life due to fatigue cracking decreases and the pavement life due to rutting increases as the gradation becomes coarser and the binder content decreases, which is the same observation made from the %Damage and %APS contours in Figure 33-C and figure 33-D, respectively.

figure 36-C shows the pavement life calculated based on the minimum pavement life due to fatigue failure and rutting failure. The pavement life contour in the figure does not show gradual, monotonous change from the top-right corner to the bottom-left corner; rather, a band of volumetric properties with the longest pavement life is found perpendicular to the diagonal direction from the top-right corner to the bottom-left corner and about one third of the distance from the top-right corner. As shown, the RS9.5B mixture life is dominated by fatigue failure. This observation is consistent with engineers' experience with North Carolina mixes.

Figure 37 and figure 38 present the predicted pavement life for the SM12.5 and RI19C mixtures, respectively. Similar patterns to Figure 36 can be found in these figures, except that the longest pavement life is found at the top-right corner in Figure 37-C and figure 38-C when the pavement lives due to fatigue cracking and rutting are combined. As shown, these two mixtures are dominated by fatigue cracking as well. All 3 mixtures were compared to mixtures in the material database maintained by the research team where more than 100 mixtures are documented; the 3 study mixtures show high rutting resistance.

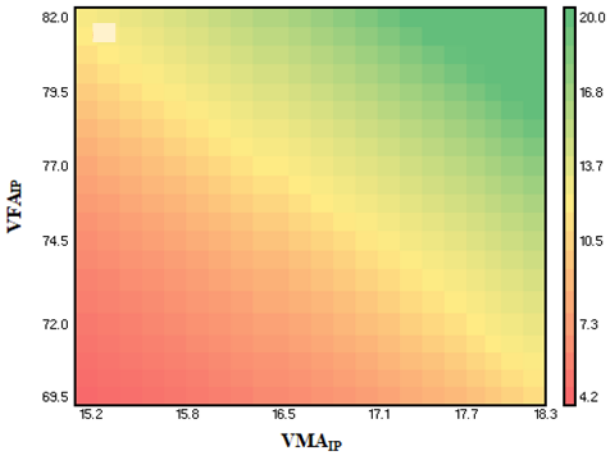

Note: The unit for life is year.

A. Pavement life based on fatigue %Cracking.

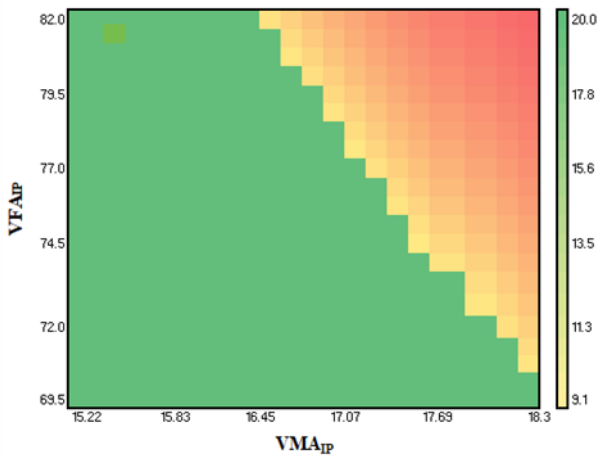

Note: The unit for life is year.

B. Pavement life based on percent permanent strain.

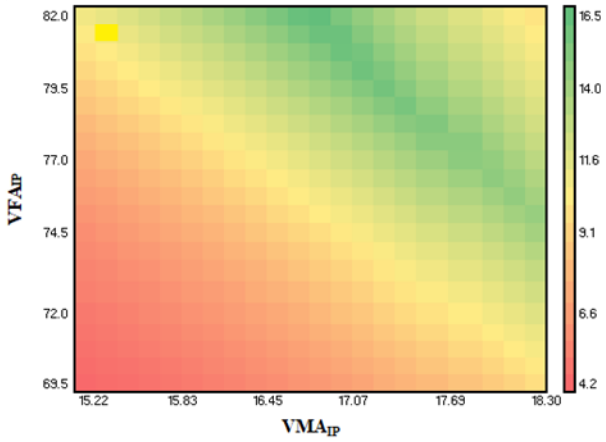

Note: The unit for life is year.

C. Pavement life with combined %Cracking and percent permanent strain.

Figure 36. Illustrations. Predicted pavement life based on different volumetric conditions of RS9.5B mixture.[(26)]

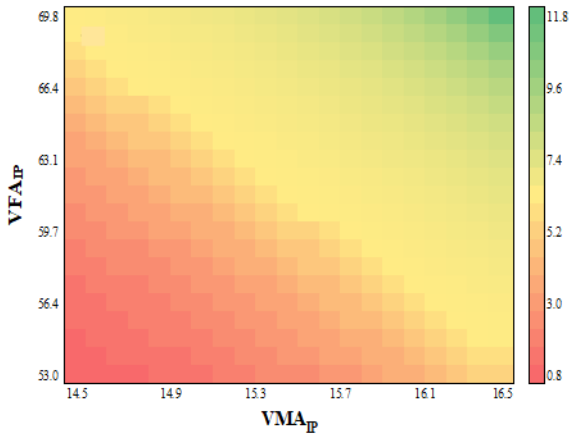

Note: The unit for life is year.

A. Pavement life based on fatigue %Cracking.

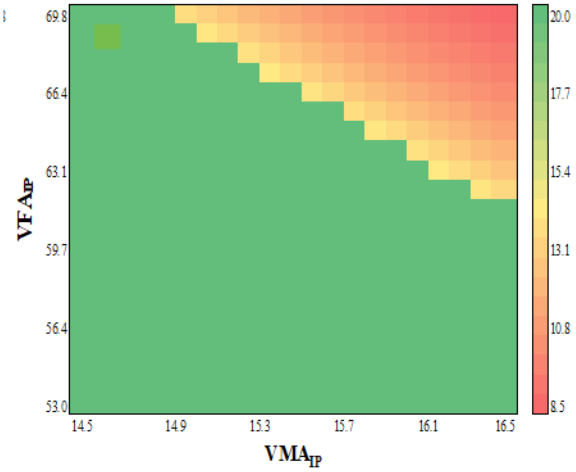

Note: The unit for life is year.

B. Pavement life based on percent permanent strain.

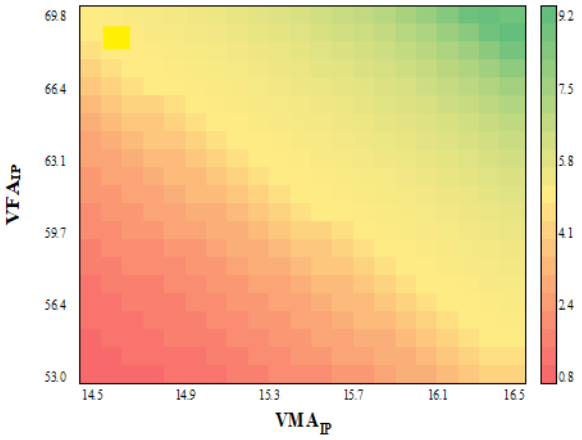

Note: The unit for life is year.

C. Pavement life with combined %Cracking and percent permanent strain.

Figure 37. Illustrations. Predicted pavement life based on different volumetric conditions of SM12.5 mixture.[26]

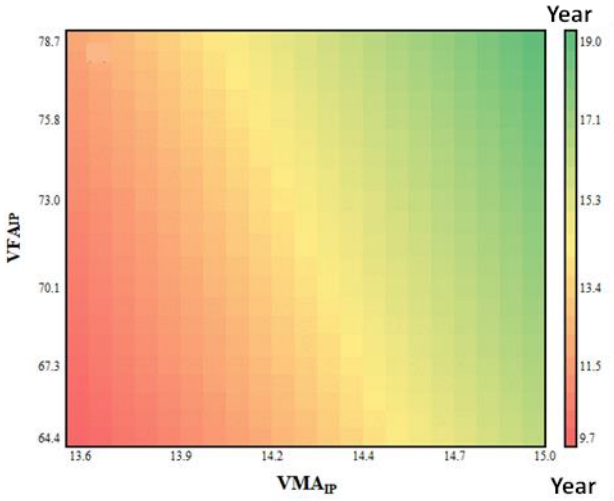

Note: The unit for life is year.

A. Pavement life based on fatigue %Cracking.

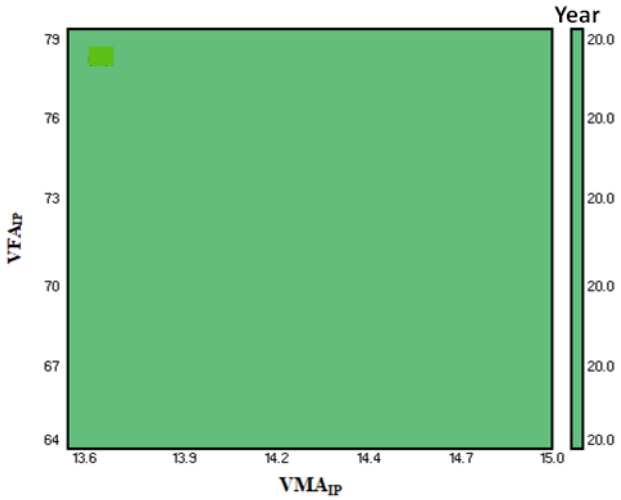

Note: The unit for life is year.

B. Pavement life based on percent permanent strain.

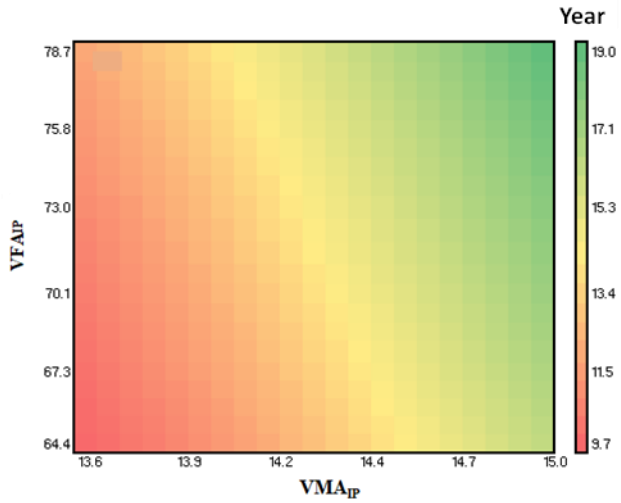

Note: The unit for life is year.

C. Pavement life with combined %Cracking and percent permanent strain.

Figure 38. Illustrations. Predicted pavement life based on different volumetric conditions of the RI19C mixture.[26]

Step 4. Determine the Candidate Design

After obtaining the mixture life contours, the performance-optimum design can be determined for the desired pavement life. In this step, the amount of each component material that is needed to formulate the performance-optimum design is determined.

In figure 36, each point in the volumetric space corresponds to a condition in the binder content-air void content (AC-AV) space, as shown in figure 30 where the RS9.5B mixture is used as an example. Therefore, the pavement life contour in figure 36 can be plotted in the design AC-AV space, as shown in figure 39-A. Although pavement engineers at different agencies may use different design air void contents, this study used 4 percent as the target design air void content at the N_{des}. The final design is determined along the horizontal line at the design air void content, as shown in figure 39-C.

The performance-optimum conditions are determined based on the desired pavement life. In the example of the RS9.5B mixture, the performance-optimum design, i.e., where the maximum pavement life is located, is marked with a circle labeled PEMD in figure 39-A. In figure 39-A, each point corresponds to one point in figure 39-B, which means that, moving along the x-axis, not only does the binder content change, but the gradation varies correspondingly. The corresponding gradation, which is CUW 54 (based on the Bailey method designation), is presented in figure 39-B, and table 28–table 30 present the design results.[25] Figure 39-C and figure 39-D present the life contours for the SM12.5 and RI19C mixtures, respectively. The circles in figure 39-C and figure 39-D indicate the performance-optimum conditions based on the predictive BMD method. The original Superpave design of the RI19C mixture yielded 4.1 percent air void content at the N_{des}. Different failure criteria would result in different pavement life data, and the performance-optimum design would be located at different locations in the design space. For example, if 2 percent APS is applied as the rutting failure criterion instead of 2.5 percent, then the performance-optimum position will move toward the left in the design space in figure 39-A, figure 39-C, and figure 39-D.

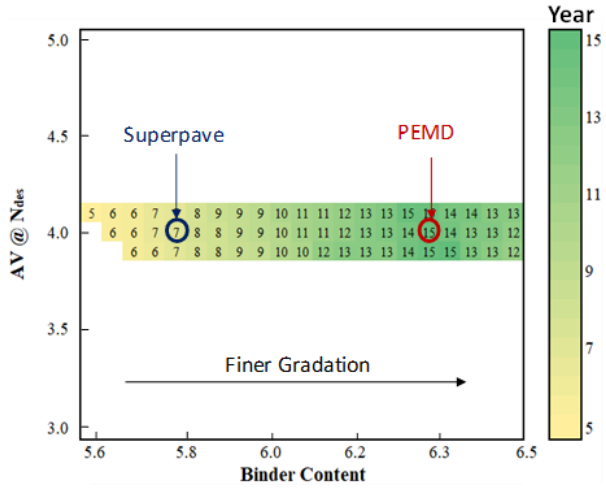

A. RS9.5B mixture.

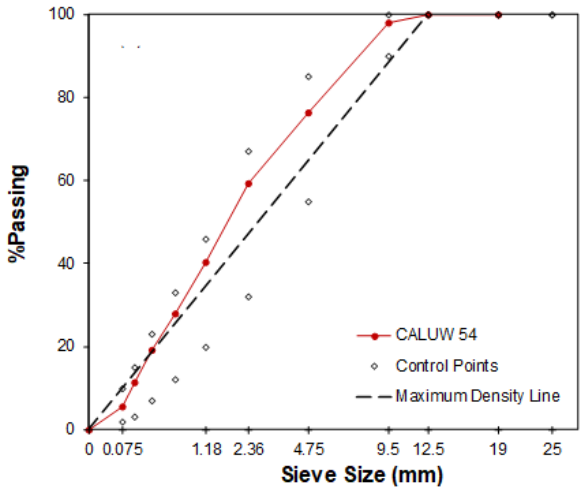

B. Predictive BMD final gradation of RS9.5B mixture.

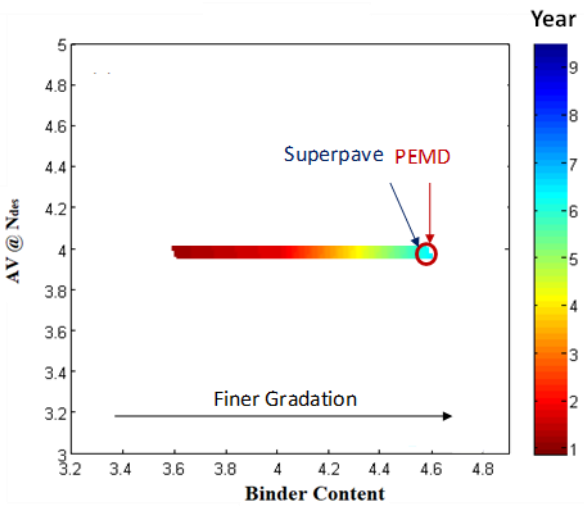

C. Pavement life in design AC-AV space and predictive BMD conditions for SM12.5 mixture.

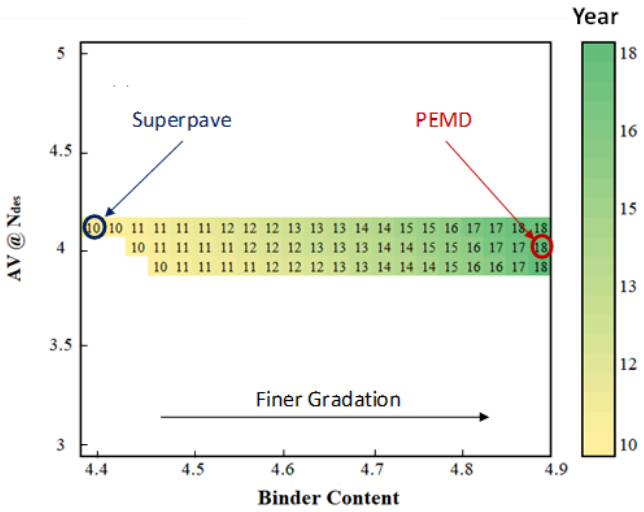

D. Pavement life in design AC-AV space and predictive BMD conditions for RI19C mixture.

Figure 39. Illustrations. Pavement life in the design AC-AV space and design results.[26]

Table 28. Performance-optimum design results for RS9.5B mixtures.

Mixture	Gradation	Raw Binder Content (Percent)	RAP Binder Content (Percent)	Stockpile #78	Stockpile DS	Stockpile WS	RAP	N/A
RS9.5B	CUW 50	5.1	1.4	33	7	30	30	—

DS = dry screenings; WS = washed screenings.
Note: #78, DS, and WS are the name designations of the stockpiles.

Table 29. Performance-optimum design results for SM12.5 mixtures.

Mixture	Gradation	Raw Binder Content (Percent)	RAP Binder Content (Percent)	Stockpile #78's-Chantilly	Stockpile #78's-Loudon	Stockpile DS	RAP	N/A
SM12.5	CUW 110	3.6	0.9	18	37	23	22	—

Note: 78's are the name designations of the stockpiles.

Table 30. Performance-optimum design results for RI19C mixtures.

Mixture	Gradation	Raw Binder Content (Percent)	RAP Binder Content (Percent)	Stockpile #67	Stockpile 78M	Stockpile Screening	Stockpile MS	RAP
RI19C	CUW 60	3.9	1	17	26	14	23	20

Note: #67, 78M, and MS are the name designations of the stockpiles.

The analysis results show that the pavement life for each of the three study mixtures is dominated by fatigue damage. As a result, the fine gradations and high binder contents have been selected by the predictive BMD algorithm. The Superpave volumetric-optimum condition for the RS9.5B mixture is marked with an X in figure 39-A. In this case, the predictive BMD suggests a finer gradation and higher binder content compared to the mixtures designed by Superpave volumetric design to obtain the performance-optimum condition. The performance-optimum and the Superpave volumetric-optimum conditions of the SM12.5 mixture share the same gradation and binder content because both design methods suggest the finest gradation and highest binder content in the design volumetric space as the optimal design.

Step 5. Check Volumetric Properties and Moisture Susceptibility

The design candidate mixture is selected based primarily on its fatigue and rutting behavior. However, designers also should evaluate other properties before the final job mixture formula is determined. Moisture susceptibility is one such property of asphalt mixtures. Designers can check the mixture's behavior under moisture damage using different methods, such as the tensile strength ratio test (AASHTO T 283), boiling test (ASTM D 3625), etc.[50,51] In addition, even though the mixture is designed based directly on performance such that some of the existing volumetric criteria that are related to mix performance become negotiable, the mixture still should meet some volumetric requirements. For example, the binder-to-dust ratio is believed to be related to mixture permeability.[19] Such parameters should be evaluated to ensure the mixture's durability. In the predictive BMD method, moisture susceptibility and the volumetric parameters can be tested after the design candidate is determined. If the criteria are not satisfied, the user can return to the step where the candidate design is determined. Because the performance of the entire volumetric space is predicted and known, users should be able to determine another design condition based on performance without needing to conduct additional tests.

Table 31 presents a comparison between the PPO designed mixtures and the SVO designed mixtures. The table shows that, for the RS9.5B mixture and the RI19C mixture, the PPO exhibits 110 and 77 percent improvement in pavement life compared with the SVO, respectively. For the SM12.5 mixture, the predictive BMD method and Superpave method yield the same design, which indicates little room for improvement in performance with the given materials without changing the coarse-graded gradation type.

Table 31. Comparison between predictive BMD performance-optimum and SVO mixture designs for the three study mixtures.

Mixture ID	Mixture Design	Percent CUW	Percent P_b	VMA (Percent)	VFA (Percent)	D/B	Fatigue Life (Years)	Rutting Life (Years)	Combined Life (Years)
RS9.5B	PPO	50	6.5	17.8	77.6	0.9	15.4	14.7	14.7
RS9.5B	SVO	60	5.8	16.3	71.3	0.97	6.9	20	6.9
SM12.5	PPO	110	4.5	14.5	73.8	0.8	7	19	7
SM12.5	SVO	110	4.5	14.5	73.8	0.75	7	19	7
RI19C	PPO	61	4.9	15	73.7	0.8	17.7	20	17.7
RI19C	SVO	75	4.4	13.6	70.6	0.77	10	20	10

P_b = binder content; D/B = dust to binder ratio; PPO = predictive BMD performance-optimum; SVO = Superpave volumetric-optimum.

Figure 40 presents a flowchart of the steps in the predictive BMD design. Table 32 presents a timeline for conducting the predictive BMD for a single mixture. Although the time required to conduct predictive BMD for a mixture is longer than for mix designs that are based on volumetrics only, the benefits of designing asphalt mixtures using the predictive BMD method are significant. Not only is the predictive BMD method expected to produce longer-lasting asphalt mixtures and pavements, as demonstrated in table 31, but it also produces mixture performance data that can be used for the mechanistic-empirical pavement design of asphalt pavements and for PRS. Therefore, investment in AMPT BMD implementation would allow the integration of mix design, pavement design, and construction QA specifications using the same test methods and underlying engineering principles.

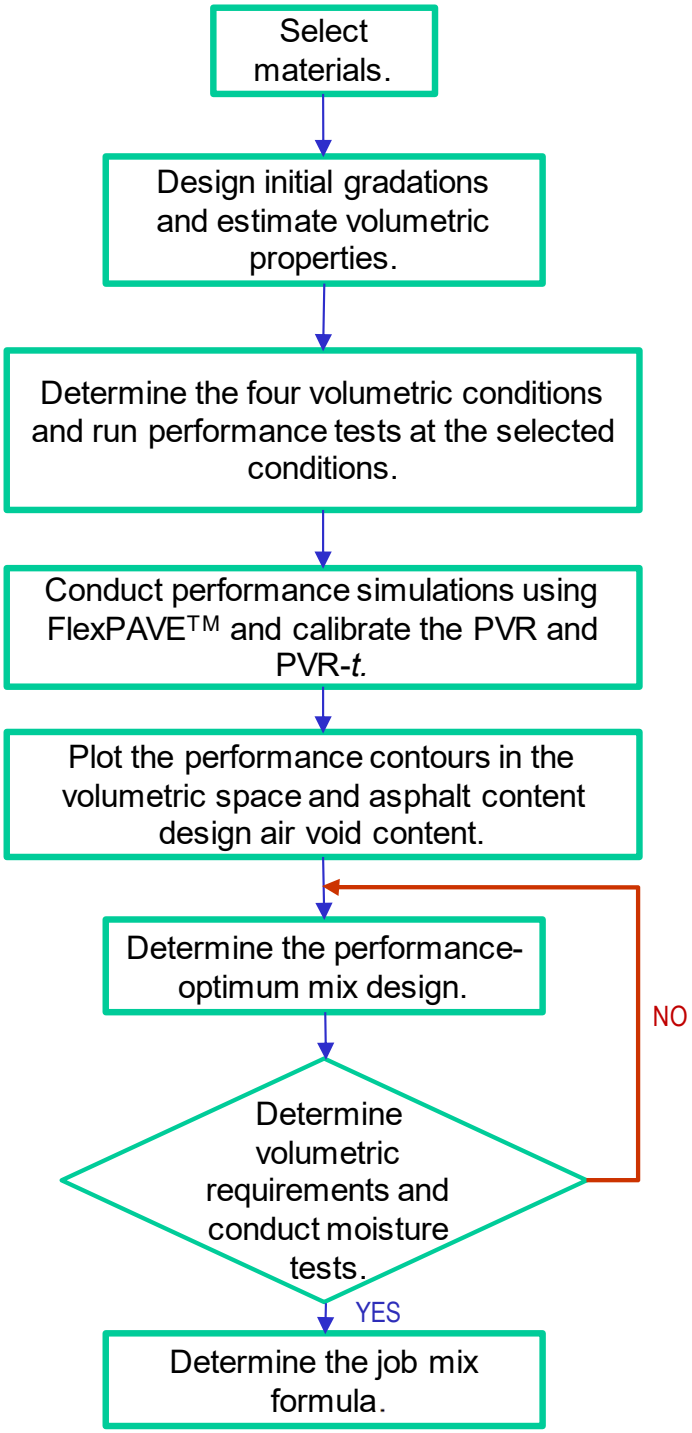

Figure 40. Flowchart. The framework of predictive BMD.[26]

Table 32. Timeline for performing AMPT BMD.

BMD Steps	1–2 d	3 d	4–5 d	6–7 d	8–10 d	11 d	12 d
Prepare gyratory samples and perform volumetric tests.	x	—	—	—	—	—	—
Prepare gyratory samples and perform volumetric tests.	x	—	—	—	—	—	—
Prepare gyratory samples and perform air void study.	—	x	—	—	—	—	—
Prepare gyratory samples for the performance tests.	—	—	x	—	—	—	—
Prepare test specimens (core, cut, dry, and measure air voids).	—	—	—	x	—	—	—
Conduct AMPT performance tests.	—	—	—	—	x	—	—
Perform data analysis.	—	—	—	—	—	x	—
Conduct moisture tests and generate mix design.	—	—	—	—	—	—	x

—No step.
Note: The timeline is estimated based on one person for all laboratory tests using one AMPT. The use of two AMPTs, one for fatigue cracking and the other for rutting, can shorten the testing period.

Summary

This section presents a framework for an AMPT BMD procedure and process. Three example mixtures demonstrate the design procedure. A summary of findings, limitations, and some future recommendations are as follows:

- The AMPT BMD method aims to predict mixture performance across the entire volumetric space and determine the performance-optimum mixture by optimizing the aggregate gradation and binder content for a given set of component materials and given aggregate gradation type (e.g., fine versus coarse).

- The AMPT BMD method can predict the performance of all reasonable component material combinations by using AMPT performance tests, mechanistic material and pavement models, and the PVR. The performance-optimum design is selected by comparing pavement life data based on fatigue cracking and rutting.

- In general, the performance-optimum mixture designed by the AMPT BMD is expected to provide a longer service life than Superpave volumetric-optimum design.

- Details of the proposed design procedure might need to be adjusted as more mixtures are tested and more experience is gained. Users can adjust the design limits, e.g., the design air void contents, performance criteria, in the design procedure based on their experience and conventions.

CHAPTER 3. ASPHALT MIXTURE PROCEDURAL IMPROVEMENT

RELIABILITY ANALYSIS OF MATERIAL MODELS IN FLEXPAVE

Since the mid-2000s, interest in the use of mechanistic-empirical pavement performance analysis has increased. Although mechanistic-empirical methods strive to systematically account for the physical properties and active mechanisms in a pavement, they are not perfect representations of the real system. As such, the mechanistic-empirical prediction of pavement performance is an inherently uncertain approach. Many of these sources of uncertainty are challenging to understand quantitatively, but the effects of uncertainty in the characterization and modeling of the mechanical properties of the asphalt concrete are technically possible to understand. These effects are inherently linked to the model chosen and the repeatability required to measure or determine the properties of the model. In the study described in this chapter, the Bayesian inference-based Markov Chain Monte Carlo (MCMC) was used to investigate ways that the uncertainties from the S-VECD and shift model input parameters propagate to pavement performance simulation errors.[12,52] The goal is to estimate the reliability of %Cracking and rut depth predictions in pavement simulations. Five different mixtures with different test variations were used to develop the predictive models to quantify the uncertainty.

Pavement performance prediction is a complex process that heavily relies on models that capture the essential mechanics of the physical system. These models often have a test or tests to characterize the relevant coefficients and other functional relationships of the model. These testing methods and material models include many uncertainties, approximations, and variabilities. Although these issues have been known for many years, recent research has focused on this issue in more detail. (See references 51–58.) Some of these studies have characterized the effect of testing uncertainties on the material models, while others have evaluated the effects of the material uncertainties on pavement performance. (See references 55–58.)

One of the essential principles behind these uncertainty evaluation studies is that material models are commonly based on test results, which have some uncertainties such as homogeneity, specimen fabrication, and measurement errors. For example, Mohammad et al. quantified the levels of variability in the measurement of volumetrics in asphalt mixtures.[54] They compared the levels of mixture variability for different States and concluded that the NMAS is the most critical factor that affects the magnitude of variability in volumetric measurements.[54] In another study, Caro et al. showed that the assumption of asphalt mixture homogeneity could be considered as one of the primary sources of uncertainty in pavement performance predictions.[55] Though heterogeneity is critical, the fact that an asphalt mixture is a composite material cannot be ignored. Thus, fabricating multiple specimens that are the same is not possible. Therefore, sample-to-sample variation in test procedures will always be a problem with material models.

To control errors, the AASHTO standard specifications define a range of sample-to-sample variability to minimize the errors as much as possible. However, even a small error can affect pavement performance predictions.[55,58] Although not explicitly stated in the literature, these effects become even more noticeable as the models become more complicated and describe more behaviors. The FlexPAVE prediction platform is one complicated modeling approach. This platform integrates the S-VECD, shift model, and LVE-based pavement response model to

predict pavement performance.[12,59] This software explicitly considers many of the physical conditions highlighted as potential sources of uncertainty. However, the FlexPAVE results are deterministic and rely on the average best-fit values of all the relevant models.

Reliability analysis, where the statistical certainty of the predictions is predicted based on the known uncertainties in the model inputs, represents an improvement to current capability and serves as an intermediate step to fully capturing, considering, and ultimately reducing the full breadth of uncertainty in the pavement performance prediction process. This reliability analysis consists of two critical components:

- Uncertainty quantification in the material models.
- Propagation of material uncertainty into the structural simulations.

A systematic study that uses different mixtures and structures could quantify these uncertainties by calculating the range of variation for each mixture and analyzing the effect of these variations in the structural level. The study's main objective should be to investigate the impact of the uncertainty that occurs in asphalt pavements predicted by FlexPAVE in the S-VECD fatigue model and rutting shift model on the %Cracking and rut depth respectively.[12]

Uncertainty Quantification in the Material Model

Many research studies have investigated the effect of uncertain material properties on the asphalt mixture's performance. The studies that this report identifies have focused on fatigue, but the essential frameworks that those studies lay out could be equally applicable to rutting.
Kassem et al. used Monte Carlo simulations to quantify the uncertainty in the dynamic modulus ($|E^*|$) master curve.[57] Those Monte Carlo simulations showed that the dynamic modulus master curve's uncertainty depends on the mixture type and NMAS.[60] Different studies quantify the uncertainty in the S-VECD fatigue model. (See references 57, 61–63.) Ding et al. quantified the S-VCED fatigue model's uncertainty via parameter estimation and calculated the predictive envelope using the MCMC method.[63] The predictive envelope is a range that the new observation falls within with a defined level of probability. The propagation of the damage characteristic curve due to the dynamic modulus uncertainty was assumed to be negligible.[63] Therefore, the dynamic modulus uncertainty and the damage characteristic model can be considered independently. The same approach that Ding et al. used was employed in this study to quantify the uncertainty in the S-VECD fatigue model (dynamic modulus, damage characteristics, and failure criterion models). More information about the methodology can be found elsewhere.[63]

Propagation of Material Uncertainty into Structural Simulations

The reliability analysis for structural level simulations goes back at least as far as 1985 when an update to the AASHTO design models was made.[64,65] In AASHTO Pavement ME™, the reliability analysis was based on the overall variability of the measured distresses from the long-term pavement performance (LTPP) program database.[66] In the database, the reliability level was incorporated using the standard deviation of the measured data compared with the predicted data. Equation 28 shows the adjusted distress level based on the reliability level and standard deviation of the measured data. As mentioned, the standard deviation in this formula is obtained from a database, so this formula cannot capture the effect of project-specific uncertainties.[67]

$$Distress = \overline{Distress} + Z_P \times Std_{measured} \quad (28)$$

Where:

$Distress$ = predicted distress at the reliability level P.

$\overline{Distress}$ = predicted distress for a given mean input value (50 percent reliability level).

Z_p = standard normal deviate corresponding to reliability level P.

$Std_{measured}$ = standard deviation of the measured distress from LTPP sections.

Timm et al. employed Monte Carlo simulations in a computer pavement design tool, ROADENT, to run reliability analysis and see the effect of input variations on the pavement performance for the Minnesota Cold Weather Pavement Testing Facility (MnROAD) research project.[68,69] The Monte Carlo method could also capture the effect of material uncertainty on the Pavement ME performance predictions; however, the Monte Carlo simulations using this program were impractical due to the extensive computing time and the number of iterations involved.[67,70] Khazanovich et al. developed a Latin hypercube simulation to combine DAKOTA and Pavement ME.[71,72] DAKOTA is a common toolkit to run uncertainty quantification on mechanical modeling in engineering. Although this study successfully reduced the number of simulations, the computation time was still impractical.[72]

Running FlexPAVE on High-Performance Computers

Thousands of FlexPAVE simulations must be performed and analyzed to generate the %Cracking and rut depth predictive envelopes necessary to meet the stated objectives of this work. Limitations of running performance prediction programs such as Pavement ME and FlexPAVE include the computation time. For example, running one case of FlexPAVE on a typical computer (quad-core central processing unit (CPU) and 8 gigabytes (GB) random-access memory (RAM)) takes approximately 30 min, depending on the structure and timeframe being analyzed. For this study, FlexPAVE was run using a cloud computing service, the NCSU-HPC center, which allowed 1,000 runs of FlexPAVE simulation in 4 h.

In research studies that involve Monte Carlo simulations, a key question is how many simulations need to be performed to achieve sufficient statistical convergence. To address this question, the researchers relied on past studies from one author and conducted a set of pilot

pavement simulations that involved 5,000 trials.[61,63] For the pilot simulations, the prediction envelope with the confidence interval of 98 percent for the dynamic modulus, damage characteristic, and failure criterion models for a mixture was generated using 5,000 data points. Then, FlexPAVE was run at the NCSU-HPC for each of those 5,000 cases. Figure 41-A shows the structure for these simulations. The climate was consistent with that of Raleigh, North Carolina, the simulation covered 20 yr, and the total equivalent single-axle loads (ESALs) over this time was 30 million. For each simulation, the %Damage throughout the 20 yr analysis was calculated and plotted, as shown in figure 41-B. In this figure, the deterministic value from the material models is shown as a red line, and the predictive envelope from the MCMC-generated cases is shown as a series of light gray lines.

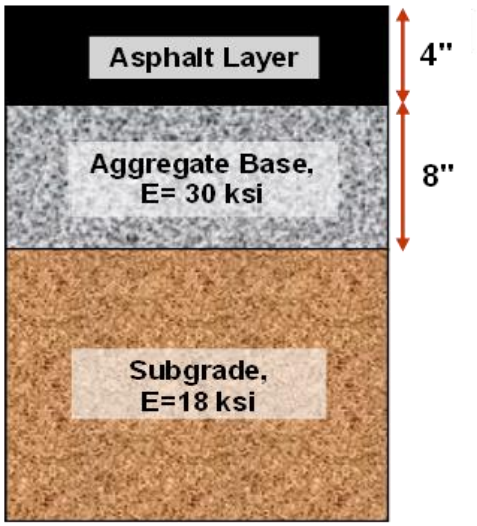

Source: FHWA.

A. Standard pavement structure used to determine %Damage in the asphalt layer.

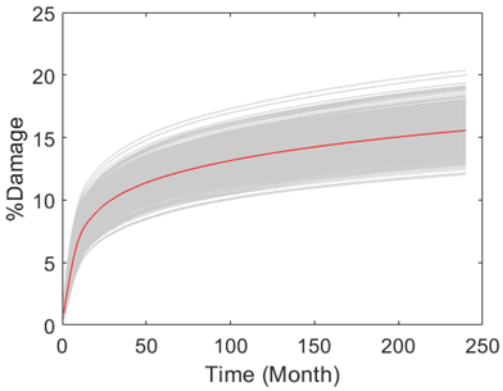

Source: FHWA.

B. %Damage in the asphalt layer under specified loading conditions.

Figure 41. Illustrations. Standard pavement structure used to determine %Damage in the asphalt layer and %Damage in the asphalt layer under specified loading conditions.

To find the minimum number of simulations, the research team selected %Damage at the end of 20 yr as a decision-making parameter. The team considered 5,000 %Damage value at the end of 20 yr as the population, and performed random sampling with different sizes. The team repeated sampling 30 times for each of the sample sizes. The average of %Damage at the end of 20 yr was calculated for each sample size and the variational statistics. Figure 42 shows the box plot distributions for the average %Damage at the end of 20 yr using the 30 samples for each sample size. As the sample size increases, the distribution for the average of %Damage at 20 yr becomes narrower.

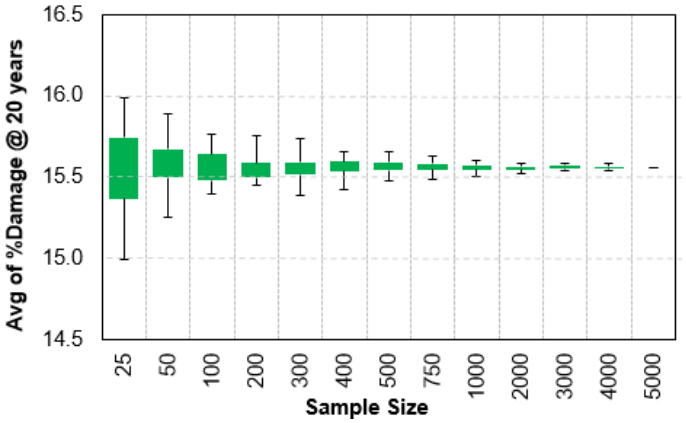

Source: FHWA.

Figure 42. Graph. Box plots for different sample sizes.

Ding et al. proposed the MCMC technique to generate the predictive envelope at the material level.[63] To find the minimum sample size for that analysis, two statistical test methods were suggested: the z-test and Kolmogorov-Smirnov test (K-S test). A z-test checks for significant differences between the means of two samples. The K-S test is a nonparametric test that is used to compare two samples and check whether or not these two samples are from the same distribution.[73] In this study, both tests were used to find a representative sample size of 1,000 runs.

RELIABILITY ANALYSIS OF DAMAGE PREDICTION IN ASPHALT PAVEMENT SECTIONS USING FLEXPAVE AND THE SIMPLIFIED VISCOELASTIC CONTINUUM DAMAGE FATIGUE MODEL

The research team used the S-VECD fatigue model and FlexPAVE to develop a framework to quantify the uncertainty in the structural level.[12] The Bayesian MCMC method was used to generate predictive envelopes, and FlexPAVE was used to study the effect of material uncertainty on the structural simulation.[63] %Damage is calculated based on the damaged area simulated in FlexPAVE and %Cracking is defined as the measurable percentage of cracking on the pavement surface.[59,73] The S-VECD model includes three major modeling components: the dynamic modulus ($|E^*|$), damage characterization (C versus S curve), and failure criterion (D^R).[63] FlexPAVE calculates the %Damage in the asphalt layer using the inputs from these three modeling components under given loading conditions. Details about FlexPAVE simulations can be found elsewhere.[59]

Figure 43 shows the framework to evaluate the effects of material characterization uncertainty on the %Cracking of the asphalt mixtures predicted by FlexPAVE. In the first step of the framework, a range of results that define the predictive intervals at predefined levels of statistical certainty is defined for each of the three aforementioned parameters. These results define the predictive envelope. Each of the parameters' predictive envelopes was generated using the Bayesian MCMC method.(63) In the next step, the three envelopes are randomly combined. For example, suppose the predictive envelopes for each parameter (dynamic modulus, damage characteristics, and D^R failure criterion) contain 1,000 sets of model inputs. In that case, the three groups of 1,000 model inputs were randomly sampled without replacement and combined. As a result, a set of 1,000 different FlexPAVE inputs was generated. Then, the 1,000 FlexPAVE simulations using a specific structure and loading conditions were conducted. At the end of the 1,000 simulations, the %Cracking predictive envelope could be generated for the particular structure and loading conditions.

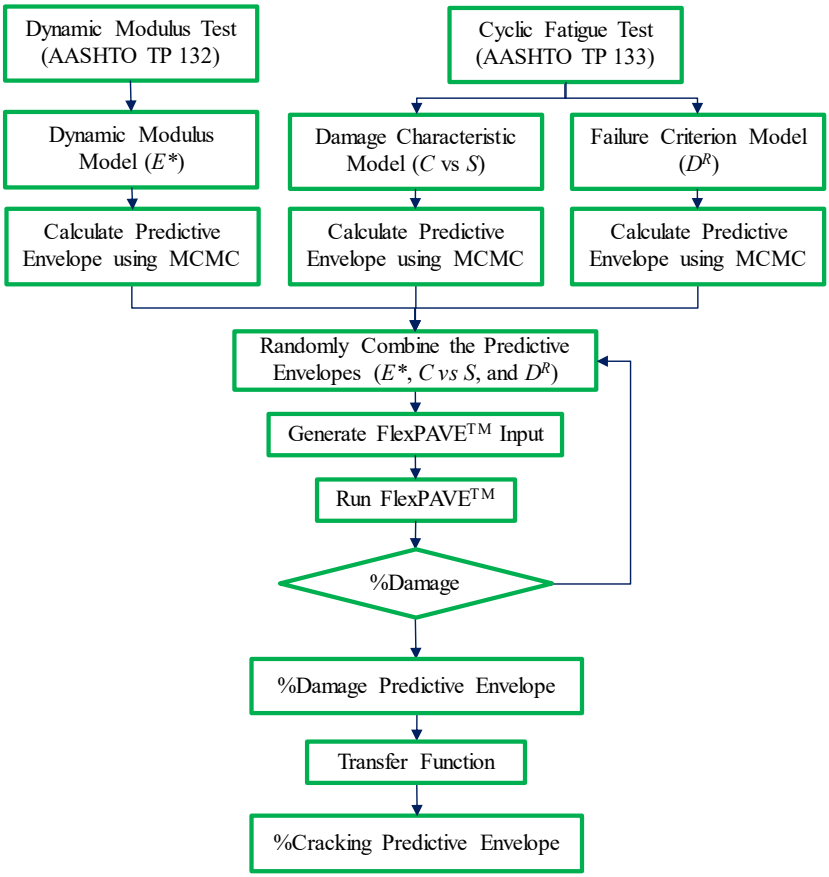

Source: FHWA.

Figure 43. Illustration. Framework for uncertainty quantification of %Cracking.

Materials and Data

Table 33 presents the relevant information for the study mixtures. These mixtures were chosen because they cover different climate zones. Only surface mixtures were used in this study.

Table 33. Mixture information.

Mixture	NMAS (mm)	Binder Grade	Binder Content (Percent)	RAP Content (Percent)	Source	Prediction Levels (Percent)
Mixture A	9.5	PG 58-28	5.8	30	NC	50, 90, 98, and 99.99
Mixture B	9.5	PG76-22	5.4	20	NC	50, 90, 98, and 99.99
Mixture C	12.5	PG 64-22	5.3	30	NC	50 and 98
Mixture D	12.5	PG 64E-28	5.3	20	ME	90 and 99.99
Mixture E	12.5	PG64-28	4.7	33	MO	90, 98 and 99.99

The predictive envelope for each study mixture was generated by the method proposed by Ding et al.[(63)] Figure 44 illustrates the results of this process for mixture A at different significance levels. The figure clearly shows that the size of the predictive envelope increases as the statistical significance level increases. The figure also shows that the visual spread of the uncertainty is more remarkable for the *C* versus *S* curves than for the dynamic modulus. Likewise, the figure shows that the envelope for D^R is visually wide, even at relatively low statistical levels of certainty, highlighting that the uncertainty for this parameter is somewhat greater than for the other two.

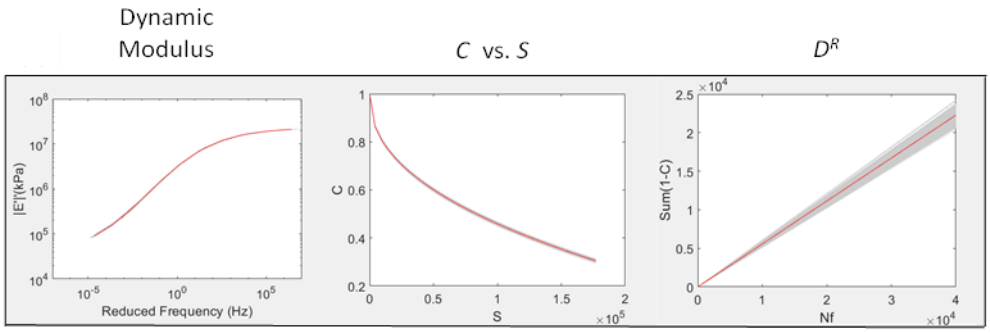

Source: FHWA.
1 kPa = 0.145 psi.

A. 50 percent.

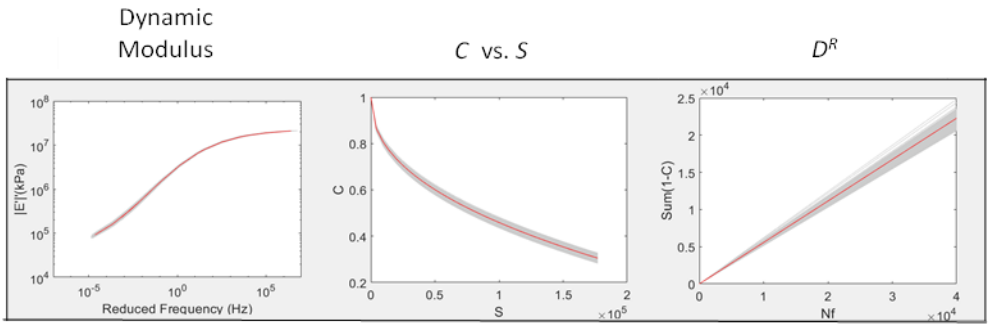

Source: FHWA.
1 kPa = 0.145 psi.

B. 90 percent.

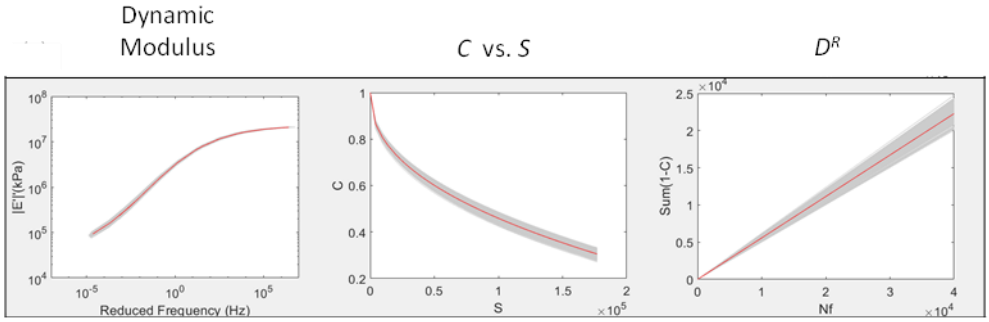

Source: FHWA.
1 kPa = 0.145 psi.

C. 98 percent.

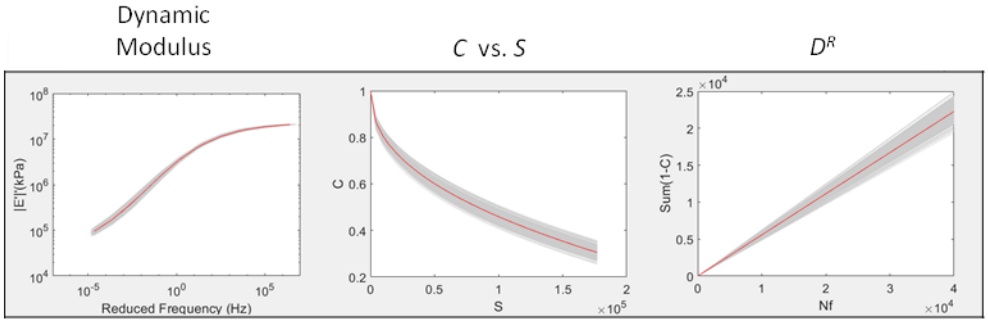

Source: FHWA.
1 kPa = 0.145 psi.

D. 99.99 percent.

Figure 44. Illustrations. Dynamic modulus, C versus S, and DR predictive envelopes for mixture A based on different levels of prediction.

Effect of Structural Factors on %Damage Propagation

In the previous sections, the standard structure was defined (figure 41-A). This section examines the effects of different structural factors on the %Damage predictive envelope:

- Climate.
- Traffic level.
- Asphalt layer thickness.
- Aggregate base and subgrade moduli.
- Aggregate base thickness.

The dynamic modulus, *C* versus *S*, and D^R 98 percent predictive envelopes for mixture A were used to investigate the effects of different structural factors on the %Damage predictive envelope. For the FlexPAVE analysis, figure 41-A was used as the reference structure, and the other structural elements were changed individually. For example, the reference structure was analyzed for three different climatic conditions. The three sites used to represent climate were Arizona, North Carolina, and Maine. The asphalt layer thickness, base thickness, base modulus, and subgrade modulus values used for these simulations were selected after studying typical mixtures used in North Carolina and other locations.[59] Table 34 shows the details of the structural factors used in this study.

Table 34. Structural information for S-VECD reliability analysis.

Structure Number	Structural Factor	Climate	Traffic (MESAL)	Asphalt Layer Thickness (Inches)	Base Thickness (Inches)	Base Modulus (ksi)	Subgrade Modulus (ksi)
1	Reference	Raleigh, NC	30	4	8	30	18
2	Climate	Phoenix, AZ	30	4	8	30	18
3	Climate	Bangor, ME	30	4	8	30	18
4	Traffic	Raleigh, NC	3	4	8	30	18
5	Traffic	Raleigh, NC	10	4	8	30	18
6	Asphalt layer thickness	Raleigh, NC	30	3	8	30	18
7	Asphalt layer thickness	Raleigh, NC	30	5	8	30	18
8	Asphalt layer thickness	Raleigh, NC	30	6	8	30	18
9	Base thickness	Raleigh, NC	30	4	16	30	18
10	Base thickness	Raleigh, NC	30	5	16	30	18
11	Base modulus	Raleigh, NC	30	4	8	15	18
12	Base modulus	Raleigh, NC	30	4	8	45	18
13	SG modulus	Raleigh, NC	30	4	8	30	5
14	SG modulus	Raleigh, NC	30	4	8	30	10

The FlexPAVE simulations were performed using all the 14 conditions listed in table 34. In the next step, the research team generated %Damage predictive envelopes for each of the structures. Figure 45 shows an example of the output generated for one of the simulations. Figure 45-A shows the %Damage predictive envelope as a function of time. Figure 45-B shows the probability distribution for the %Damage distribution at the end of 2, 5, 10, and 20 yr. The immediate observation from this figure is that as the %Damage grows, so too does the standard deviation.

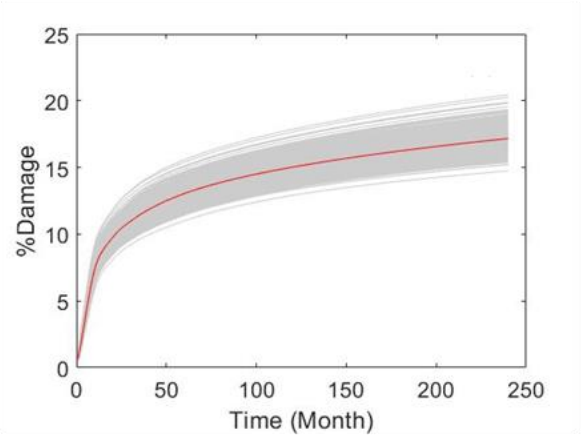

Source: FHWA.

A. %Damage versus time.

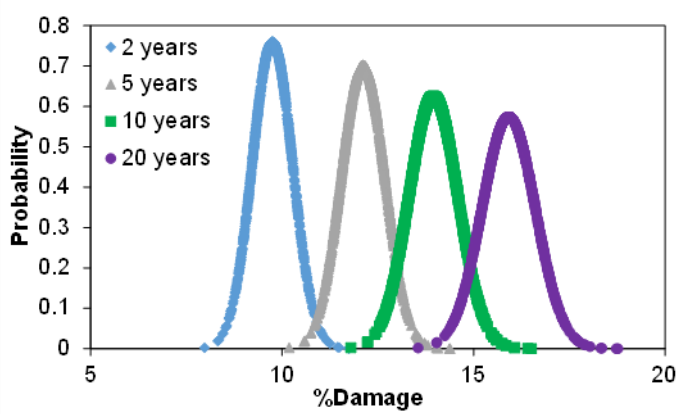

Source: FHWA.

B. %Damage distribution for different periods during the design life.

Figure 45. Graphs. %Damage versus time and %Damage distribution for different periods during the design life.

The average and standard deviations of %Damage at the end of each month for the 1,000 FlexPAVE runs were used to provide quantification for this observation. This study was repeated using the different structures listed in table 34. Figure 46-A through figure 46-F present the effects of various structural factors, including climatic condition, traffic level, asphalt layer thickness, aggregate base modulus, aggregate base thickness, and subgrade modulus, respectively, on the %Damage distribution using the 98 percent predictive envelope for

mixture A. All these figures show that the standard deviation of %Damage and the average of %Damage are strongly correlated and this relationship is not dependent on the structural factors. Figure 46-G shows the standard deviation of %Damage versus the average of %Damage using 14,000 FlexPAVE simulations from 14 different cases, indicating that this relationship is independent of the structural factors considered in this study. The standard deviation of %Damage distribution at any period of design life can be assumed to strongly correlate with the average of %Damage at the given period. In this figure, a power function was fitted to the data and the power relationship obtained. To confirm the power relationship of standard deviation and average of %Damage, the same study was repeated using the 98 percent predictive envelope for mixture B. Figure 47 shows the standard deviation of %Damage versus the average %Damage for 98 percent predictive envelopes. Therefore, the relationship between the standard deviation and the average %Damage distribution depends on the material variation. Equation 29 shows the general form of the mentioned relationship.

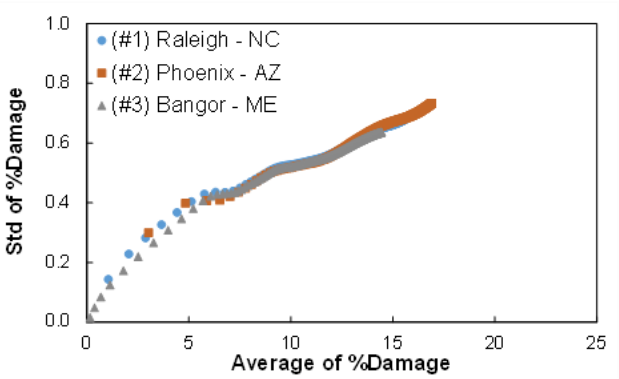

Source: FHWA.

A. Climatic conditions.

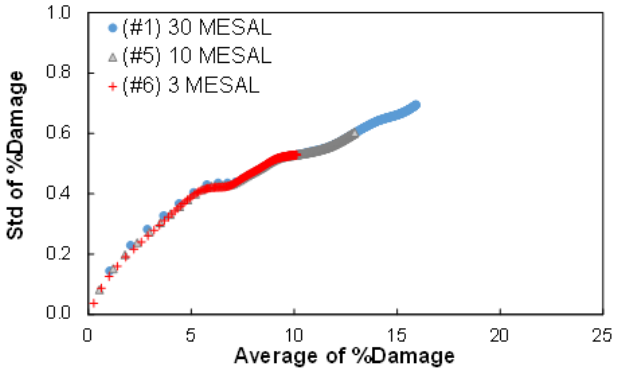

Source: FHWA.

B. Traffic levels.

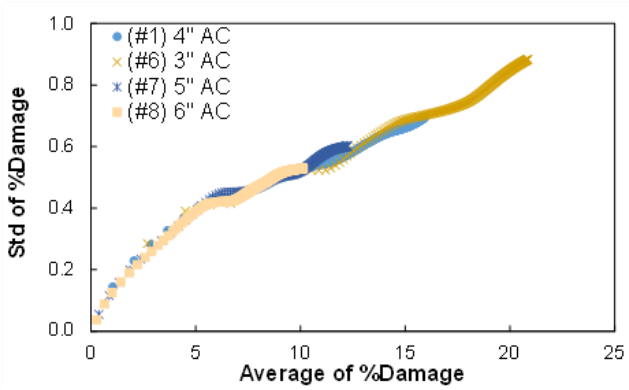

Source: FHWA.

C. Asphalt layer thicknesses.

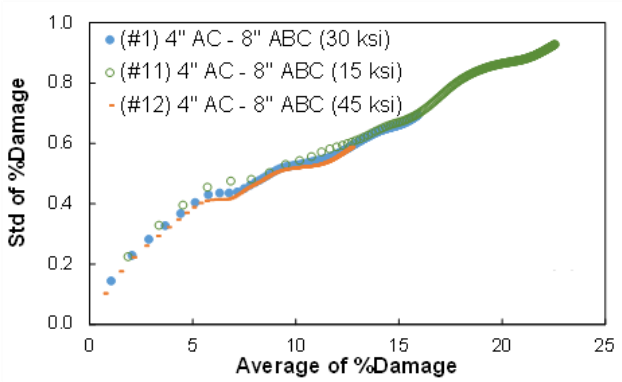

Source: FHWA.

D. Aggregate base moduli values.

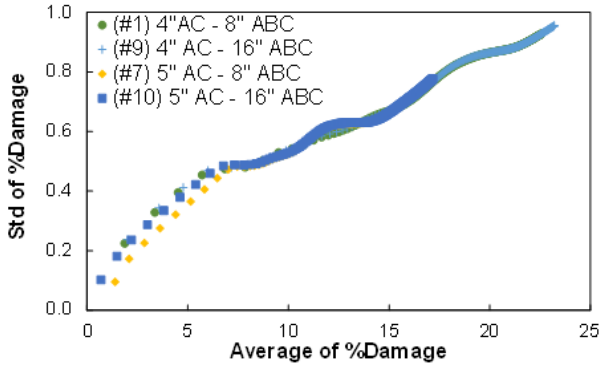

Source: FHWA.

E. Aggregate base thicknesses.

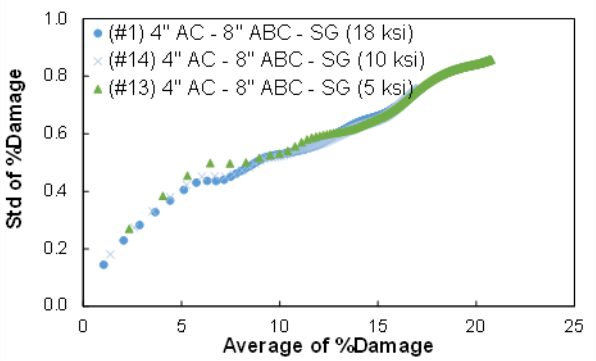

Source: FHWA.

F. Subgrade moduli values.

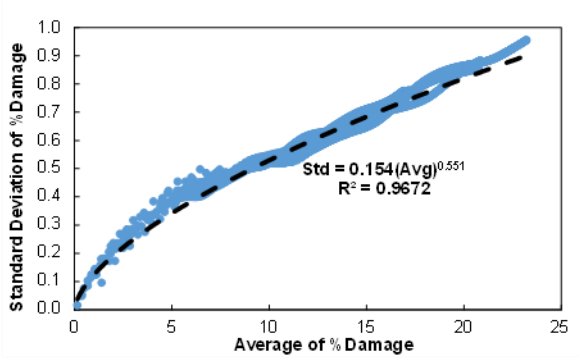

Source: FHWA.

G. All conditions.

Figure 46. Graphs. Standard deviation versus average of %Damage using different structural factors (table 34).

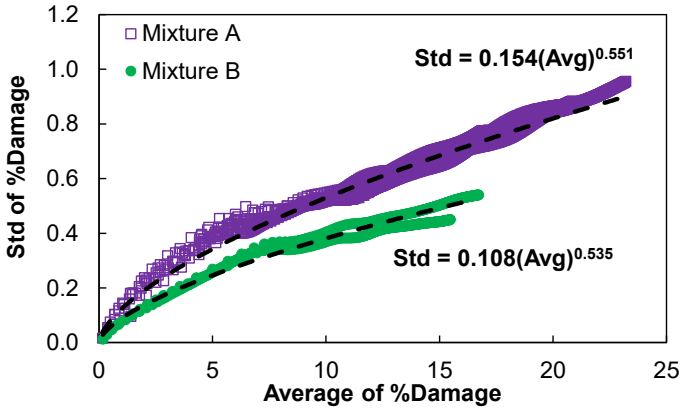

Source: FHWA.

Figure 47. Graph. Standard deviation versus average %Damage for mixture A and mixture B.

$$Std = a\left(\%D\right)^{b} \tag{29}$$

Where:

%D = %Damage at the given time.
Std = standard deviation of %Damage distribution.
a = deviation function intercept in log-log space.
b = deviation function slope in log-log space.

For each mixture and each prediction level, *a* and *b* in equation 29 were calculated using the Curve Fitting toolbox in MathWorks® MATLAB®.[74] This toolbox finds the best fit via regression analysis. Table 35 shows the fitting results for the mixtures in this study. After optimizing the coefficients, coefficient *b* was found to vary only slightly by mixture type. Thus, in a second iteration, variable *b* was treated as a universal constant, and the data were collectively reoptimized. This assumption simplifies the model without losing much accuracy. Therefore, a universal *b* value (*b* = 0.544) was used for all the mixtures via optimization.

Table 35. Fitting results using equation 29 for different mixtures.

Mixture	Prediction Level (Percent)	*a* (Varying b Values)	*b* (Varying b Values)	R^2 (Varying b Values)	*a* (Universal b Value)	*b* (Universal b Value)	R^2 (Universal b Value)
A	50	0.105	0.501	0.967	0.087	0.544	0.934
A	90	0.165	0.513	0.985	0.149	0.544	0.982
A	98	0.191	0.545	0.986	0.188	0.544	0.986
A	99.99	0.207	0.541	0.985	0.202	0.544	0.985
B	50	0.072	0.591	0.970	0.078	0.544	0.968
B	90	0.100	0.593	0.980	0.111	0.544	0.977
B	98	0.117	0.596	0.982	0.129	0.544	0.979
B	99.99	0.133	0.602	0.981	0.150	0.544	0.977
C	50	0.015	0.543	0.951	0.015	0.544	0.954
C	98	0.145	0.541	0.980	0.142	0.544	0.984
D	90	0.232	0.510	0.998	0.207	0.544	0.953
D	99.99	0.257	0.593	0.999	0.293	0.544	0.962
E	90	0.183	0.509	0.998	0.163	0.544	0.965
E	98	0.211	0.538	0.997	0.204	0.544	0.978
E	99.99	0.219	0.576	0.997	0.235	0.544	0.940

Finding a Relationship Between Mixture Variation and Performance Prediction Reliability

The previous sections describe the standard deviation of %Damage distribution as a function of the average %Damage, and this function is mix-dependent. This section models this behavior on a material-by-material basis. The first step of this process involves developing material-level

indexes to capture the variations that stem from mixture characterization. In the next step, the relationship between the defined material indexes and %Damage distribution is investigated. In this way, the research team undertook a systematic study to capture the effects of dynamic modulus, damage characteristics, and failure criterion variations on the %Damage distribution. Details regarding the development for each material index are described in the following subsections.

Dynamic Modulus

The dynamic modulus master curve can be obtained using the AMPT dynamic modulus test (AASHTO TP 132).[30] In this test, the mixture strain response to applied haversine loading is measured and used to determine the modulus and phase angle of the mixture as a function of temperature (4 °C, 20 °C, and 35 °C or 40 °C) and frequency (0.1 Hz, 1 Hz, and 10 Hz). Thus, the results from the dynamic modulus test can be summarized into nine measured data points. Subsequently, the storage modulus (E') is calculated. The storage modulus can account for both the norm and the phase angle in the dynamic modulus test. Therefore, the variation in the storage modulus of the nine measured data points can be used to define the LVE variation index (I_{LVE}). The LVE variation index is defined in equation 30.

$$I_{LVE} = \frac{1}{N}\sum_{i=1}^{N}\sum_{j=1}^{9}\left|\frac{E'_{fit\_i,j} - E'_{fit\_avg,j}}{E'_{fit\_avg,j}}\right| \quad (30)$$

Where:

I_{LVE} = LVE variation index.

N = number of MCMC simulations.

$E'_{fit\_i,j}$ = fitted storage modulus from the fitted curve for the ith dataset at the jth temperature and frequency.

$E'_{fit\_avg,j}$ = storage modulus from the fitted curve using all of N specimens at the jth temperature and frequency.

To define the relationship between the LVE variation index and the %Damage distribution, FlexPAVE simulations were run using the materials listed in table 36 with the structure shown in figure 41. For the dynamic modulus, different predictive envelopes were systematically input to FlexPAVE. For these simulations, the damage characteristics and failure criterion models were set as the mixture-specific mean values (i.e., the dynamic modulus variation was the only variation in these sets of simulations). In this way, the effect of the dynamic modulus on the %Damage distribution could be studied independently for different mixtures and prediction levels. Figure 48-A shows the standard deviation of %Damage versus the average %Damage for the different predictive envelopes for mixture A. Equation 31 shows the general relationship for the standard deviation of %Damage and the average %Damage. a_1 was found to be the only variable of this function, so finding this parameter is the key to finding the %Damage distribution.

Table 36. Mixture information.

Mix	NMAS (mm)	Binder Grade	Binder Content (Percent)	RAP Content (Percent)	Source
Mixture A	9.5	PG 58-28	5.8	30	NC
Mixture B	9.5	PG 58-28	6.1	30	NC
Mixture C	9.5	PG 58-28	5.3	30	NC
Mixture D	12.5	PG 64E-28	5.3	20	ME
Mixture E	12.5	PG 64-28	4.7	33	MO

$$Std_{LVE} = a_1 \times (\%D)^{0.544} \quad (31)$$

Where:

Std_{LVE} = standard deviation of %Damage distribution due to LVE variation.
a_1 = fitting coefficient.

The research team repeated this same analysis for all the mixtures listed in table 36. For each case, the team calculated a_1 in equation 31. In addition, the team calculated the I_{LVE} for every prediction level using equation 30. In the next step, the team investigated the relationship between I_{LVE} and a_1, shown in figure 48-B for the mixtures in this study. Four points appear for each mixture and correspond to the four different predictive envelopes mentioned in table 33 (i.e., 50, 90, 98, and 99.9 percent). These results are from 15 different conditions, representing a total of 15,000 FlexPAVE simulations. The research team developed equation 32 based on this figure. In this equation, a_1 can be calculated by knowing the I_{LVE} from the AMPT dynamic modulus test.

$$a_1 = 0.2026(I_{LVE}) \quad (32)$$

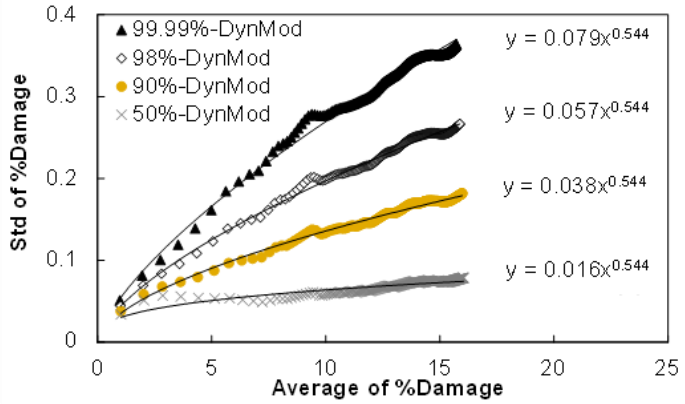

Source: FHWA.

A. Effect of dynamic modulus variation on %Damage variation.

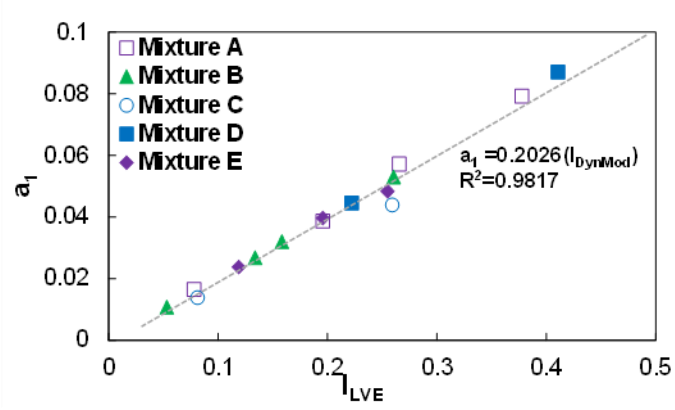

Source: FHWA.

B. a_1 versus I_{LVE} for different mixtures.

Figure 48. Graphs. Effect of dynamic modulus variation on %Damage variation using different levels of the predictive envelopes for mixture A and a_1 versus I_{LVE} for different mixtures.

Damage Characteristic

A similar approach as that described in the Dynamic Modulus subsection was considered to find the effect of the damage characteristic parameters on the %Damage distribution. The first step defined the *C* versus *S* variability index. Equation 33 shows the proposed index that represents the variability for the *C* versus *S* curve. This equation calculates the area between the fitted *C* versus *S* curve for the *ith* specimen (dataset) and the *C* versus *S* curve using all the samples (datasets).

$$I_{CvsS} = \frac{1}{N}\sum_{i=1}^{N}\int_{0}^{S_{max}} |C_i - \overline{C}_{fit}|\,dS \tag{33}$$

Where:

I_{CvsS} = index parameter representing the damage characteristic curve variation.
C_i = pseudostiffness for the *i*th specimen.
$\overline{C}_{fit}$ = fitted pseudostiffness using all the specimens.
S_{max} = internal state variable at $S = 200{,}000$.

The next step inputs the damage characteristic envelopes into FlexPAVE while the dynamic modulus and D^R parameters were fixed at the mixture-specific mean values. Then, the research team plotted the standard deviations of %Damage versus the average %Damage for all mixtures and different prediction levels. Figure 49 shows an example for the different prediction levels for mixture A. Equation 34 shows the general function to relate the standard deviation of %Damage and the average %Damage.

$$Std_{CvsS} = a_2 \times (\%D)^{0.544} \quad (34)$$

Where:

Std_{CvsS} = standard deviation of %Damage distribution due to damage characteristic variation.
a_2 = fitting coefficient.

In the next step, a_2 versus I_{CvsS} was plotted for all the 15 conditions listed in table 36. Equation 35 was developed to calculate a_2 by knowing I_{CvsS}.

$$a_2 = 9.09 \times 10^{-5} (I_{CvsS}) \quad (35)$$

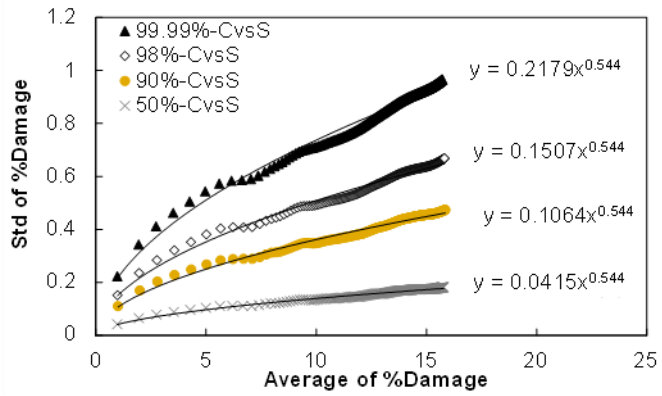

Source: FHWA.

A. Effects of damage characteristic variation on the %Damage variation.

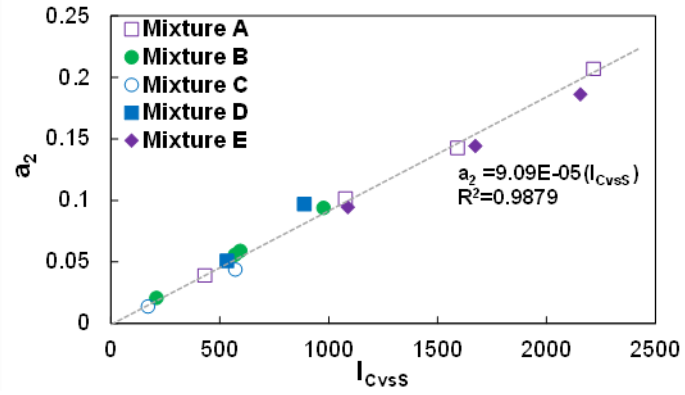

Source: FHWA.

B. a_2 versus I_{CvsS} for different mixtures.

Figure 49. Graphs. Effects of damage characteristic variation on the %Damage variation using different levels of the predictive envelopes for mixture A and a_2 versus I_{CvsS} for different mixtures.

Failure Criterion (D^R)

To find the effect of the D^R parameter on the %Damage distribution, a similar approach as that described in the previous subsection Damage Characteristics was employed. The first step defines the variability of the D^R variability index. Because D^R is a single parameter, the research team chose standard deviation as the variability index, equation 36. This equation simply defines the index variability as the standard deviation of D^R values compared to the regressed D^R.

$$I_{DR} = \sqrt{\frac{1}{N}\sum_{i=1}^{N}\left(D_i^R - D_{fit}^R\right)^2} \tag{36}$$

Where:

I_{DR} = index parameter representing failure criterion variation.

D_i^R = D^R value for the *ith* specimen.

D_{fit}^R = regressed D^R value considering all the samples.

In the next step, a plot similar to the plots for the dynamic modulus and *C* versus *S* curve in the previous subsections shows that the standard deviation of %Damage correlates with the average %Damage in the power form. Equation 37 shows the general form of this function.

$$Std_{DR} = a_3 \times \left(\%D\right)^{0.544} \tag{37}$$

Where:

Std_{DR} = standard deviation of %Damage distribution due to D^R variation.

a_3 = fitting coefficient.

The next step plots a_3 versus I_{DR} for all the conditions listed in table 36, as shown in figure 50. Therefore, equation 38 could be defined as follows:

$$a_3 = 5.07\left(I_{DR}\right) \tag{38}$$

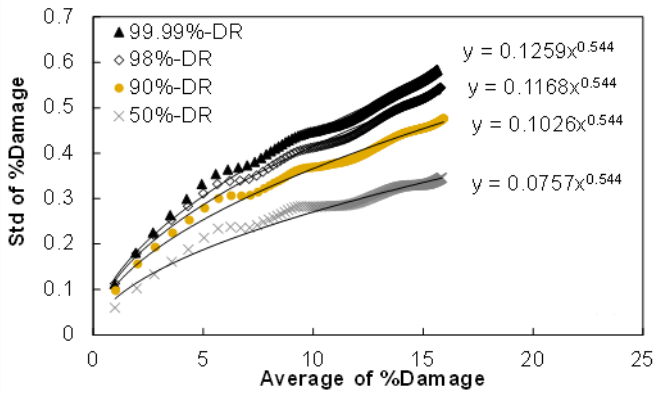

Source: FHWA.

A. Effect of failure criterion (D^R) variation on %Damage variation.

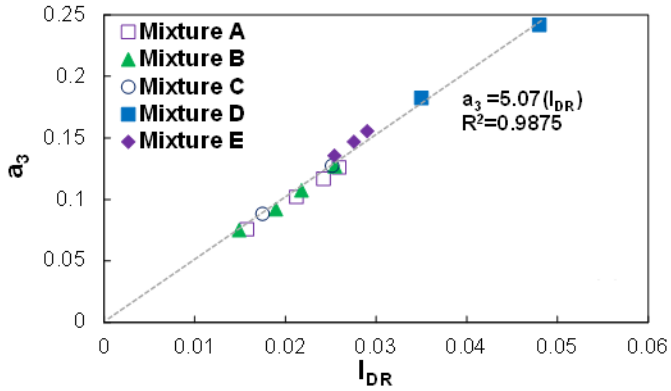

Source: FHWA.

B. a_3 versus I_{DR} for different mixtures.

Figure 50. Graphs. Effect of failure criterion (D^R) variation on %Damage variation using different levels of the predictive envelopes for mixture A and a_3 versus I_{DR} for different mixtures.

%Damage Distribution

The Failure Criterion (D^R) section developed three models to calculate the %Damage distribution using I_{LVE}, I_{CvsS}, and I_{DR}. The research team investigated these parameters individually, but in the pavement simulations, the %Damage distribution is a function of the combined uncertainty of dynamic modulus (a_1), damage characteristic (a_2), and D^R (a_3). Thus, the way these three variations interact within the FlexPAVE simulation must be understood to produce the final propagated uncertainty. The first step selects the 99.99 percent predictive envelopes for the three models. These three envelopes were randomly combined and input to FlexPAVE. The team repeated the same study for 98, 90, and 50 percent predictive envelopes. Figure 51 shows the standard deviation of %Damage versus the average %Damage for four different prediction levels for mixture A. As in the previous graphs, a power relationship can be observed.

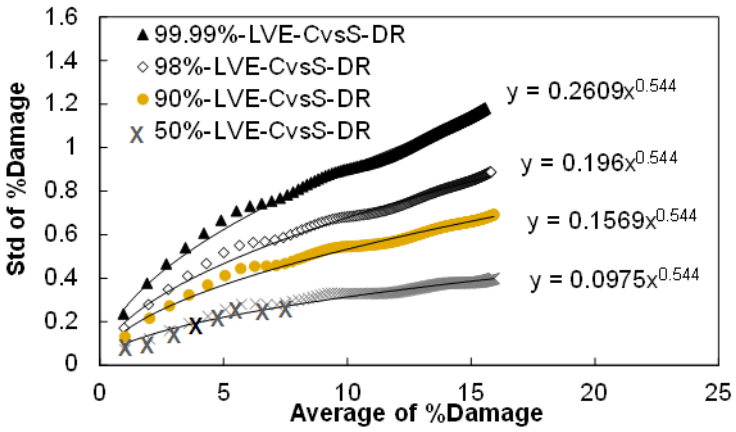

Source: FHWA.

Figure 51. Graph. Effects of dynamic modulus, damage characteristic, and failure criterion (D^R) variations on %Damage variation.

Equation 39 shows the general function of the standard deviation of %Damage and the average %Damage.

$$Std_{Total} = a_{Total}\left(\%D\right)^{0.544} \tag{39}$$

Where:

Std_{Total} = standard deviation of %Damage distribution.
a_{Total} = fitting coefficient.

After some trial and error, the research team found that a linear combination that involved weighted factors for each parameter's contribution to the total variation (as shown in equations 40 to 43) described succinctly and sufficiently the relationship between individual parameter variation and total simulation uncertainty.

$$Std_{Total} = w_1 \times Std_{LVE} + w_2 \times Std_{CvsS} + w_3 \times Std_{DR} \tag{40}$$

$$a_{Total}\left(\%D\right)^{0.544} = w_1 a_1 \left(\%D\right)^{0.544} + w_2 a_2 \left(\%D\right)^{0.544} + w_3 a_3 \left(\%D\right)^{0.544} \tag{41}$$

$$a_{Total}\left(\%D\right)^{0.544} = \left(\%D\right)^{0.544}\left(w_1 a_1 + w_2 a_2 + w_3 a_3\right) \tag{42}$$

$$a_{Total} = w_1 a_1 + w_2 a_2 + w_3 a_3 \quad (43)$$

Where w_1, w_2, w_3 is linear regression coefficients.

To find w_1, w_2, and w_3, the research team carried out a series of performance simulations using various combinations of variability indexes. The team then used the resulting variation in %Damage to calibrate the values of the respective weight factors. For example, for mixture A, four different predictive envelopes for the dynamic modulus, four different predictive envelopes for the damage characteristics, and four different predictive envelopes for the D^R parameter are available. Therefore, the team could create 64 possible combinations with varying levels of prediction certainty for each respective parameter. FlexPAVE simulations were performed for each condition. The next step calculated a_{Total} for each combination using equation 43. Also, a_1, a_2, and a_3 are known from the I_{LVE}, I_{CvsS}, and $I_{DR,}$ respectively. Therefore, the team could find w_1, w_2, and w_3 for each mixture through regression analysis.

Table 37 shows the regression results for each mixture individually. The table shows that the coefficients for the different mixtures are similar. As a result, the team examined the possibility of using a global set of coefficients by performing another regression analysis of all the data together. The result of this analysis is in the last row of table 37. Figure 52 shows the results of the predicted a_{Total} versus fitted a_{Total} using the global linear regression coefficients. The last two columns in table 37 present the mean standard squared error (SSE) for two different scenarios. The Mean SSE column shows the SSE for a respective mixture after optimizing the mixture-specific weight factors. The Mean SSE for All 171 Conditions column presents the mean SSE when the mixture-specific weight factors were used to predict all 171 conditions. Because the global calibration was developed using all these 171 conditions, the values of the SSE in both columns are the same. The research team provided both columns to give a sense of the overall efficacy of using the globally calibrated coefficients.

Table 37. Linear regression coefficients for different mixtures.

Mixture	w_1	w_2	w_3	Mean SSE*	Mean SSE for All 171 Conditions
Mixture A	0.32	0.63	0.72	5.4E-05	2.0E-04
Mixture B	0.26	0.42	0.91	4.8E-06	2.0E-04
Mixture C	0.15	0.35	0.96	4.1E-08	5.8E-03
Mixture D	0.34	0.29	0.92	2.9E-07	5.2E-03
Mixture E	0.24	0.62	0.77	6.3E-06	3.6E-04
All (global)	0.28	0.55	0.83	3.8E-05	3.8E-05

Note: Mean SSE is the average of the sum of squared errors.

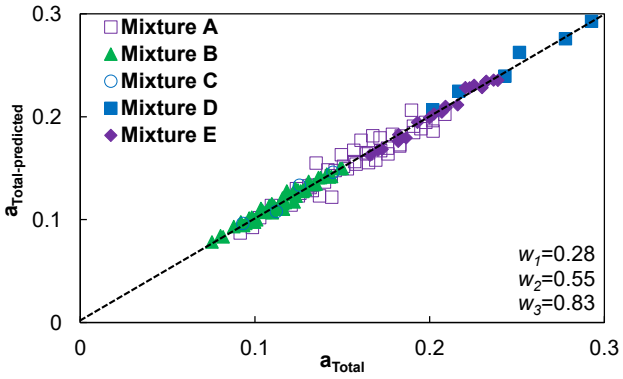

Source: FHWA.

Figure 52. Graph. Prediction results obtained from linear regression analysis.

The next step investigates the effect of using the global coefficient on the %Damage propagation. To find the %Damage distribution, $\%Damage_P$ is defined in equation 44.

$$\%Damage_P = \overline{\%Damage} + Z_P \times Std_{Total} \quad (44)$$

Where:

$\%Damage_P$ = %Damage at the P reliability level.

$\overline{\%Damage}$ = %Damage for the mean input value (50 percent reliability level).

Z_p = standard normal deviate corresponding to the P reliability level.

To quantify the error between the observed and predicted %Damage, %Error is defined in equation 45.

$$\%Error = \frac{\left(D20_{98\%-a_{Total-Predicted}} - D20_{98\%-a_{Total}}\right)}{D20_{98\%-a_{Total}}} \quad (45)$$

Where:

$D20_{98\%-a_{Total-Predicted}}$ = %Damage at 20 yr corresponding to 98 percent reliability level using $a_{Total\text{-}Predicted}$.

$D20_{98\%-a_{Total}}$ = %Damage at 20 yr corresponding to 98 percent reliability level using a_{Total}.

The final step studies the %Error for all of 171 conditions for 2 different scenarios using the globally calibrated coefficients and the mixture-specific coefficients. In this study, the mixture-specific coefficient cases are considered as the reference point for comparisons in %Error. Figure 53-A shows the %Error when using the global coefficients. Figure 53-B shows the %Error using the mixture-specific coefficients. Based on this figure, the maximum %Error

for all 171 conditions is less than 2 percent. Comparing these two figures can confirm that the global regression coefficients can be used to find the %Damage distribution.

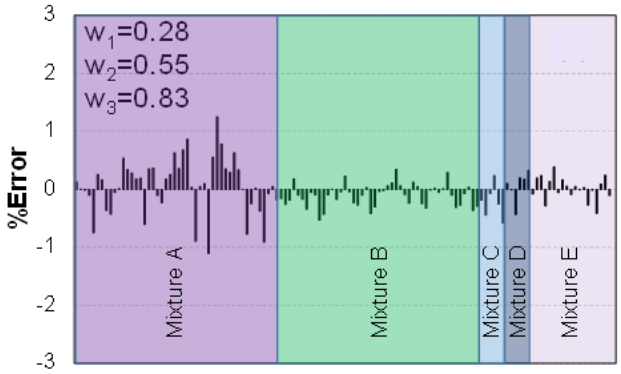

Source: FHWA.

A. Global regression coefficients.

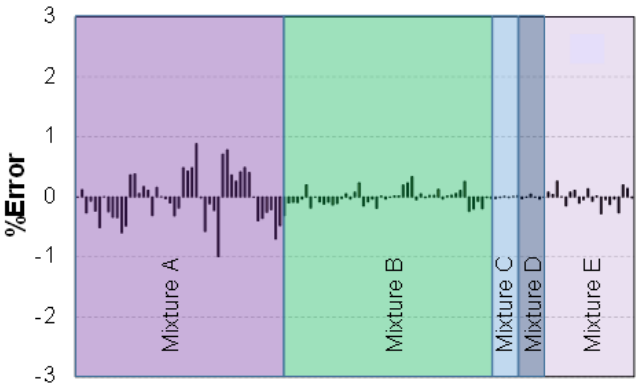

Source: FHWA.

B. Mixture-specific coefficients.

Figure 53. Graphs. %Error for different mixtures.

%Cracking Envelope

To calculate %Cracking, the research team used the preliminary transfer function for %Damage. Equation 150 in Volume I of this report presents the general form of the transfer function.[18,73] Figure 54 shows the 98 percent %Damage and %Cracking envelopes for mixture A in structure 1 (table 36). These data were generated following the framework presented in this section.

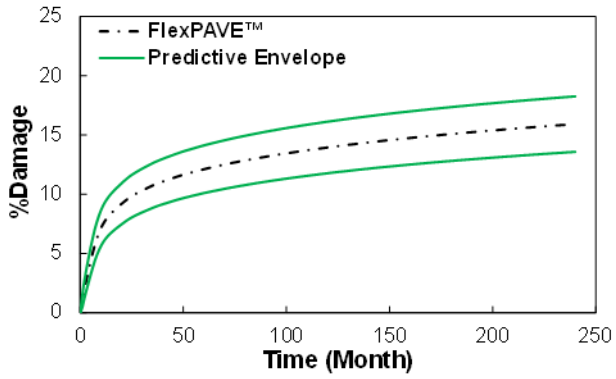

Source: FHWA.

A. %Damage.

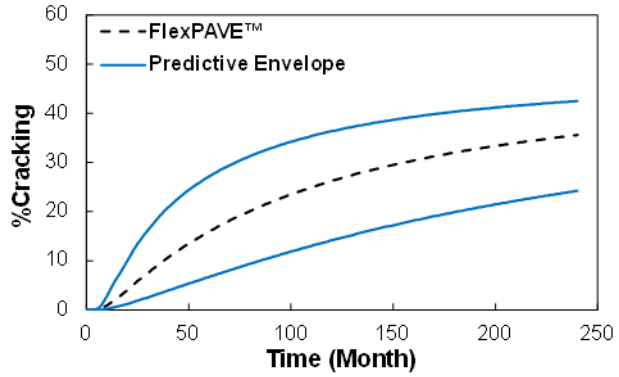

Source: FHWA.

B. %Cracking.

Figure 54. Graphs. Predictive envelopes.

Model Verification

The final step verified the models. The research team obtained the %Cracking envelope under structure 1 loading conditions for all the study mixtures using two different approaches. In the first approach, the team obtained the %Cracking envelope by using FlexPAVE simulations through NCSU-HPC and considered the results as the prediction interval. These results can be regarded as the reference data for model verification. In the second approach, the team used the proposed models to generate the %Cracking envelope with the reliability level of 98 percent.

Figure 55 shows the %Damage and %Cracking bands using the two approaches. These figures show the results for the best case (where the %Error is the least) and for the worst case (where the %Error is the highest). For the worst case, based on the predictive model, the %Damage at the end of 20 yr falls within 15.8 percent ±2.2 percent with 98 percent reliability. However, based on the FlexPAVE simulations on NCSU-HPC, this value falls within 15.8 percent ±1.6 percent with 98 percent reliability. For the %Cracking at the end of 20 yr, the upper band from the FlexPAVE-HPC simulations is 40.3 percent, and is 41.8 percent from the predictive model. Therefore, for the worst case, the errors in predicting the upper band of %Damage and %Cracking are 0.6 and 1.5 percent, respectively.

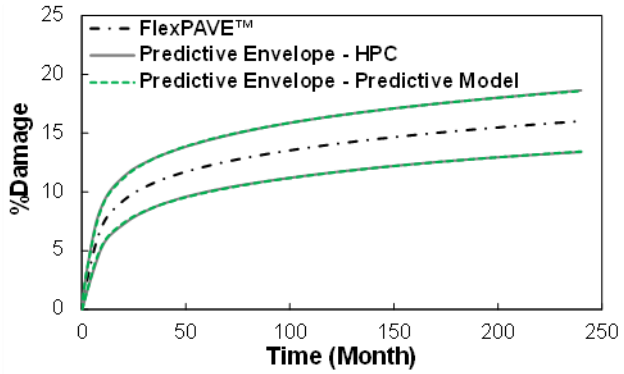

Source: FHWA.

A. %Damage for best case.

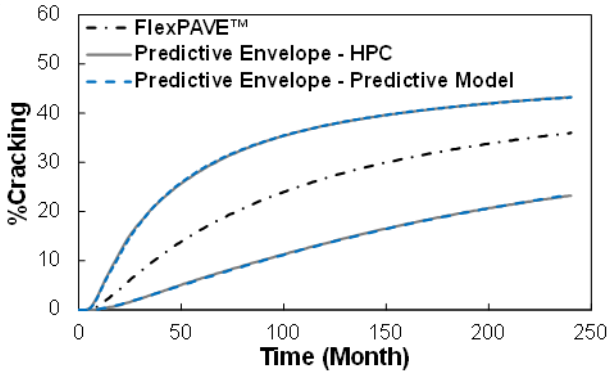

Source: FHWA.

B. %Cracking for best case.

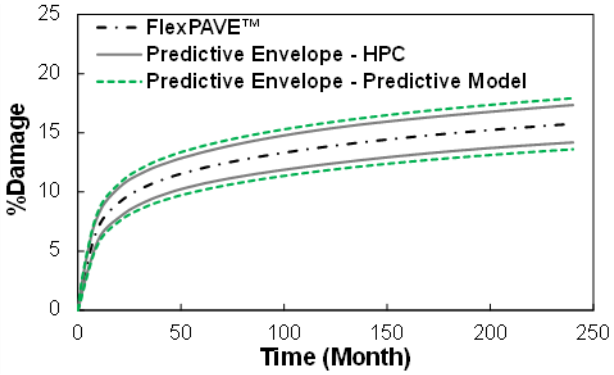

Source: FHWA.

C. %Damage for worst case.

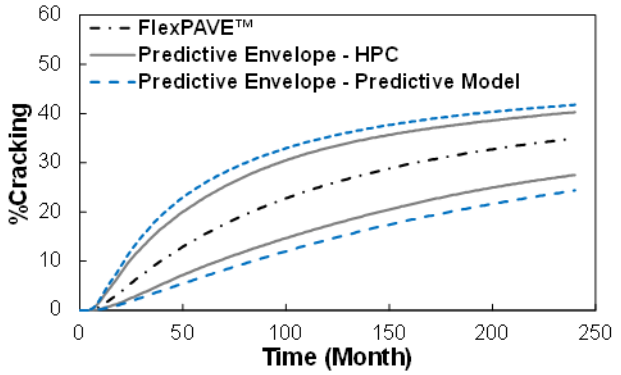

Source: FHWA.

D. %Cracking for worst case.

Figure 55. Graphs. FlexPAVE results and predictive envelopes.

Figure 56 summarizes the proposed framework. Using this framework saves a substantial amount of computation time and allows users to find the %Cracking envelope at any given reliability level. To run MCMC simulations, users should run 1,000 FlexPAVE simulations, which take approximately 500 h of computing time (approximately 20 d). However, using the proposed framework, users do not need to run additional FlexPAVE cases and can calculate the %Cracking envelope using the FlexPAVE results for %Damage values obtained from the mean input values (approximately 30 min).

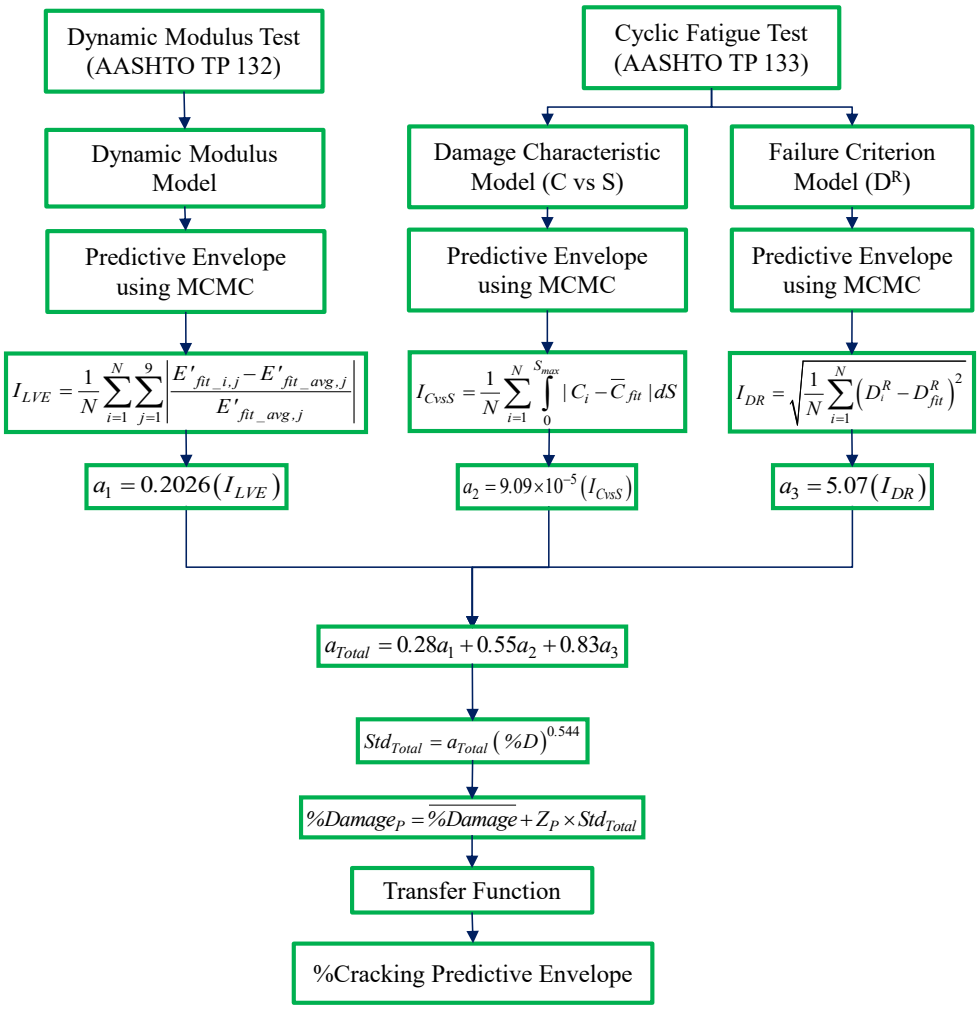

Source: FHWA.

Figure 56. Illustration. Framework to find %Cracking predictive envelope.

RELIABILITY ANALYSIS OF RUT DEPTH PREDICTION IN ASPHALT PAVEMENT SECTIONS USING FLEXPAVE AND THE PERMANENT DEFORMATION SHIFT MODEL

To develop the framework for rut depth prediction, this study used the simplified FlexPAVE algorithm whereby the asphalt layer's rut depth is independent of aggregate base thickness, base modulus, and subgrade modulus. For this model, the variation in the asphalt mixture dynamic modulus does not significantly affect the rut depth in the asphalt layer. Therefore, different from the %Cracking calculation, the dynamic modulus variation is not a critical factor in the rut depth predictive envelope.

As noted earlier, the main drawback to calculating the %Cracking predictive envelope was the extensive computation time for the FlexPAVE simulation to run 1,000 cases of MCMC generated inputs. As a result, the predictive models were developed to bypass running 1,000 FlexPAVE simulations. However, with the simplified algorithm developed in chapter 3 in Volume I of this report, this concern does not exist for the rut depth calculations.[18] Using the

simplified version of the FlexPAVE algorithm, 1,000 FlexPAVE for Rutting simulations can be performed in 1 or 2 min on a typical computer (quad-core CPU and 8 GB RAM). The research team did not need to develop new models to find the rut depth predictive envelope. Users can obtain the rut depth predictive envelope by running 1,000 cases of the simplified FlexPAVE algorithm. To verify the simplified FlexPAVE, the research team performed 1,000 cases of FlexPAVE simulations on a high-performance computer and compared the results to the results from the simplified version of FlexPAVE.

Figure 57-A shows the results obtained by FlexPAVE simulations using a high-performance computer. Figure 57-B shows the results when the same simulations were performed using the simplified version of FlexPAVE. Because maximum percentage of difference in the predicted rut depths obtained by the two methodologies was 0.1 percent, the simplified FlexPAVE was used to run the structural simulations. Figure 58 shows the preliminary framework to calculate the rut depth predictive envelope.

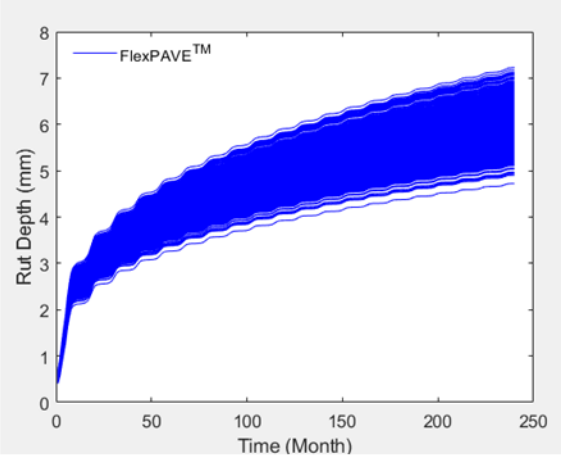

Source: FHWA.
1 mm = 0.04 inches.

A. Obtained by FlexPAVE.

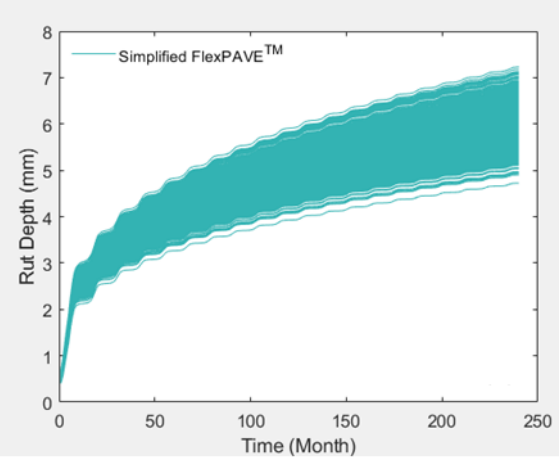

Source: FHWA.
1 mm = 0.04 inches.

B. Obtained by Simplified FlexPAVE.

Figure 57. Illustrations. Comparison of rut depth calculation.

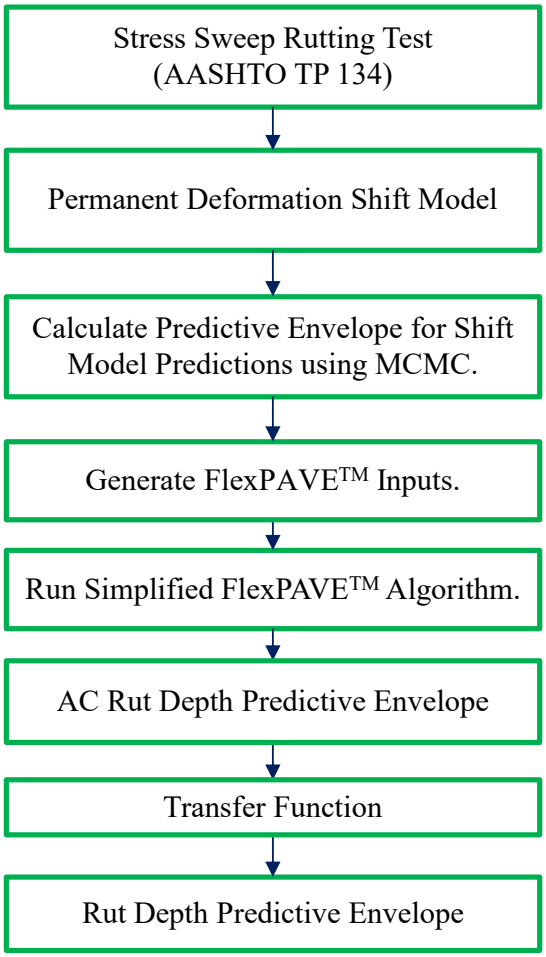

Source: FHWA.

Figure 58. Illustration. Framework for uncertainty quantification of rut depth.

Materials and Data

To investigate the effects of uncertainty on the permanent deformation in asphalt pavements, the SSR test results from different materials were used. Table 36 provides general information about these mixtures.

Finding a Relationship between Mixture Variation and Performance Prediction Reliability

Uncertainty in Rut Depth Predictions

Equations 46 to 50 show the permanent deformation shift model, which is calibrated by SSR test results. This model is calibrated using six model coefficients (ε_0, N_I, β, p_1, d_1, and d_2). This section studies three major uncertainties in the rut depth prediction.

$$\varepsilon_{vp} = \frac{\varepsilon_0 N_{red}}{\left(N_I + N_{red}\right)^{\beta}} \tag{46}$$

$$N_{red} = N \times 10^{a_T} \tag{47}$$

$$a_T = a_{\xi_p} + a_{\sigma_v} \tag{48}$$

$$a_{\xi_p} = p_1\left(\log\left(\xi_p\right) + 0.398\right) \tag{49}$$

$$a_{\sigma_v} = \left(d_1 \times T + d_2\right) \times \left(\log\left(\sigma_v / P_a\right) - 0.877\right) \tag{50}$$

Where:

ε_{vp} = viscoplastic strain.
N_{red} = reduced number of cycles.
a_T = total shift factor.
$a_{\xi p}$ = reduced load time shift factor.
$a_{\sigma v}$ = vertical stress shift factor.
ξ_p = reduced load time, s.
σ_v = vertical stress, kPa.
T = test temperature, °C.
P_a = atmospheric pressure used to normalize the stress, kPa.
ε_0, N_I, β, p_1, d_1, and d_2 = fitting coefficients.

Variation in the Stress Sweep Rutting Test Results

The SSR test records the viscoplastic strain at the end of each cycle. Based on this AASHTO TP 134 standard test procedure, when the difference in the viscoplastic strain at the end of 600 cycles between two replicates is less than 25 percent, the third replicate is not needed.[16] Figure 59 shows the SSR test results for mixture A described in table 36. The research team performed this test with two replicates at the low temperature (LT) (T_L = 30 °C) and two replicates at the high temperature (HT) (T_H = 51 °C). In this test, the differences between the viscoplastic strain for the two replicates at the HT and LT are 23.2 and 21.1 percent, respectively. Therefore, based on the AASHTO TP 134, these results are acceptable, and the third replicate is not needed.[16] This section investigates the effects of these variations on the shift model calibration and rut depth prediction.

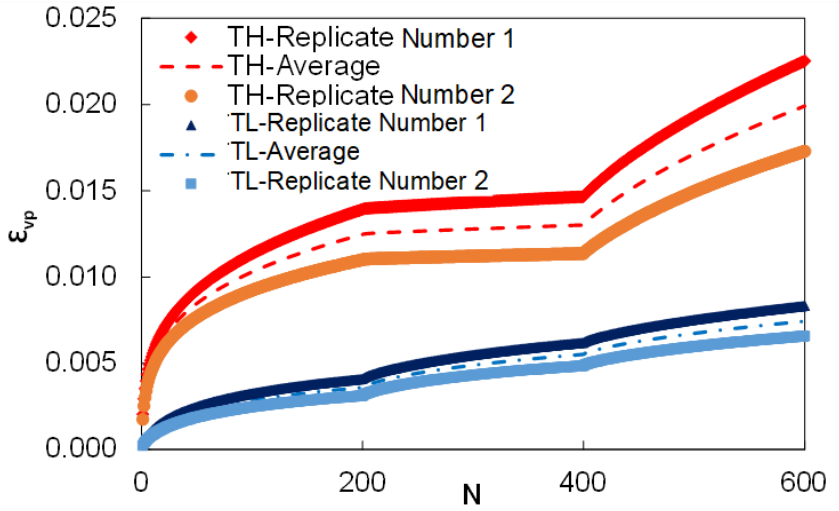

Source: FHWA.

Figure 59. Graph. Viscoplastic strain versus number of cycles from SSR test results for mixture A.

Variation in Shift Model Coefficients

To calibrate the permanent deformation shift model, the viscoplastic strain versus the number of cycles for each temperature is needed. The research team used the average of two replicates' viscoplastic strain at each temperature to calibrate the shift model. This section studies the effect of sample-to-sample variation on the shift model calibration using only results from measured tests. The first step defines five different approaches based on the measured results and then uses the approaches to calibrate the permanent deformation shift model. The first approach, which is the AASHTO TP 134 standard procedure for the shift model calibration, is based on the average viscoplastic strain obtained from two tests at each temperature (approach 1).[16] Approach 2 through approach 5 use the four possible combinations of individual replicates to calibrate the shift model (table 38). The research team then calibrated the shift model using the five different approaches and generated five different sets of model coefficients. Table 38 shows the shift model coefficients that the team calibrated based on five different approaches and the differences between the model coefficients and the measured data.

Table 38. Different approaches to calibrate the permanent deformation shift model.

Approach	T_H	T_L	ε_0	N_I	β	p_1	d_1	d_2
1	Average	Average	2.95E-03	0.9	0.727	0.66	0.140	−1.37
2	Replicate 1	Replicate 1	3.00E-03	0.7	0.710	0.63	0.124	−0.95
3	Replicate 2	Replicate 1	2.92E-03	1.2	0.748	0.52	0.150	−1.20
4	Replicate 1	Replicate 2	3.00E-03	0.7	0.710	0.79	0.137	−1.64
5	Replicate 2	Replicate 2	2.92E-03	1.2	0.748	0.69	0.172	−2.33

Variation in Rut Depth Predictions

The research team used the simplified FlexPAVE algorithm to investigate the effects of the variation in the model coefficients on pavement rut depth predictions. The team selected structure 1 (table 34) to carry out the predictions. The team also used structure 1 to develop the RSI. The next step predicted the asphalt layer rut depth for 20 yr. Figure 60 shows the simplified FlexPAVE simulations using the different approaches listed in Table 38. In this figure, the rut depth at the end of 20 yr for approach 2 has the highest value compared to the other approaches (5 mm) and approach 5 has the lowest value (3 mm). Therefore, 3 mm to 5 mm is the expected range of rut depth predictions for this specific test result and structure.

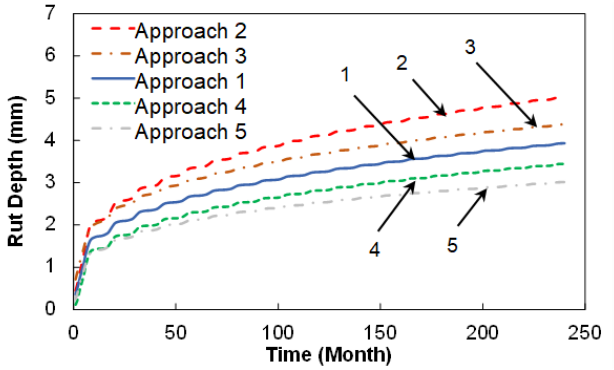

Source: FHWA.
1 mm = 0.04 inches.

Figure 60. Graph. Rut depth predictions by simplified FlexPAVE using permanent deformation shift model and SSR test results.

Bayesian Inference-Based Markov Chain Monte Carlo Method

The research team used the same approach employed to calculate the rut depth predictive envelope the to predict the %Cracking envelope. To calculate the rut depth predictive interval, the team used the Bayesian inference-based MCMC methodology to generate the model coefficients.[(63)] This method treats the shift model coefficients as random variables. The team used the MCMC method to generate the probability distribution for each of the six model coefficients, which is the posterior distribution. The posterior distribution shows the credible interval of the model predictions. This methodology can quantify the shift model uncertainties because it provides the model coefficient density and can quantify the effect of the model coefficients' density through the posterior distribution.

The first step generates 1,000 sets of the shift coefficients using the MCMC method. The team applied no restriction to the posterior distribution and generated the coefficients using the MCMC method without any constraints on the coefficients.

The next step propagates the posterior density values of the shift model coefficients to construct the distributions of the viscoplastic strain at the test temperatures (ε_{vp} at T_L and ε_{vp} at T_H). To find the effect of this variation on the structural level, the research team input 1,000 sets of model coefficients to the simplified FlexPAVE algorithm and calculated the rut depth over 20 yr for each set of coefficients. Figure 61 shows the credible intervals of the viscoplastic strain and rut depths predicted by the simplified FlexPAVE version for structure 1.

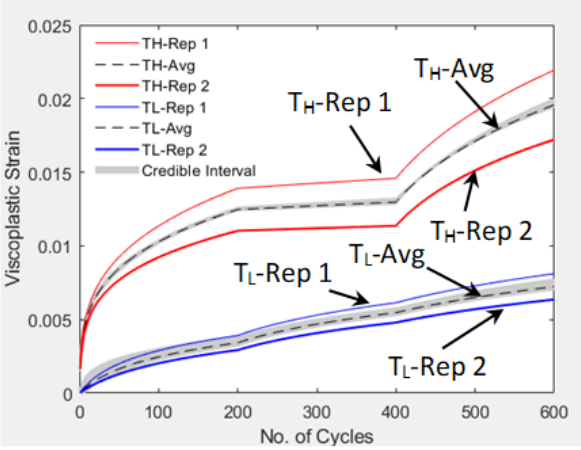

Source: FHWA.

A. Viscoplastic strain.

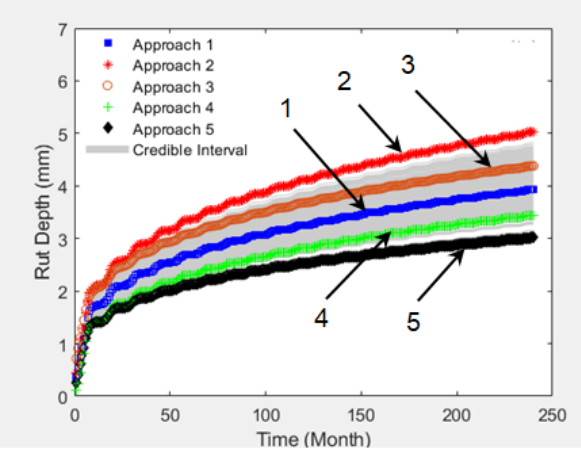

Source: FHWA.
1 mm = 0.04 inches.

B. Rut depth.

Figure 61. Graphs. 95 percent credible intervals for mixture A using unconstrained MCMC method.

The next step generates the prediction interval data using MCMC methodology. Figure 62 shows the 95 percent prediction intervals of the viscoplastic strain and rut depth predictions for structure 1. Although the credible interval range for the viscoplastic strain looks small, this uncertainty has a substantial impact on the rut depth predictions. Because the rut depths obtained using approach 2 and approach 5 are considered extreme cases, these two approaches are expected to cover the variation in rut depth predictions. However, the prediction interval band in Figure 62 is wider than the range provided by the measured data.

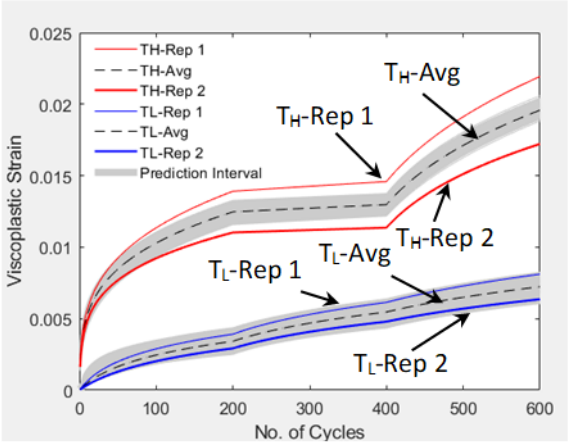

Source: FHWA.

A. Viscoplastic strain.

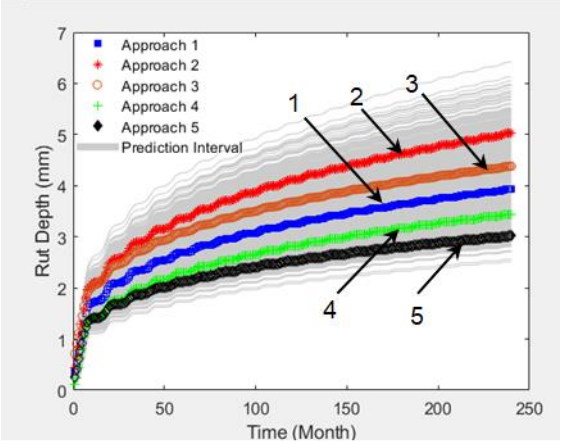

Source: FHWA.
1 mm = 0.04 inches.

B. Rut depth.

Figure 62. Graphs. 95 percent prediction intervals for mixture A using unconstrained MCMC method.

Constrained Parameter Estimation

To find the reason for the vast range in the rut depth prediction intervals, the research team investigated the variation in the shift model's coefficients. The first step of this detailed analysis investigated the range of the parameter estimations required to construct the credible interval and prediction interval. The team then compared the posterior distribution variation to the model coefficients calibrated using the five different approaches (table 38). The team obtained the three model coefficients, ε_0, N_I, and β, required to construct the reference curve by fitting the viscoplastic strain versus the number of cycles at the reference condition. Table 39 shows the range of these three coefficients obtained from the measured data, credible interval, and prediction interval.

Table 39. Range of shift model coefficients in parameter estimation for mixture A.

Data Type	ε_0 Min*	ε_0 Max*	N_I Min*	N_I Max*	β Min*	β Max*
Measured data	2.92E-03	3.00E-03	0.7	1.2	0.710	0.748
Credible interval	2.59E-03	3.07E-03	0.1	1.7	0.695	0.736
Prediction interval	2.26E-03	3.29E-03	0.1	1.1	0.691	0.737

Min = minimum; Max = maximum.

Table 39 shows that the model coefficient range for the measured data is narrower than that for the credible and prediction intervals. Therefore, the broader range for the shift model coefficients in the credible and prediction intervals could be a possible reason for the considerable variation in figure 61-B and figure 62-B. The next step generates the posterior distribution in a constrained range. The research team limited the three coefficients (ε_0, N_I, and β) to the range of the coefficients for the measured data. The next step generates the viscoplastic strain levels at the test temperatures using the MCMC posterior distribution method. Figure 63 shows the credible interval for the viscoplastic strain and the predicted rut depth using the new sets of coefficients. As expected, the range of 95 percent credible interval for the rut depth narrowed significantly. Therefore, constraining the coefficients can be a possible approach to generate the posterior distribution.

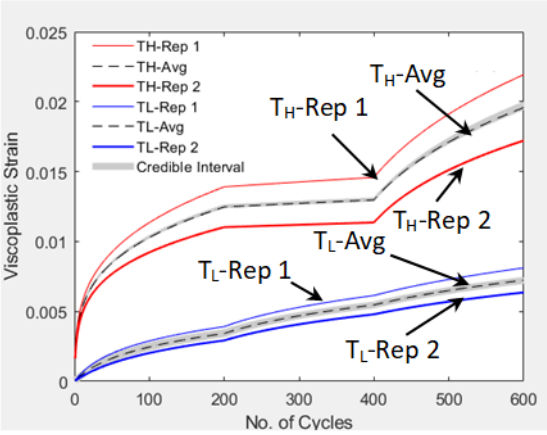

Source: FHWA.

A. Viscoplastic strain.

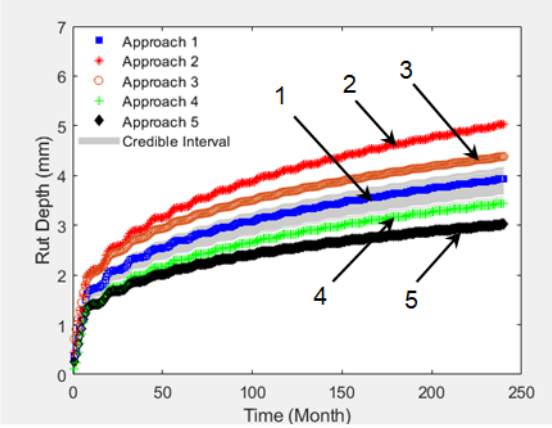

Source: FHWA.
1 mm = 0.04 inches.

B. Rut depth.

Figure 63. Graphs. 95 percent credible intervals for mixture A using constrained MCMC method.

The next step used the posterior distribution for the prediction interval and the MCMC method to generate the model coefficients. Similar to the credible interval posterior distribution, the model coefficients were generated in the same range as the measured coefficients. Figure 64-A shows the 95 percent prediction interval for the viscoplastic strain at the SSR test temperature.
Figure 64-B presents the 95 percent rut depth prediction interval under structure 1. As expected, constraining the model coefficients decreased the variation in rut depth predictions. The research team reported the SSR test results variation for mixture A as 23.2 and 21.1 percent for the HT and LT, respectively. These variations led to a maximum variation of 49.9 percent for mixture rut depth.

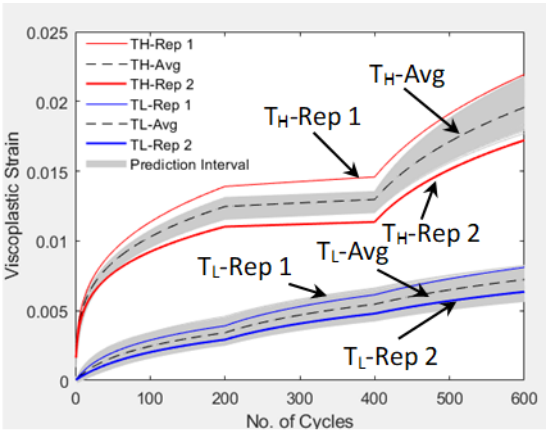

Source: FHWA.

A. Viscoplastic strain.

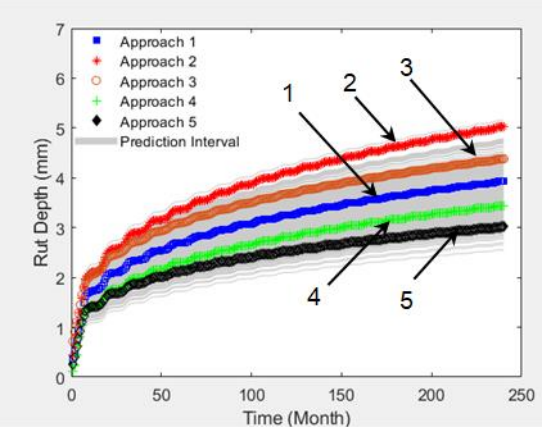

Source: FHWA.
1 mm = 0.04 inches.

B. Rut depth.

Figure 64. Graphs. 95 percent prediction intervals using constrained MCMC method.

Previous research studies have shown that ε_0 and N_I represent the primary region and (1- β) represents the slope of the permanent strain growth in the log-log scale in the secondary region.[59,75,76] Therefore, these three parameters represent the asphalt mixture's viscoplastic behavior in the primary and secondary regions. For mixture A, the unconstrained MCMC method leads to considerable variation in ε_0, N_I, and β. These variations result in a larger deviation in rut depth predictions. For example, the range of β from the measured data is from 0.710 to 0.748 (table 39). Based on the unconstrained MCMC method, this range from the parameter estimation (β) was from 0.691 to 0.737. As a result, the MCMC method tends to generate low β values. As mentioned, (1- β) controls the permanent strain growth; therefore, a lower β value leads to higher viscoplastic strain values. On the other hand, a lower ε_0 value results in lower viscoplastic strain values. For mixture A, the MCMC method generates lower ε_0 values in comparison with the measured data. Therefore, ε_0 and β are competing against each other, which may contribute to the larger variation in the predictive envelope in Figure 64.

To confirm the finding that structural factors do not have a significant effect on rut depth variations, the research team calculated the asphalt layer rut depth variation for mixture A using a different structure. Figure 65 shows a comparison of the results for the simplified FlexPAVE simulations using structure 1 and structure 8. In this case, the same results for both structures (maximum variation of 49.9 percent) were obtained, which confirms the independence of rut depth variation to the structure.

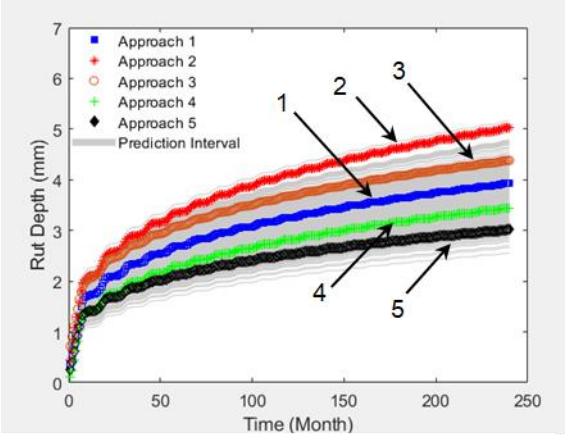

Source: FHWA.
1 mm = 0.04 inches.

A. Structure number 1.

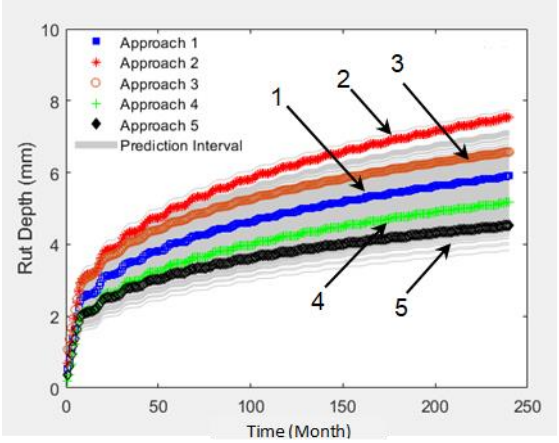

Source: FHWA.
1 mm = 0.04 inches.

B. Structure number 8.

Figure 65. Graphs. 95 percent prediction intervals for asphalt rut depth using constrained MCMC method.

To see the effect of the SSR test results variation on the rut depth predictions, the research team used another set of SSR test results with less variability compared to mixture A to repeat the same study. For mixture B, the SSR test results variation was less than for mixture A. Similar to mixture A, the test was performed with two replicates at the LT (T_L = 30 °C) and two replicates at the HT (T_H = 51 °C). The differences between the viscoplastic strain levels for the two replicates at the HT and LT were 4.7 and 6.9 percent, respectively. Based on the measured data and results obtained from approach 1 to approach 5, the maximum difference in rut depth predictions was 16.8 percent. Similar to mixture A, the research team performed two different scenarios of MCMC simulations to generate a 95 percent predictive envelope. Table 40 shows the range of the shift model coefficients obtained from the measured data, unconstrained credible interval, and unconstrained prediction interval. Figure 66 and figure 67 show the 95 percent

predictive envelopes using the unconstrained and constrained MCMC method, respectively. Based on the unconstrained MCMC method, the maximum difference in the rut depth predictions was 34.5 percent. For these simulations, the maximum difference using the constrained MCMC method was 21.3 percent. A comparison of the results for mixture A and mixture B shows that as the variation in the test results decreases, the variation in the rut depth predictions likewise decreases.

Table 40. Range of shift model coefficients in parameter estimation for mixture B.

Data Type	ε_0 Min	ε_0 Max	N_I Min	N_I Max	β Min	β Max
Measured data	3.69E-03	3.76E-03	0.5	0.7	0.685	0.687
Credible interval	3.37E-03	3.73E-03	0.1	0.6	0.667	0.689
Prediction interval	3.23E-03	3.62E-03	0.1	0.4	0.667	0.678

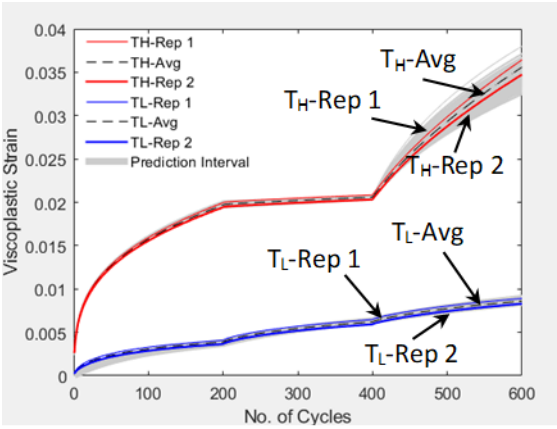

Source: FHWA.

A. Viscoplastic strain.

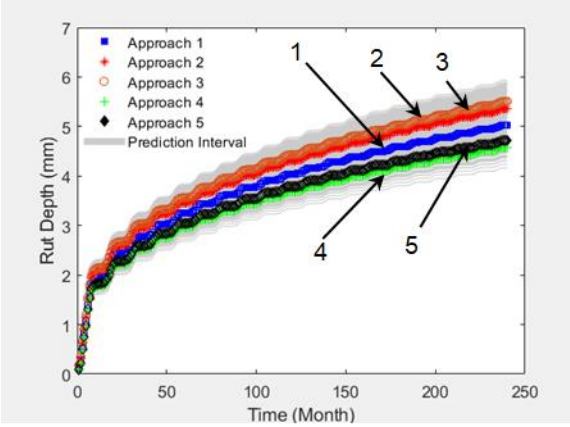

Source: FHWA.
1 mm = 0.04 inches.

B. Rut depth.

Figure 66. Graphs. 95 percent credible intervals using unconstrained MCMC method.

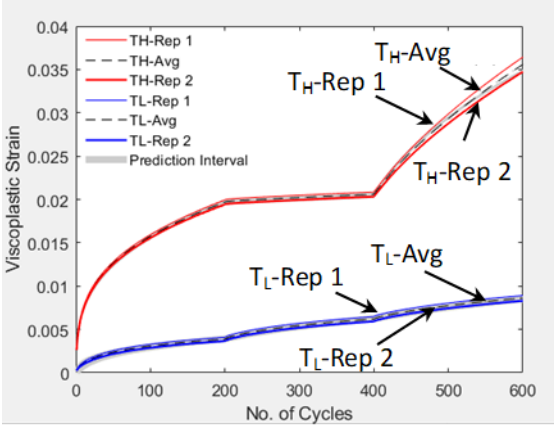

Source: FHWA.

A. Viscoplastic strain.

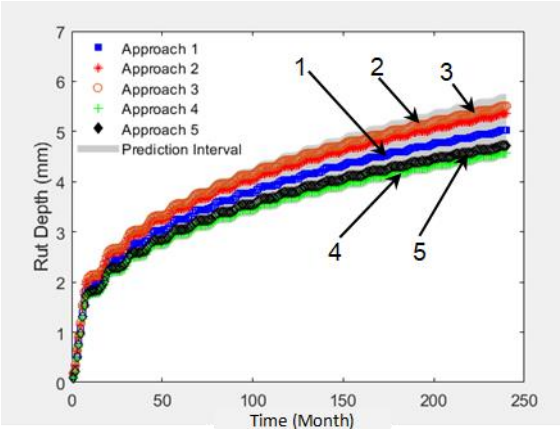

Source: FHWA.
1 mm = 0.04 inches.

B. Rut depth.

Figure 67. Graphs. 95 percent credible intervals using constrained MCMC method.

As mentioned earlier, the variation at both the HT and LT affects the rut depth variation. The research team performed the same analysis described for mixtures A and B for mixture C, mixture D, and mixture E (table 36). Table 41 shows the variation in the SSR test results and the measured rut depths for all the mixtures in this study. The next step investigates the variation in the predictive envelope using the constrained and unconstrained MCMC methods.

The results show that the variation in rut depth depends on the climatic conditions, variation at the LT, and variation at the HT. Thus, defining a global function that relates the variation at the material level to the structural level variation is complex. A rule of thumb for the analysis of the study mixtures shows that the variation in the rut depth predictive envelope is 1.5 to 3.5 times that of the variation in the viscoplastic strain. However, with the simplified FlexPAVE, developing a predictive model is not necessary. The simplified FlexPAVE algorithm calculates the variation in the rut depth given the climatic conditions and variation at the material level.

Table 41. Variation in test results and MCMC data generation for all study mixtures.

Mixture ID	Climate	Viscoplastic Strain at T_L (Percent)	Viscoplastic Strain at T_H (Percent)	Measured Rut Depth (Percent)	Rut Depth Predictive Envelope (Constrained) (Percent)
Mixture A	NC	21.1	23.2	40.0	49.9
Mixture B	NC	6.9	4.7	16.8	21.3
Mixture C	NC	6.3	8.4	17.5	16.3
Mixture D	ME	0.2	8.6	1.5	7.6
Mixture E	MO	2.5	1.8	11.4	8.6

SUMMARY OF FINDINGS IN RELIABILITY ANALYSIS

This chapter describes the development of the framework for calculating the %Cracking predictive and rut depth envelopes based on the S-VCED model and rutting shift model.[12] To develop the %Cracking framework, the research team performed thousands of FlexPAVE simulations using five different mixtures with different levels of prediction. The team used the MCMC method to generate the dataset for the FlexPAVE inputs.[52] The team defined three material variability indexes and developed a model to relate these indexes to the %Damage distribution. The following list summarizes the findings from the %Cracking study:

- The variation in %Damage and %Cracking increases as %Damage grows.
- The variation of %Damage at any period of the design life strongly correlates with the average %Damage at the given period, regardless of the pavement structure and loading condition.
- The relationship between the standard deviation and the average %Damage distribution depends on the material variation.
- The predictive models can predict the propagation of the testing variability to %Cracking variations at any desired level of reliability with more than 98 percent accuracy (less than 2 percent error).

With respect to the rut model reliability, table 42 presents the predicted rut depths after 20 yr for all the mixtures listed in table 36. Table 42 also presents a comparison of the range of the rut depth predictive envelope for all the mixtures based on the unconstrained MCMC and constrained MCMC methods.[52] The first method generated the rut depth predictive envelopes using the unconstrained MCMC method and the second method generated the coefficients in constraint to the measured model coefficients.

Table 42. Range for rut depth predictions using different methodologies.

Mixture	Minimum or Maximum	Measured Rut Depth at 20 yr (mm)	Unconstrained Rut Depth at 20 yr (mm)	Constrained Rut Depth at 20 yr (mm)
Mixture A	Minimum	3.0	2.5	2.6
Mixture A	Maximum	5.0	6.4	5.1
Mixture B	Minimum	4.6	4.0	4.5
Mixture B	Maximum	5.5	6.1	5.7
Mixture C	Minimum	1.7	1.5	1.7
Mixture C	Maximum	2.0	2.1	2.0
Mixture D	Minimum	1.8	1.8	1.7
Mixture D	Maximum	1.8	2.2	1.9
Mixture E	Minimum	2.9	3.2	2.9
Mixture E	Maximum	3.3	3.5	3.2

The results show that constraining the shift model coefficients to the measured data generates a posterior distribution with a narrower range than the unconstrained MCMC generation.[52] Therefore, this constraining approach could be used to generate the predictive envelopes for rut depth. Figure 68 shows the proposed framework for the rut depth predictive envelope.

However, because the shift model coefficients are calibrated using two replicates at each temperature, the main drawback of the proposed methodology could be constraining the coefficients to the limits obtained using the measured data. Therefore, the limits are forced to those of the measured data, which come from two replicates at each temperature. A ruggedness study to identify the effects of the SSR test factors on the shift model's coefficients could improve the accuracy of the test results. If the ruggedness study on AASHTO TP 134 is done, the effect of sample-to-sample variability on the model coefficients could be studied.[16] Therefore, the limits for the Bayesian inference-based MCMC method could be selected based on the more robust analysis.[63]

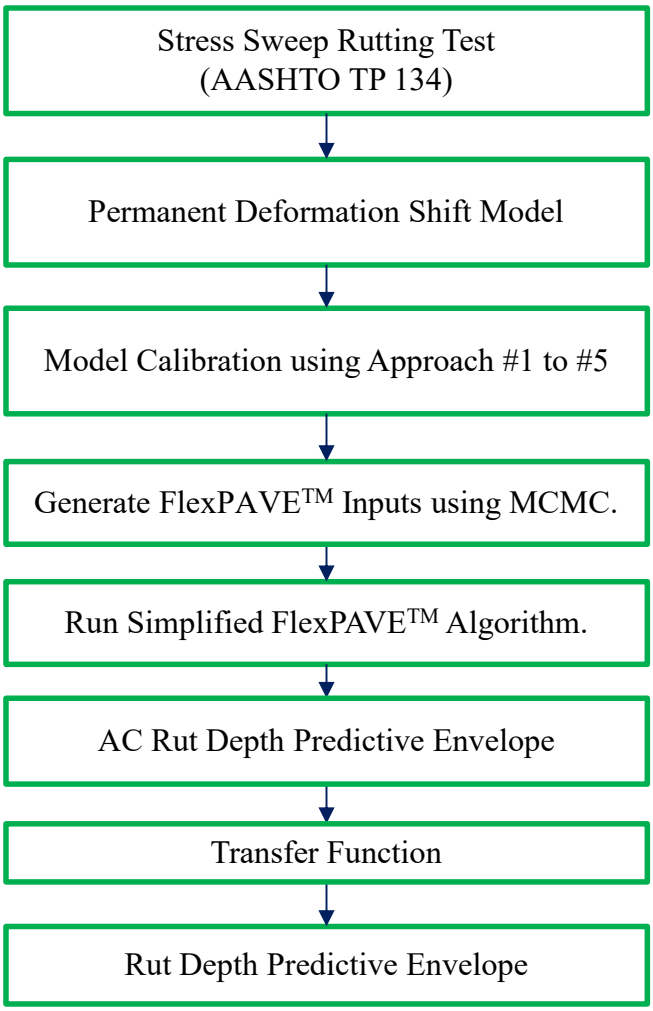

Source: FHWA.

Figure 68. Illustration. Proposed framework to calculate rut depth predictive envelope.[16]

DEVELOPMENT OF PASSFLEX

This section discusses the underlying concepts and models that are used as the basis for the performance prediction approaches used in the tools necessary to operate PASSFlex. The three software components for these prediction approaches are as follows.

FlexMAT is the material-level evaluation software used in this framework to characterize the models that describe asphalt concrete's behavior. FlexMAT version 2.1 is the current version in which the dynamic modulus, fatigue cracking, aging, thermal contraction, and rutting models are calibrated using up-to-date approaches.

FlexPAVE uses a three-dimensional finite element method to simulate pavement performance. Formerly known as LVECD, FlexPAVE combines the models calibrated in FlexMAT to EICM climatic characteristics to perform moving load simulations and predict pavement life.[22]

PASSFlex is the software that combines FlexMAT and FlexPAVE into a PRS framework intended to support the user (e.g., agencies, contractors, researchers) in the different steps of a PRS-based project. PASSFlex was designed to offer the user five main tools:

- A local database of mixtures can be developed based on AMPT testing.
- PRS can be developed using a choice of protocol.
- Mixture approval based on an index or performance.
- QA evaluation by measured AQCs and calibrated volumetric relationships.
- A toolbox that contains FlexMAT and FlexPAVE in a single environment.

Before this section discusses the details of PASSFlex, three PRS protocols developed under the auspices of the Transportation Research Board and FHWA Research Support (TFRS) project, TRFS-01 Quality Assurance (QA) Aspects of Performance Related Specifications (PRS), are introduced. Among these three protocols, protocol A was selected to be implemented in PASSFlex.

Performance-Related Specifications Protocols

A statistically robust QA system within PRS is based on three possible protocols. Protocol A uses the IVR from four corners for the pay table development and QA. Protocol B uses the PVR for pay table development and QA. Protocol C is essentially the same as protocol B with the addition of periodic performance testing during construction. The sampling size and frequency, and associated lot and sublot sizes, are governed by the testing needs and the time required to conduct these tests. A brief description of the three protocols and the expectation regarding the sampling frequency for each of them is in the following sections.

Protocol A: Pay Tables Developed Using Index-Volumetrics Relationships, Mixture Design Approval Using Index Values, and Field Acceptance Using Conventional AQCs

Protocol A is the simplest form of PRS. Protocol A bases the pay adjustments on the difference in index values between as-designed and as-constructed pavements. Protocol A's major strength over higher level protocols is protocol A uses the index parameters for the entire protocol and therefore does not require FlexPAVE. Protocol A uses the IVRs, which allow the index values to be predicted as a function of AQC values, to develop pay tables, and uses the index parameters for mixture approval.

Protocol A uses the relationship between the index parameters and volumetric properties to develop pay tables. In most cases, the sampling frequency and size, the lot sizes, and other QA processes currently used by State highway agencies do not change substantially in this PRS approach. Samples are taken on a traditional random sampling basis at a frequency of one per sublot. Common mixture properties, i.e., the volumetric optimum binder content (P_b), mixture bulk specific gravity (G_{mb}), and maximum specific gravity (G_{mm}), then are determined and used to calculate the V_a, VMA, and VFA. One critical issue unique to PRS is ensuring that roadway lots and plant lots represent the same material, because the IVR requires in-place density and mixture control variables. Finally, because this QA approach utilizes conventional volumetric properties and in-place density as AQCs, users can undertake approved agency verification and independent assurance processes without changes to current practice, and technicians do not

need training to learn new test methods. Agencies that do not currently utilize volumetric properties as AQCs would need to change the QA requirements.

On completion of each sublot, the user inputs measured properties (P_b, V_a, VMA) of mixtures from the plant along with in-place density values (percentage of G_{mm}) from the roadway mixtures into the IVR with generalized project conditions to predict the index values for each sublot. On completion of the lot, the user calculates the average and standard deviations of the index values for each lot and uses those average and standard deviations of the index values to estimate the percentage of pay established by the agency.

Protocol B: Pay Tables Developed Using Performance-Volumetrics Relationships, Mixture Design Approval Using Predicted Pavement Life, and Field Acceptance Using Conventional Acceptance Quality Characteristics

Protocol B differs from protocol A for the pay table development and mixture approval because protocol B uses the pavement life predicted from FlexPAVE instead of S_{app} and RSI values. In protocol B, once the pavement design for the project is complete and the agency is ready to develop PRS for the project, the agency should use the performance properties for a representative mixture design in the material database along with the project-specific traffic, climate, and pavement structural design data to predict the pavement performance using FlexPAVE. The agency then uses predicted performance and volumetric properties obtained from the four corners to develop the fatigue cracking and rutting PVRs. Finally, pay tables for the project PRS are developed based on the agency's historical cost information.

After a contractor is awarded the project, the contractor will submit a mixture design for approval. The State highway agency or a consultant will conduct the performance tests (dynamic modulus, cyclic fatigue, and SSR) at the optimum mixture design conditions. The performance test results are then input into FlexPAVE along with the project-specific traffic data, climate data, and pavement structural design (that were used to develop the project PRS) to predict the pavement performance. The predicted pavement life should meet the minimum pavement life set forth in the PRS for the mixture design to be approved.

Because protocol B uses the relationship between pavement performance and volumetric properties to develop the pay tables, the QA processes currently used by agencies do not change substantially in this PRS approach, similar to protocol A. This QA approach continues to utilize conventional volumetric properties and in-place density as AQCs, so approved agency verification and independent assurance processes can be undertaken without changes to current practice, and no new training is necessary for technicians to learn new test methods. For agencies that do not currently utilize volumetric properties as AQCs, the QA requirements would need to change.

Protocol C: Pay Tables Developed Using Performance-Volumetric Relationships, Mixture Design Approval Using Predicted Pavement Life, and Field Acceptance Using Conventional AQCs and Periodic Performance Testing

Considering the challenges agencies face in conducting performance tests during construction, protocol B uses PVRs to predict as-built pavement life from traditional mixture AQCs (i.e., volumetric properties and in-place density). Although these AQCs can be used to measure changes in mixture proportioning, they are not necessarily sensitive to the changes in asphalt binder quality that result from changes in recycled materials content or binder source. To address these shortcomings, protocol C follows the same steps as protocol B with the addition of periodic performance testing during construction. This protocol adopts true PRS as envisioned in FHWA's PRS research in predicting as-built pavement life from FlexPAVE using actual performance test results determined during construction, while at the same time considering the practical limitations of conducting these performance tests during production.

In protocol C, in addition to the traditional AQCs routinely measured for acceptance testing as proposed in protocol B, pavement life also is predicted from FlexPAVE using periodically conducted performance tests that serve as another quality indicator for adjusting the payment for the asphalt mixture. During construction, agencies will measure the traditional AQCs in accordance with the agency's QA sampling frequency. Agencies will then conduct additional performance testing at a lesser frequency, depending on several practical considerations, including but not limited to where the performance test samples are fabricated, where the AMPT performance tests are conducted, and AMPT testing durations, etc. Consideration of these factors will lead to guidance on the sampling frequency in the form of one set of tests per sublot or 5,000 tons of production (the agency determines the exact number). The agency then will predict pavement life for each set of performance test results. This predicted life will determine the incentives and disincentives of the production mix from which the representative sample for performance testing is taken.

Material Testing

This report refers to the initial step in the development of the PRS framework as prePRS because it is a lab and analysis-intensive stage where the goal is to develop a database of the materials that will be used in the future PRS project stages. The distinction between prePRS and PRS, although theoretical, is made because the development of this database is independent of actual project development and may start many years before a project is envisioned and may be updated continuously and independently of the other steps in the PRS as new mix designs are created and tested. This step, however, is the starting point, because all the subsequent steps depend on the characterization that occurs at this stage.

The complete set of material characterization used in PASSFlex requires information from different properties that, optimally, would come from lab specimens but, for some cases, may also be obtained in higher level approaches via relationships with other material properties, similar to level 3 in the *Mechanistic-Empirical Pavement Design Guide*.[8] Table 43 provides a summary of the characterization, models, and lab effort requirement for the implemented methodology in FlexMAT.

Table 43. Summary of characterizations needed in the development of the PASSFlex database.

Properties Characterization	Model	Lab Testing
Dynamic modulus	2S2P1D	Required
Fatigue cracking	S-VECD[12]	Required
Permanent deformation	Shift model	Required
Aging	PAM-AMAC	Multilevel alternative
Thermal cracking	CTC	Multilevel alternative

2S2P1D = two springs, two parabolic elements, one dashpot; PAM = pavement aging model; AMAC = asphalt mixture aging-cracking; CTC = coefficient of thermal contraction.

The basic, or required, proposed testing system is based on the AMPT, a servo-hydraulic closed-loop testing machine designed for asphalt mixture materials. AMPTs are normally less expensive than other generic servo-hydraulic testing machines. AMPTs are specifically designed for asphalt materials and thus the necessary ranges of loading and temperatures do not have to be as wide as for other purposes, which reduces the production cost.

Four main types of distress can be evaluated using the experimental steps of the prePRS:

- Fatigue cracking.
- Thermal cracking.
- Aging.
- Rutting.

The first three types of distress have the dynamic modulus as a common fundamental property denominator and then their own procedures to characterize individual properties, whereas rutting is characterized only by its own testing procedure without the need for dynamic modulus testing.

The dynamic modulus, cyclic fatigue, and permanent deformation (or rutting) tests are performed in an AMPT following specific standards, but because the characterization of aging and thermal contraction do not have standardized procedures, a multilevel approach for the characterization of aging and thermal contraction is offered in PASSFlex. The test methods for aging and thermal contraction may not involve an AMPT, but rather other equipment, depending on the level selected. Three levels of analysis were designed so that users can calibrate the aging and thermal cracking models according to the amount of lab effort needed.[77]

Understanding the purpose of each test is fundamental for building a strong database and, consequently, reliable components in the QA of the mix. Combining the test characterization that is required for each project's needs with the available resources for that project is a task with importance that must not be neglected. The amount of effort required for the characterization of aging and the coefficient of thermal contraction (CTC), for example, has a certain flexibility given the multilevel approach available and, therefore, users who have projects with restrictions on material testing can opt for higher level analyses.

It is well known that certain distress types are more common in certain climatic regions than others and sometimes the way agencies and contractors handle these distress types may tip the scale toward the opposite direction. One example is using softer mixes in cold regions to prevent fatigue cracking but incurring a premature increase in rut depth. Finding the balance between material characteristics and specific project needs is another complicated task that, although not deeply explored in this report, will have certain elements in common with the presented framework. These elements from mixture design combine with the methods presented in this report to generate a powerful tool that agencies can use to achieve optimum performance through a combination of material selection and volumetric characteristics.

Even though FlexMAT is treated as a single software for overall workflow understanding, FlexMAT comprises two separate spreadsheets because of the different needs of the two spreadsheets during FlexMAT development. At a certain point, the climatic database needed for RSI calculation was included within FlexMAT Rutting's spreadsheet, what would cause it to become a file much larger than FlexMAT Cracking. During that time, the research team decided it was best to leave FlexMAT Cracking and FlexMAT Rutting as separate files to avoid the hindrances related to big file sizes on FlexMAT Cracking and isolate them into FlexMAT Rutting, since the climatic database was only used in FlexMAT Rutting. Details about the current database format in FlexMAT Rutting will be given in this section when the same is covered.

In this approach, FlexMAT Cracking is responsible for most of the models related to material characterization and the simple explanation is that cyclic fatigue, CTC analysis (levels 2 and 3) and aging analysis (all levels) are all based on the dynamic modulus characterization. Therefore, the first model to be characterized in FlexMAT Cracking should be the current implemented dynamic modulus model, which for FlexMAT Cracking version 2.1 is two springs, two parabolic elements, one dashpot (2S2P1D). The exception to that case is level 1 of CTC analysis, where CTC has been measured in the lab and the calibrated coefficients are the actual input.

Performance-Related Specifications Development Using PASSFlex

PASSFlex is the most important product from this work. It is software developed in Microsoft Visual Basic for Applications® (VBA) and uses Microsoft Excel as the host platform.[32,78] PASSFlex serves as a base-tool for contractors and agencies adopting performance specifications that use robust mechanistic models combined with AMPT testing and pavement performance predictions, thereby laying down a solid framework for a QA system.

In the conceptual design phase, developers considered different coding languages as alternatives to Microsoft VBA for developing the PASSFlex source code. However, the positive feedback from FlexMAT users and the natural compatibility between FlexMAT version 2.1 and FlexPAVE version 2.0 graphical user interface (GUI), which are part of the framework and are coded using Microsoft VBA and Microsoft Excel, were deciding factors in the choice of coding language.

PASSFlex combines different elements from FlexMAT and FlexPAVE to generate reliable performance predictions that can be transferred into prePRS steps, such as pay table generation, mix approval, or pay adjustments based on AQCs. Within the protocols envisioned in the PASSFlex framework, the user is presented with different alternatives to obtain life predictions based on volumetric AQCs so that both mix and pavement quality can be evaluated and adequate pay factors generated. Figure 69 presents an overview of the PASSFlex operational scheme.

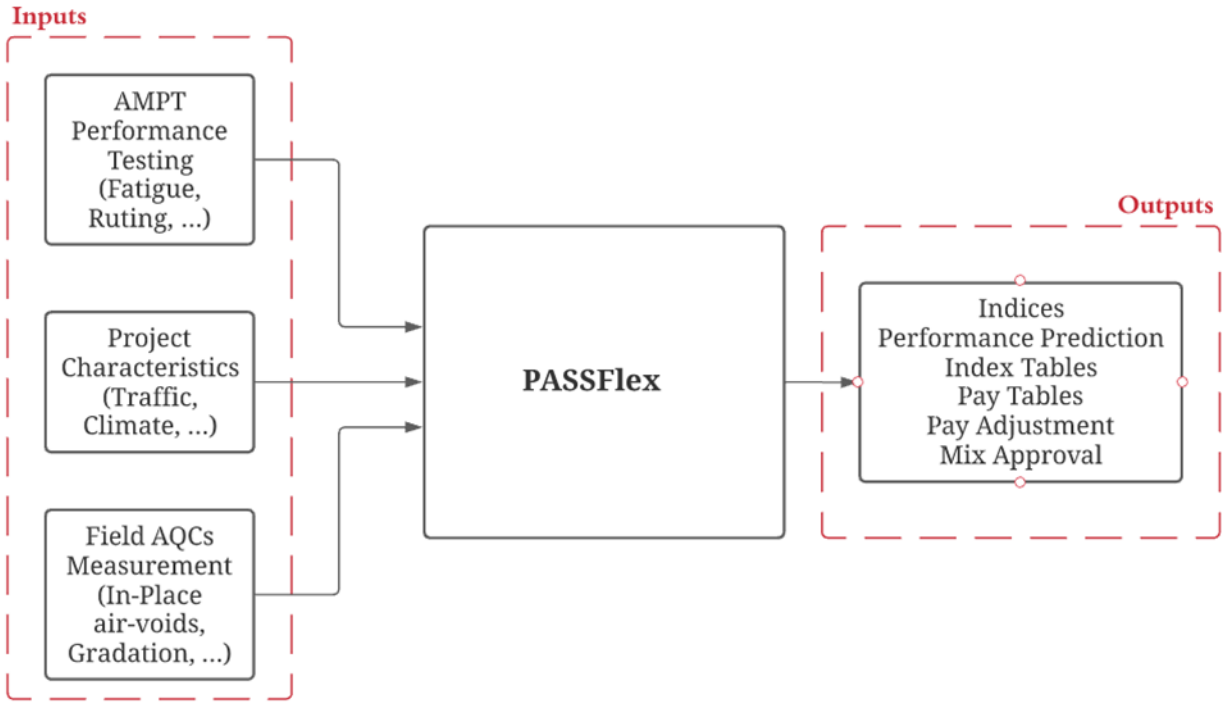

Source: FHWA.

Figure 69. Illustration. Overall PASSFlex flow scheme.

The four main functionalities of PASSFlex guide the user through the different possible parts that compose the workflow of QA analysis of a project using a PRS system. These four main functionalities have different buttons in the initial screen of the software:

- Develop Material Database.
- Develop PRS.
- Approve Mix.
- Adjust Payment Using QA Data.

Figure 70 presents a screenshot of this initial PASSFlex screen.

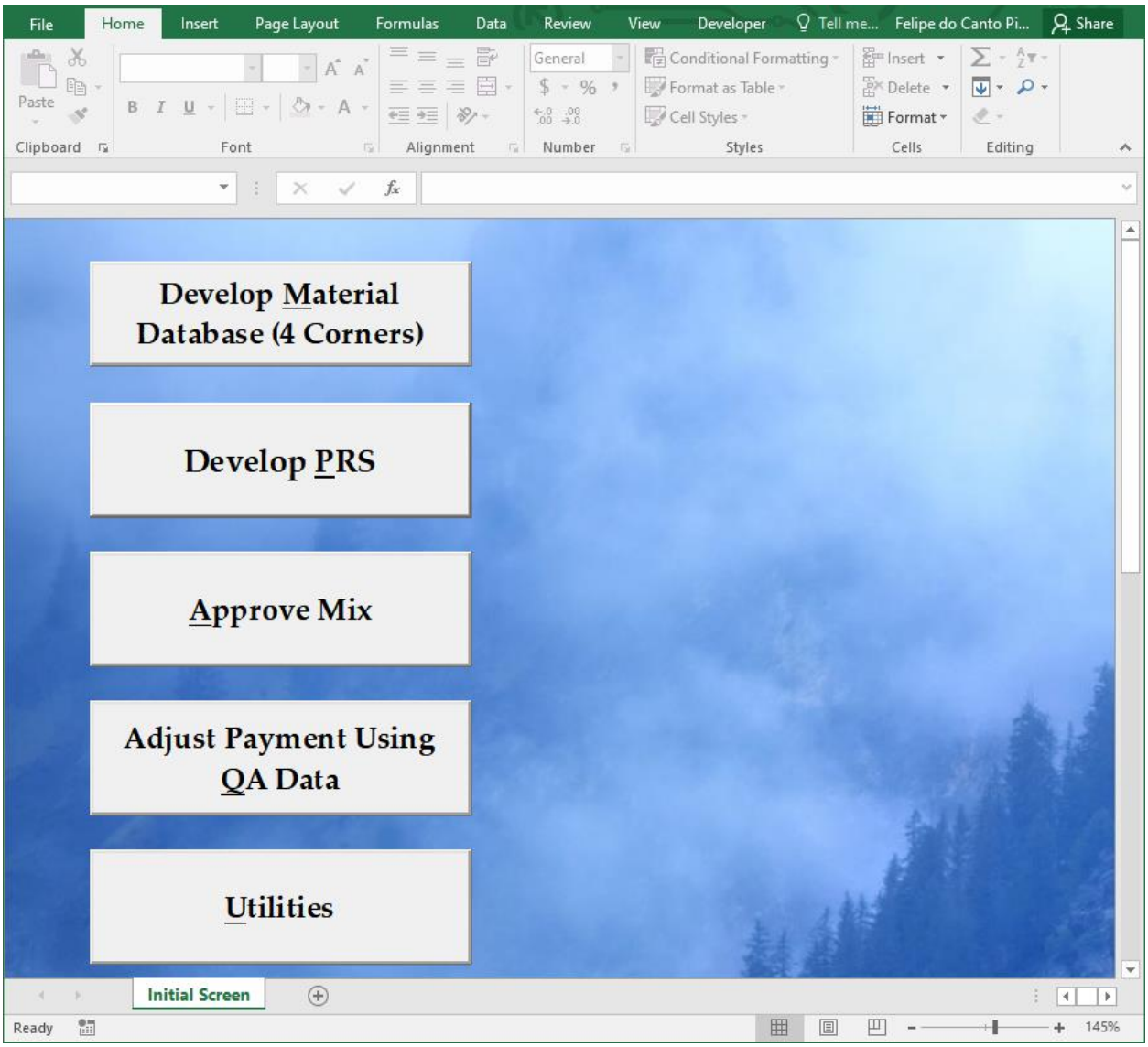

Source: FHWA.

Figure 70. Screenshot. PASSFlex initial screen.

A fifth functionality, Utilities, is an accessory tool that simplifies access to other software that are part of the PASSFlex framework. In this sense, PASSFlex can be seen as a toolbox of multiple functionalities and software. Currently, the Utilities functionality allows the user to store the latest version of FlexMAT Cracking and FlexMAT Rutting in a directory of choice. Developers expect future implementations of PASSFlex to include the same system for FlexPAVE version 2.0 usage, once it is available.

This report defines a protocol before describing the functionalities of PASSFlex because a PRS project will always be tied to a protocol in PASSFlex. A protocol is a part of the adopted PRS framework that describes the different steps and effort needed to achieve the goals of the PRS. In other words, a protocol is the plan of development for PRS that specifies the steps needed to achieve the PRS objectives. Because there is no single method to achieve such goals, users can develop multiple protocols to describe different approaches and assumptions to achieve these objectives. In the PASSFlex system, protocols are the guidelines for the procedures in the following three basic stages:

- Pay tables development: Pay tables are a tabular output in which the pay factors are given to the user as a function of the in-place AQCs and the cost model is adopted. Protocols determine the means to calibrate a relationship between the volumetric characteristics and a performance indicator to calculate a pay table.

- Mix design approval: The approval stage is dependent on the selected protocol. It is an important stage where the contractor's mix design will go through a mix approval process based on threshold values given the characteristics of the project. A pass or fail result ends this stage.

- Field acceptance: The final stage of field acceptance uses the volumetric functions calibrated in the initial stage to predict, based on the measured in-place AQCs of a certain representative sample of the constructed pavement, the pay factors for that lot. This stage applies incentives (or disincentives) based on the contractor's efforts over the QA elements.

Current PASSFlex implementation depends on a single protocol implementation, protocol A. Protocol A makes the predictions of field performance without pavement simulations by FlexPAVE. Figure 71 presents a simplified overview of protocol A.

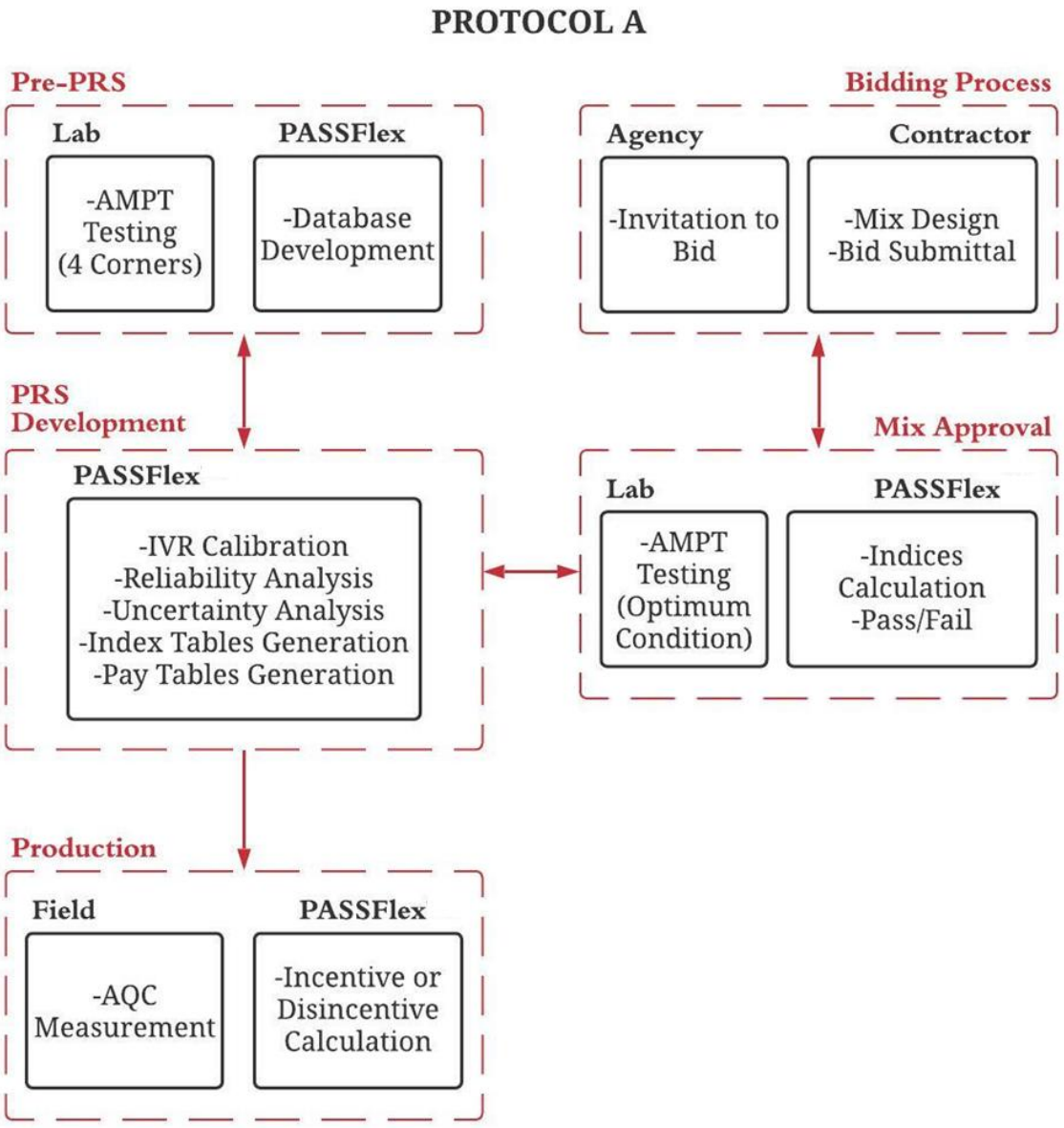

Source: FHWA.

Figure 71. Illustration. Protocol A overview.

The following sections explain the implementation of protocol A and clarify the elements of Figure 71.

Development of Material Database

The material database in PASSFlex is the basis for any PRS protocol that is created. This database stores a list of material properties characterized during FlexMAT analysis so that users can access those material properties without reanalyzing or reinputting data from AMPT tests of mixes once those mixtures have been analyzed and added to the database. Agencies and other PASSFlex users are expected to develop their own database of mixtures and continuously build on this database, adding new mixtures as the mixtures are designed and tested.

This section reinforces the concept of four corners to help clarify the expected data inputs in the database. The four corners are four different volumetric conditions for a mixture created using the same materials. Users can obtain these four volumetric conditions with a combination of varying granulometry, binder content, and compaction level. The volumetric space is normally defined by two of the following three main in-place volumetric variables:

- VMA.
- VFA.
- Air void content (V_a).

These three properties form a linearly dependent system in which knowing two is sufficient to characterize the third. Equations 4 and 6 show the relationships between these three properties and the in-place volumetric prop, respectively.

Figure 72 illustrates a mix's different volumetric conditions in the volumetric space. The CUW of a given number is used for identifying conditions that use the same granulometry.

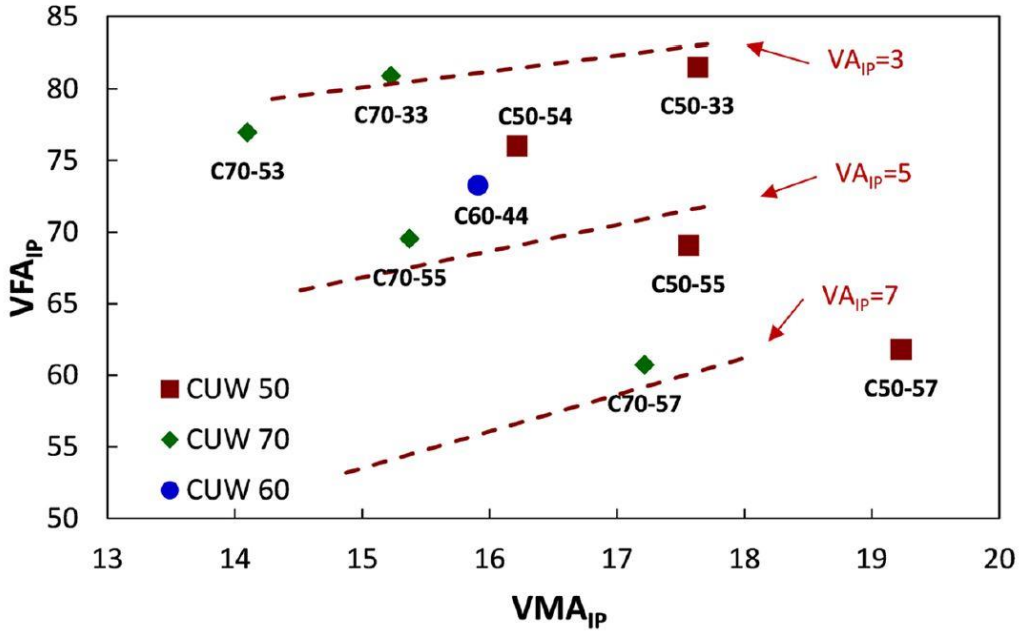

Figure 72. Graph. Volumetric space characterization.[19]

The distinction between mixture and volumetric condition becomes important at this stage for the four corners context. One mixture may be tested at multiple volumetric conditions, i.e., volumetric modifications of a mixture and, for the purposes of this work, still considered one single mixture even though the different modified versions may differ in performance. In fact, the purpose of defining a mixture as a combination of materials that may assume different volumetric conditions is to predict the mixture's behavior through the volumetric state of that mixture, which generates the concepts that underlie the IVR and PVR.[19]

The four corners are four different volumetric conditions that enclose a specific region in the volumetric space. Users can calibrate the IVR or PVR to predict the indexes (i.e., S_{app} and the RSI) or performance (i.e., pavement life) of volumetric conditions that fall within the enclosed space that the four corners create. The calibration of the IVR and PVR is one of the proposed features of PASSFlex that users achieve by running the performance tests (dynamic modulus, cyclic fatigue, and SSR tests) in the four corners and calculating the index values or performance for each condition. This summary of the four corners concept helps explain the database structure for PASSFlex mixtures file storage. The database is a three-level structure in which one or more volumetric conditions are stored under a single mixture and one or more mixtures are stored under a mixture category. Figure 73 presents an illustrative overview of the file structure. The "Performance testing results" box in figure 73 indicates a set of files that in PASSFlex's internal algorithms use. These files include, in the current version, one FlexMAT Cracking file, one FlexMAT Rutting file, and one ASCII based file with the summarized properties of each FlexMAT file for the given condition.

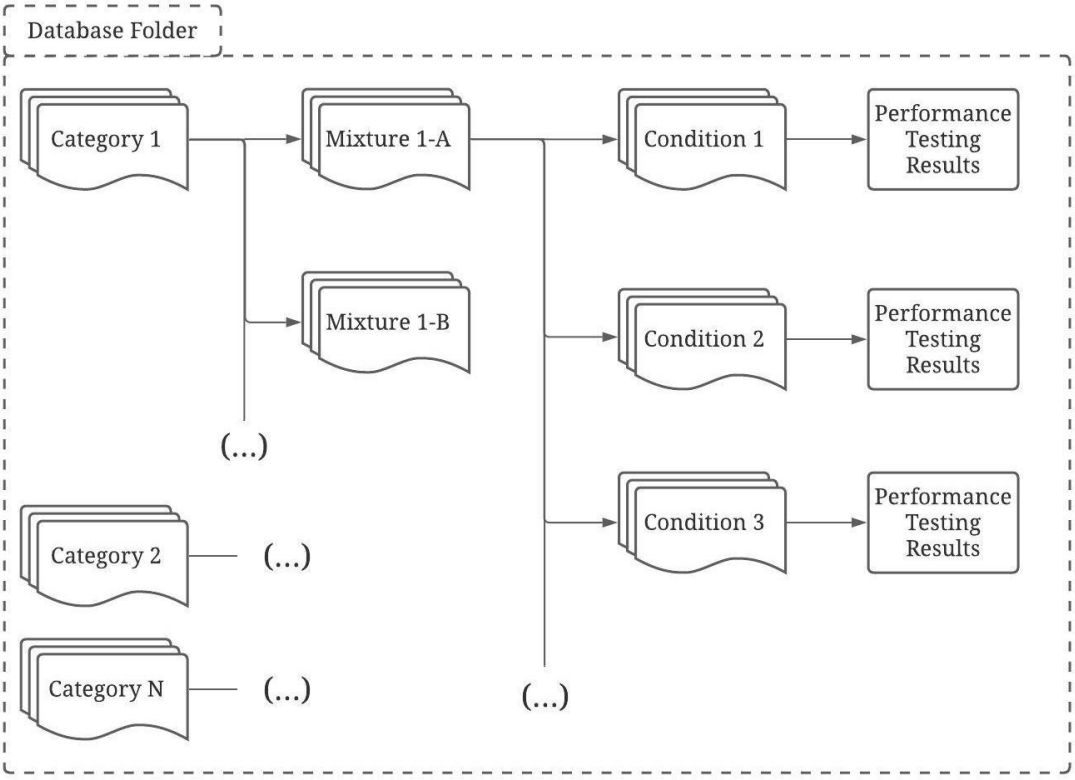

Source: FHWA.

Figure 73. Illustration. Schematic of database folder organization for PRS development.

A user can choose among three alternatives to handle the development of the database of mixtures in PASSFlex. Clicking the "Develop Material Database (4 Corners)" button in the initial screen starts the database development process. The "Develop Material Database" dialog box in figure 74 is displayed.

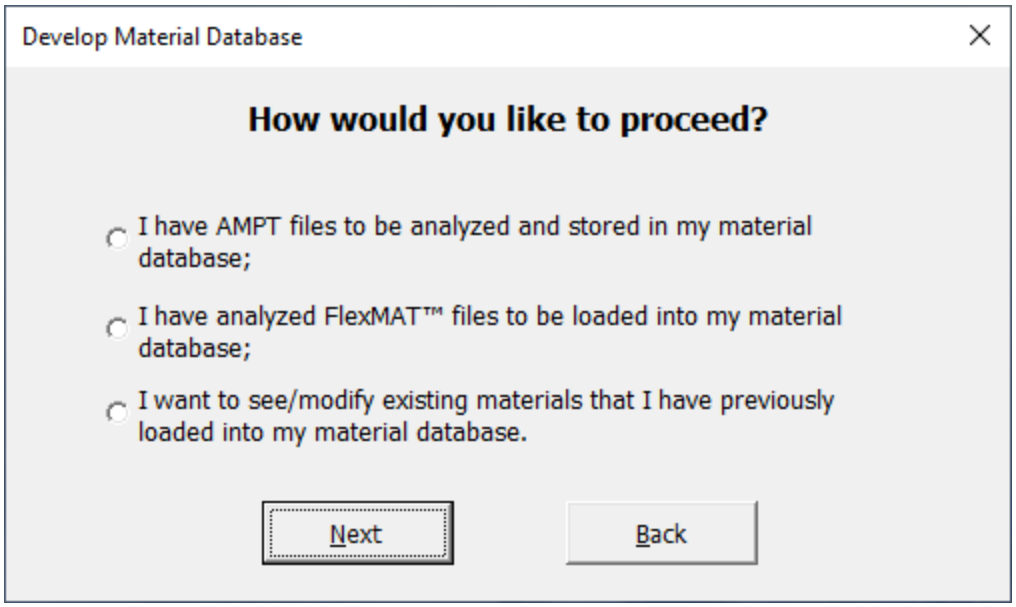

Source: FHWA.

Figure 74. Screenshot. "Develop Material Database" dialog box.

The user selects the "I have AMPT files to be analyzed and stored in my material database" radio button in situations where the user has performed the necessary laboratory tests described in previous sections and wishes to analyze the AMPT data by using FlexMAT files directly connected to the PASSFlex database. In this case, the expected inputs are files output from an AMPT in specific formats. PASSFlex will generate and open the necessary FlexMAT files when needed so that the user can complete data selection and analysis process.

When the user selects the "I have AMPT files to be analyzed and stored in my material database" radio button and then clicks the "Next," the "Analyze AMPT Data" dialog box in figure 75 is displayed. In the "Analyze AMPT Data" dialog box, the user can perform the following tasks:

- Select an existing condition that was previously added to the database and update that condition with new AMPT tested data.
- Create a new volumetric condition on the database so that the analysis can be performed.
- Load FlexMAT Cracking and FlexMAT Rutting for the analysis of the AMPT files and store the AMPT files in the appropriate database folder.

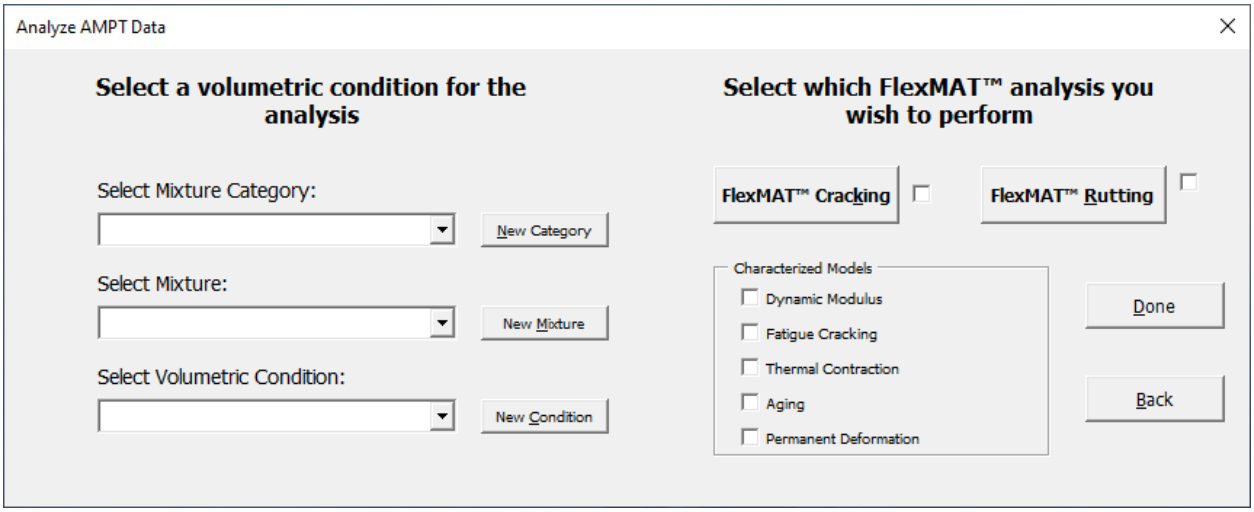

Source: FHWA.

Figure 75. Screenshot. "Analyze AMPT Data" dialog box for database development with AMPT files.

Once the intended FlexMAT analyses are complete, the user clicks "Done" to generate the summary file with the characterization coefficients for each of the FlexMAT files analyzed. Clicking "Done" also updates the "Characterized Models" area with a mark in the check box of every model for which coefficients were calibrated.

The user selects the "I have analyzed FlexMAT™ files to be loaded into my material database" radio button (figure 74) to handle previously analyzed FlexMAT files. Because FlexMAT is compatible with PASSFlex but independent of it, some users may use FlexMAT separately and independently from PASSFlex. Users should select the "I have analyzed FlexMAT™ files to be loaded into my material database" radio button in the following situations:

- The user ran their own analysis using FlexMAT before having access to PASSFlex.
- The user lost access to the AMPT output data but possesses FlexMAT files.
- The user possesses a FlexMAT (for Cracking or for Rutting) file without the corresponding AMPT files.

When the user selects the "I have analyzed FlexMAT™ files to be loaded into my material database" radio button and then clicks "Next" (figure 74), the "Load FlexMAT Data" dialog box (figure 76) is displayed. Even though the "Analyze AMPT Data" dialog box and the "Load FlexMAT Data" dialog box are similar, the methods for each approach are fundamentally different. in the "Load FlexMAT Data" dialog box (figure 76) is used to upload existing FlexMAT files from a known directory.

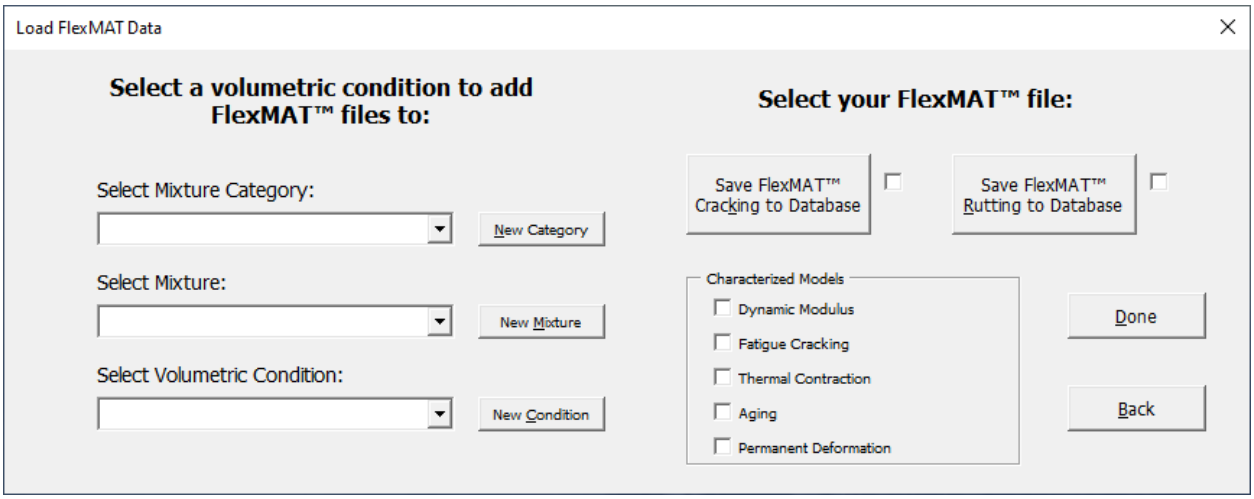

Source: FHWA.

Figure 76. Screenshot. "Load FlexMAT Data" dialog box for database development with external FlexMAT file.

If the FlexMAT version used outside of PASSFlex is FlexMAT version 2.1 (for users who have lost access to the AMPT output data but are in possession of FlexMAT files), no differences between the results from the first and second input approaches should be evident. If the versions are consistent, the calibrated coefficients should be the same. Users can expect minor deviations concerning the number of decimal places used when reading the coefficients. Users should always use the latest released version of FlexMAT because the latest version will have the most updated and verified algorithms and corrections to potential bugs and unexpected behaviors.

The "I want to see/modify existing materials that I have previously loaded into my material database" radio button is more for organization than development because the user cannot use the "I want to see/modify existing materials that I have previously loaded into my material database" radio button to add any new material to the database, but only to verify and modify existing inputs. When the user selects the "I want to see/modify existing materials that I have previously loaded into my material database" radio button and then clicks "Next," the "Material Database" dialog box in figure 77 is displayed. With the "Material Database" dialog box, users can verify already existing categories, mixtures, and volumetric conditions of the database, with the value of each coefficient and the models calibrated for each condition.

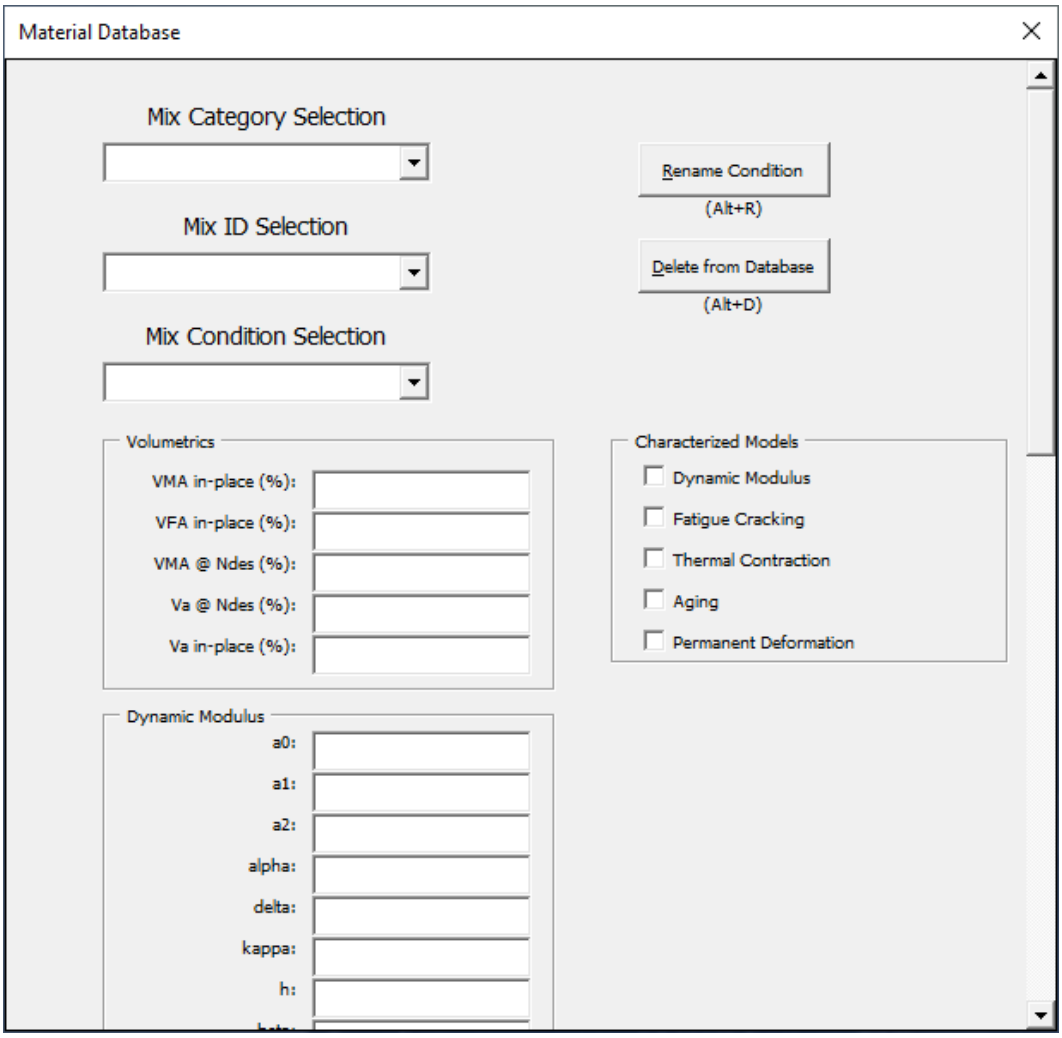

Source: FHWA.

Figure 77. Screenshot. "Material Database" dialog box for properties verification.

The user can begin verifying the characteristics of the existing mixtures by using the following lists in the top-left corner of the dialog box, which present all the materials currently in the database:

- The "Mix Category" list.
- The "Mix ID" list.
- The "Mix Condition" list.

Whenever a user selects one hierarchically higher list item, the following lists will automatically update their existing list of alternatives to those linked to the previous selection to provide the user with those lists for selection.

Once a user selects a volumetric condition, the "Characterized Models" area is updated with marks in the check boxes that indicate which models are characterized for the selected condition. Scrolling down, each model has a list of coefficients, and the respective values (when available)

are displayed. Users cannot edit these properties, but their presence is a visual verification of the actual values for each coefficient, cueing the user when a new condition has been loaded and potentially helping the user develop a sense of expected values for each coefficient.

Currently, users can perform two possible actions with the “Material Database” dialog box:

- The user can click the “Rename Condition” button to rename a given condition to change the nomenclature selected during that condition’s inclusion in the database.

- The user can click the “Delete from Database” button to delete any category, mixture, or condition.

If a user deletes higher hierarchical levels, any lower hierarchical levels will also be permanently deleted. For example, if a user deletes a mixture, any volumetric condition stored under that Mix ID will automatically be deleted.

Development of Performance-Related Specifications

The “Develop PRS” button on the PASSFlex initial screen calibrates the volumetric predictive models by using the tested information in the material database and, through those models, generates a pay table capable of linking AQCs to pay factors by following the stages of development.

The first stage begins when the user clicks the “Develop PRS” button on the initial PASSFlex screen, and then clicks “Next” to display the “PRS Project Selection” dialog box shown in figure 78. The “PRS Project Selection” dialog box separates creating a new project from updating a previously existing project; the user can either click the “Create a New Project” button under “New Project,” or select a project in the “Existing Projects” list. To continue working on an existing project (or to review an existing project’s details), the user clicks the “Existing Projects” list to display the list of existing projects, and then clicks a project. Under “Selected Project’s Protocol,” the text box displays a preview of the selected project’s protocol.

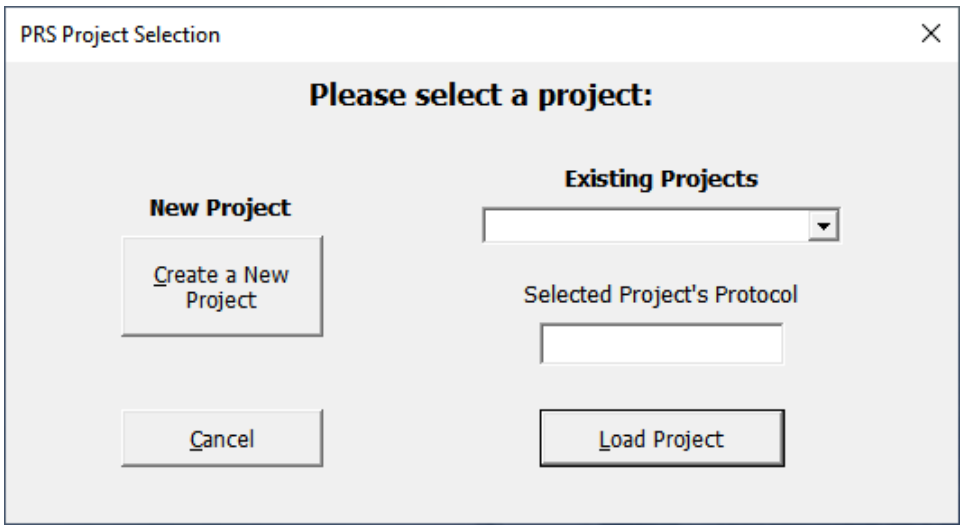

Source: FHWA.

Figure 78. Screenshot. "PRS Project Selection" dialog box.

PRS projects are always linked to a protocol in PASSFlex. When the user clicks the "Create a New Project" button, the "Protocol Selection" dialog box in figure 79 is displayed. In the "Project's Name" text box, the user types the name for the project, and then in the "Protocol Selection" area, click the correct protocol. Once the user clicks a protocol, the box in the "Informational" area is updated with a brief preview and description of that protocol and the steps involved. Protocols B and C are unavailable because these protocols are not implemented in the current PASSFlex version. However, this dialog box is expected to receive updates in the future to include protocols other than the existing protocols.

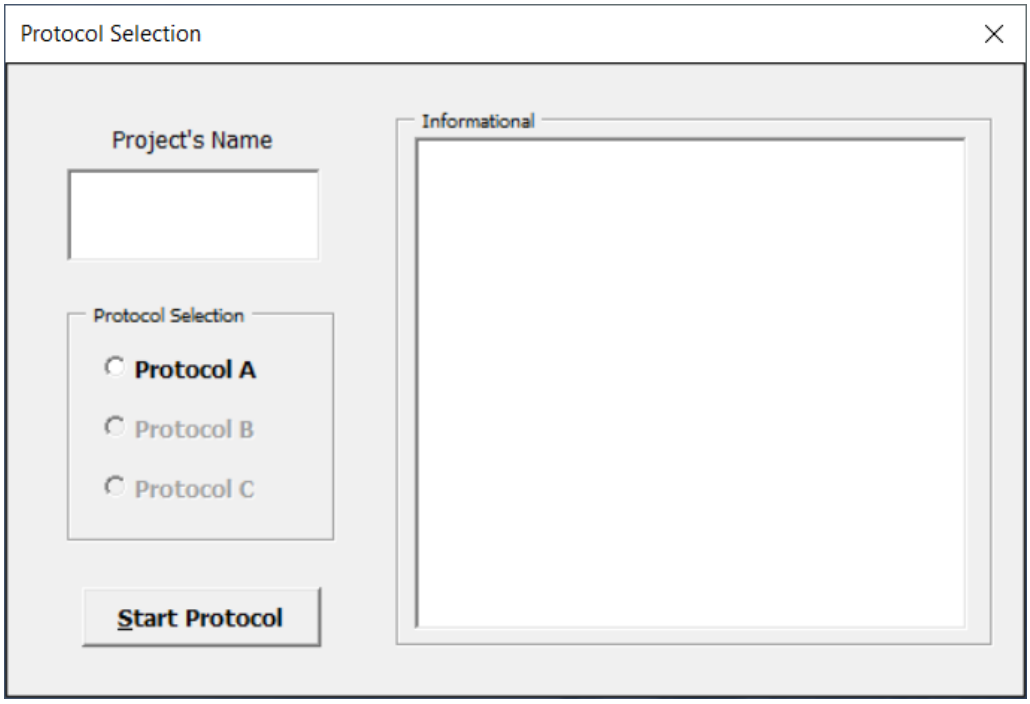

Source: FHWA.

Figure 79. Screenshot. "Protocol Selection" dialog box for a new project.

When the user clicks the "Start Protocol" button, the "Protocol A Step 1: Mixture Selection" screen in Figure 80 is displayed. Figure 80 identifies a few of the most important elements. On the "Protocol A Step 1: Mixture Selection" screen, the user can access all the mixtures previously added to the database through cells B3 and B4. When the user selects a mix category in cell B3, the available mix IDs for that category are displayed in cell B4.From there, when the user selects a mixture, all the volumetric conditions available (for that mixture) are updated into the "Table 1. Volumetric Conditions of Selected Mixture" table of properties at the bottom of the "Protocol A Step 1: Mixture Selection"' screen. This table is dynamically updated for each volumetric condition to summarize the index values (for S_{app} and the RSI) as a function of VMA_{IP} and VFA_{IP} in preparation for the second step.

S_{app} and the RSI, however, are project-dependent indexes and require a climatic component is to calculate their values. To incorporate this climatic component, users select the State and city in cells B7 and B8. When a user selects a location, PASSFlex searches for the nearest climatic station in the database of climatic stations and displays that nearest climatic station's coordinates (latitude and longitude) in cell B11 and updates the "Climate PG" cell (cell B12) with the corresponding values for the displayed location. PASSFlex uses this climate PG value for the S_{app} calculation and uses the "Station Code" cell (cell B14) to find the climatic summary file that the RSI calculation uses.

After the user selects the location, S_{app} is ready for the calculations required for the volumetric conditions that have had their S-VECD model calibrated.[12] When the user clicks the "Run S_{app} Analysis" button PASSFlex analyzes all the volumetric conditions and updates the volumetric conditions in the existing table. However, the layer type for the RSI still needs to be defined. To define the RSI layer type, in the "Layer Type – for RSI Calc." list (cell B9), the user clicks one

of the three listed items. Once the user selects the correct items in the "State" cell (B7), "City" cell (B8), and "Layer Type – for RSI Calc." cell (B9), clicking "Run RSI Analysis" determines the RSI value for each of the volumetric conditions that have permanent deformation characterized. The results are updated in the table.

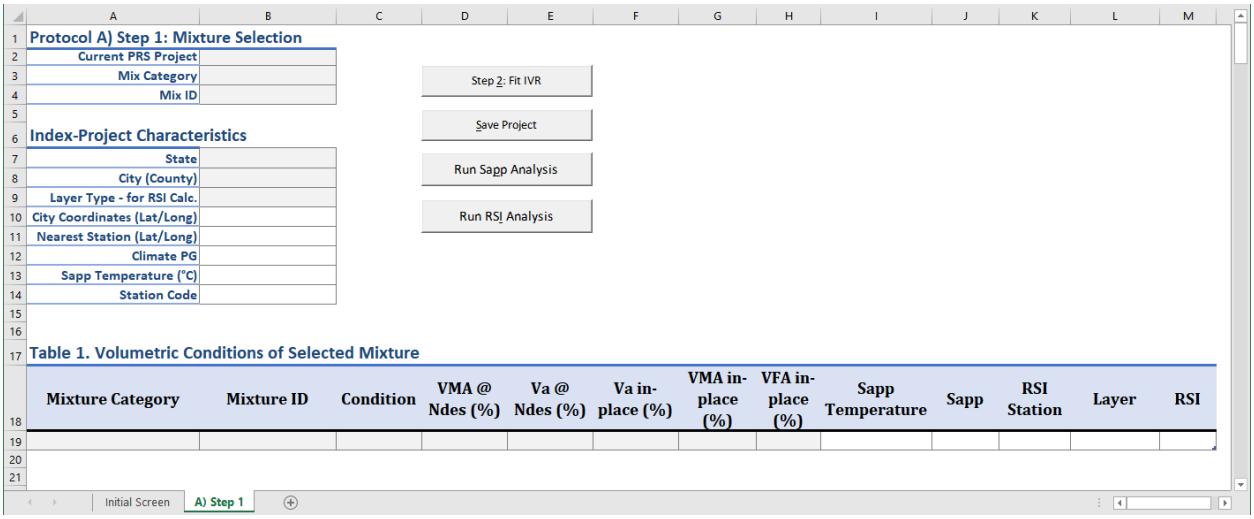

Source: FHWA.

Figure 80. Screenshot. "Protocol A Step 1: Mixture Selection" screen.

Table 44 presents a summary of functionalities and requirements for each of the possible actions presented in step 1 of protocol A. According to table 44, each index needs at least four volumetric conditions, which relates to the work of Wang et al., in which four conditions are considered an adequate number of conditions to balance accuracy of prediction and laboratory effort.[(19)]

Table 44. Summary of actions in step 1 of protocol A.

Action	Functionality	Requirement
The "Mix Category" cell (cell B3)	Select a mixture category from the available categories in the developed database.	• A mixture category exists in the database.
The "Mix ID" cell (cell B4)	Select a mixture from the available mixtures under the selected mixture category in the developed database.	• A mixture category is selected. • A mixture exists under the selected mixture category in the database.
The "Step 2: Fit IVR" button	Initialize step 2 of protocol A, fitting the index-volumetric relationship (IVR) to the volumetric conditions of the selected mixture.	• A mixture category is selected (cell B3). • A mixture is selected (cell B4). • At least four volumetric conditions have S_{app} calculated. • At least four volumetric conditions have RSI calculated.

Action	Functionality	Requirement
The "Save Project" button	Override the existing PRS project file in the database with the current project values.	• A project name is selected (cell B2).
The "Run S_{app} Analysis" button	Calculate the S_{app} value for each volumetric condition in the "Table 1. Volumetric Conditions of Selected Mixture" table that has been fatigue-damage characterized.	• A State is selected (cell B7). • A city is selected (cell B8). • A dynamic modulus model characterization exists in FlexMAT Cracking. • A fatigue cracking model characterization exists in FlexMAT Cracking.
The "Run RSI Analysis" button	Calculate the S_{app} value for each volumetric condition present in the "Table 1. Volumetric Conditions of Selected Mixture" table that has been permanent deformation characterized.	• A State is selected (cell B7). • A city is selected (cell B8). • A layer type is selected (cell B9). • A permanent deformation model characterization exists in FlexMAT Rutting.

After the user fills the "Table 1. Volumetric Conditions of Selected Mixture" table with a minimum of four values for S_{app} and the RSI, if the user clicks the "Step 2: Fit IVR" button, the "Protocol A Step 2: Index-Volumetric Relationship (IVR) Fitting" screen is displayed for the next step of this protocol. Clicking the "Step 2: Fit IVR"' button starts the process of minimization as a background calculation, thereby fitting the first-order linear function given by equations 21 and 22 to the assembled index-volumetric space in protocol A's step 1.

The "Protocol A Step 2: Index-Volumetric Relationship (IVR) Fitting" screen in PASSFlex contains details about the fitting quality of the IVR function and, most importantly, the fitting coefficients (β_i) for the IVR. Two plots provide the user with the means to visually inspect the fit quality and show the predicted index values versus the measured values obtained from the four corners. Figure 81 presents a brief overview of the "Protocol A Step 2: Index-Volumetric Relationship (IVR) Fitting" screen. Two cells, C5 and C6, were designed to select different fitting models for the IVRs, but currently the only available option is the First-Order model described in equations 21 and 22.

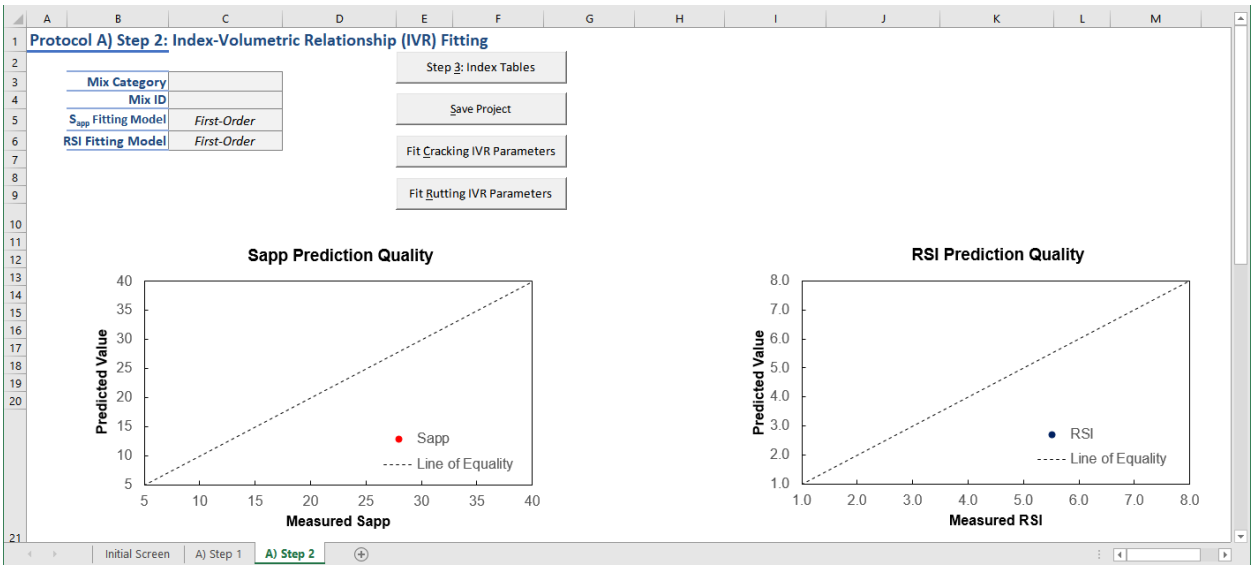

Source: FHWA.

Figure 81. Screenshot. "Protocol A Step 2: Index-Volumetric Relationship (IVR) Fitting" screen.

Table 45 provides a summary of the actions available in step 2 of protocol A, with the respective descriptions and requirements.

Table 45. Summary of actions in step 2 of protocol A.

Action	Functionality	Requirement
The "Step 3: Index Tables" button	Generate index tables based on the fitted IVRs given the limits for the volumetric variables.	• The IVR is fitted for both S_{app} and RSI predictions. • A volumetric limit is selected for index tables.
The "Save Project" button	Override the existing PRS project file in the database with the current project values.	A project name is selected (cell B2 on the "Protocol A Step 1: Mixture Selection" screen).
The "Fit Cracking IVR Parameters" button	Rerun the minimization of error between predicted and measured S_{app} values by refitting the IVR coefficients.	A minimum of four S_{app} values exist in different volumetric conditions.
The "Fit Rutting IVR Parameters" button	Rerun the minimization of error between predicted and measured RSI values by refitting the IVR coefficients.	A minimum of four RSI values exist in different volumetric conditions.

The next step, step 3, generates index tables based on the fitted IVRs for multiple volumetric conditions. When the user clicks the "Step 3: Index Tables" button, the "VMA-VFA Range Selection" dialog box is displayed to select the volumetric range. Figure 82 shows the "VMA-VFA Range Selection" dialog box and its elements.

Source: FHWA.

Figure 82. Screenshot. "VMA-VFA Range Selection" dialog box for protocol A's step 3 volumetric range selection.

Each index table forms a grid of 16 by 16 values, i.e., PASSFlex uses 16 VMA_{IP} values and 16 VFA_{IP} values to calculate the index values using the IVRs. The "VMA-VFA Range Selection" dialog box (figure 82) determines the range of each of the volumetric variables used to characterize the indexes in the generated table, given lower and upper limits. The values will be equally distributed between the limits if each incremental step is greater than or equal to 0.1 percent (adopted precision of the volumetric variables); if not, the upper limit will be assumed as the minimum limit plus 1.5 percent to ensure the minimum precision as an incremental step.

The three following alternatives set the limits of the volumetric variables for index tables:

- The user selects the "Suggested Limits" radio button to define the minimum and maximum available limits as those limits are presented among the tested conditions and update the four text boxes on the right of the dialog box accordingly for the user's visual verification. If the user modifies the values, the other values are maintained as unmodified, but the "Suggested Limits" radio button changes to unselected and the "Custom Limits" radio button changes to selected.

- The user selects the "Custom Limits" radio button to freely select the limiting values of the volumetric variables.

- The "Project Based Limits" radio button is based on the Superpave method that defines the volumetric limits according to the mixture's NMAS and on the project's expected traffic level. The user selects the "Project Based Limits" radio button to select the limits. In the "Mix/Project Information area, the drop-down lists change from "Locked" to empty values so that the user can select among the existing limits. The presented list of limits follows The Superpave Mix Manual for new Construction and Overlays and are given in Table 46 and Table 47.[79] Because VMA has no upper limit, the upper limit is left to the user's discretion, but is still required.

Table 46. Criteria for minimum VMA.[79]

Nominal Maximum Size	Minimum Voids in Mineral Aggregate (percent)
9.5 mm	15.0
12.5 mm	14.0
19.0 mm	13.0
25.0 mm	12.0
37.5 mm	11.0
50.0 mm	10.5

Table 47. Criteria for voids filled with aggregate range.[79]

Traffic Level (ESALs)	Design Voids Filled with Asphalt (percent)
$< 3 \times 10^5$	70 – 80
$< 3 \times 10^6$	65 – 78
$< 1 \times 10^8$	65 – 75
$> 1 \times 10^8$	65 – 75

When the user selects the four limits and then clicks the "Done" button, PASSFlex verifies the validity of the inputs for possible typographical errors or invalid information (e.g., non-numeric inputs) and displays the "Protocol A Step 3: Index Tables Generation" screen. Step 3 has a dedicated screen (similar to steps 1 and 2) with two index tables (one for each index) where the index values are calculated for each volumetric condition given in the top row (VMA_{IP}) and leftmost column (VFA_{IP}). Figure 83 shows the "Protocol A Step 3: Index Tables Generation" screen.

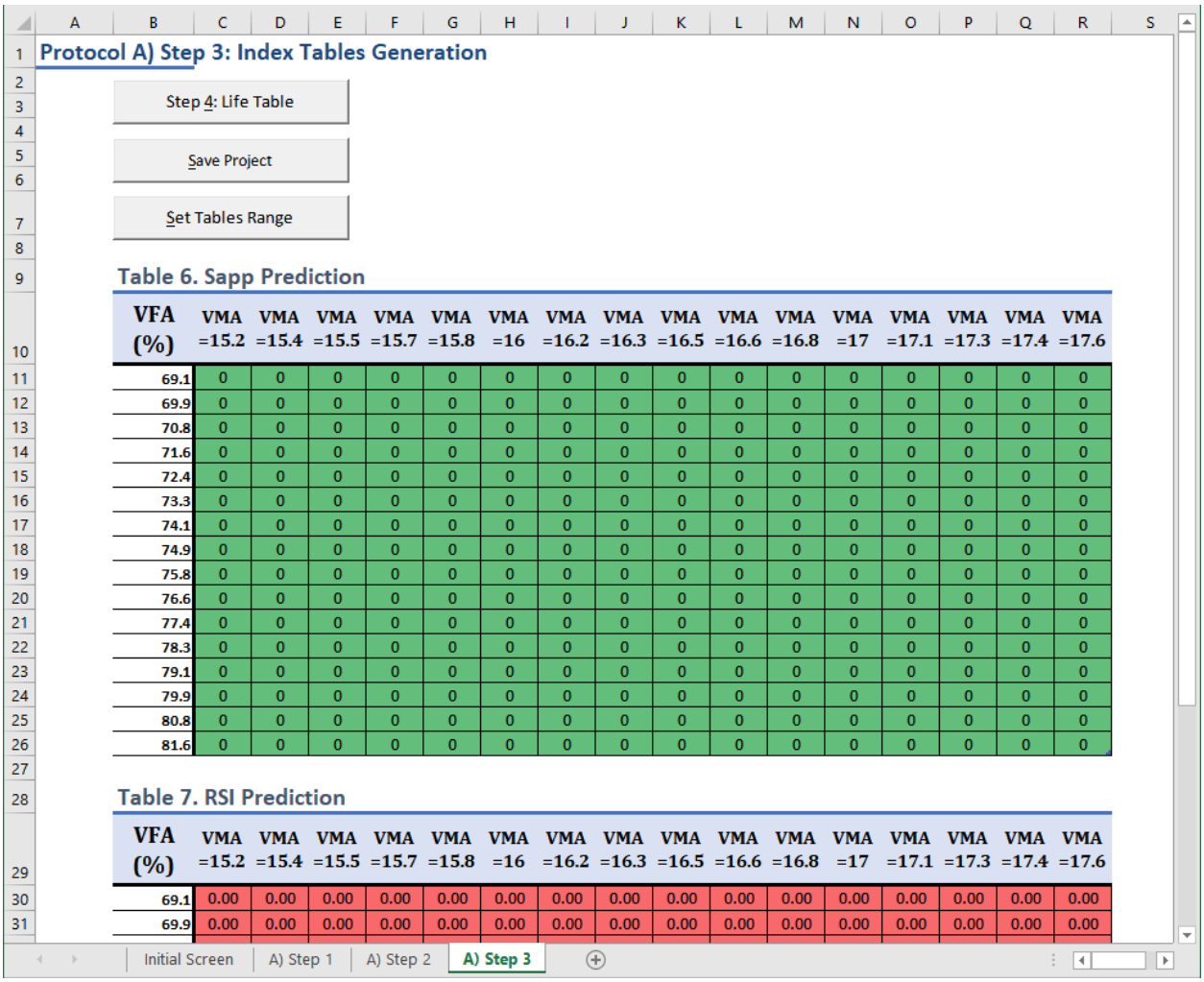

Source: FHWA.

Figure 83. Screenshot. "Protocol A Step 3: Index Tables Generation" screen.

During the development of the index table generation procedure, the developers considered AQCs other than VMA_{IP} and VFA_{IP} as alternatives for the display variables, and those other AQCs may still be implemented in a future version to accommodate the needs of different agencies. The simplicity of generating index tables based on the same two volumetric variables used to calibrate the coefficients in equations 21 and 22 was the governing strategy for the current implementation, because that strategy removed the need for additional dimensions on the displays when a user needs a set of more than two variables. Agency and contractor feedback regarding the common practice of AQCs as display variables is important for the acceptance and usability of PASSFlex, so the current implementation may be changed once developers collect evaluation input about PASSFlex from the intended public.

Table 48 provides a summary of the available actions in step 3 of protocol A with the respective description and requirements.

Table 48. Summary of actions in step 3 of protocol A.

Action	Functionality	Requirement
The "Step 4: Life Table" button	*Generate the life table based on the fitted IVRs, given the limits for the volumetric variables.	—
The "Save Project" button	Override the existing PRS project file on the database with the current project values.	A project name is selected (cell B2 on the "Protocol A Step 1: Mixture Selection" screen).
The "Set Tables Range" button	Reload the volumetric variables limit selection window.	—

—No requirement.
*Dummy deterministic solution implemented.

Once the user is satisfied with the current setting of the index tables, the user clicks the "Step 4: Life Table" button to generate pavement life predictions through the indexes.

This step is currently not validated for the conversion between the index values and pavement life. The development of this relationship is currently outside the scope of work. This research creates the space in which this relationship can be implemented once a research team can conduct an indepth study and develop and validate a method for the conversion. Once the solution is ready, developers will then update PASSFlex to accommodate this conversion step by adjusting the inputs to inputs that the developed method may require and modifying the background algorithm accordingly. The research team expects that this solution will be based on a probabilistic approach, taking historical variations of the AQCs and running MCMC method simulations to generate the probability distribution of the predictions.(52)

The current PASSFlex implementation presents a deterministic relationship between expected pavement life and the generated index values. Again, the current relationship is a placeholder for the finalized conversion method. The currently implemented method is not validated or representative of the expected material behavior by any means. The implemented function is not specified in this work and should be viewed as a generic closed-form function that converts indexes into life.

Figure 84 presents the "Protocol A Step 4: Life Table Generation" screen and a respective deterministic life table. In the current implementation, the life table follows the same limits used for the index tables, which may or may not be modified, depending on the needs of the index-to-life solution.

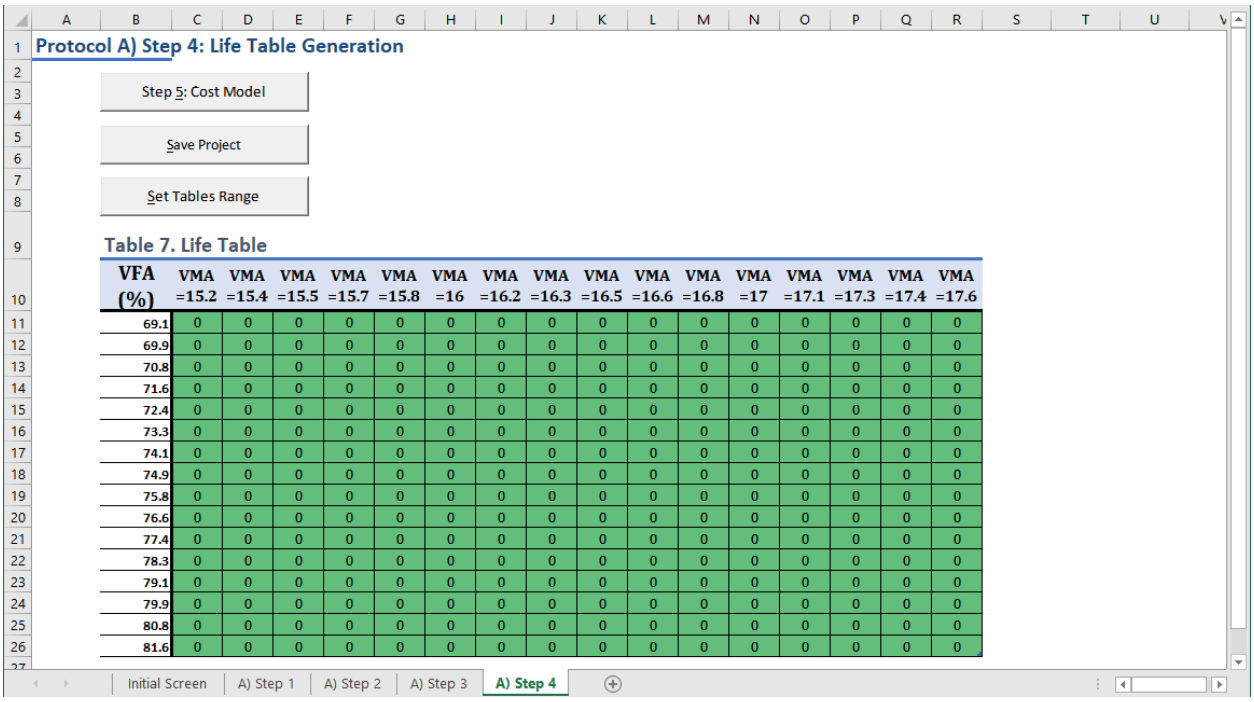

Source: FHWA.

Figure 84. Screenshot. "Protocol A Step 4: Life Table Generation" screen.

Even though the current implementation is subject to changes, table 49 provides a brief description of the existing actions of step 4 so that the example presented later can be better understood.

Table 49. Summary of actions in step 4 of protocol A.

Action	Functionality	Requirement
The "Step 5: Cost Model" button	Display the "Protocol A Step 5: Cost Model Definition" screen to define the cost model.	—
The "Save Project" button	Override the existing PRS project file on the database with the current project values.	A project name is selected (cell B2 on the "Protocol A Step 1: Mixture Selection" screen).
The "Set Tables Range" button	Reload the volumetric variables limit selection window.	—

—No requirement.

Moving to step 5 from step 4 has no requirement; as soon as the user clicks the "Step 5: Cost Model" button, the "Protocol A Step 5: Cost Model Definition" screen in figure 85 is displayed. Step 5 defines the cost-model function that relates incentives and disincentives to the predicted life difference (PLD). The two complementary elements on the "Protocol A Step 5: Cost Model Definition" screen are the "Table 8. Cost Model" table and the "Cost Model" chart. The information in the "Table 8. Cost Model" table is reproduced graphically in the "Cost Model" chart so that the user can visually inspect the defined model and verify its adequacy for the

intended relationship. The cost model uses the difference between the expected design life and the predicted life defined in step 4 to generate an incentive and disincentive factor (%I/D) that will be used to calculate the adjustment of the final payment.

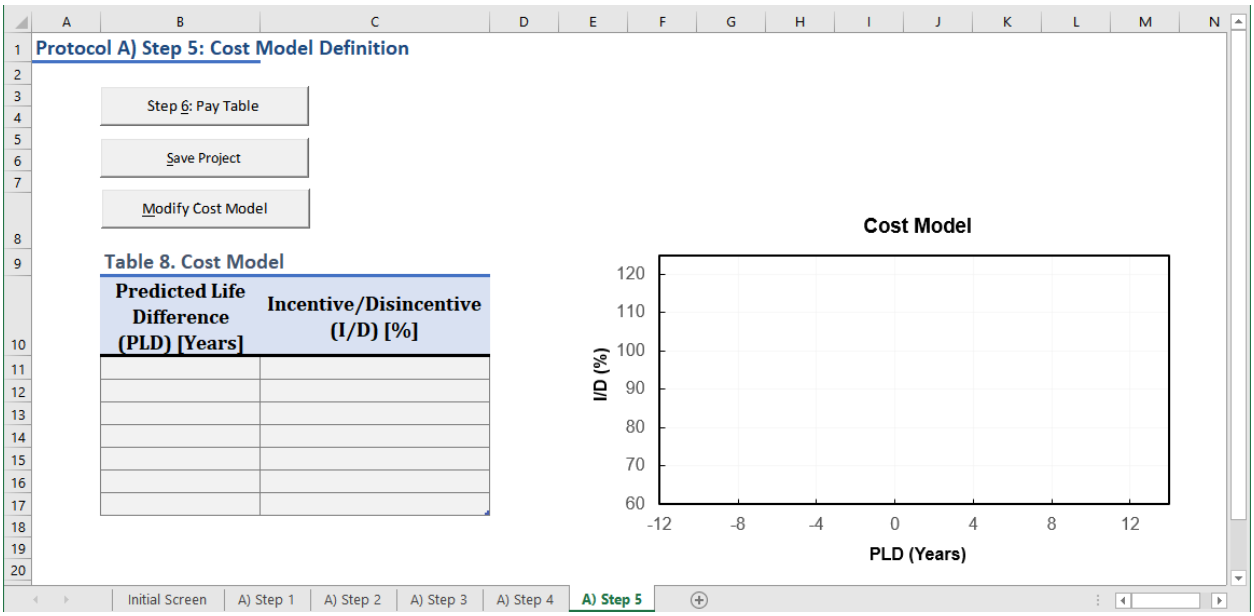

Source: FHWA.

Figure 85. Screenshot. "Protocol A Step 5: Cost Model Definition" screen.

Table 50 presents an overview of the actions in step 5 of protocol A with the corresponding descriptions and restrictions shown in the "Protocol A Step 5: Cost Model Definition" screen.

Table 50. Summary of actions in step 5 of protocol A.

Action	Functionality	Requirement
The "Step 6: Pay Table" button	Display the "Protocol A Step 6: Pay Table Generation" screen and apply the characterized cost model to the life table in step 4 to generate the pay table.	A set of at least two coordinate points exist in the cost model.
The "Save Project" button	Override the existing PRS project file in the database with the current project values.	A project name is selected (cell B2 on the "Protocol A Step 1: Mixture Selection" screen).
The "Modify Cost Model" button	Display the "Cost Model Update" dialog box.	—

—No requirement.

When the user clicks the "Modify Cost Model" button, the "Cost Model Update" dialog box in Figure 86 is displayed. The "Cost Model Update" dialog box guides the user through updating the cost model, instead of simply modifying the "Table 8. Cost Model" table with the cost model's definition points.

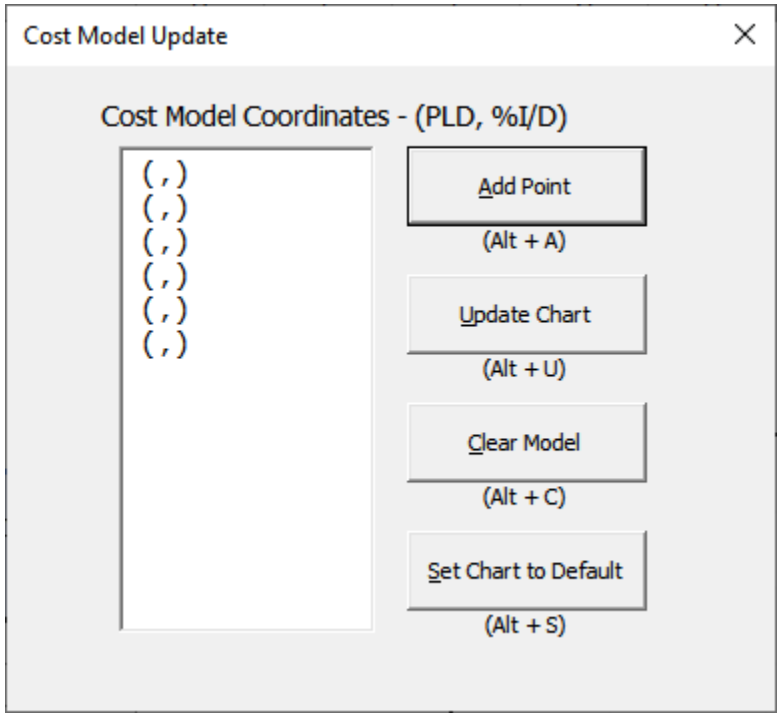

Source: FHWA.

Figure 86. Screenshot. "Cost Model Update" dialog box.

The following four actions are available in the "Cost Model Update" dialog box:

- When the user clicks the "Add Point" button, the "Add Point to Cost Model" dialog box in figure 87 is displayed. The user can enter a coordinate pair: PLD in the "Predicted Life Difference (PLD)" box and %I/D in the "Percent Incentive/Disincentive (%I/D)" box. After the user enters the values, PASSFlex verifies the values to ensure that typographical errors and non-numeric values are not present and then adds the values to the set of coordinates that define the cost model.

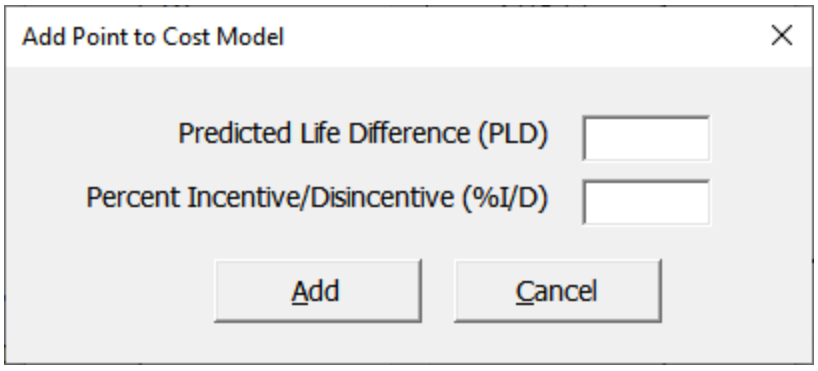

Source: FHWA.

Figure 87. Screenshot. "Add Point to Cost Model" dialog box.

- When the user clicks the "Update Chart" button, PASSFlex converts the current set of coordinates in the "Cost Model Coordinates – (PLD, %I/D)" box to the cost model on the "Protocol A Step 5: Cost Model Definition" screen and updates both the table and graph. PASSFlex checks the validity and completion of the input coordinates and provides the user with guidance if an error is found.

- When the user clicks the "Clear Model" button, PASSFlex clears the current cost model's coordinates from the "Cost Model Coordinates – (PLD, %I/D)" box, and in the "Protocol A Step 5: Cost Model Definition" screen, deletes the values in the "Table 8. Cost Model" table and clears the "Cost Model" chart. This action cannot be undone.

- When the user clicks the "Set Chart to Default," PASSFlex overrides the current cost model and loads a predefined, arbitrarily chosen cost model. This predefined default cost model is mainly illustrative. An alternative functionality (not implemented) is an agency-specific library of cost models, where agencies would have the option to create a database of cost models to be readily available once a new cost model is stored.

The cost model implemented from the set of input coordinates is a piecewise linear function, i.e., a function that assumes linear behavior for interpolation between coordinate points. For extrapolations of a PLD less than the minimum PLD established by the coordinates, %I/D is assumed to have a value of 0 percent, which represents a material that has such poor behavior compared to the expected pavement life that a complete replacement would be required for the contractor to receive any payment. On the other hand, for PLD values greater than the maximum PLD defined in the cost model's coordinates, %I/D is assumed to become a constant value equal to the %I/D that corresponds to the maximum PLD value. This approach represents a limit to the incentives, indicating that beyond a certain quality level of the material, increments in the material quality would not receive additional financial incentives.

Once a valid cost model is set, when the user clicks the "Step 6: Pay Table" button PASSFlex initializes the last step, generating the pay table. This step generates the output from PASSFlex's second block, the pay tables, based on the design life of the input in cell C7. Figure 88 presents the "Protocol A Step 6: Pay Table Generation" screen.

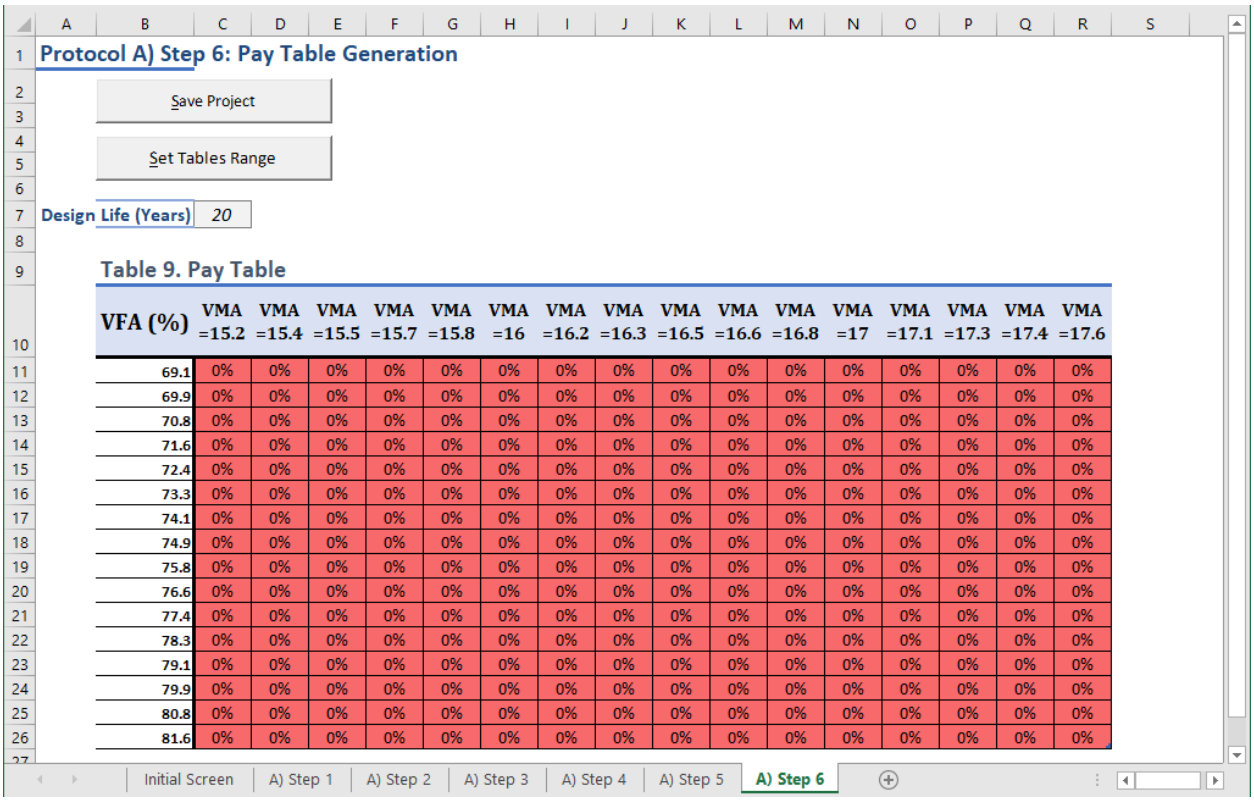

Source: FHWA.

Figure 88. Screenshot. "Protocol A Step 6: Pay Table Generation" screen.

Table 51 presents an overview of the available actions in step 6.

Table 51. Summary of actions in step 6 of protocol A.

Action	Functionality	Requirement
The "Design Life (Years)" cell (C7)	Set the design life, in years, for the calculation of the pay table.	—
The "Save Project" button	Override the existing PRS project file in the database with the current project values.	A project name is selected (cell B2 on the "Protocol A Step 1: Mixture Selection" screen).
The "Set Tables Range" button	Reload the volumetric variables limit selection window.	—

—No requirement.

The pay table is the combined result of all the previous steps and converts the volumetric characteristics into the payment percentage. This information is valuable because this information will be applied at different times in a project. For agencies, the pay table is an item in the set of QA tools that establishes the quality standards that are expected of the final product and provides contractors with rational, justifiable information about how payments are adjusted based on AQCs.

Figure 89 presents a flowchart of the procedure to develop PRS in protocol A.

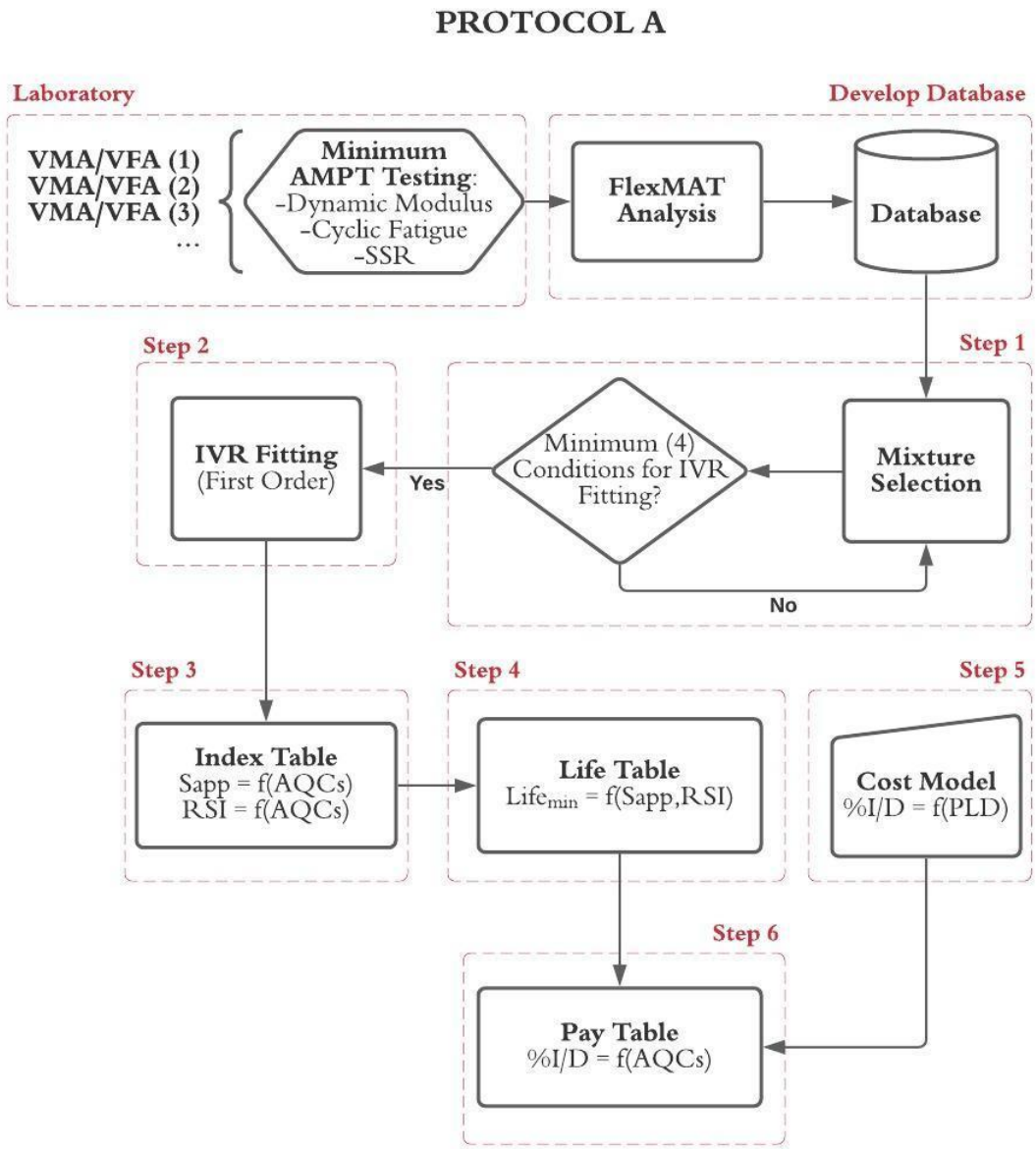

Source: FHWA.

Figure 89. Illustration. Summary flowchart of protocol A's pay table development.

Mix Approval

The “Approve Mix” button on the initial PASSFlex screen guides the user through the acceptance procedure for a mixture. In the expected workflow of a PRS project, the mixture would be submitted by the contractor who won the project bid and now needs to have the mix design approved by the agency. The agency would be responsible for performing the AMPT laboratory performance tests of this mixture, which should be in the form of an optimized design process (e.g., Superpave mix design, performance-engineered mix design (PEMD)), which this report refers to as the optimum condition. This procedure is different from the procedure in the “Development of Performance-Related Specifications” section, which uses the different volumetric conditions tested to predict the material’s performance in the volumetric space. The optimal condition is no longer submitted as a calibration resource but rather as a condition under direct evaluation, and its characteristics are used to determine the mix’s quality and adequacy.

Making a distinction between the use of mixtures for various purposes helps avoid confusion. A mixture can be defined by a set of materials (aggregate, binder, RAP) and can be mixed under different volumetric conditions (typically four conditions, i.e., the four corners used to calibrate the volumetric relationships). However, mixture approval sees a mixture in terms of a single volumetric condition, the optimum condition, which is representative of that mixture’s characteristics and responsible for the mixture passing (or failing) the approval criteria.

The version of PASSFlex developed from this study uses protocol A, which has an approval criterion based on indexes (S_{app} and the RSI) to determine if the mix is acceptable or not. PASSFlex creates and manages a database for the submitted optimum conditions to access and verify the mixtures, and the software is responsible for managing the database and running the analyses.

The user clicks the “Approve Mix”’ button to initialize the mixture approval process. The first step is deciding between managing the mixture approval database and approving the actual mix. Figure 90 presents the “Start Mix Approval” dialog box that guides the user through this selection process.

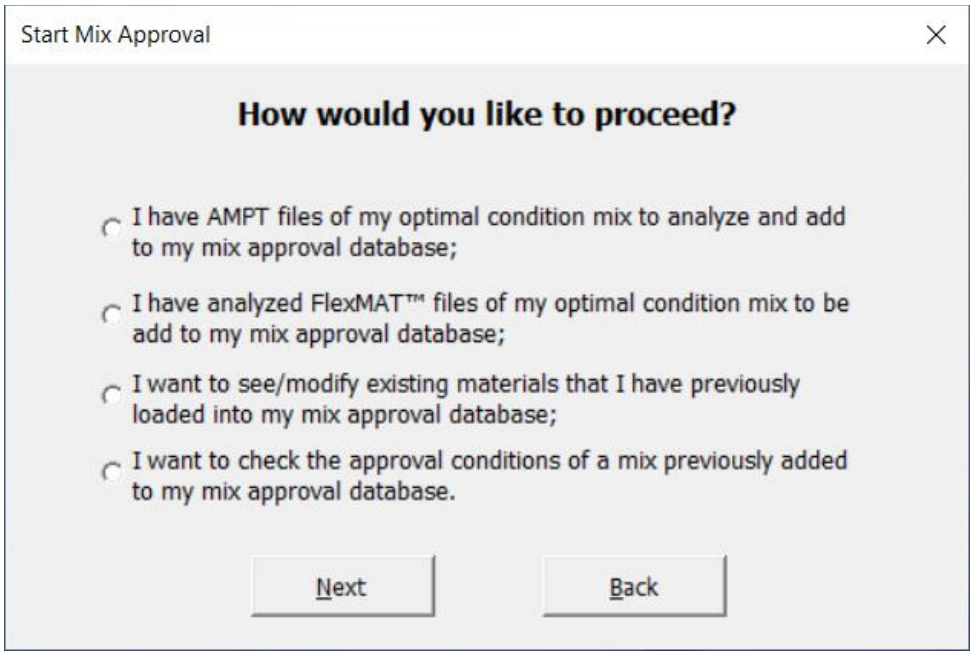

Source: FHWA.

Figure 90. Screenshot. "Start Mix Approval" dialog box, the action filter dialog box for mix approval.

The "Start Mix Approval" dialog box contains four radio buttons for different analysis stages of an optimum condition mixture to be checked for approval. To start any stage, the user selects one of the following radio buttons, and then clicks the "Next" button:

- The "I have AMPT files of my optimal condition mix to analyze and add to my mix approval database" radio button: The user selects this radio button when AMPT performance testing has been performed in the lab and the results are ready to be analyzed through FlexMAT. The user can modify or create an entry for the mixture's optimum condition in the database and create and open the required FlexMAT files in the "Analyze AMPT Data for Mix Approval" dialog box in figure 91 (similar to the "Analyze AMPT Data" dialog box in figure 75 except for the simplification of the number of needed inputs). Also, the mixtures are no longer separated into categories and volumetric conditions; instead, PASSFlex requires a single identification for the optimum condition's name. The similarity between the "Analyze AMPT Data for Mix Approval" dialog box and the "Analyze AMPT Data" dialog box is intentional and based on the assumption that the user's experience with either method of database handling is directly transferable to the other method.

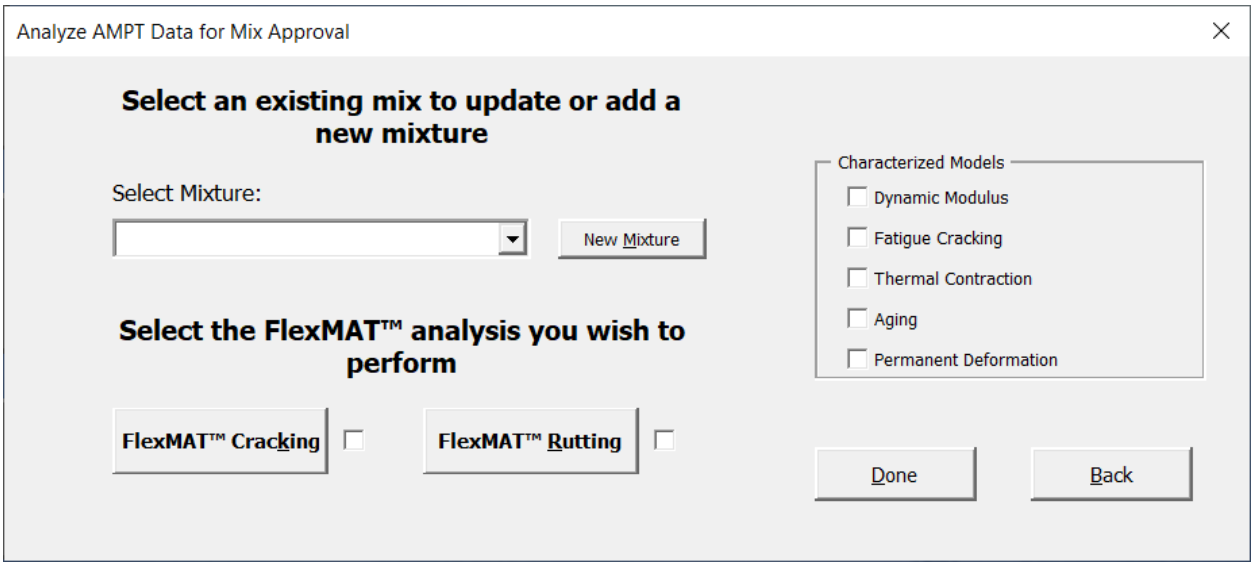

Source: FHWA.

Figure 91. Screenshot. "Analyze AMPT Data for Mix Approval" dialog box.

- The "I have analyzed FlexMAT™ files of my optimal condition mix to be added to my mix approval database" radio button: The user selects this radio button to display the "Load FlexMAT Data for Mix Approval" dialog box (figure 92) to choose from preanalyzed FlexMAT files, i.e., FlexMAT files that correspond to the mixture to be added to the database. Although selecting the "I have AMPT files of my optimal condition mix to analyze and add to my mix approval database" radio button (the first option in the "Start Mix Approval" dialog box) generates the necessary files to perform the analysis, selecting the "I have analyzed FlexMAT™ files of my optimal condition mix to be added to my mix approval database" radio button (the second option in the "Start Mix Approval" dialog box) creates a database entry for a mixture with the expectation that selecting FlexMAT files will complete the material's characterization without requiring further analysis.

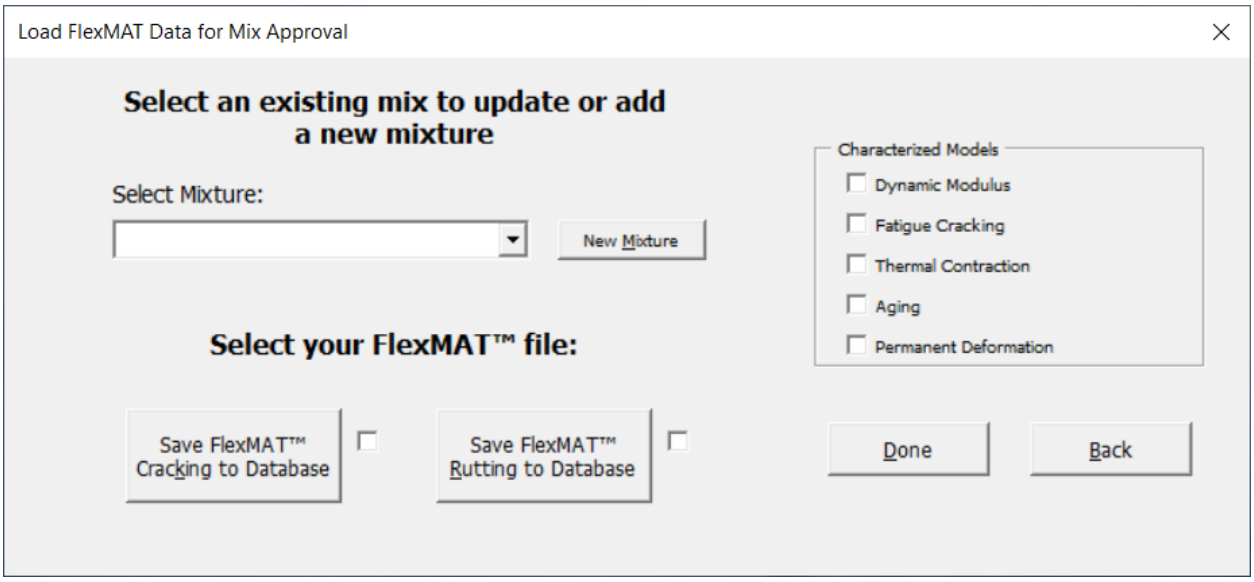

Source: FHWA.

Figure 92. Screenshot. "Load FlexMAT Data for Mix Approval" dialog box.

The user selects the FlexMAT files by clicking the "Save FlexMAT™ Cracking to Database" and "Save FlexMAT™ Rutting to Database" buttons under "Select your FlexMAT™ file" (similar to the "Load FlexMAT Data" dialog box in figure 76 and for the same reasons as the "Analyze AMPT Data for Mix Approval" dialog box in figure 91). After PASSFlex loads the FlexMAT files, PASSFlex marks the check boxes next to the "Save FlexMAT™ Cracking to Database" and "Save FlexMAT™ Rutting to Database" buttons to indicate the presence of the files in the selected mixture's database entry and updates the check boxes in the "Characterized Models" area accordingly.

- The "I want to see/modify existing materials that I have previously loaded into my mix approval database" radio button: The user selects this radio button to display the "Mix Approval Material Database" dialog box (figure 93), which provides access to any mixture that has been previously added to the mixture approval database. In the "Mix Approval Material Database" dialog box, the user can rename mixtures, delete mixtures, and show the calibrated models with the respective coefficients (when available).

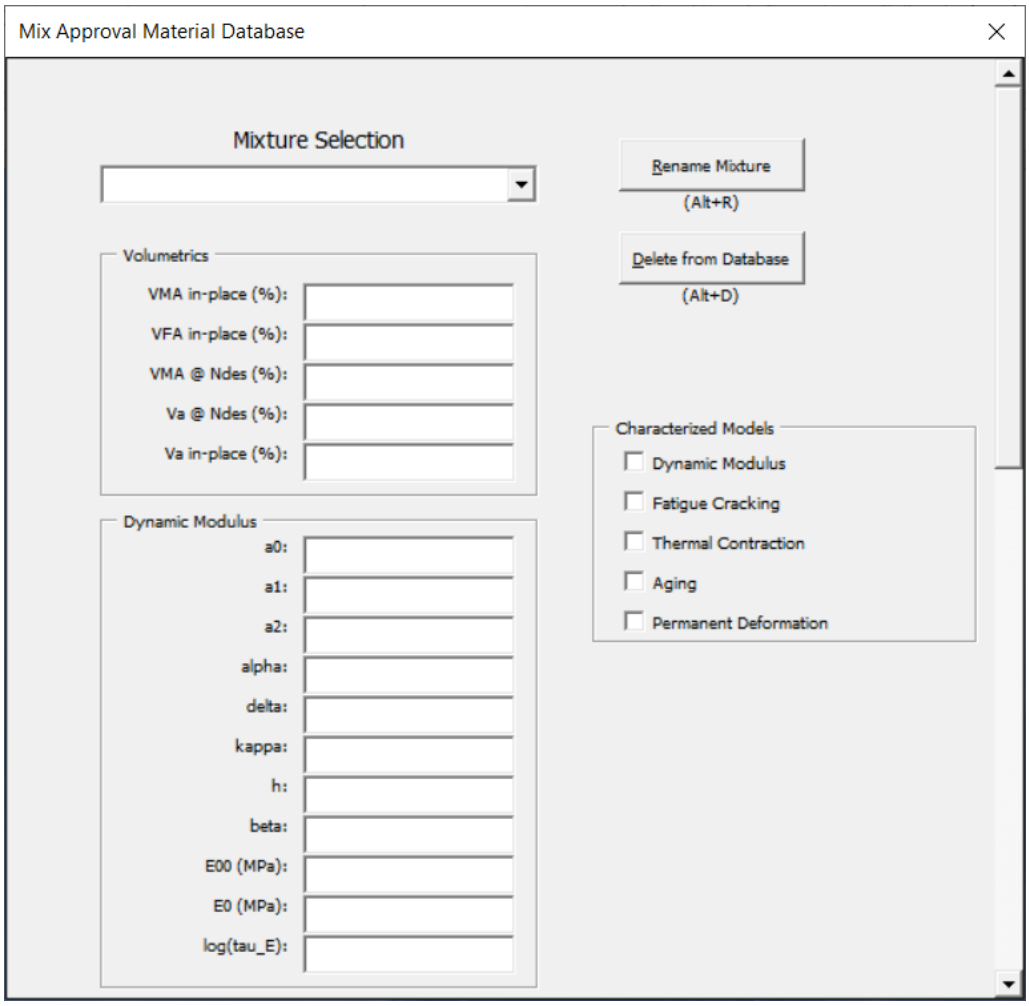

Source: FHWA.

Figure 93. Screenshot. "Mix Approval Material Database" dialog box.

- The "I want to check the approval conditions of a mix previously added to my mix approval database" radio button: The user clicks this radio button to display the "Protocol Selection for Mix Approval" dialog box (figure 94) and start the mix approval process. Because protocols B and C are still under development, their alternatives are still locked, but once protocols B and C are implemented, their alternatives also will be selected on the "Protocol Selection for Mix Approval" dialog box. When the user selects a protocol, PASSFlex updates the "Informational" box with a summary of the respective mix approval procedure for the selected protocol. This feature provides the user with brief in-program guidance about the protocol selection process. Clicking the "Start Mix Approval" button displays the "Mix Approval – Protocol A" screen (figure 95).

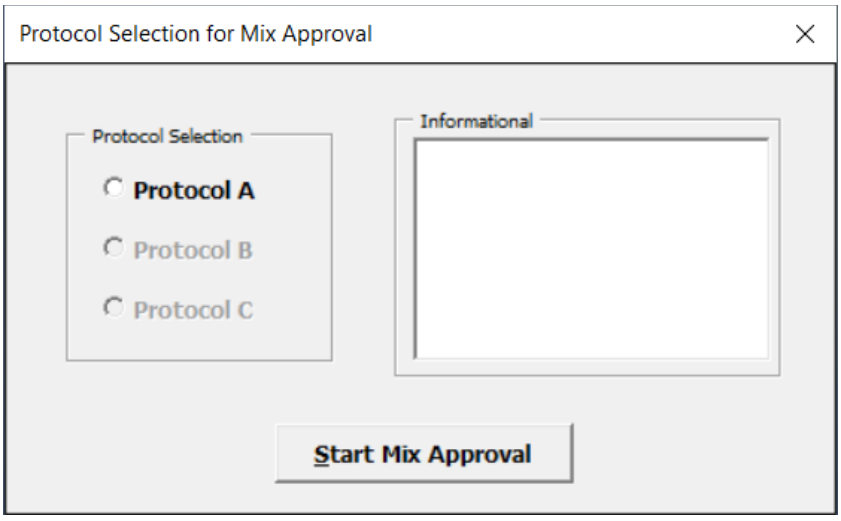

Source: FHWA.

Figure 94. Screenshot. "Protocol Selection for Mix Approval" dialog box.

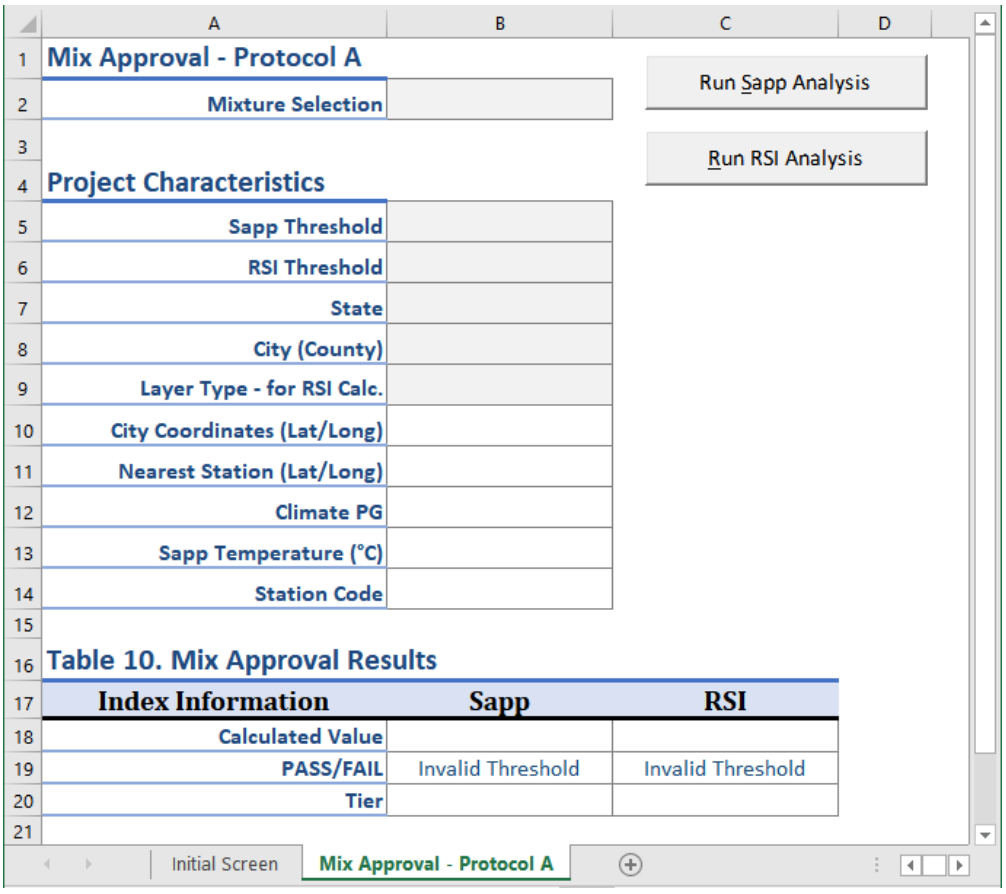

Source: FHWA.

Figure 95. Screenshot. "Mix Approval - Protocol A" screen.

Protocol A's mix approval procedure is based on indexes. A comparison between a threshold value and the calculated index value determines if the mixture is approved or not. For the RSI, the calculated value needs to be smaller than the threshold, whereas for S_{app}, the calculated value needs to be greater than the threshold. The "Mix Approval – Protocol A" screen in figure 95 guides the user toward the index calculation and threshold limit comparison process. Table 52 presents a summary of the available actions and their respective functionalities and requirements.

Table 52. Summary of actions on the "Protocol A - Mix Approval" screen.

Action	Functionality	Requirement
The "Mixture Selection" list (cell B2)	Select the mixture submitted for approval among the available optimum condition mixtures added to the mixture approval database.	Mixture exists in the mixture approval database.
The "S_{app} Threshold" cell (cell B5)	Determine the minimum allowable value for S_{app} for the mixture to be approved with respect to fatigue cracking.	—
The "RSI Threshold" cell (cell B6)	Determine the maximum allowable value for the RSI for the mixture to be approved with respect to permanent deformation.	—
The "State" cell (cell B7)	Update the list of cities selection (cell B8) to match selected State.	—
The "City (County)" cell (cell B8)	Determine the temperature profile used in the calculation of S_{app} and RSI values.	A State is selected (cell B7).
The "Layer Type - for RSI Calc." cell (cell B9)	Determine the type of layer used in the RSI calculation.	—

Action	Functionality	Requirement
The "Run S_{app} Analysis" button	Calculate the S_{app} value for the selected mixture.	• A mixture is selected (cell B2). • A State is selected (cell B7). • A city or county is selected (cell B8). • A dynamic modulus model is characterized in FlexMAT Cracking. • A fatigue cracking model is characterized in FlexMAT Cracking.
The "Run RSI Analysis" button	Calculate the RSI value for the selected mixture.	• A mixture is selected (cell B2). • A State is selected (cell B7). • A city or county is selected (cell B8). • A layer type is selected (cell B9). • A permanent deformation model is characterized in FlexMAT Rutting.

—No requirement.

When the user enters information in the "Protocol A - Mix Approval" screen, PASSFlex updates the "Table 10. Mix Approval Results" table, which presents a simple compilation of the following information:

- The index values calculated when the user clicks the "Run S_{app} Analysis" and "Run RSI Analysis" buttons.
- The mix approval results based on the threshold limits the user selects.
- The traffic tier based on the recommended thresholds for S_{app} and RSI, given in volume I of this report.[18]

These limits are not enforced in PASSFlex, but are recommended such that passing or failing is determined by the input thresholds, which are completely up to the user's discretion. PASSFlex calculates the determined tier regardless of the threshold values the user selects and the tier does not affect the comparison with the threshold values.

Figure 96 presents a flowchart that summarizes the mixture approval procedure in protocol A of PASSFlex.

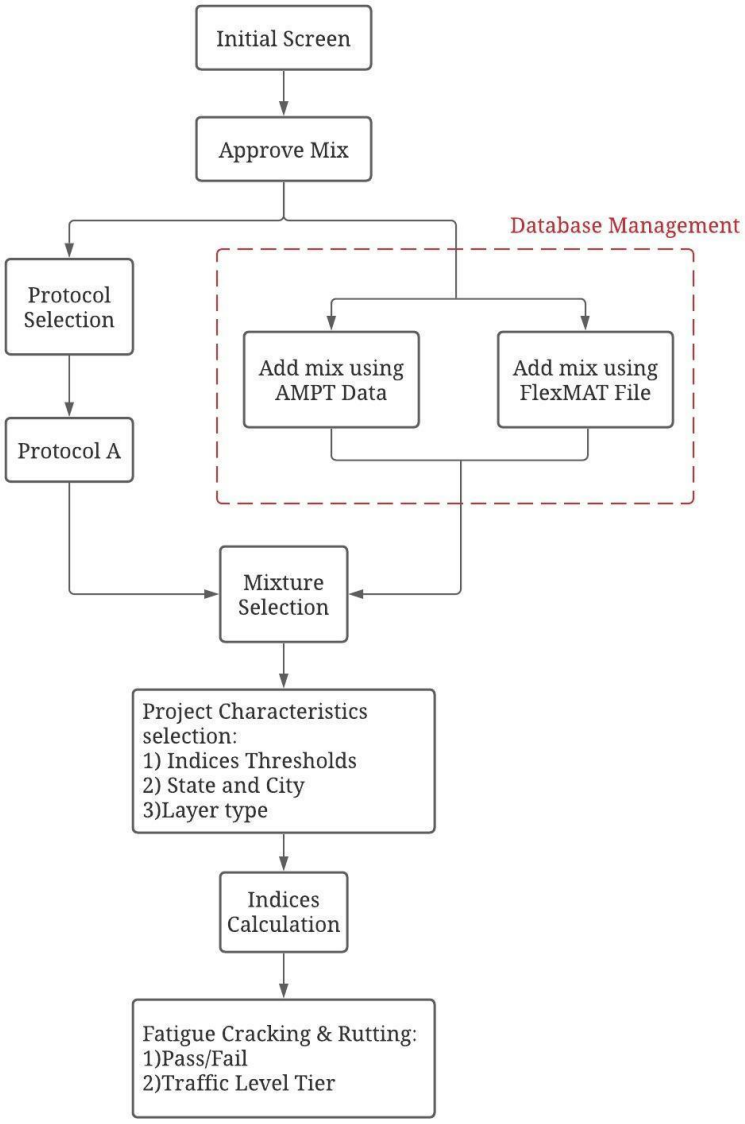

Source: FHWA.

Figure 96. Illustration. Protocol A's mixture approval flowchart.

Payment Adjustments Using Quality Assurance Data

The final stage of the PRS framework in PASSFlex is predicting the pay adjustment factors using AQCs. The "Adjust Payment Using QA Data" button is on the initial PASSFlex screen with the "Develop Material Database (4 Corners)," "Develop PRS," and "Approve Mix" buttons.

This procedure uses one of the developed PRS projects to calculate the amount of incentive or disincentive relative to a determined volume of constructed material based on the construction quality of a representative sample of that material. To obtain the pay adjustments for a given

mix, the project developed in the 'Develop PRS' stage needs to be complete, i.e., the final step (pay table generation) is a requirement for the calculation of the pay factors for as-built material.

When the user clicks the "Adjust Payment Using QA Data" button in the initial PASSFlex screen, the "PRS Project Selection" dialog box in figure 97 is displayed. The "Existing Projects" list contains all the PRS projects in the database, including any projects that are not finalized. However, if the user selects an incomplete project, a warning message is displayed that specifies the missing necessary parts of the project and directs the user where to go to complete the project.

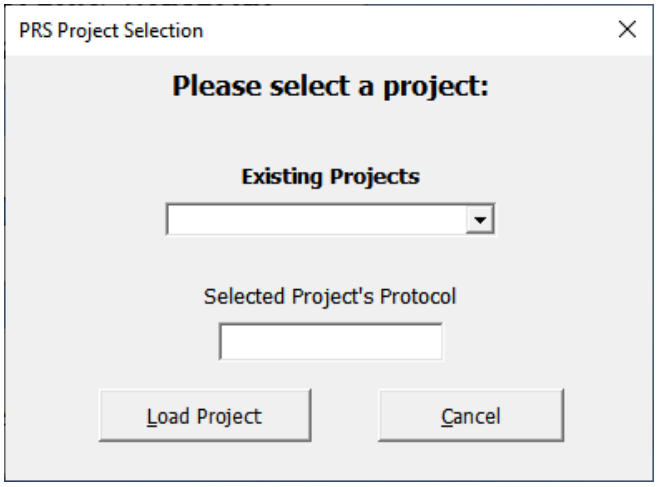

Source: FHWA.

Figure 97. Screenshot. "PRS Project Selection" dialog box for pay adjustment.

In protocol A, the project must have IVR model calibration parameters, a cost model, and a design life. When a user successfully loads a project, all the steps in that project's pay table development are loaded (on the "Protocol A Pay Adjustment Calculation" screen in figure 98) so that the user can review details of interest in that PRS project while inputting the information for the calculation of the pay adjustments.

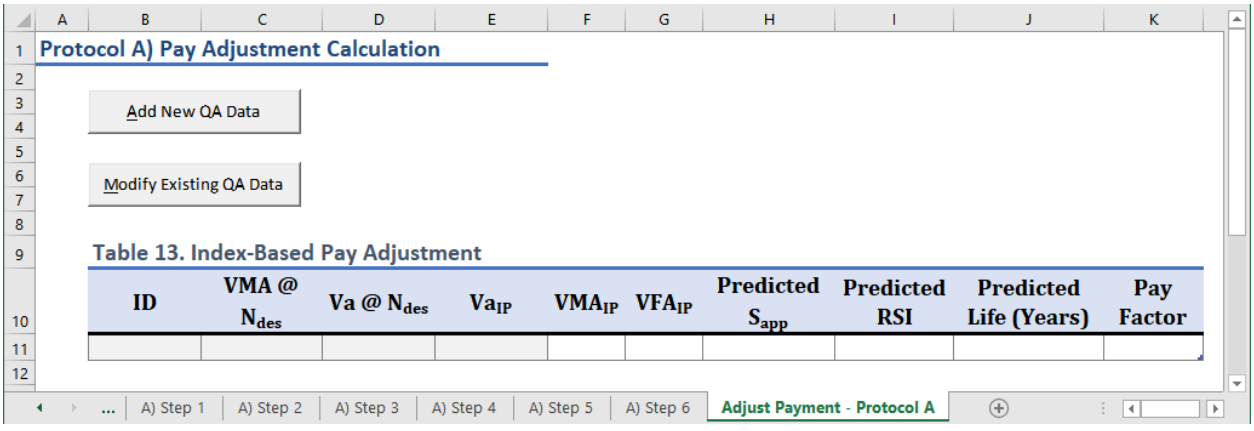

Source: FHWA.

Figure 98. Screenshot. "Protocol A Pay Adjustment Calculation" screen.

Table 53 presents the actions on the "Protocol A Pay Adjustment Calculation" screen. Both available actions display dialog boxes for the user to input and modify information for PASSFlex. Direct modifications of the "Protocol A Pay Adjustment Calculation" screen in figure 98 are not expected.

Table 53. Summary of actions on protocol A's payment adjustment screen.

Action	Functionality	Requirement
The "Add New QA Data" button	Display the "Add New QA Data from Field Representative Sample" dialog box to add a new representative sample's AQCs, which are needed to calculate that sample's pay factor.	—
The "Modify Existing QA Data" button	Display the "Modify QA Data" dialog box to update values previously added to the calculation table.	One or more sets of QA data exist in the "Table 13. Index-Based Pay Adjustment" table.

—No requirement.

When the user clicks the "Add New QA Data" button, the "Add New QA Data from Field Representative Sample" dialog box in figure 99 is displayed, which adds new QA data to calculate the pay factor for a representative sample. To calculate the pay factor, under "New QA Data ID," the user must add an identifier for the sample, and in the "Quality Assurance Inputs" area, add the three currently implemented volumetric characteristics that are used to calculate VMA_{IP} and VFA_{IP}. Once the user adds the three characteristics, PASSFlex performs the volumetric conversion automatically. Clicking the "Done" button adds the data to the "Table 13. Index-Based Pay Adjustment" table on the "Protocol A Pay Adjustment Calculation" screen where a summary of the relevant information is provided in the row identified by the selected ID.

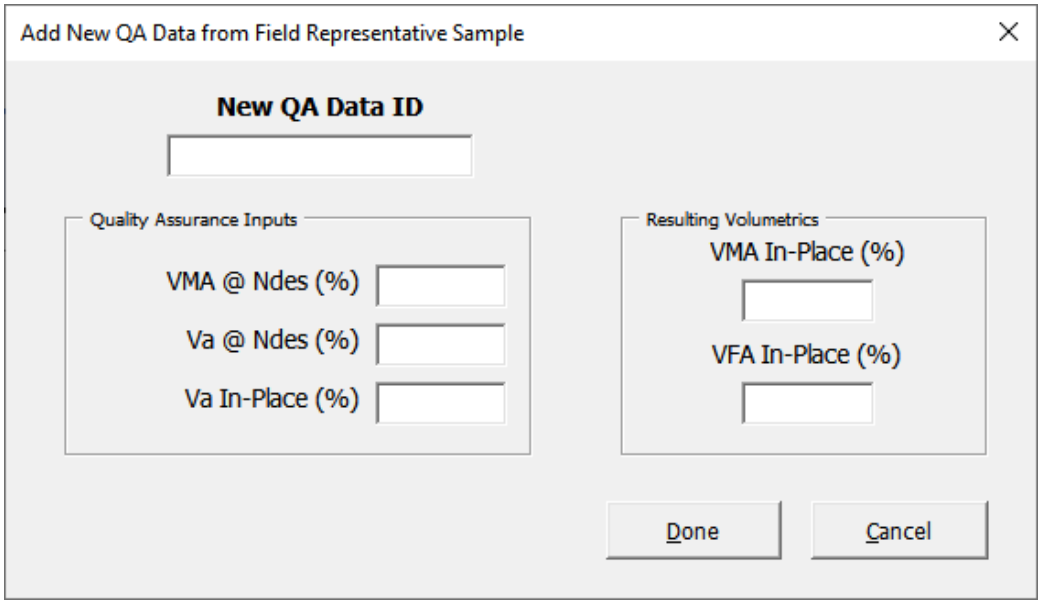

Source: FHWA.

Figure 99. Screenshot. "Add New QA Data from Field Representative Sample" dialog box.

The current PASSFlex implementation of these calculations is deterministic in nature, and the definition of a representative sample is open to the user's interpretation. The deterministic implementations in the current framework are related to the ongoing nature of the project and not because defining the calculated quantities deterministically is an inherently better approach than defining them stochastically. On the contrary, that PASSFlex developers should take the variability in asphalt materials and construction methods into account when determining QA elements and evolving versions of the software.

When the user clicks the "Modify Existing QA Data" button on the "Protocol A Pay Adjustment Calculation" screen, the "Modify QA Data" dialog box in figure 100 is displayed. The user can modify the values of the input AQCs for any added sample by deleting individual samples and all the information in the table.

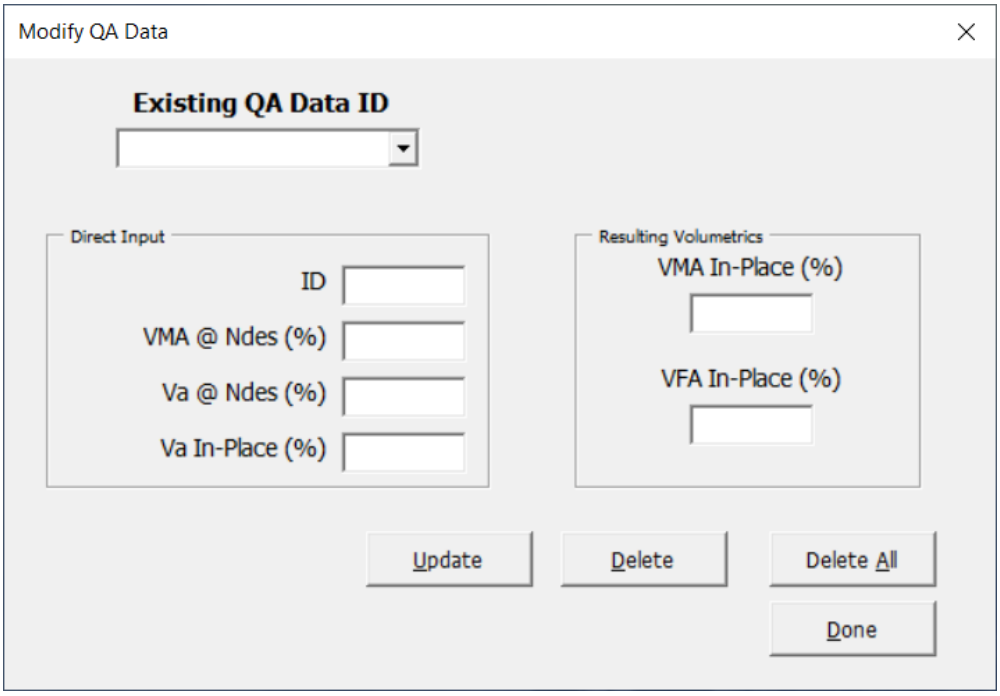

Source: FHWA.

Figure 100. Screenshot. "Modify QA Data" dialog box for pay factor calculations.

The user can select the data to be modified; any modifications will populate the "Protocol A Pay Adjustment Calculation" screen only after the user clicks one of the buttons on the "Modify QA Data" dialog box. The "Delete" and "Delete All" buttons cannot be reversed and, for that reason, a prompt for confirmation is displayed before the action is performed. When the user completes all the changes, clicking the "Done" button displays the "Protocol A Pay Adjustment Calculation" screen.

CHAPTER 4. SHADOW PROJECTS

This chapter describes three shadow projects that the research team undertook in concert with the Western Federal Lands Highway Division (WFLHD), MaineDOT, and Missouri Department of Transportation (MoDOT) to introduce the AMPT suite of performance tests and the performance models to State DOTs. The research team used samples from real-world construction projects to develop PVRs and evaluate their accuracy as a function of mixture volumetrics and in-place density values. The data from the shadow projects have no bearing on currently specified payments to contractors; however, the shadow projects will allow agencies and the research team to evaluate the methods in realistic environments and prepare agencies for the deployment of PRS in the future. The following section provides information applicable to all three shadow projects, followed by separate descriptions of each shadow project.

STEPS INCLUDED IN A SHADOW PROJECT

A shadow project's primary goal is to demonstrate to the agency (and contractor) the project acceptance and contractor payment process if performance testing and analysis are used within a contract document. Shadow projects also help the agency understand how the testing and analysis may impact the agency's normal testing and volumetric-based acceptance operations. To achieve these goals, the research team, WFLHD, MaineDOT, and MoDOT undertook several activities during the shadow projects, e.g., an AMPT workshop, onsite training, regular conference calls, and proficiency testing. This overview describes the flow of the sequential steps that agencies should take for all such shadow projects.

Asphalt Mixture Performance Tester Testing

Three performance tests (described earlier in this report) utilize the AMPT:

- The dynamic modulus test.
- The direct tension cyclic fatigue test.
- The SSR test.

For sample preparation, the large cylindrical specimens are fabricated according to AASHTO R 83 and the small cylindrical specimens are fabricated according to AASHTO PP 99.[48,80] Shadow project agencies must have facilities for asphalt mixture fabrication and test sample preparation. Table 54 provides a summary of the AMPT testing requirements for shadow projects.

Table 54. Performance tests that use the AMPT.

Performance Testing	AASHTO Specifications	Number of Gyratory-Compacted Specimens	Test Specimen Geometry	Test Specimens
Dynamic modulus	TP 132[30]	1	Small cylindrical	3
Cyclic fatigue	T 411[15]	1	Small cylindrical	3
SSR	TP 134[16]	4 (2 for LT, 2 for HT tests)	Large cylindrical	4 (2 for LT, 2 for HT tests)

Mixture-Level Data Analysis Using FlexMAT Software

The AMPT test results are input to FlexMAT for mixture-level analysis. The research team developed this Microsoft Excel-based data analysis software to characterize performance models using data files generated by the AMPT. FlexMAT performs complex analysis algorithms that are involved in generating dynamic modulus master curves, calibrating the S-VECD model, and calibrating the shift model for rutting predictions.[12] Using simple clicks, FlexMAT generates output files that the FlexPAVE pavement performance analysis software can use.[59]

Pavement Performance Simulations Using FlexPAVE version 1.1

The research team also developed FlexPAVE. This software employs viscoelastic continuum damage theory to account for the effects of loading rate and temperature on pavement responses and distress mechanisms. FlexPAVE also allows the creation of pavement structures that consist of asphalt concrete and unbound materials. Users can assign each asphalt concrete layer various material properties by inputting the output files that FlexMAT generates. Lastly, users can assign project location, traffic conditions, and design vehicle configurations for the given project.[59] FlexPAVE uses the EICM to determine climatic conditions based on the project location.[22] The major output from FlexPAVE simulations is pavement performance, which FlexPAVE provides in the form of damage percentage (%Damage) and rut depth over the design life of the pavement. The research team has not yet completed transfer functions for FlexPAVE. However, the research team's previous research showed a good relationship between simulated %Damage and field-measured cracking area and between simulated asphalt concrete rut depth and field-measured total rut depth.[14,81]

Asphalt Mixture Performance Tester Training

The research team provides two types of AMPT training for agency personnel before the shadow project: A 2-d AMPT workshop held at NCSU and an onsite training session held at the agency's laboratory. For the AMPT workshop, the research team provides hands-on training for technical procedures and analysis. The technician team from the shadow project agency learns about test specimen preparation and AMPT protocol and the data analysis team learns to analyze test results using FlexMAT and FlexPAVE. For the onsite training, a member of the research team visits the shadow project agency and reviews all the shadow project test procedures with agency

personnel. In this training session, a trainer checks and records the condition of the agency's lab to determine whether any modifications or improvements are necessary.

Proficiency Testing

Once the shadow project agency completes AMPT training, the agency conducts tests using materials that the research team also tests. This process constitutes proficiency testing and consists of the following steps:

- The shadow project agency fabricates 12 gyratory-compacted samples using a mixture commonly used by that agency and targets 5 percent ±0.5 percent air void content for the cored and cut test specimens.
- The shadow project agency ships six of these gyratory-compacted samples to the research team.
- The agency uses the six retained samples to core and cut two of the gyratory-compacted samples to make eight smaller specimens for the dynamic modulus and cyclic fatigue tests and core and cut the remaining four gyratory-compacted specimens for the SSR tests.
- The research team performs the same coring and cutting procedure using the six samples that the agency shipped to NCSU.
- The shadow project agency and the research team both run AMPT tests.
- The agency sends its AMPT test results to the research team, and the team analyzes the data, compares the results to the team's reference test results, and holds a debrief call with agency personnel to discuss the results.

The two main purposes of the proficiency testing are to familiarize the agency's personnel with the test equipment and processes before testing during the shadow project and to check whether the performance test results the agency generates are repeatable compared to the results the research team generates. Proficiency testing ranges from test specimen fabrication to FlexMAT analysis. Once the test results are considered reasonable, the agency's personnel are considered proficient regarding conducting AMPT tests. Then the shadow project can begin.

Shadow Project Selection

Once the proficiency testing is completed, the participating agency selects a real-world construction project to serve as the shadow project. The project selection guidelines state that the project must use a mixture that is part of a mainline pavement structure (e.g., not used in ramps, shoulders, aprons, intersections, or turning lanes). The project should also be large enough that the mixture can be placed over multiple days to simulate the variability that naturally occurs over the course of larger projects. The agency should obtain samples from multiple truck loads (normally more than ten) for the shadow project. For projects that involve multiple mixture types (for example, surface and intermediate layers), the agency has the option to sample from each of

the mixture types. In these cases, the agency is required to sample 11 times for each mixture type included in the study.

Material and Information Acquisition

Next, the agency acquires the asphalt concrete for the AMPT tests from the selected project following the AASHTO T 168 method.[82] The agency must obtain 11 samples from 11 different truck loads to enable the research team to investigate meaningful variations among the 11 samples. The agency must acquire approximately 400 lb of asphalt concrete samples from each truck, and must store the acquired samples in temperature-controlled storage to maintain a consistent target temperature that is below 25 °C (77 °F) to avoid material aging and oxidation before the samples are shipped to the research team. The 400 lb asphalt mixture sample is calculated using 80 lb for AQC testing and 120 lb for six gyratory-compacted samples (20 lb for each sample) with a safety factor of two. In addition, the agency must track the field locations where the 11 samples were obtained, referring to station and truck numbers, to measure field densities. The agency must conduct volumetric tests using its own method and the acquired samples to collect AQC data, such as design air voids, VMA, VFA at the design compaction level (N_{des}), maximum specific gravity, and binder content. The agency uses the AQCs to calculate the samples' volumetric characteristics. The agency then uses the calculated volumetric characteristics to calibrate and build the mixture's PVR. Before the PVR calibration process, the agency assigns the samples for either calibration or verification. The agency keeps the calibration samples to run the AMPT tests and sends the rest of the samples, i.e., the verification samples, the AQCs, and the in-place density data, to the research team.

Selection of Four Corners

The underlying concept of the PVR is that the performance of an asphalt mixture under any volumetric conditions can be predicted by testing the asphalt mixture at a few selected volumetric conditions and developing the relationship between the performance and the volumetric conditions. Four volumetric conditions are sufficient to develop the PVR for a given mixture. The agency should select these four corners (the furthest distances within the quadrangular range of volumetric conditions) at the widest points within the range of volumetric conditions to capture the performance of the mixture at any given volumetric condition. For the shadow projects, the agency selects the four corners using three or four samples and three additional samples to verify the PVR function.

Shadow Project Asphalt Mixture Performance Tester Testing and Data Analysis

The protocol for the AMPT tests used in the shadow projects is identical to that used for the proficiency tests. The shadow project agency and the research team conduct AMPT tests with target air voids determined in the PVR calibration phase. For the data analysis, FlexPAVE utilizes the AMPT test results to simulate pavement performance.

Performance-Volumetrics Relationship Development

Based on the FlexPAVE simulation results and the samples' volumetric characteristics, the research team then develops the PVRs. The research team uses IP-VMA, IP-VFA, %Damage, and asphalt concrete surface rut depth data for the four corners to build PVRs for fatigue cracking and rutting.

Figure 101 presents a flowchart for the main processes in a shadow project.

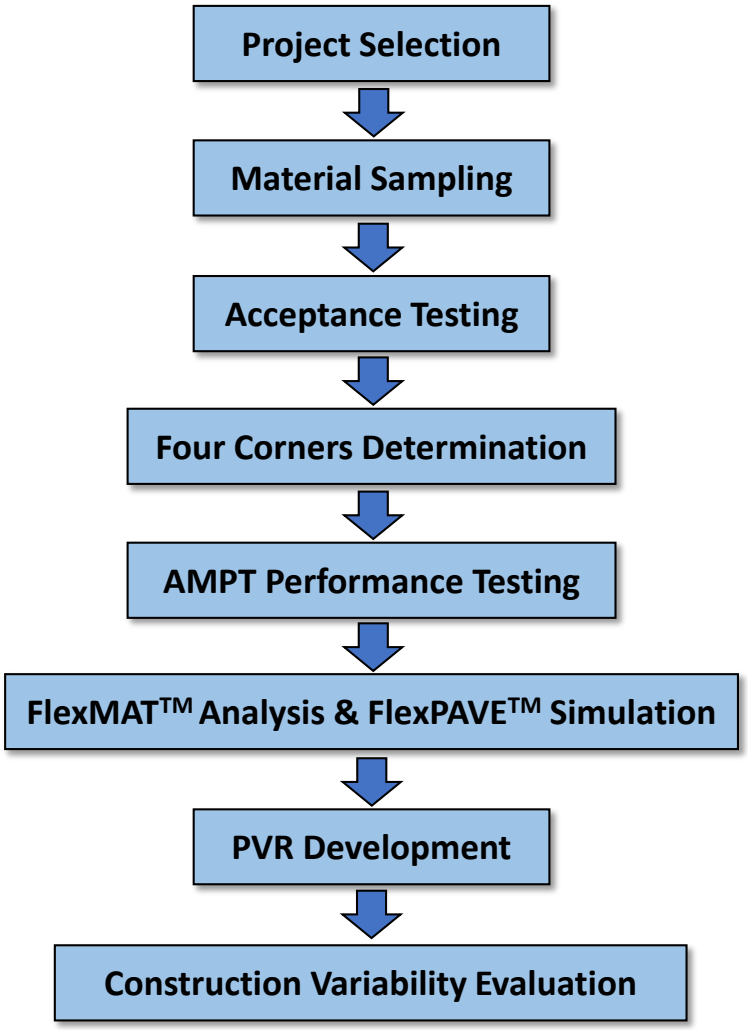

Source: FHWA.

Figure 101. Illustration. Flowchart of PRS shadow project.

THE SKYLINERS WESTERN FEDERAL LANDS HIGHWAY DIVISION SHADOW PROJECT

The WFLHD of FHWA conducted the first shadow project using the Skyliners Road Improvement Project in Deschutes County, west of Bend, OR.[83] This report refers to the project as the WFLHD shadow project; the project reconstructed approximately eight miles of two-lane

roadway in the Deschutes National Forest. The agency pulverized, shaped, and recompacted existing pavement to form the foundation for the new pavement structure that consists of 4 inches of asphalt pavement over 6 inches of emulsified asphalt-treated aggregate base course. The roadway receives automobile, recreational vehicle, and occasional logging truck traffic. The estimated 20-yr design traffic for this roadway is 200,000 ESALs.

The agency constructed the roadway in two phases in 2015 and 2016. The agency collected samples of the asphalt mixture for testing in the Bituminous Mixtures Laboratory at FHWA's TFHRC. The samples included:

- Component asphalt binder and aggregate.
- Plant-produced loose asphalt mixture.
- Compacted pavement roadway cores.

The WFLHD shadow project was conducted before the research team fully developed the PVR and PEMD methodology and calibrated the performance models in FlexPAVE; therefore, this shadow project did not include a full application of PRS. The focus of the testing and analysis of the WFLHD shadow project was assessing the effect of in-place density on fatigue cracking and rutting that the uncalibrated FlexPAVE performance models predicted. Figure 102 shows photographs taken during construction and the completed pavement.

Source: FHWA.

A. Pulverization of existing road.

Source: FHWA.

B. Placement of emulsion-treated base.

Source: FHWA.

C. Placement of asphalt pavement.

Source: FHWA.

D. Finished Skyliners roadway.

Figure 102. Photos. WFLHD shadow project.

Western Federal Lands Highway Division Statistical Asphalt Pavement Acceptance Data

Statistical acceptance for asphalt pavement found in *The Standard Specifications for Construction of Roads and Bridges on Federal Highway Projects* (FP-14) includes separate material and ride quality payment provisions.[(84)] The FP-14 material pay factors include AQCs for mixture volumetric properties and performance-graded binder properties. The mixture volumetric AQCs in FP-14 are:

- AC.
- VMA.
- In-place density.

A lot in FP-14 is typically defined as the total quantity of work produced. A project may have more than one lot due to project scheduling, changes in material sources, the job mixture formula, or target values. The project schedule for the Skyliners Road Improvement Project initially divided the planned 36,000 tons of asphalt mixture into two lots, one for each phase. The second lot was terminated after four samples because the lot's calculated FP-14 pay factor fell below the minimum for continuous production due to difficulties controlling the mixture's binder content. After the contractor took corrective action, a third lot was commenced and most of the phase 2 production was completed under the third lot.

Table 55 provides a summary of in-place density data for lot 1 and lot 3. The table only presents the in-place density data because the focus of the shadow testing for the Skyliners Road Improvement Project was the effect of in-place density on fatigue cracking and rutting. Table 55 includes the data for each sample, the mean and standard deviation for the lot, the percent within limits based on the WFLHD specification lower quality limit of 91 percent theoretical maximum

specific gravity, and the in-place density pay factor. Based on the WFLHD in-place density specification, the two lots received an incentive payment of 4 percent.

Table 55. WFLHD shadow project: Summary of in-place density acceptance data for lot 1 and lot 3.

Sample	Lot 1 Percent G_{mm}	Lot 1 Air Voids, Percent	Lot 3 Percent G_{mm}	Lot 3 Air Voids, Percent
1	93.76	6.24	92.71	7.29
2	94.45	5.55	92.53	7.47
3	93.38	6.62	91.87	8.13
4	92.13	7.87	91.52	8.48
5	94.48	5.52	92.61	7.39
6	93.68	6.32	94.20	5.80
7	95.03	4.97	92.12	7.88
8	93.63	6.37	92.04	7.96
9	94.09	5.91	92.94	7.06
10	93.87	6.13	92.36	7.64
11	94.17	5.83	93.89	6.11
12	92.43	7.57	94.43	5.57
13	93.85	6.15	93.96	6.04
14	93.08	6.92	93.20	6.80
15	94.03	5.97	93.41	6.59
16	95.79	4.21	92.41	7.59
17	92.38	7.62	92.38	7.62
18	92.38	7.62	92.71	7.29
19	92.96	7.04	93.02	6.98
20	91.80	8.20	94.79	5.21
21	92.80	7.20	92.58	7.42
22	91.72	8.28	92.15	7.85
23	91.05	8.95	—	—
24	91.11	8.89	—	—
25	93.10	6.90	—	—
Average	93.25	6.75	92.90	7.10
Standard Deviation	1.19	1.19	0.88	0.88
PWL	97	97	99	99
Pay Factor	1.04	1.04	1.04	1.04

—No data.
G_{mm} = maximum specific gravity; PWL = percent within limits.

Effect of In-Place Density on Asphalt Mixture Properties

The focus of the laboratory testing for this shadow project was the effect of air voids on the FlexPAVE material properties: the dynamic modulus, cyclic direct-tension fatigue properties, and SSR properties. The agency prepared test specimens from laboratory-batched component materials and from plant-produced loose asphalt mixture at three nominal air void contents: 4, 7, and 10 percent.

Figure 103, figure 104, and figure 105 show the effect of air void content on selected properties from the three tests used to characterize asphalt mixtures for FlexPAVE performance analyses. These figures show the data for test specimens prepared from plant-produced loose asphalt mixture samples. The research team obtained similar trends for test specimens prepared from component materials. Figure 103 shows the effect of air void content on the dynamic modulus master curve; the dynamic modulus decreases with an increase in air void content. Using 7 percent air void content as the basis for comparisons, decreasing the air void content from 7 to 4 percent results in an increase in stiffness, whereas increasing the air void content from 7 to 10 percent results in a decrease in stiffness. Figure 104 shows the effect of air void content on the damage characteristic curve derived from cyclic fatigue testing. The damage characteristic curve tracks the reduction in the pseudosecant modulus that indicates the structural integrity (C) of the asphalt mixture with increasing damage (S). Figure 104 shows the reduction in C as a function of S for different air void contents. Finally, figure 105 shows the effect of air void content on the accumulated permanent deformation in the HT SSR test; permanent deformation increases with an increase in air void content.

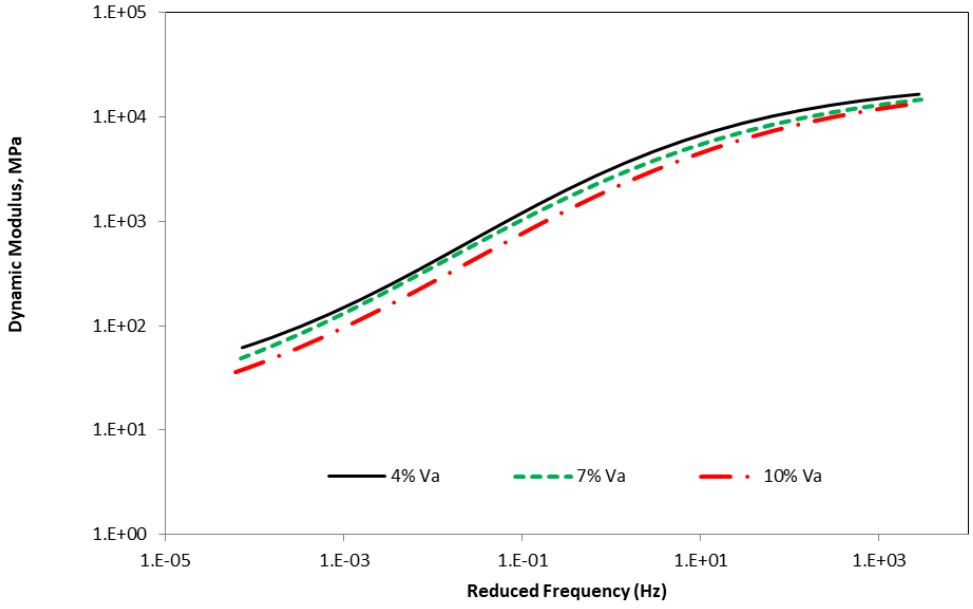

Source: FHWA.
1 MPa = 145.04 psi.

Figure 103. Graph. WFLHD shadow project: Effect of air void content (V_a) on the dynamic modulus master curve.

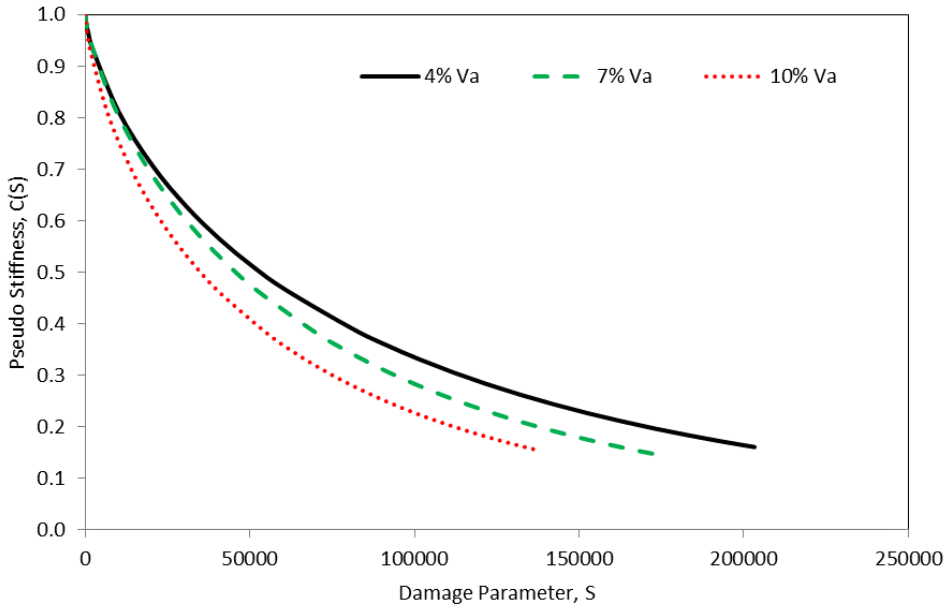

Source: FHWA.

Figure 104. Graph. WFLHD shadow project: Effect of air void content (V_a) on the damage characteristic curve.

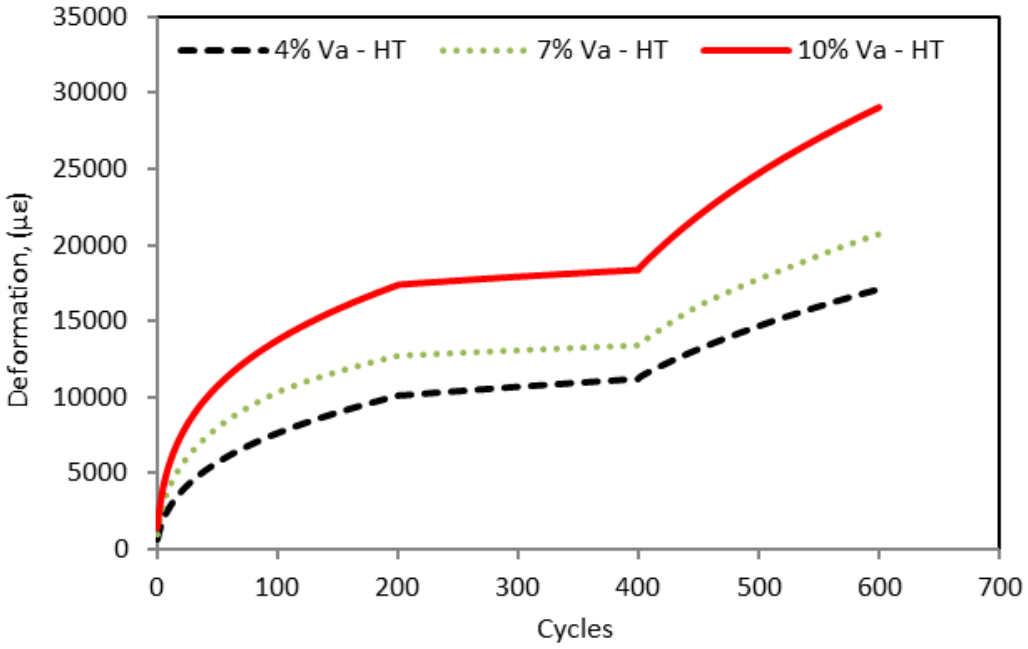

Source: FHWA.

Figure 105. Graph. WFLHD shadow project: Effect of air void content (V_a) on permanent deformation.

Effect of In-Place Density on Pavement Effect of In-place Performance

The research team used asphalt mixture material properties for 4, 7, and 10 percent air void contents in FlexPAVE to determine the effect of air void content on the rutting and fatigue cracking performance of the pavement section for the Skyliners Road Improvements Project. The team used traffic volume of 50 ESALs per day over a 20-yr analysis period in the analysis. The team used climatic data for Redmond, OR, the closest site location in the EICM, in the analysis.[22] The analysis showed that fatigue cracking was the critical distress for this pavement, because the rutting in the asphalt layer was less than 0.2 mm for all air void contents.

Figure 106 shows fatigue damage from FlexPAVE over the 20-yr analysis period. This analysis shows the negative effect of increasing the air void content on the pavement's fatigue cracking performance. At the time that this analysis was conducted, the rutting and cracking models in FlexPAVE were not field calibrated; therefore, the extent of fatigue cracking associated with the percentage of fatigue damage shown in figure 105 is not known. Figure 106 shows the life of pavements constructed with 4 and 10 percent air void contents relative to a pavement constructed with 7 percent air void content for fatigue damage levels greater than about 15 percent. Increasing the air void content from 7 to 10 percent decreases the pavement fatigue life by approximately 40 percent. This finding is similar to the finding of a field study from the State of Washington that concluded that each 1 percent increase in in-place air void content above 7 percent resulted in a 10 percent reduction in pavement life.[85] Figure 106 shows that decreasing the air void content from 7 to 4 percent increases pavement life about 75 percent. Figure 107 shows the effect of air voids on relative fatigue life for Skyliners Road.

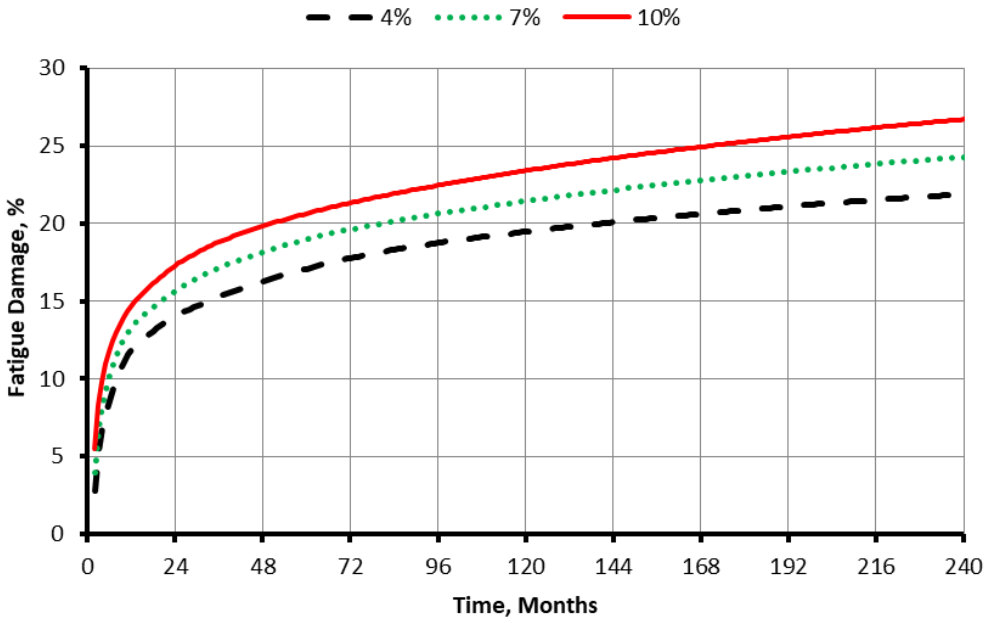

Source: FHWA.

Figure 106. Graph. WFLHD shadow project: Skyliners FlexPAVE fatigue analysis.

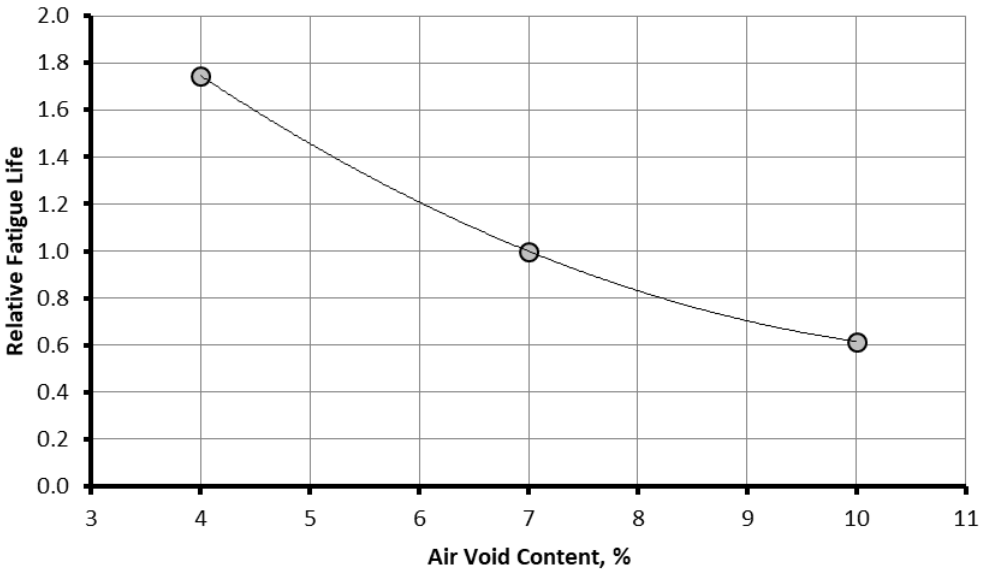

Source: FHWA.

Figure 107. Graph. WFLHD shadow project: EFFECT of air voids on relative fatigue life for Skyliners Road.

To compare the uncalibrated FlexPAVE fatigue results to the WFLHD acceptance data, the agency should use the fatigue life for the air void content that corresponds to a pay factor of 1.0 for the WFLHD QA specifications as the basis, having a relative fatigue life of 1.0. For a typical lot size of 25 samples and in-place density standard deviation of 1.25 percent, the WFLHD QA specifications provide a pay factor of 1.0 for an average air void content of 7.5 percent. Figure 108 presents a histogram of the relative fatigue life for the Skyliners asphalt pavement using the combined in-place density data for lot 1 and lot 3. The relative fatigue life ranges from 0.78 to 1.85 with an average of 1.14. From the earlier analysis of the WFLHD density data, the pavement project received an incentive payment, which appears justified based on the relative life analysis.

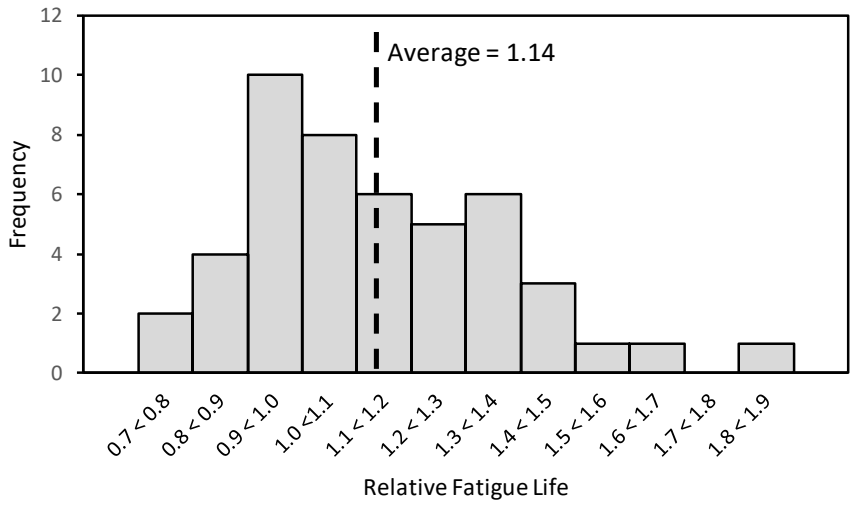

Source: FHWA.

Figure 108. Graph. WFLHD shadow project: Histogram of relative fatigue life of Skyliners pavement.

An interesting evaluation is to compare the WFLHD QA specification pay factors to the relative pavement life from the FlexPAVE fatigue analysis. Assuming a typical lot size of 25 samples and in-place density standard deviation of 1.25 percent, the WFLHD pay factor and relative life were computed for various average air void contents. Based on these assumptions, the maximum pay factor of 1.05 can be reached for average air void contents of 5.9 percent or less. Remove-and-replace is in the WFLHD specifications for an average air void content of 8.8 percent or greater. Figure 109 compares the pay factors and relative pavement life data for lot average air void contents ranging from 5.9 to 8.8 percent. The disincentive pay factors are in good agreement with the relative pavement life. The incentive pay factors are lower than the relative pavement life.

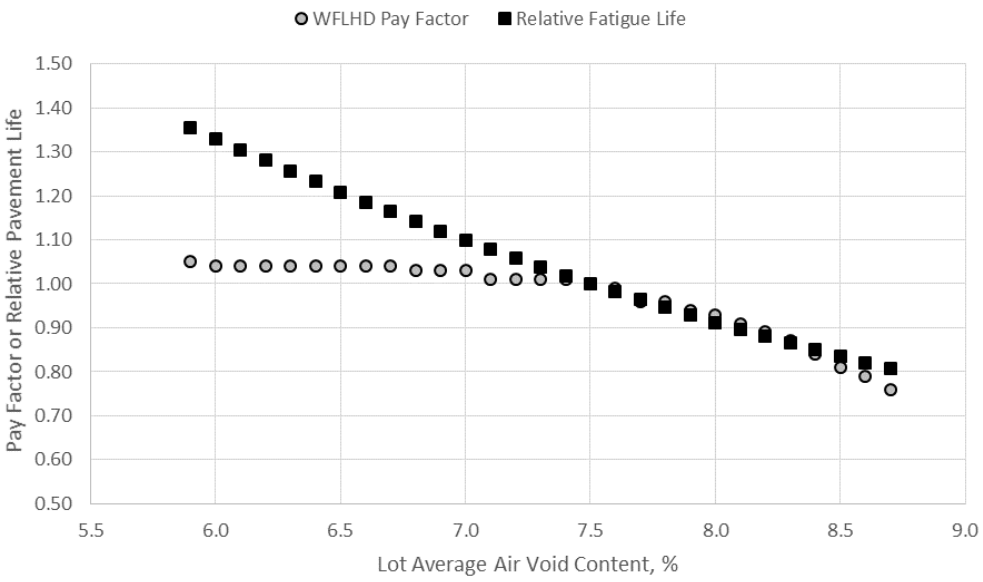

Source: FHWA.

Figure 109. Graph. WFLHD shadow project: Comparison of WFLHD pay factors and FlexPAVE relative pavement life.

Summary

Although the WFLHD shadow project did not include a full application of PRS, the shadow project used uncalibrated pavement performance models, and the analysis considered only the effect of in-place density. The application of the approach in this project illustrated the following important concepts:

- The asphalt mixture testing for PRS is sensitive to changes in air void content. Changes in air void content significantly affect dynamic modulus, fatigue, and permanent deformation properties in a rational way.

- The pavement performance must be used as the basis for specifications and payment (rather than only material properties). Although material properties associated with both rutting and fatigue cracking are affected by changes in air void content, pavement performance modeling clearly shows that fatigue cracking is the critical distress mode for asphalt layers in this low-volume pavement.

- The FlexPAVE fatigue cracking model indicates that fatigue cracking performance can be significantly improved by increasing the target in-place density in construction specifications (for the Skyliner project's roadway conditions).

- The agencies and contractors can apply PRS to tailor mixture designs to the critical distress mode for a specific pavement. FlexPAVE analysis results for the Skyliner project indicate that the mixture design for low-volume roads should place greater emphasis on fatigue performance. Only pavement performance analyses can determine the relative

emphasis that should be placed on permanent deformation versus cracking, which will be different for different traffic volumes and pavement structures.

- The relative fatigue life analysis based on pavement fatigue damage analysis from FlexPAVE confirms the reasonableness of the disincentive payment adjustments included in the WFLHD QA specifications for in-place pavement density. However, the relative fatigue life analysis results indicate that the maximum 5 percent incentive for in-place density warrants additional evaluation and risk analysis.

- The relative fatigue life analysis, based on uncalibrated performance models, suggests that significant differences in pavement life should be expected, even for pavements that are well constructed based on current QA specifications. The Skyliners roadway project received nearly the maximum incentive payment for in-place density under the WFLHD QA specifications, indicating that the project was well constructed. The relative fatigue life based on the FlexPAVE analysis showed a range in relative fatigue life from a low of 0.78 to a high of 1.85 with an average of 1.14. A 20-yr design life has a range in pavement life from 15.6 to 37.0 yr with an average of 22.8 yr. This project shows that guidance is needed to address variability when establishing payment provisions based on pavement performance.

THE MAINE DEPARTMENT OF TRANSPORATION SHADOW PROJECT

Although the MaineDOT shadow project needs to meet a few more objectives to familiarize the State agency personnel with formal PRS project components, such as AMPT BMD and the pay table concept, this section describes the technical and analytical sides of the MaineDOT shadow project, personnel training, field material sampling, field variability investigation, and pavement performance predictions using the PVR, all of which should be generally applicable for any State agency shadow project. Therefore, this study focuses on the bulk of the MaineDOT shadow project implementation process and ignores the pay table work that has not been completed at the time of this writing.

To accomplish the goals of the MaineDOT shadow project, MaineDOT and the research team undertook several key activities, including AMPT training, proficiency testing, shadow project selection, material sampling, AMPT testing, data analyses, performance simulations, and PVR development. In this section, the MaineDOT shadow project process and results are described and the field variability and its impact on pavement performance.

Maine Department of Transportation Proficiency Testing and Results

Table 56 lists the mixture information used for the proficiency testing.

Table 56. MaineDOT shadow project: Proficiency test mixture information.

Property	Information
NMAS (mm)	9.5
Binder type	PG 64-28
RAP content (percent)	20

Property	Information
Virgin binder content (percent)	5.0
Total binder content (percent)	6.3
Superpave design	75 gyrations, 3–10 MESALs

Figure 110 presents comparisons of typical proficiency test results MaineDOT and the research team obtained. Figure 110-A to figure 110-D show no markable differences between the two sets of test results. The dynamic modulus and damage characteristic curves collapse well and the averaged percentage of difference of the measured dynamic modulus values and the averaged difference of the area of the damage characteristic curves from both MaineDOT and the research team were 5.8 percent for each. The strain levels in the cyclic fatigue tests of the MaineDOT and research team test specimens required different inputs: 500, 550, and 600 microstrain for the MaineDOT specimens and 630, 670, and 770 microstrain for the research team specimens. The larger strain levels the research team used for the specimens caused early failure, as shown in figure 110-D. Good collapse of the damage characteristic curves in figure 110-C and the high R^2 value in figure 110-D demonstrate the strain level independence of the damage characteristic curve and the D^R failure criterion, which is the slope of the line in figure 110-D. For figure 110-E, the difference between the two sets of SSR test results at the LT is 38.6 percent, which is greater than the 25 percent that the current SSR test specification (AASHTO TP 134) sets as allowable repeatability for two replicates.[16] However, the SSR test results at the HT for both the MaineDOT and research team tests did not show a significant difference (7 percent difference). Also, the test repeatability generated by MaineDOT was acceptable (2.6 percent). The reason for the relatively large difference at the LT is not known. Other than the LT data, the research team considered the test results acceptable and the AMPT training successful.

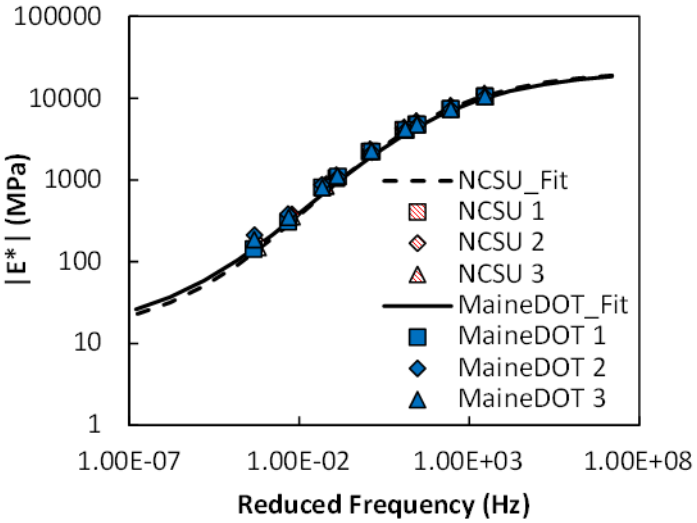

1 MPa = 145.04 psi.

A. Dynamic modulus master curves.

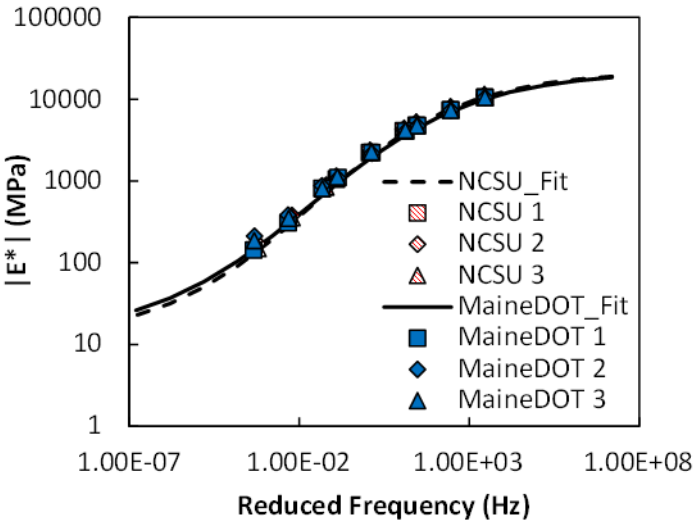

0 °C = 32 °F.

B. Time-temperature shift factors.

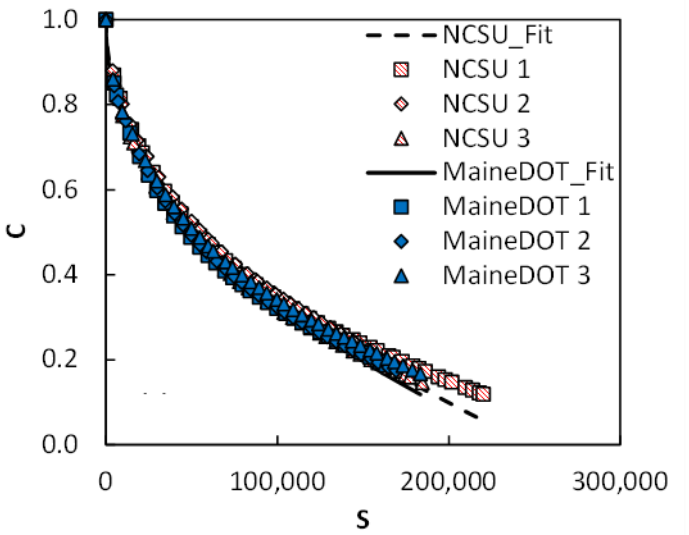

C. Damage characteristic curves.

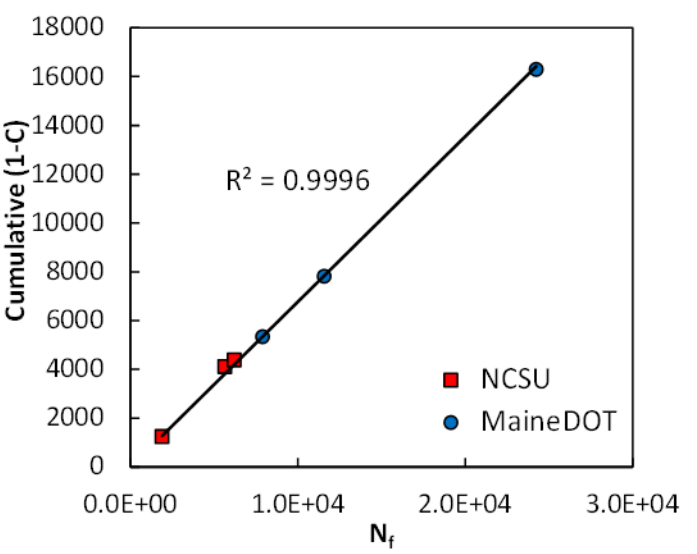

D. Pseudoenergy-based failure criterion.

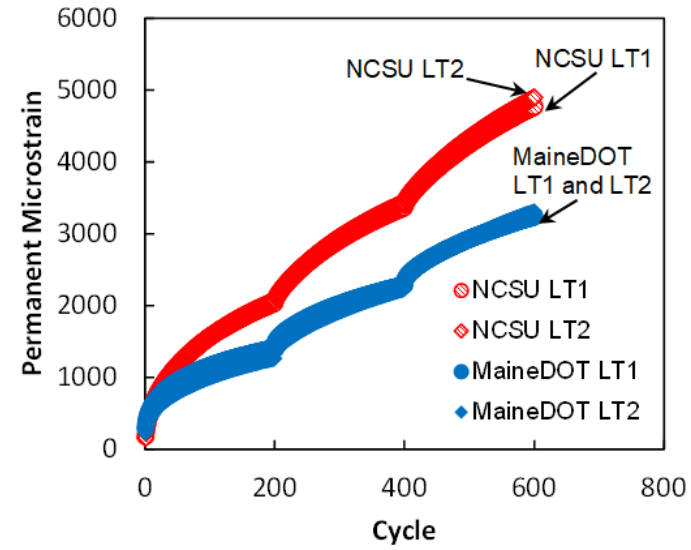

E. SSR test LT results.

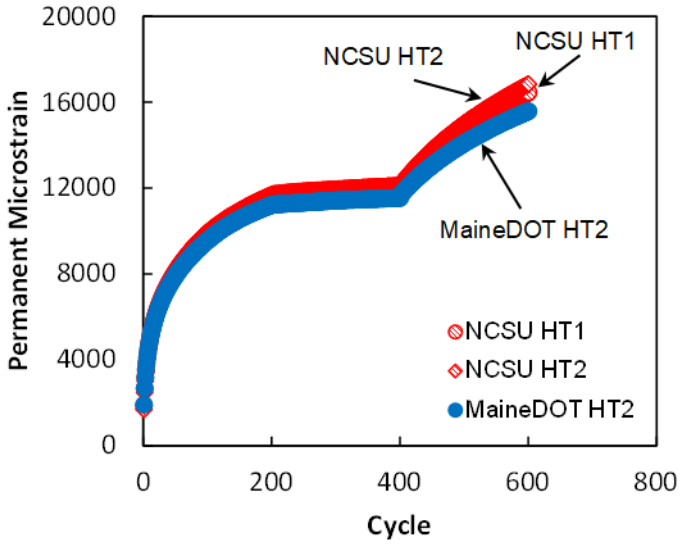

F. SSR test HT results.

Figure 110. Graphs. Proficiency test results from MaineDOT and research team.[23]

Maine Department of Transportation Project Selection

MaineDOT selected a project that is part of a mainline pavement structure that contains sufficient paving for the shadow project. The project location is Interstate 95 northbound beginning 0.04 mi north of Johnson Flat Road in Pittsfield and extending northerly 13.57 mi to the bridge over the Maine central railroad line in Newport. Table 57 presents a summary of the MaineDOT shadow project.

Table 57. MaineDOT shadow project: General information and material description.

Pavement Structural Design	NMAS (mm)	Binder Type	RAP Content (Percent)	Virgin Binder Content (Percent)	Total Binder Content (Percent)	Superpave Design
100 mm HMA pavement (50 mm wearing course +50 mm base course) 300 mm aggregate base type B	12.5 (Fine-graded)	PG 64E-28	20	4.7	5.6	75 Gyrations, 10–30 MESALs

Material Sampling for Maine Department of Transportation Shadow Project

MaineDOT acquired samples from 11 different truck loads and conducted material tests to obtain the AQCs of each sample. Table 58 presents details regarding these AQC data.

Table 58. AQC data collected by MaineDOT.

Sample ID	Air Void (Percent)	VMA (Percent)	G_{mb}	G_{mm}	G_{sb}	VFA (Percent)	Binder (Percent)	In-Place Density (Percent)
159352	4.7	15.5	2.426	2.546	2.72	70	5.3	96.5
159353	4.5	16.4	2.406	2.537	2.72	73	5.5	96.0
159354	3.5	16.2	2.418	2.505	2.72	78	5.7	93.1
159355	4.4	15.9	2.412	2.524	2.72	72	5.2	94.6
159356	4.7	16.3	2.404	2.523	2.72	71	5.3	94.9
159357	4.3	16.5	2.402	2.511	2.72	74	5.5	95.3
159358	4.6	16.4	2.402	2.518	2.72	72	5.3	95.4
159359	4.3	16.1	2.416	2.524	2.72	73	5.5	96.8
159360	3.9	16.8	2.404	2.502	2.72	77	5.9	92.5
159361	4.7	17.3	2.391	2.509	2.72	73	5.9	92.9
159362	4.4	17.0	2.396	2.507	2.72	73	5.8	94.3
Average	4.4	16.4	2.407	2.519	2.72	73.3	5.5	94.8

G_{mb} = mixture bulk specific gravity; G_{mm} = maximum specific gravity; G_{sb} = aggregate bulk specific gravity.

Performance-Volumetrics Relationship Calibration Conditions and Construction Variability

As a first step to building the PVRs, the research team began to formulate a PVR calibration plan using the 11 samples. The research team referred to MaineDOT's specifications for this effort and then created the specification limits for the shadow project mixture within the VMA_{IP} and VFA_{IP} domains. Table 59 outlines the agency's volumetric acceptance criteria and limits (for use in a percent-within-limits specification) for the shadow project mixture.

Table 59. Specification limits for MaineDOT 12.5-mm mixture.

Property	Criteria and Limits (Percent)
VMA	Minimum 15
VFA	60–84
PGAB content	Target ±0.4
Air void content	4.0 ±1.5
In-place density	95 ±2.5

PGAB = performance graded asphalt binder.

The research team obtained the target performance graded asphalt binder (PGAB) content from the mixture's job mix formula, and used the maximum VMA value of 18 percent, based on the volumetric calculations, when the air void content changed from 2.5 to 5.5 percent with the same PGAB content, because no maximum VMA is shown in table 59.

Figure 111-A presents the calculated VMA_{IP} and VFA_{IP} for the specification limits and 11 samples within the volumetric domain; the research team obtained these results by inputting the information in table 58 into equations 4 and 6. Although the information for the 11 samples falls within the specification limits, the research team found sample-to-sample variations that could be considered construction variability. The maximum differences in the VMA_{IP} and VFA_{IP} among the 11 samples are 32 and 23 percent, respectively. The movement of the VMA_{IP} and VFA_{IP} shows patterns when the in-place density, binder content, and aggregate gradation change in the VMA_{IP} and VFA_{IP} domains, as shown in figure 111-B. The VMA_{IP} and VFA_{IP} of the samples move diagonally from top right to bottom left when the binder content or gradation changes and move diagonally from top left to bottom right when the in-place density (air void content) changes. The gradation and binder content were not changeable for each of the 11 samples because the agency acquired the samples for the shadow project in a plant-produced state. Therefore, one way to change the VMA_{IP} and VFA_{IP} of the 11 samples using equations 4 and 6 to make four corners is to change the in-place density values, which would be the same as the target air void contents of the test specimens.

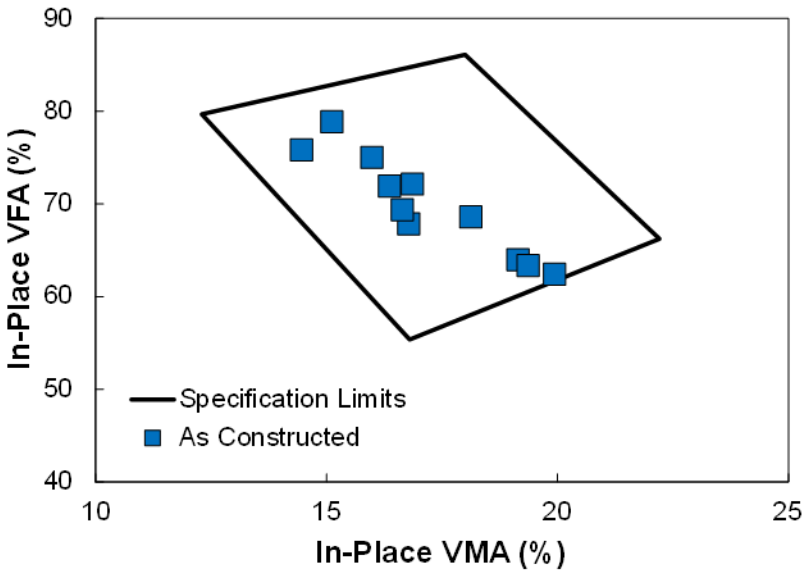

A. Calculated VMA_{IP} and VFA_{IP} for specification limits for 11 samples.

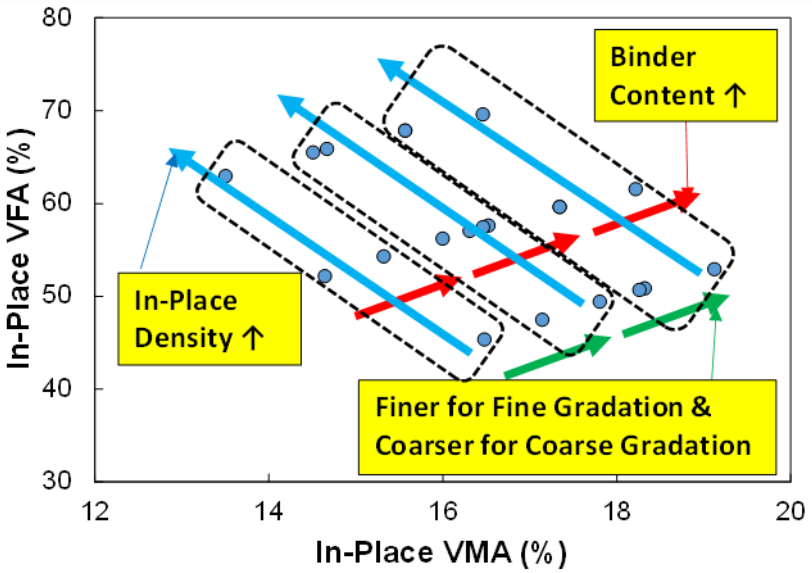

B. Movement of VMA_{IP} and VFA_{IP} with mixture properties.

Figure 111. Graphs. MaineDOT shadow project.[23]

The research team selected 3 samples located the furthest away within the 11 samples to create 4 corners. Typically, four samples are chosen in this phase. However, three samples can be selected when the three samples can make the widest quadrangular volumetric range. If three samples are used to build four corners, one sample should be compacted with two different target air void contents. For the MaineDOT shadow project, samples 159352, 159360, and 159361 were selected to build the four corners, as presented in figure 112-A. Figure 112-B shows the final PVR calibration plan for the four corners and verification purpose samples. The research team rearranged the selected three samples in the volumetric domain by changing the target air void contents to low and high values to establish a quadrangular range. The figure reflects that sample 159352 is compacted at two different target air void contents, 7.5 and 3.5 percent, denoted as A and B, respectively, and at 2.5 and 7.5 percent for samples 159360 and 159361, respectively. The verification purpose samples that the research team will test later remain in the same locations as in figure 112-A. Furthermore, MaineDOT implemented performance tests using other samples, including a sample outside the four corners, to check whether the PVR can capture a point that is outside the area encompassed by the four corners. Once the testing plans were set, MaineDOT shipped the test samples to the research team and stored the remaining three samples in temperature-controlled storage as backup.

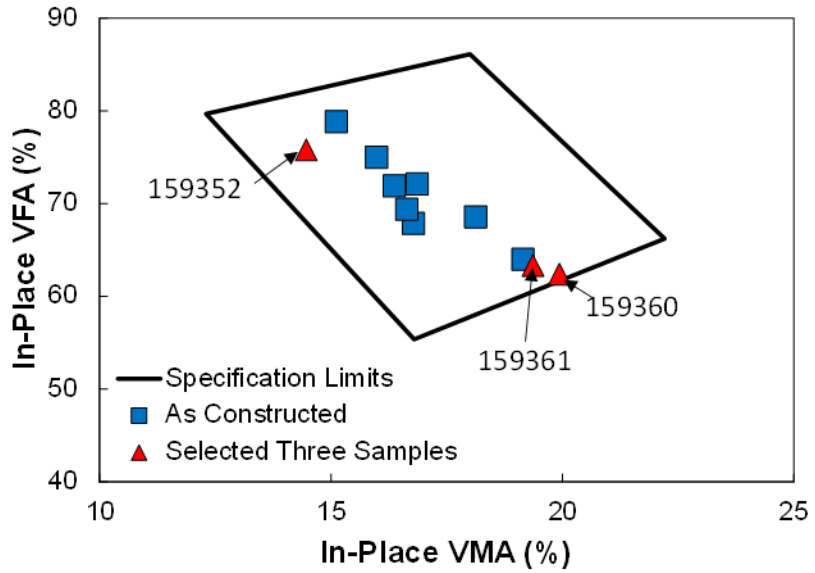

A. Selected three samples to create four corners.

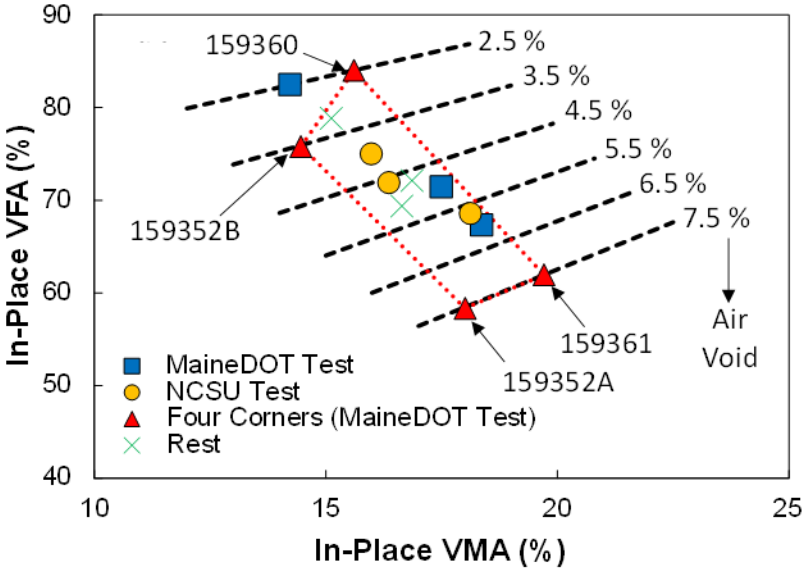

B. Determined PVR calibration conditions.

Figure 112. Graphs. MaineDOT shadow project.[(23)]

The research team estimated the minimum amount of mixture and preparation time for one sample (one volumetric condition) to complete the PVR development 5 d, which includes mixture fabrication, coring and cutting, air void measurements, three AMPT performance tests, and 120 lb of mixture based on 20 lb for a gyratory-compacted specimen times six. The PVR uses four volumetric conditions, and at least two samples are recommended to verify the

developed PVR. Therefore, the PVR needs a minimum of 30 d and 720 lb of mixture to develop and be verified. Also, FlexMAT analysis and FlexPAVE simulations based on the AMPT performance test results may take a day to complete. The time needed to complete the FlexPAVE simulations for the four corners and verification samples depends on the performance of the hardware, but the software will automatically run simulations if the user chooses the batch mode. Therefore, users are not required to do anything while the simulation is running. The PVR calibration of takes less than 2 h using the Microsoft Excel regression data analysis function.

Asphalt Mixture Performance Tester Tests and Performance Prediction

MaineDOT and the research team conducted the AMPT tests based on the determined PVR conditions inFigure 112-B. Table 60 presents the target and achieved air void contents of the test specimens fabricated by both MaineDOT and the research team. MaineDOT and the research team used test temperatures of 4 ℃, 20 ℃, and 40 ℃ for the dynamic modulus tests, 15 ℃ for the cyclic fatigue tests, 20 ℃ for the LT SSR tests, and 45 ℃ for the HT SSR tests.

Table 60. MaineDOT shadow project: Measured air voids of test specimens.

Sample ID	Target Air Voids (Percent)	Air Voids for Dynamic Modulus Test (Percent)	Air Voids for Cyclic Fatigue Test (Percent)	Air Voids for SSR Test (Percent)	Testing By
159352A	7.5	7.2	7.2	7.5	MaineDOT
159352B	3.5	3.3	2.9	3.3	MaineDOT
159360	2.5	2.4	2.5	2.2	MaineDOT
159361	7.5	7.6	7.6	7.6	MaineDOT
159354A	5.0	5.1	4.6	5.2	MaineDOT
159354B	6.0	5.8	5.8	6.0	MaineDOT
159355	2.5	2.3	2.2	2.3	MaineDOT
159353	4.0	4.3	4.4	3.7	NCSU
159358	4.6	4.7	4.7	4.3	NCSU
159362	5.7	5.8	5.8	5.9	NCSU

After the AMPT performance tests were completed, both MaineDOT and the research team separately carried out data analysis using FlexMAT. The research team gathered all the analyzed data to run pavement performance simulations using FlexPAVE. The research team input the same information in table 57 to FlexPAVE to simulate real situations as much as possible, except for the thickness of the asphalt layer. The project was a mill-and-fill project where the top 50 mm of the existing asphalt layer was replaced by the study mixture. Because fatigue damage in a relatively thin pavement, such as the selected pavement, starts mostly at the bottom of the asphalt layer, changing the mixture for the top 50 mm of the asphalt layer would not yield information about the effects of changes in the mixture volumetric conditions on the pavement performance. Therefore, the research team used FlexPAVE to model the entire 100 mm of the asphalt layer for the study mixture. The team selected Bangor, ME in the EICM for the climate conditions.[22] The team input daily ESAL as 1,389, which the team calculated from the design ESAL (10,000,000) divided by 20 yr. The research team input the traffic speed as 70 mph, which is the same as the

design speed, and assumed the traffic growth rate as 0 percent. Table 61 presents the analyzed results of the FlexPAVE performance simulations and the volumetric information for the tested specimens.

Table 61. MaineDOT shadow project: Volumetric information and test results.

Sample ID	Cyclic Fatigue IP-VMA	Cyclic Fatigue IP-VFA	SSR IP-VMA	SSR IP-VFA	%Damage at 20 yr	Asphalt Surface Rut Depth at 20 yr (mm)
159352A	17.7	59.4	18.0	58.3	14.3	1.6
159352B	13.9	79.2	14.3	76.9	9.9	1.0
159360	15.6	84.0	15.3	85.7	10.6	0.9
159361	19.8	61.6	19.8	61.6	14.3	1.6
159354A	17.1	73.2	17.7	70.6	14.2	1.2
159354B	18.2	68.1	18.4	67.3	11.5	1.4
159355	14.0	84.2	14.1	83.6	10.3	0.9
159353	15.7	72.0	15.1	75.5	12.5	1.3
159358	16.5	71.4	16.1	73.3	11.4	1.3
159362	18.2	68.2	18.3	67.8	12.1	1.6

Performance-Volumetrics Relationship Development

The research team calibrated the PVR function based on the results of the simulated performance and the volumetric information for the four corners samples. This calibration effort used equations 17 and 18. Table 62 presents the coefficients for both equations.

Table 62. MaineDOT shadow project: Performance volumetric relationship coefficients for %Damage and rut depth.

Performance	a_f / a_r	b_f / b_r	d_f / d_r	R^2
%Damage	0.41	−0.11	13.46	0.98
Asphalt rut depth	0.058	−0.019	1.681	1.00

Users can predict performance by inputting the volumetric information into the developed PVR function. Table 63 presents the numerical results for the performance predicted from the PVR and simulated by FlexPAVE and figure 113-A and figure 113-B present comparisons of the %Damage and rut depths, respectively, obtained from the PVR and FlexPAVE.

Table 63. MaineDOT shadow project: Comparison of performance derived from FlexPAVE and performance volumetric relationship.

Sample ID	%Damage Simulated by FlexPAVE	%Damage Predicted from PVR	%Damage %Error	Asphalt Surface Rut Depth Simulated by FlexPAVE (mm)	Asphalt Surface Rut Depth Predicted from PVR (mm)	Asphalt Surface Rut Depth %Error
159352A	14.3	14.0	2.0	1.6	1.6	0.7
159352B	9.9	10.2	2.8	1.0	1.0	1.0
159360	10.6	10.4	2.3	0.9	0.9	0.9
159361	14.3	14.6	1.8	1.6	1.6	0.6
159354A	14.2	12.2	14.0	1.2	1.3	11.4
159354B	11.5	13.2	15.1	1.4	1.4	1.2
159355	10.3	9.7	6.5	0.9	0.9	3.0
159353	12.5	11.8	5.9	1.3	1.1	12.5
159358	11.4	12.1	6.3	1.3	1.2	8.0
159362	12.1	13.2	9.1	1.6	1.4	7.7
Average	—	—	6.6	—	—	4.7

—No data.

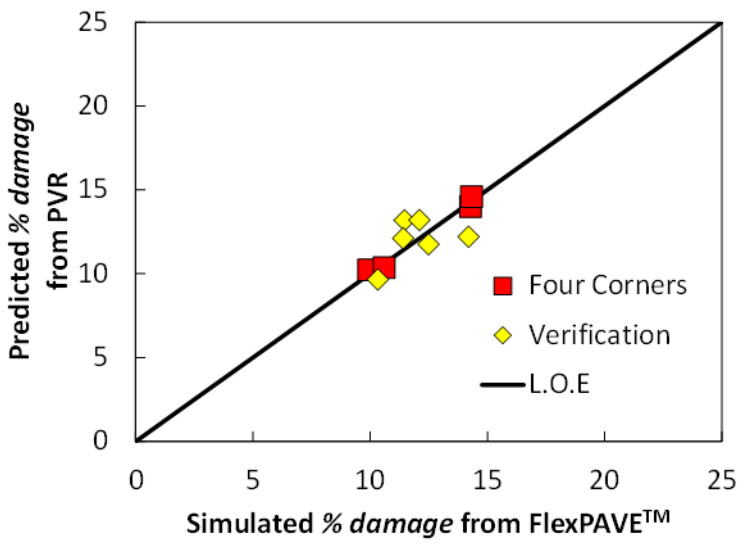

A. %Damage.

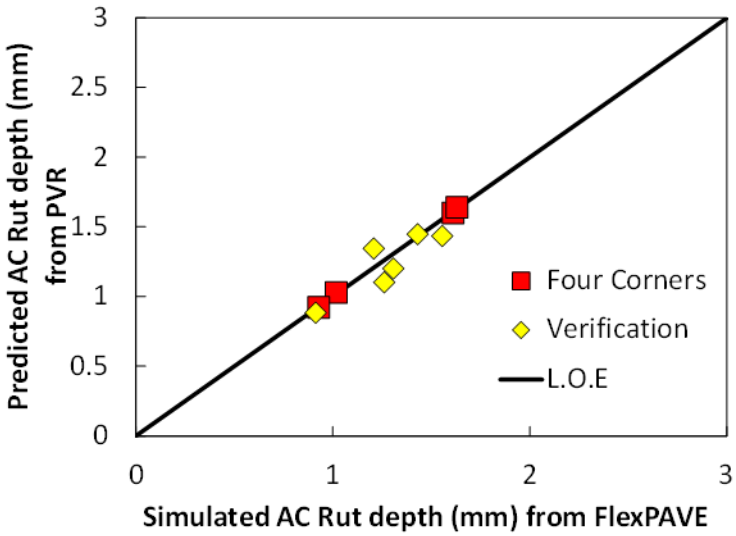

B. Asphalt concrete rut depth.

Figure 113. Graphs. MaineDOT shadow project: Comparison of results obtained from FlexPAVE and PVR.(23)

The %Error between the predicted and simulated performance of all samples is 6.6 percent for %Damage and 4.7 percent for rut depth. The largest %Error is 15.1 percent in %Damage, and most of the samples showed less than 10 percent for both %Damage and rut depth, except a few samples. These findings indicate that the developed PVRs worked well to predict pavement performance. In other words, users can predict pavement performance without running performance tests once PVRs are developed. Only volumetric tests are needed to predict pavement performance, which will save a significant amount of both materials and time.

Investigation into Field Variability and Its Impact on Pavement Performance Using the Performance-Volumetrics Relationship

The research team used the developed PVR function to investigate the effect of construction variability on pavement performance. Although 11 samples were paved for the same project, the samples had various binder contents, G_{mm} values, and in-place density values that affected the volumetric conditions, as shown in table 58. Therefore, the research team had to select appropriate variables to represent the field variability. During field pavement construction, the most changeable factor is the field density or in-place air voids. The research team focused on the field density of the constructed 11 samples and the field density's impact on performance using the PVR. Table 64 shows the in-place density percentages, volumetric conditions, and predicted performance in terms of predicted %Damage and rut depth at the design life (20 yr) based on the PVRs of the constructed 11 samples. Figure 114-A and figure 114-B present the volumetric information and the PVR-predicted performance with in-place air voids.

Table 64. MaineDOT shadow project: In-place density, volumetric conditions, and predicted performance obtained using performance volumetric relationships of 11 samples.

Sample ID	IP-Density (Percent)	IP-Air Void (Percent)	VMA_{IP} (Percent)	VMA_{IP} (Percent)	%Damage Predicted from PVR	Asphalt Surface Rut Depth Predicted from PVR (mm)
159352	96.5	3.5	14.5	75.8	10.8	1.1
159353	96.0	4.0	16.0	75.0	11.5	1.2
159354	93.1	6.9	19.1	64.0	14.0	1.6
159355	94.6	5.4	16.8	67.8	12.7	1.3
159356	94.9	5.1	16.6	69.3	12.4	1.3
159357	95.3	4.7	16.9	72.1	12.2	1.3
159358	95.4	4.6	16.4	71.9	12.0	1.2
159359	96.8	3.2	15.1	78.8	10.7	1.0
159360	92.5	7.5	19.9	62.4	14.5	1.6
159361	92.9	7.1	19.4	63.3	14.2	1.6
159362	94.3	5.7	18.1	68.6	13.1	1.4

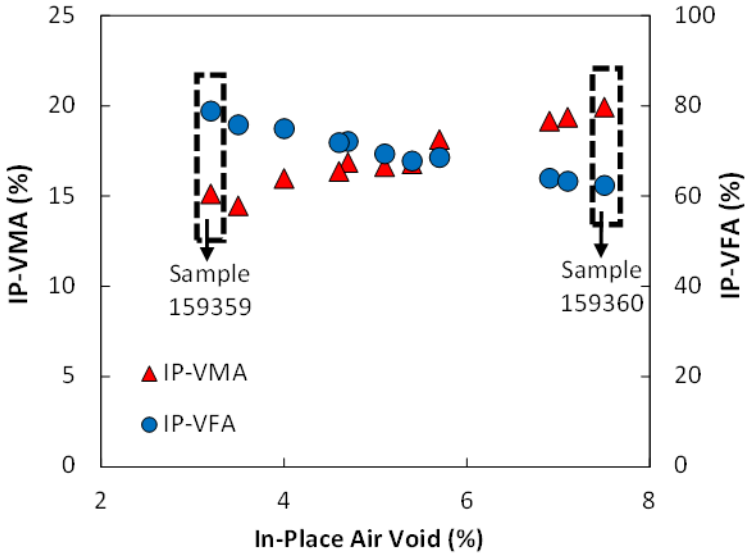

1 mm = 0.04 inches.

A. Volumetric conditions.

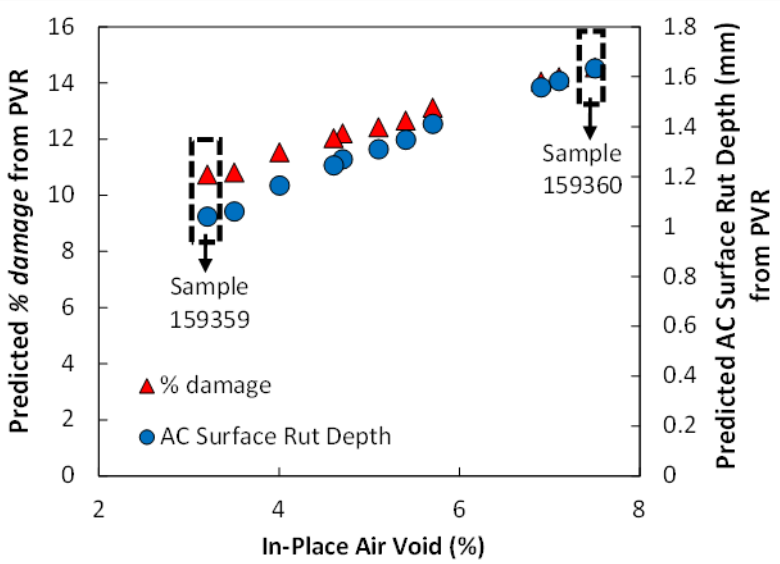

1 mm = 0.04 inches.

B. Predicted performance at design life derived from PVRs of constructed 11 samples.

Figure 114. Graphs. MaineDOT shadow project.[(23)]

The results indicate that the sample with the lowest in-place density, sample 159360, was predicted to have the worst performance in terms of least resistance to fatigue cracking and rutting and the sample with the highest in-place density, sample 159359, was predicted to have the best performance. The percent difference of these two samples was calculated as 30.1 percent for fatigue cracking and 44.5 percent for rutting. Although these percentages would change when the transfer functions are included in FlexPAVE, these results clearly show that field construction variability can affect pavement performance significantly. In addition, the performance predicted using the PVRs and the field variability show reasonable trends.

Summary

The results of this study are summarized in the following findings:

- The proficiency test results indicated that the AMPT workshop and onsite training helped the shadow project agency (MaineDOT) personnel become proficient with AMPT testing.
- The proficiency tests that MaineDOT undertook were performed well and the quality of the test results was acceptable.
- MaineDOT acquired 11 samples. Through the AQC tests, marked field variability was noticeable within the same project.
- MaineDOT and the research team successfully carried out all the AMPT tests using the shadow project materials. The test results presented no problems in developing the PVRs.

- The research team developed the PVR using the four corners method. The PVRs were able to predict pavement performance based on the input volumetric conditions. On average, the errors were 6.6 and 4.7 percent for the fatigue damage and rutting predictions, respectively obtained from the PVR, compared to the performance derived from FlexPAVE simulations.

- The research team investigated field variability and field variability's impact on pavement performance in this study. Within the 11 constructed samples, the maximum percentage differences were 30.1 and 44.5 percent for the predicted fatigue damage and rutting, respectively, at the design life using the PVR function.

- The PVR function predicted the expected trend of pavement performance as a function of field density. However, an additional field study is needed to validate the performance that the PVRs predicted. Once the PVR functions are verified, State highway agencies will be able to use the PVR functions and volumetric information to predict performance of the pavement instead of running performance tests, which will lead to significant savings in terms of materials and time.

For State highway agencies to use the PVR concept in projects, a future study is needed to evaluate the sensitivity of PVRs to changes in pavement structure, traffic volume and speed, and climatic conditions. Agencies could use this sensitivity analysis to determine how to group different paving projects so that the agencies can use the same PVR functions for the projects within each group without having to calibrate PVRs for individual projects.

THE MISSOURI DEPARTMENT OF TRANSPORTATION SHADOW PROJECT

This chapter provides a chronological overview of MoDOT's shadow projects and analysis of the AMPT test results. MoDOT conducted three shadow projects, J6I3114, J6I3157, and J5P3054. The research team's role was to help MoDOT prepare for the shadow projects and understand the procedures and modeling concepts, data collection, testing protocols, data analysis, and other required activities. The primary contact person at MoDOT was Daniel J. Oesch at Daniel.Oesch@modot.mo.govD. The following chronological list contains the primary events:

- Material sampling: J6I3114 Project (June 2017), J6I3157 Project (June 2017), J5P3054 Project (October 2017).

- Onsite training: December 20–21, 2017.

- Proficiency testing (MoDOT): February 2018.

- Proficiency testing (NCSU): March 2018.

- Shadow project testing (MoDOT): March 2018–January 2019.

Training Resources

MoDOT personnel attended a 2-d AMPT hands-on workshop held at NCSU from January 31 to February 1 in 2017. The research team provided onsite training December 20–21, 2017.

Communication Log

Table 65 provides a summary of the important communications and reasons and outcomes.

Table 65. MoDOT shadow project: Communication log.

Date	Type	Major Communication Log
3-29-2018	Conference call	• The team reviewed proficiency test results. • The team compared MoDOT's test results to the research team's test results.
11-26-2018	Conference call	• Discussed issues surrounding shadow project data quality. • The team identified some minor issues in the dynamic modulus test results. • The team determined that the quality of cyclic fatigue test results for several samples was not acceptable. • The team determined that several SSR tests were conducted with an incorrect template, i.e., the HT template was used for the low-temperature test. • The team informed MoDOT of missing shadow data in the shared database.
4-25-2019	Conference call	• The team reviewed the testing procedures to enhance the test quality. • The team informed MoDOT of the missing data again. • The team requested that MoDOT quantify the remaining materials to conduct additional tests. • The team suggested MoDOT conduct a second round of proficiency testing.

Date	Type	Major Communication Log
5-21-2019	Conference call	• MoDOT uploaded additional tests results. The SSR test results were completely corrected. • MoDOT confirmed that they do not have sufficient materials to conduct additional tests for PVR development.
2-26-2021	Video meeting	• MoDOT stated that the second proficiency test did not happen due to test scheduling problems at MoDOT. • MoDOT conducted AMPT performance tests using another project. Because the most important part of the project is to practice conducting AMPT performance tests, the team decided to alter the project plan to focus on securing MoDOT's proficiency for AMPT performance testing. • The team informed MoDOT that except for the AMPT performance testing, the other techniques of the shadow project are tools that can be learned relatively easier than the test procedure. • MoDOT provided the most recent AMPT performance test results.

Proficiency Testing

The research team used one of the collected shadow project mixture samples for the proficiency tests. Table 66 provides a summary of the proficiency test mixture.

Table 66. MoDOT shadow project: Mixture properties for proficiency testing.

Mixture ID	NMAS (mm)	Virginia Binder Type	RAP Content (Percent)	Total Binder Content (Percent)
17MFO0050	12.5	PG 76-22	28	5.2

According to onsite training and shadow project guidelines, the agency should fabricate 12 gyratory-compacted samples with the target specimen air void content of 4 percent ±0.5 percent and then ship 6 randomly selected samples to the research team. However, the gyratory-compacted samples MoDOT fabricated were 170 mm in height (instead of the specified 180 mm) with target air voids of 4 percent ±0.5 percent. This outcome highlights the importance of the time interval between the onsite training and project start. If the time between onsite training and the project start date is too long, then the chance is greater that the agency will not remember the details in sample fabrication and testing and will make mistakes. MoDOT personnel and the research team each cored and cut six gyratory-compacted samples to obtain test specimens. The research team had only five gyratory-compacted samples shipped from MoDOT due to delivery limitations. The team therefore used one gyratory-compacted sample for the dynamic modulus and cyclic fatigue tests and three samples for the SSR tests. The remaining gyratory-compacted sample was kept as a backup. Table 67 provides a summary of the number of tested specimens and average measured air void contents of the test specimens.

Table 67. MoDOT shadow project: Averaged measured air void contents and test temperatures of proficiency test specimens.

Test Conducted By	Dynamic Modulus Test (Number of Specimens, Air Void Content Percent)	Cyclic Fatigue Test (Number of Specimens, Air Void Content Percent)	SSR Test (Number of Specimens, Air Void Content Percent)
MoDOT	4, 4.2	3, 4.3	LT: 1, 3.5 HT: 1, 3.7
NCSU	2, 4.5	2, 4.3	LT: 1, 3.9 HT: 2, 4.0

Dynamic Modulus Testing

MoDOT personnel and the research team each conducted dynamic modulus tests. Based on the MoDOT's dynamic modulus test results, the research team found that the target strain range of the dynamic modulus test was set to 75 to 125 microstrain. According to test standards (AASHTO TP 132), the target microstrain range for the small geometry specimen test is specified as 50 to 75 microstrain.[30] MoDOT used a strain range that is intended for large geometry test specimens. The dynamic modulus tests were conducted at 4 ℃, 20 ℃, and 40 ℃. The number of test loading rates at each test temperature was six (25 Hz, 10 Hz, 5 Hz, 1 Hz, 0.5 Hz, and 0.1 Hz) when the onsite training and proficiency tests were conducted. Figure 115 presents a comparison of the two sets of results. Although MoDOT conducted the two sets of tests at different target strain ranges, the measured dynamic modulus values are not significantly different. Figure 115-0 shows that most of the dynamic modulus values that MoDOT obtained from tests conducted at 4 °C and 20 °C are visually similar for both sets of results. FlexMAT Cracking was used to develop the dynamic modulus master curves presented in figure 115-0. The MoDOT curves for the tests conducted at 40 °C are slightly higher than the researcher's curves.

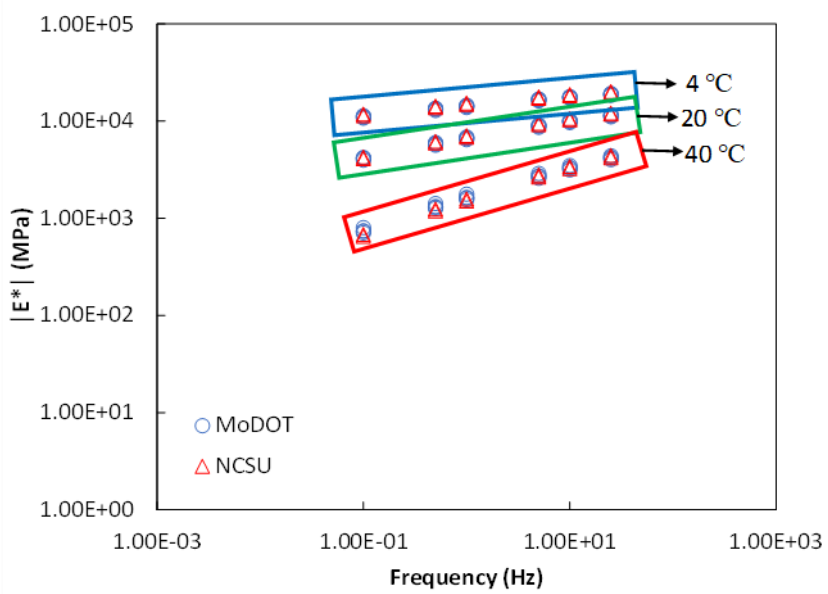

Source: FHWA.
1 MPa = 145.04 psi.

A. Proficiency test results—dynamic modulus test results before shifting.

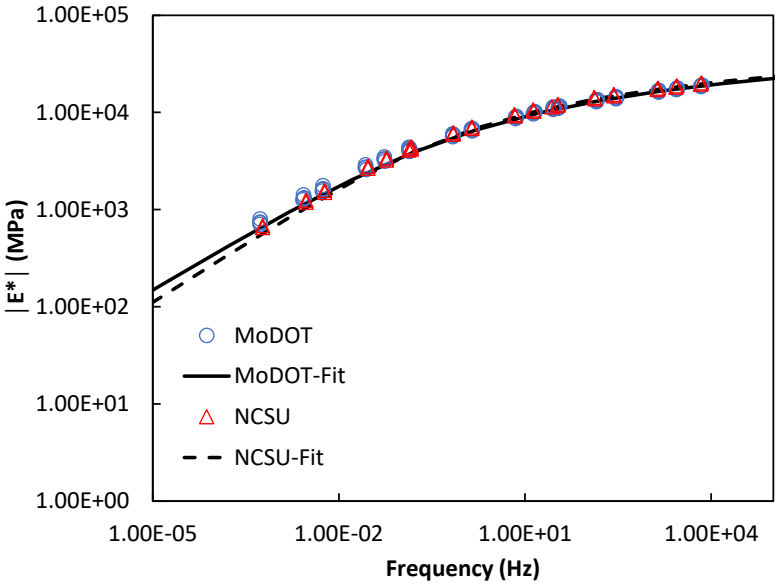

Source: FHWA.
1 MPa = 145.04 psi.

B. Proficiency test results—dynamic modulus test results after shifting.

Figure 115. Graphs. MoDOT shadow project: Dynamic modulus proficiency test results.

According to AASHTO TP 132, several factors that are measured during dynamic modulus tests should be evaluated by comparing them to the acceptable limits in the test standard to determine the data quality.[30] During a dynamic modulus test, the AMPT automatically measures various factors, as summarized in table 68 with the acceptance limits. Except for MoDOT's first specimen (with the 25 Hz at 4 °C data), all the data met the quality requirements. Based on these results, the test data quality can be considered acceptable for both institutions.

Table 68. MoDOT shadow project: Dynamic modulus test results compared to data quality requirements.

Test Conducted By	Specimen ID	Deformation Drift (Negative Sign)	Load Std. Error (<10 Percent)	Deformation Std. Error (<10 Percent)	Deformation Uniformity (<30 Percent)	Phase Uniformity (<3°)
MoDOT	1	All met	All met	All met	32.8 percent at 25 Hz, 4 °C	All met
MoDOT	2	All met	All met	All met	All met	All met
MoDOT	3	All met	All met	All met	All met	All met
MoDOT	4	All met	All met	All met	All met	All met
NCSU	1	All met	All met	All met	All met	All met
NCSU	2	All met	All met	All met	All met	All met

As a next step, the research team compared dynamic modulus test data from the two institutions using the Multilaboratory Precision (Reproducibility) method from AASHTO T 378.[86] This comparison used all the dynamic modulus values from both MoDOT and the research team, with the assumption that the number of test specimens was four for each institution. The assumption of four test specimens for each institution is based on the different number of tested specimens (four specimens tested by MoDOT and two specimens tested by the research team) and leads to tighter threshold values for a pass or fail criterion. Table 69 presents the reproducibility comparison results. The research team corrected the acceptance limits by multiplying the current acceptance limit values in AASHTO T 378 by 2.8, because this test standard has incorrect acceptance limit values.[86] Also, the research team extrapolated the acceptance limit values of the loading rates, 25 Hz and 10 Hz at 4 °C, because AASHTO T 378 does not specify limits for dynamic modulus values above 16,400 MPa.[86]

Table 69. MoDOT shadow project: Reproducibility of dynamic modulus test results from two institutions.

Temperature (°C)	Loading Rate (Hz)	Average Dynamic Modulus (MPa)	Reproducibility	Acceptance Limit	Pass or Fail
4	25	18,482	10.4	14.4	Pass
4	10	17,199	10.7	14.4	Pass
4	5	16,201	10.9	15	Pass
4	1	13,869	11.4	15.4	Pass

Temperature (°C)	Loading Rate (Hz)	Average Dynamic Modulus (MPa)	Reproducibility	Acceptance Limit	Pass or Fail
4	0.5	12,884	11.7	15.4	Pass
4	0.1	10,750	12.4	15.4	Pass
20	25	11,311	12.2	15.4	Pass
20	10	9,902	12.7	15.4	Pass
20	5	8,855	13.1	19.4	Pass
20	1	6,636	14.4	19.4	Pass
20	0.5	5,810	15.0	19.4	Pass
20	0.1	4,119	16.7	24.6	Pass
40	25	4,386	16.4	24.6	Pass
40	10	3,482	17.6	24.6	Pass
40	5	2,888	18.6	24.6	Pass
40	1	1,767	21.7	32	Pass
40	0.5	1,421	23.2	32	Pass
40	0.1	801	27.8	39.7	Pass

These results show that the measured dynamic modulus test values the research team obtained from both institutions are not statistically different because all the values met the acceptance limits. In conclusion, the research team did not find any significant problems with MoDOT's dynamic modulus testing.

Cyclic Fatigue Testing

The cyclic fatigue tests were performed at 18 °C. For the cyclic fatigue tests, the damage characteristic curves indicate that the MoDOT curves deviated compared to the researcher's curves, as shown in figure 116-A. Also, the researcher's curves are relatively above the MoDOT curves. This outcome is due to a dynamic modulus ratio (DMR) problem caused by the lack of conditioning time. Table 70 provides a summary of the measured DMRs that MoDOT and the research team obtained. The DMR indicates the difference between the condition of the fatigue test specimen and the dynamic modulus test results. Because the dynamic modulus test and cyclic fatigue test should use the same mixture and target air void contents, the physical specimen properties for these two tests must be similar. Therefore, at the test temperature, the fingerprint dynamic modulus ($|E^*|$) value of the cyclic fatigue test specimen should be in the acceptable DMR range (0.85 to 1.15) of the corresponding dynamic modulus value from the developed dynamic modulus master curve. If the DMR is 1, then the physical specimen properties of the dynamic modulus and cyclic fatigue tests are the same. The measured DMR value of the research team was 1.02, but only one specimen of MoDOT's measured DMR values was within the range. Two MoDOT specimens were out of the range, indicating that the two specimens were not fully conditioned. For the cyclic fatigue tests, the conservative conditioning time is 1 hr 30 min in the AMPT chamber after the chamber reaches the target test temperature. This information was covered at the onsite training level. Figure 116-B shows the damage characteristic curves for the specimens within the DMR range. When the DMR values are in the

acceptable range, the curves collapse well. Figure 116-C shows the pseudoenergy-based failure criterion (D^R) value is lower for the MoDOT results than the research team's results. However, the numerical D^R values of the specimens within the acceptable DMR range are similar, as shown in table 70. The cyclic fatigue test index, S_{app}, shows the same trend as D^R. The research team used Jefferson City, MO, as the location when calculating the S_{app} values.

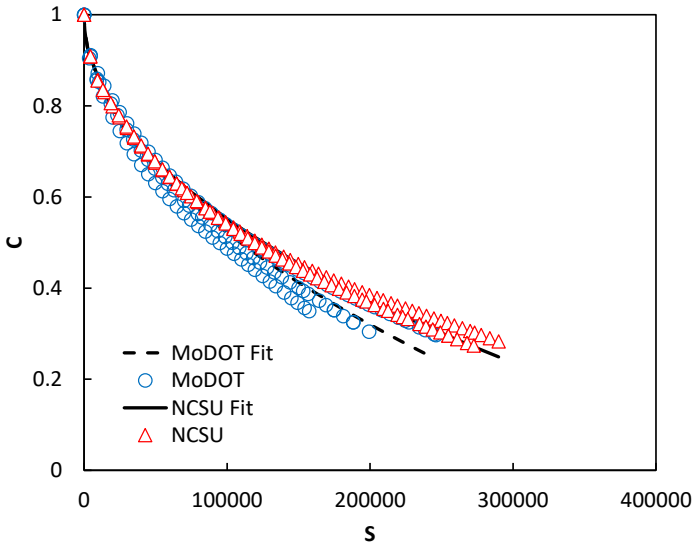

Source: FHWA.

A. Proficiency test results—damage characteristic curves.

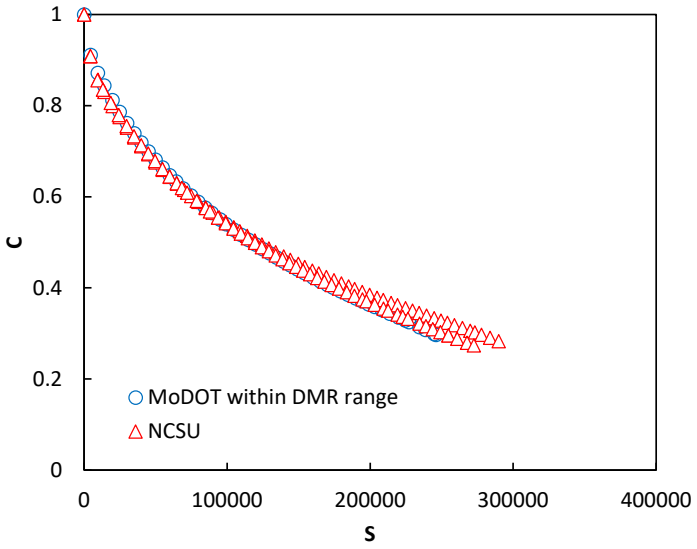

Source: FHWA.

B. Proficiency test results—damage characteristic curves within DMR range.

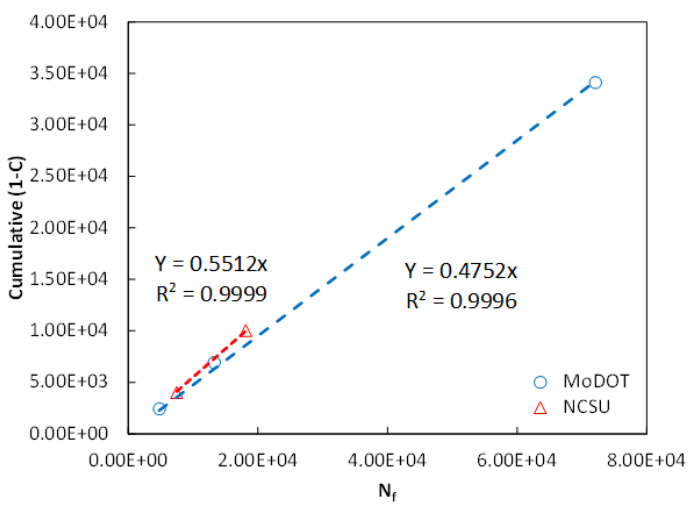

Source: FHWA.

C. Proficiency test results—pseudoenergy-based failure criterion.

Figure 116. Graphs. MoDOT shadow project: Cyclic fatigue proficiency test results.

Table 70. MoDOT shadow project: Cyclic fatigue proficiency test results.

Institution	Test Specimen	Air Void Content (Percent)	DMR	N_f	D^R	S_{app}
MoDOT	1	4.2	1.08	13,250	0.52	20.7
MoDOT	2	4.6	0.73	4,770	0.51	17.0
MoDOT	3	4.0	0.81	72,080	0.47	13.1
NCSU	1	4.1	1.02	18,110	0.55	26.4
NCSU	2	4.4	1.02	7,460	0.54	23.8

N_f = number of cycles to failure; D^R = pseudostrain energy-based fatigue failure criterion of a mixture; and S_{app} = the fatigue index parameter of a mixture.

In addition, the research team investigated the proportional integral derivative (PID) tuning of the cyclic fatigue tests for both institutions. A PID is a control loop mechanism that continuously calculates the error value as the difference between the desired set point and a measurement. In AMPT performance testing, the better-tuned PID values produce smaller errors between the command and output. During the onsite training, the research team trained the MoDOT engineers to tune the PID. In another project the research team is currently working on for FHWA (Ruggedness and Interlaboratory Studies for Asphalt Mixture Performance Tester (AMPT) Cyclic Fatigue Test: Phase I Report), the PID is considered well-tuned when the standard error at each cycle during the initial five cycle tests before the cyclic fatigue test is less than 10 percent.[87] Table 71 presents a summary of the calculated standard error values for both the MoDOT and researcher's tests. The standard error at any cycle for both institutions does not exceed 10 percent, which indicates that the PID is well tuned for both institutions. Table 71 also presents the tolerance values of the other quality indicators for the cyclic fatigue fingerprint test. The research team did not find any significant problems regarding PID tuning and fingerprint testing.

Table 71. MoDOT shadow project: Test results compared to fatigue test quality indicators.

Institution	Test Specimen	Fingerprint Average Load Standard Error (<10 Percent)	Fingerprint Deformation Standard Error (<10 Percent)	Fingerprint Deformation Uniformity (<30 Percent)	Fingerprint Phase Uniformity (<3°)	Cyclic Fatigue Average Deformation Standard Error (<10 Percent)
MoDOT	1	2.77	2.66	11.79	0.50	1.85
MoDOT	2	2.21	2.39	1.32	0.67	2.51
MoDOT	3	3.36	3.18	11.31	0.75	2.14
NCSU	1	2.94	2.93	4.75	0.83	1.12
NCSU	2	2.31	2.72	7.59	1.25	1.71

Stress Sweep Rutting Testing

The SSR tests were conducted at 26 ℃ and 49 ℃. Figure 117-0 and figure 117-0 present the results of SSR tests conducted at both institutions at two different temperatures, LT and HT, respectively. According to AASHTO TP 134, the acceptable strain difference between the replicates is 25 percent at the end of the test.[16] Although the MoDOT test results consistently showed lower permanent strain curves than the research team for both temperature tests, the maximum strain difference did not exceed 25 percent. One possible explanation for the MoDOT's lower permanent strain (ε_{vp}) compared to that of the research team is the conditioning time. Lastly, the measured SSR index value, the RSI value, was 2.6 percent for the MoDOT and 3.0 percent for the research team. Based on comparisons of the test results, the research team did not find any remarkable problems. Table 72 and table 73 show the numerical SSR test results and the maximum strain difference at each temperature, and table 74 presents the measured RSI index values.

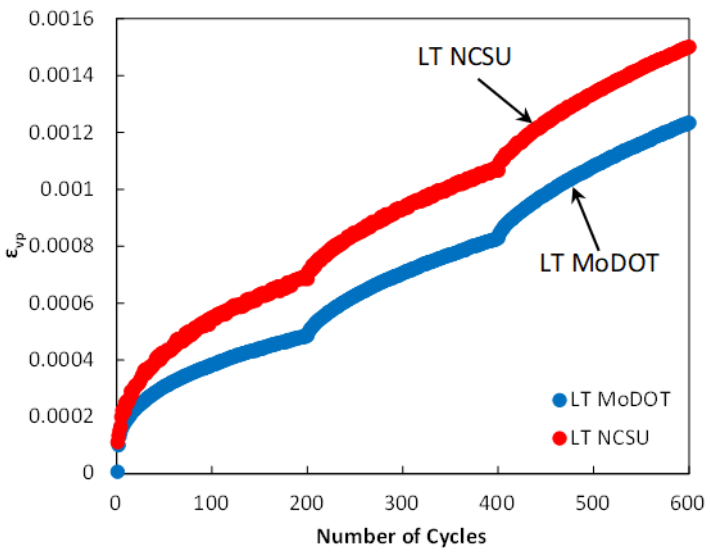

Source: FHWA.

A. Proficiency test results—SSR tests at LT.

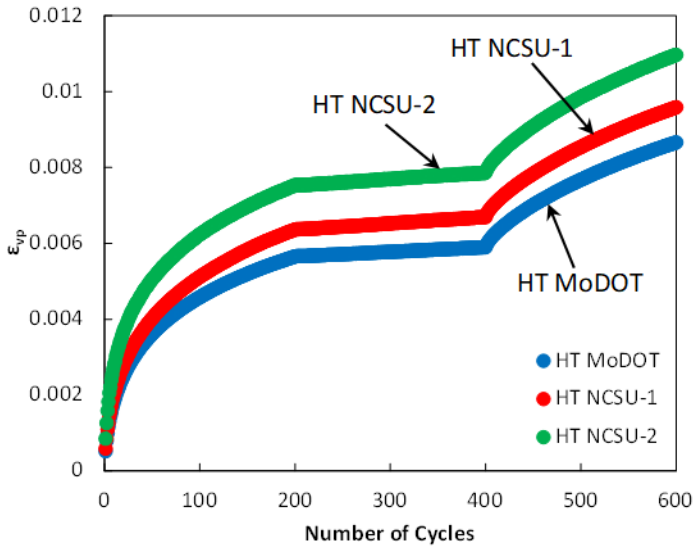

Source: FHWA.

B. Proficiency test results—SSR tests at HT.

Figure 117. Graphs. MoDOT Shadow Project: SSR proficiency test results.

Table 72. MoDOT shadow project: SSR test results (LT).

Institution	Sample	Air Void Content (Percent)	Permanent Strain at 600th Cycle	Percent Difference of Permanent Strain at 600th Cycle
MoDOT	1	3.5	0.001234	19.5
NCSU	1	3.9	0.01501	19.5

Table 73. MoDOT shadow project: SSR test results (HT).

Institution	Sample	Air Void Content (Percent)	Permanent Strain at 600th Cycle	Percent Difference of Permanent Strain at 600th Cycle
MoDOT	1	3.7	0.008665	23.5
NCSU	1	4.0	0.00959	23.5
NCSU	2	4.1	0.10969	23.5

Table 74. MoDOT shadow project: Measured RSI values.

Institution	RSI (Percent)
MoDOT	2.6
NCSU	3.0

Summary of Proficiency Test Results

Based on the proficiency test results, the team investigated the major issues presented in table 75.

Table 75. MoDOT shadow project: Major issues of proficiency testing, with solution.

Test	Major Issue	Solution
Sample fabrication	The gyratory-compacted specimen height was 170 mm.	The target height of gyratory-compacted specimens is 180 mm.
Dynamic modulus	The target strain range was 75–125 microstrain.	The target strain range should be 50–75 microstrain.
Cyclic fatigue	The MoDOT's two test specimens showed lower DMR values than those of the research team.	The test specimen should be conditioned in an AMPT chamber for 1 h 30 min at the test temperature.
SSR	The MoDOT's permanent strain curves were consistently lower than the research team's results.	The test specimen should be conditioned in an external chamber at 1 h for the LT and 3 h for the HT.

Evaluation of Proficiency Tests

Regarding the test result reproducibility from both institutions (MoDOT and NCSU), the research team concluded that the test results would be more similar if the institutions could resolve the major issues in Table 75. The test results from both institutions did not show significant differences regarding the major test parameters, such as D^R and S_{app} (only for the results within the acceptable DMR range), for the fatigue tests and the RSI values for the SSR tests. Therefore, the team determined that MoDOT was proficient at conducting AMPT tests and was ready to run the shadow project tests.

Material Acquisition for Missouri Department of Transportation Shadow Projects

Table 76 provides a summary of the MoDOT shadow projects and material properties. The research team selected 3 paving projects and MoDOT obtained 10 samples from 10 different truck loads on different dates for each project. MoDOT sealed the materials in cardboard boxes and plastic bags. MoDOT obtained around 400 lb of materials for each sample.

Table 76. MoDOT shadow project: General project information.

Project	J6I3114	J6I3157	J5P3054
Pavement type	Surface	Surface	Surface
Route	1–44	I–270	US 63
Mixture	SP125	SP125	SP125
NMAS (mm)	12.5	12.5	12.5
Mixture PG	PG76-22	PG76-22	PG70-22
RAP content (percent)	28	33	30
Total binder content (percent)	5.2	4.7	5

Missouri Department of Transportation's Quality Acceptance Test Results for 10 Samples

The MoDOT conducted acceptance tests of all acquired samples to obtain the AQCs and then provided the resultant data to the research team. Table 77–table 79 present a summary of the measured AQCs. MoDOT used a coring method to measure the in-place air void contents (in-place density).

Table 77. AQC obtained from MoDOT: J6I3114 project.

Sample ID	G_{sb}	Air Void Content at N_{des} (Percent)	Asphalt Binder (Percent)	VMA at N_{des} (Percent)	In-Place Air Void (Percent)
17MFO0050	2.603	5.0	5.58	15.4	8.07
17MFO0051	2.603	2.9	5.33	13.9	8.08
17MFO0052	2.603	4.4	5.21	14.5	7.77
17MFO0053	2.603	4.2	4.88	14.1	6.40
17MFO0054	2.603	3.4	5.43	14.0	7.67
17MFO0055	2.603	4.5	5.56	14.8	6.06
17MFO0056	2.603	4.1	5.01	14.0	7.45
17MFO0057	2.603	6.0	5.30	15.6	8.59
17MFO0058	2.603	5.3	5.19	15.3	8.92
17MFO0059	2.603	5.4	5.11	15.3	9.24

Table 78. AQC obtained from MoDOT: J6I3157 project.

Sample ID	G_{sb}	Air Void Content at N_{des} (Percent)	Asphalt Binder (Percent)	VMA at N_{des} (Percent)	In-Place Air Void (Percent)
17MFO0060	2.721	4.6	4.19	14.8	6.94
17MFO0061	2.721	4.2	4.36	14.6	5.80
17MFO0062	2.721	4.9	4.41	15.1	6.18
17MFO0063	2.721	4.0	4.17	14.3	7.18
17MFO0064	2.721	4.0	4.26	14.5	6.84
17MFO0065	2.721	5.2	4.33	15.4	4.88
17MFO0066	2.721	5.8	4.28	15.7	5.47
17MFO0067	2.721	4.4	4.38	15.2	4.87
17MFO0068	2.721	4.2	4.12	14.5	6.12
17MFO0069	2.721	5.0	4.00	14.7	6.65

Table 79. AQC obtained from MoDOT: J5P3054 project.

Sample ID	G_{sb}	Air Void Content at N_{des} (Percent)	Asphalt Binder (Percent)	VMA at N_{des} (Percent)	In-Place Air Void (Percent)
17MFO0070	2.682	2.6	5.77	14.6	4.97
17MFO0071	2.682	5.1	5.21	15.2	7.00
17MFO0072	2.682	5.0	5.21	15.2	7.93
17MFO0073	2.682	6.4	5.42	16.9	4.88
17MFO0074	2.682	3.9	5.33	14.8	4.74
17MFO0075	2.682	4.5	4.7	14.8	5.30
17MFO0076	2.682	4.5	4.93	14.6	5.27
17MFO0077	2.682	5.0	5.09	15.4	5.48
17MFO0078	2.682	4.0	5.16	13.9	6.35
17MFO0079	2.682	3.8	5.39	13.9	5.83

G_{sb} = aggregate bulk specific gravity; G_{mb} = mixture bulk specific gravity; G_{mm} = maximum specific gravity; and N_{des} = design compaction level.

Selection of Performance Volumetric Relationship Calibration Conditions

Based on the AQCs measured by the MoDOT and mixture specification limits, the research team created a plot for the 10 samples of the J6I3114 project regarding their volumetric conditions as an example, shown here in figure 118. Equations 5 and 7 were used to calculate the VMA_{IP} and VFA_{IP} values. The mixture specification limits were referred from Missouri Standard Specification for Highway Construction (2016) and are summarized in table 80.[88] Table 81 presents the numerical VMA_{IP} and VFA_{IP} of 10 samples.

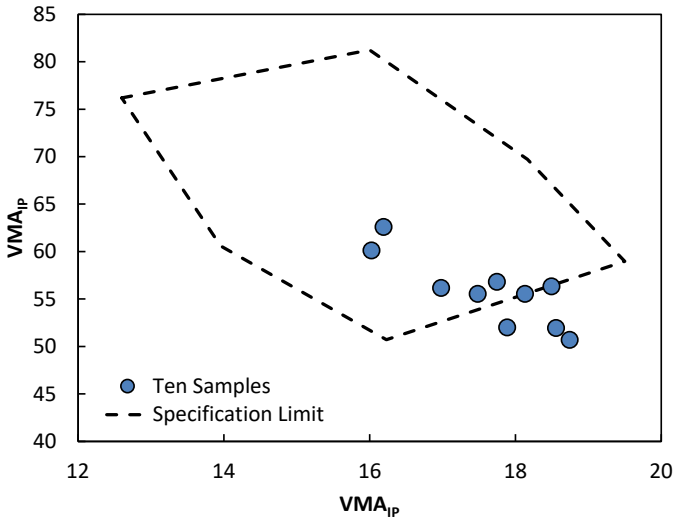

Source: FHWA.

Figure 118. Graph. Calculated IP-VMA and IP-VFA for 10 samples: MoDOT Shadow Project J6I3114.

Table 80. MoDOT shadow project: Mixture specification limits of SP125 mixture.

Condition	Air Void Content at N_{des} Limit (Percent)	VMA at N_{des} Limit (Percent)	In-Place Air Void Limit (Percent)	VMA_{IP} (Percent)	VFA_{IP} (Percent)
1	3	16.0	3.0	16.0	81.3
2	3	16.0	5.5	18.2	69.7
3	4	16.0	8.0	19.5	59.0
4	4	13.5	3.0	12.6	76.2
5	5	13.5	8.0	16.2	50.7
6	5	13.5	5.5	14.0	60.6

Table 81. MoDOT shadow project: IP-VMA and IP-VFA of J6I3114 project 10 samples.

Sample ID	VMAIP (Percent)	VFAIP (Percent)
17MFO0050	18.1	55.5
17MFO0051	18.5	56.3
17MFO0052	17.5	55.5
17MFO0053	16.0	60.1
17MFO0054	17.7	56.8
17MFO0055	16.2	62.6
17MFO0056	17.0	56.2
17MFO0057	17.9	52.0
17MFO0058	18.6	51.9
17MFO0059	18.7	50.7

To determine the four corners, the research team selected the four samples located farthest from each other, as shown in figure 119. The research team moved selected four samples in the volumetric domain by changing the target air void content to make the four corners. Within the mixture specifications, the team made the four corners plan with two low and high target air void contents. Figure 120 shows the determined four corners of the J6I3157 project samples. Three mixture samples that were not used for the four corners were used to verify the PVR and compacted at the same in-place air void contents. Using the same method, the team determined the four corners for the other two projects; table 82 provides a summary of the plans. The team planned the initial experimental work distribution for the MoDOT to conduct the AMPT performance tests for the four corners and for the research team to conduct the verification tests.

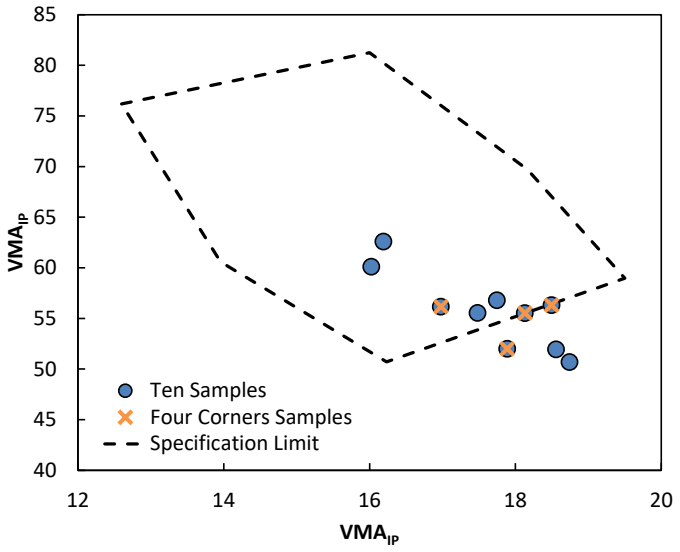

Source: FHWA.

Figure 119. Graph. MoDOT shadow project: Selected four samples for four corners.

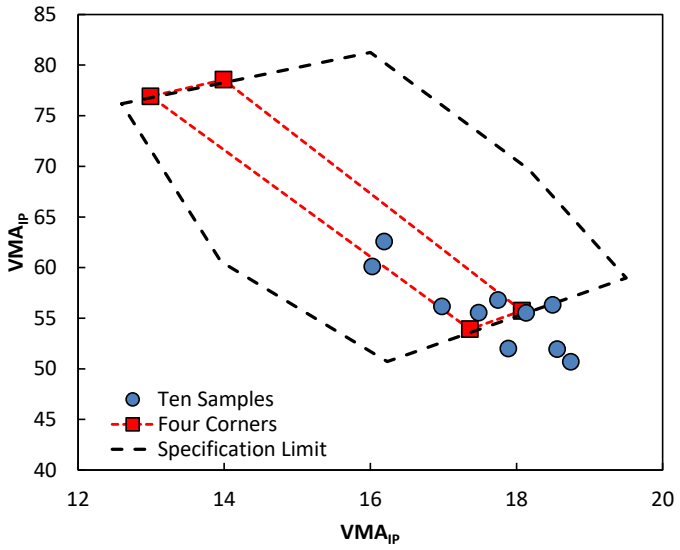

Source: FHWA.

Figure 120. Graph. Determined four corners of MoDOT J6I3157 project samples.

Table 82. MoDOT shadow project: Test plan for four corners and verification samples of three projects.

Project	Sample ID	Test Purpose	Target Test Specimen Air Void Content (Percent)	Test By
J6I3114	17MFO0050	Four corners	8.0	MoDOT
J6I3114	17MFO0051	Four corners	3.0	MoDOT
J6I3114	17MFO0056	Four corners	3.0	MoDOT
J6I3114	17MFO0057	Four Corners	8.0	MoDOT
J6I3114	17MFO0053	Verification	6.4	NCSU
J6I3114	17MFO0055	Verification	6.1	NCSU
J6I3114	17MFO0058	Verification	8.9	NCSU
J6I3157	17MFO0064	Four Corners	8.0	MoDOT
J6I3157	17MFO0066	Four Corners	3.0	MoDOT
J6I3157	17MFO0067	Four Corners	3.0	MoDOT
J6I3157	17MFO0069	Four Corners	8.0	MoDOT
J6I3157	17MFO0061	Verification	5.8	NCSU
J6I3157	17MFO0063	Verification	7.2	NCSU
J5P3054	17MFO0065	Verification	4.9	NCSU
J5P3054	17MFO0070	Four Corners	3.0	MoDOT
J5P3054	17MFO0070	Four Corners	6.5	MoDOT
J5P3054	17MFO0076	Four Corners	4.0	MoDOT
J5P3054	17MFO0078	Four Corners	8.0	MoDOT
J5P3054	17MFO0071	Verification	7.0	NCSU
J5P3054	17MFO0074	Verification	4.7	NCSU
J5P3054	17MFO0077	Verification	5.5	NCSU

Shadow Project Test Results

MoDOT personnel conducted the AMPT tests for the four corners based on the experimental plans shown in table 82. Because one of the shadow project mixtures was used for the proficiency testing, the shadow project tests were conducted at the same test temperatures, as specified in table 83.

Table 83. MoDOT shadow project: Test temperatures used for AMPT performance tests.

Performance Test	Test Temperature
Dynamic modulus	4 °C, 20 °C, and 40 °C
Cyclic fatigue	18 °C
SSR	LT: 26 °C HT: 49 °C

MoDOT conducted shadow project tests from March 2018 to January 2018, and provided the test results to the research team. The team analyzed the test results and observed no significant problems with the dynamic modulus test results. However, the team found several problems with the cyclic fatigue and SSR tests. Table 84 provides a summary of the results of tests that the MoDOT conducted. The team divided the quality of the test results into four levels: good, fair, poor, and incorrect. The research team based the levels on experience, as described in the Support column of table 85.

Table 84. MoDOT shadow project: Overall quality of results from performance tests conducted by MoDOT.

Sample ID	Dynamic Modulus Test	Cyclic Fatigue Test	SSR Test (LT)	SSR Test (HT)
17MFO0050	Good	Fair	Good	Good
17MFO0051	Good	Good	Good	Good
17MFO0056	Fair	Poor	Good	Fair
17MFO0057	Fair	Fair	Good	Good
17MFO0064	Fair	Fair	Good	Incorrect
17MFO0066	Fair	Fair	Good	Incorrect
17MFO0067	Poor	Poor	Fair	Incorrect
17MFO0069	Fair	Fair	Good	Fair
17MFO0070-AV 3 percent	Good	No data	Good	Incorrect
17MFO0070-AV 6.5 percent	No data	Fair	Specimen 1	Fair
17MFO0076	Fair	Poor	Good	Incorrect
17MFO0078	Fair	Poor	Good	Incorrect

Table 85. MoDOT shadow project: Basis for test quality level judgments.

Test	Level	Support
Dynamic modulus	Good	The master curve is well collapsed. None or only a few data quality indicator issues.
Dynamic modulus	Fair	The master curve is well collapsed. More than five data quality indicator issues.
Dynamic modulus	Poor	The master curve is not visually collapsed.
Cyclic fatigue	Good	The damage characteristic curves are well collapsed. No data quality indicator issues.
Cyclic fatigue	Fair	The damage characteristic curves are well collapsed. Data quality indicator issue.
Cyclic fatigue	Poor	The damage characteristic curves are not visually collapsed.
SSR	Good	The test was conducted correctly. The replicate percent difference is less than 25 percent.
SSR	Fair	The test was conducted correctly. The replicate percent difference is greater than 25 percent.
SSR	Incorrect	The test was conducted using an incorrect template.

Dynamic Modulus Test Results

Overall, the team did not find significant problems with the dynamic modulus testing. Table 86 provides a summary of the test results.

Table 86. Major issues found for dynamic modulus tests conducted by MoDOT.

Sample ID	Dynamic Modulus Test Issue
17MFO0050	Specimen 2—Load standard error, deformation standard error.
17MFO0051	Specimen 1—Deformation standard error.
17MFO0056	Specimens 1, 3, and 4—Load standard error, deformation standard error, and phase uniformity.
17MFO0057	Specimens 1, 2, 3, and 4—Load standard error, deformation standard error, phase uniformity, deformation uniformity, and deformation drift in opposite direction.
17MFO0064	Specimens 1, 2, and 3—Load standard error, deformation standard error, and phase uniformity.
17MFO0066	Specimens 1 and 2—Load standard error, deformation standard error, phase uniformity, and deformation uniformity.
17MFO0067	Specimens 1, 2, 3, and 4—Load standard error, deformation standard error, phase uniformity, and deformation drift in opposite direction.

Sample ID	Dynamic Modulus Test Issue
17MFO0069	Specimens 1, 2, and 3—Load standard error, deformation standard error, deformation uniformity, and deformation drift in opposite direction.
17MFO0070-AV 3 percent	Specimens 1, 3, and 4—Load standard error and deformation standard error.
17MFO0070-AV 6.5 percent	No data.
17MFO0076	Specimens 2 and 3—Load standard error, deformation standard error, and deformation uniformity.
17MFO0078	Specimens 1, 2, 3, and 4—Load standard error and deformation standard error.

All cases had issues related to the load standard error and some specimens had issues related to the deformation standard error. According to AASHTO TP 132, users should adjust the tuning of hydraulics because these errors are increased when the applied load does not have a good sinusoidal shape.[30] In addition, these issues can occur if the test specimens do not have a well-distributed aggregate structure. If coarse aggregate is positioned at a certain location, the linear variable differential transformer sensor near the aggregate will respond differently to the other side.

Some cases also had deformation standard error and phase uniformity issues. Users can solve these issues by ensuring the alignment and parallelism of the test specimens. Also, users can repeat the test several times after changing the test specimen's alignment until the test quality improves. The team provided possible solutions to MoDOT through conference calls.

Cyclic Fatigue Test Results

The cyclic fatigue tests that the MoDOT conducted showed several issues that related to the DMR, damage characteristic curve, early failure (number of cycles), and actuator strain standard error. For DMR values, the tolerance range is 0.85 to 1.15. For damage characteristic curves, figure 121 shows two examples. For number of cycles, the research team rejects tests that fail before 2,000 cycles. Table 87 presents the issues that involved individual samples.

Table 87. Major issues of cyclic fatigue tests conducted by MoDOT.

Sample ID	Cyclic Fatigue Test Issue
17MFO0050	The damage characteristic curves did not collapse. A DMR value was out of the range. A specimen failed before 2,000 cycles.
17MFO0051	No issues found.
17MFO0056	The damage characteristic curves did not collapse, and the curve shapes were not acceptable. Four specimens had higher than 10 percent actuator strain standard error.

Sample ID	Cyclic Fatigue Test Issue
17MFO0057	The number of cycles to failure (N_f) of one specimen was too low. A specimen failed before 2,000 cycles.
17MFO0064	The damage characteristic curves did not collapse. Four specimens had higher than 10 percent actuator strain standard error.
17MFO0066	Four specimens had higher than 10 percent actuator strain standard error.
17MFO0067	The damage characteristic curves collapsed, but three DMR values were out of range.
17MFO0069	The damage characteristic curves collapsed, but a DMR value was out of range. A specimen failed before 2,000 cycles.
17MFO0070-AV 3 percent	No data.
17MFO0070-AV 6.5 percent	The damage characteristic curves did not collapse. A specimen had higher than 10 percent actuator strain standard error.
17MFO0076	The damage characteristic curves did not collapse, and the curve shapes were not acceptable. A DMR value was out of range. Two specimens had higher than 10 percent actuator strain standard error.
17MFO0078	The damage characteristic curves did not collapse. A specimen failed before 2,000 cycles. Three specimens had higher than 10 percent actuator strain standard error.

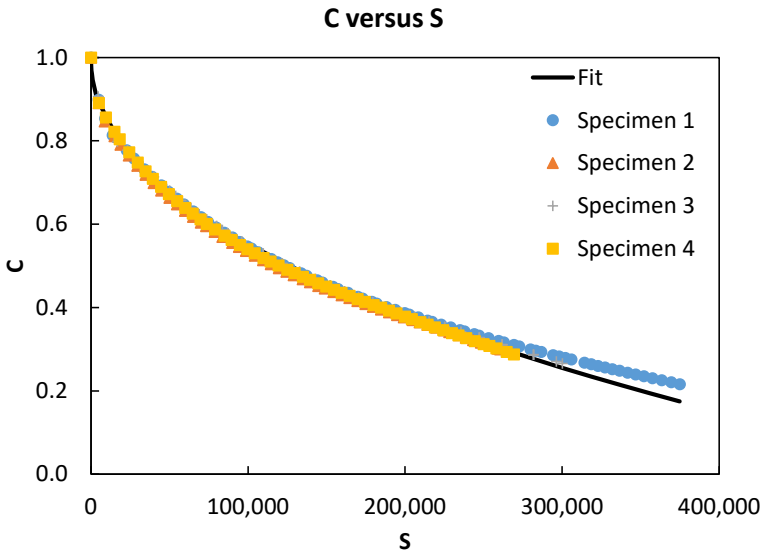

Source: FHWA.

A. Good damage characteristic curves.

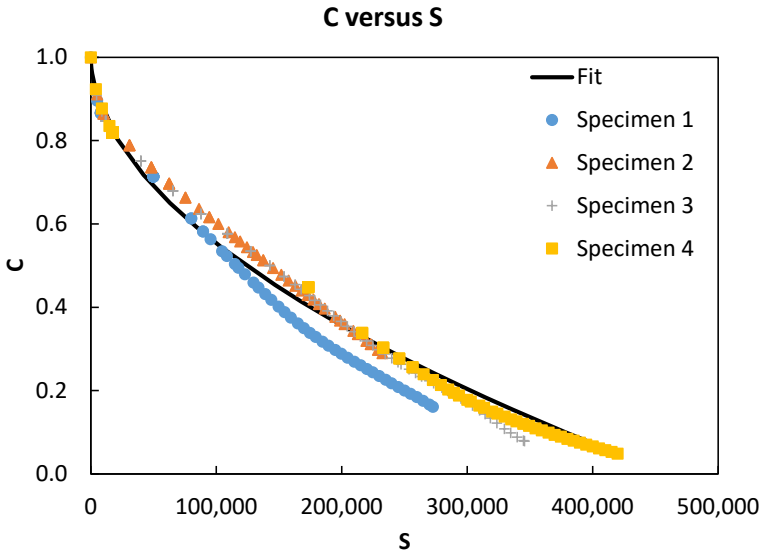

Source: FHWA.

B. Poor damage characteristic curves.

Figure 121. Graphs. MoDOT shadow project: Examples of damage characteristics curves.

The team suggested solutions to MoDOT for the test-related problems. For the DMR issue, the team highly recommended conditioning the specimen inside the AMPT chamber for 1 h and 30 min at the test temperature (18 °C) to provide sufficient preconditioning time to yield acceptable DMR values. Regarding early failure, the team suggested using a filler gauge to fill the gap between the specimen and the machine. Because test specimen ends cannot be prepared in perfect parallel, the ends are angled. When the users tighten the specimen to avoid gaps, the specimen is stretched and damaged even before the testing starts, which could induce early

failure. To address this problem, the team recommended using a filler gauge when the specimen is tightened to the machine. Lastly, actuator strain standard error occurs when users do not turn the AMPT manifold to high. The dynamic modulus test is conducted at low, which may confuse users regarding cyclic fatigue testing that should be conducted at high to apply an increasing load to the specimen.

Stress Sweep Rutting Test Results

The results of the SSR tests that MoDOT conducted were compromised due to a test temperature template issue. MoDOT personnel did not use the correct test software template. Most of the LT SSR tests were conducted using the HT SSR test template, and the same mistake (vice versa) happened for the HT SSR tests. Table 88 provides a summary of the major SSR test issues.

Table 88. Major issues of SSR tests conducted by MoDOT.

Sample ID	SSR Test Issue
17MFO0050	No issue found.
17MFO0051	No issue found.
17MFO0056	The replicate percent difference was 30.7 percent at the LT.
17MFO0057	No issue found.
17MFO0064	The LT test used the HT test template.
17MFO0066	The LT test used the HT test template.
17MFO0067	The LT test used the HT test template. The HT test used the LT test template.
17MFO0069	No data.
17MFO0070-AV 3 percent	The LT test used the HT test template.
17MFO0070-AV 6.5 percent	The HT test used the LT test template.
17MFO0076	The LT test used the HT test template.
17MFO0078	The LT test used the HT test template.

The team reminded the MoDOT about the existence of two templates for each test temperature to solve the issue. Also, the team suggested that the MoDOT conduct additional tests when the replicate percent difference is higher than 25 percent based on the test standard.

Lessons from Shadow Project Testing

Based on the test results and associated issues, the research team learned the following lessons from the MoDOT's shadow project:

- The agency and the research team should hold regular meetings in the middle of shadow AMPT performance testing to ensure communication because even if proficiency testing is conducted successfully, the State highway agency can easily make major and minor mistakes.

- The agency should keep the time between the proficiency testing and the shadow project testing short to minimize possible testing problems. In addition, the agency should go

through the entire testing procedure with the research team before the agency starts conducting the shadow performance testing.

- The research team should supply video-recorded testing guidance to help agency personnel recall the testing procedure if holding regular meetings is difficult.

- The State highway agency should assign operators who are able to work long term to avoid the loss of testing skills. If the agency assigns a temporary operator to carry out the performance test, then agency personnel will have a greater chance of compromising performance test proficiency.

Alternative to Shadow Project Plans

Due to several instances of unacceptable test quality, the research team suggested that MoDOT conduct a second set of proficiency tests using the collected mixture samples that were not used. However, the second proficiency tests did not occur due to MoDOT's project scheduling conflicts. Also, MoDOT did not have enough materials for several mixture samples to develop the four corners. Due to these reasons, the team decided to suspend the project.

One of the main objectives of a shadow project is to help the State highway agency become familiar with AMPT performance testing. Once the agency becomes proficient with the tests, then the agency can produce performance data based on its own interests. Therefore, the research team determined that the main objective of the shadow project could be met if the MoDOT acquired proficiency skills to conduct AMPT performance tests.

To meet this main objective, MoDOT provided the research team with the most recent AMPT performance test results obtained from another project. The team analyzed and evaluated the test results and focused on the most vulnerable areas, based on the shadow project test results, to verify improvement in the proficiency skills of the MoDOT personnel. MoDOT performed SSR tests (which were not performed for the shadow project) as follow up and the research team analyzed those results.

The MoDOT tested four specimens for the dynamic modulus tests. The test date was in January 2020. In contrast to the shadow project results, the data quality indicators for the four specimens met the requirements. The target strain value was changed from 75–125 microstrain to 50–75 microstrain. Table 89 summarizes the dynamic modulus test results that the research team used to verify proficiency.

Table 89. MoDOT shadow project: dynamic modulus proficiency verification test results.

Specimen ID	Deformation Drift (Negative Sign)	Load Standard Error (<10 Percent)	Deformation Standard Error (<10 Percent)	Deformation Uniformity (<30 Percent)	Phase Uniformity (<3°)
1	All met	All met	All met	All met	All met
2	All met	All met	All met	All met	All met
3	All met	All met	All met	All met	All met
4	All met	All met	All met	All met	All met

For the cyclic fatigue tests, the three test specimens showed well-collapsed damage characteristic curves, as shown in figure 122. The DMR values of the three specimens were in the 0.85–1.15 range and no early failure occurred. Also, the three specimens had similar D^R and S_{app} values. Lastly, the actuator deformation standard error (ADSE) of the three specimens did not exceed 10 percent. Table 90 provides a summary of the test results.

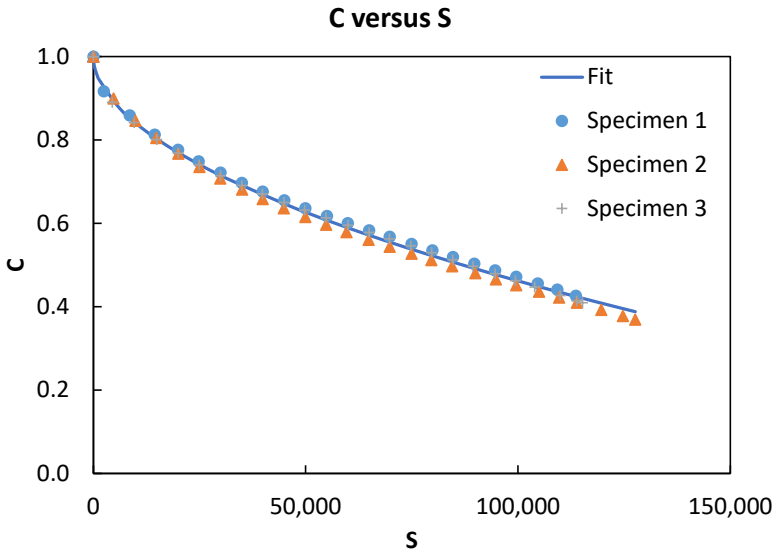

Source: FHWA.

Figure 122. Graph. MoDOT shadow project: Damage characteristic curves of proficiency verification test.

Table 90. MoDOT shadow project: Cyclic fatigue proficiency verification test results.

Specimen ID	DMR	N_f	D^R	S_{app}	ADSE (<10 Percent)
1	1.01	52,620	0.39	9.5	6.75
2	0.98	38,410	0.43	10.6	7.68
3	0.97	49,360	0.39	9.0	6.52

MoDOT conducted the SSR test again with the correct template for the samples with the issues in table 91. Except for the 17MFO0069 and 17MFO0070 samples, MoDOT successfully tested the other samples with the correct test templates.

Table 91. MoDOT shadow project: SSR proficiency verification test results.

Sample ID	SSR Test Issue
17MFO0064	LT test was conducted correctly.
17MFO0066	LT test was conducted correctly.
17MFO0067	Both temperature tests were conducted correctly.
17MFO0069	Both temperature tests were conducted correctly.
17MFO0070-AV 3 percent	Insufficient material.

Sample ID	SSR Test Issue
17MFO0070-AV 6.5 percent	Insufficient material.
17MFO0076	LT test was conducted correctly.
17MFO0078	LT test was conducted correctly.

The team did not find any testing-related problems from the proficiency verification test results. Therefore, the research team concluded that the MoDOT successfully addressed the major issues that the team found during the shadow project tests, and that MoDOT personnel are proficient in conducting AMPT performance tests.

Summary

The summary of the findings from the MoDOT shadow projects are as follows:

- The research team compared the proficiency test results generated by both MoDOT and the research team. For the dynamic modulus tests, test repeatability and reproducibility were acceptable even if the tests were conducted within different target strain ranges. For the cyclic fatigue tests, MoDOT test results showed lower DMR values than the researcher's results due to lack of conditioning time. Despite some specimens having DMR-related problems, the S_{app} values did not show significant differences. For the SSR tests, the reproducibility was within the tolerance and the difference in RSI values was 0.4 percent, which is not significant.

- The MoDOT obtained 10 samples from different truckloads for each of 3 projects and measured the AQCs. The research team selected four corners and verification samples to develop PVRs based on the volumetric conditions calculated from the measured AQCs.

- The MoDOT first conducted AMPT performance tests for the four corners samples. However, the research team found that the overall quality of the test results was not acceptable to develop the PVR. This outcome was due to lack of communication between the MoDOT and the research team. The research team highly recommends regular meetings during shadow projects.

- The research team could not proceed with the project because the amount of material was not sufficient to conduct additional performance tests. Considering the main objective of the shadow project, the team decided to focus on the proficiency of the MoDOT to conduct AMPT performance tests.

- The research team provided possible solutions to the MoDOT to solve the major problems that occurred during the shadow projects. With these solutions in hand, the MoDOT conducted the AMPT performance test for another project and shared the test results with the team. The team and MoDOT considered the test as the MoDOT's proficiency verification test. The test results did not indicate any major or minor issues.

- The team determined that MoDOT is completely proficient to conduct AMPT performance tests, based on the proficiency verification test. The test results that MoDOT generated can be used for MoDOT's own interests.

CHAPTER 5. CONCLUSIONS AND FUTURE WORK

CONCLUSIONS

Over the past few decades the research team has developed advanced test methods and mechanistic models for the characterization of asphalt concrete and software programs for mixture-level analysis and pavement performance analysis. The research efforts that this report documents are designed to advance these methodologies to aid the deployment of FHWA's PRS for asphalt pavements.

The research team developed a thermal cracking model based on the S-VECD model.[12,77] The developed model utilizes three hierarchical levels to determine one of the most important material properties for thermal cracking prediction, the CTC. In addition, the team developed a dissipated pseudostrain energy (DPSE)-based failure criterion to predict fracture in the thermal stress restrained specimen test (TSRST). The algorithm for TSRST predictions is used in the thermal cracking analysis framework, FlexTC, to determine the crack depth in a pavement subjected to thermal fluctuations. The team verified the TSRST prediction algorithm and FlexTC using eight MnROAD test sections.[69] The FlexTC framework's main strength is that the required material characterization methods are identical to those for fatigue cracking, thus reducing the efforts required for material characterization in mechanistic-empirical pavement analysis compared to other methods.

Another advancement at the material level that stemmed from this research is the development of S_{app} and RSI parameters as the cracking and rutting indexes, respectively. S_{app} accounts for the effects of a mixture's modulus and toughness on the mixture's fatigue resistance and is a measure of the amount of fatigue damage the material can tolerate under loading. The RSI is the APS (in percent) and is defined as the ratio of the permanent deformation in an asphalt layer to the thickness of that layer at the end of a 20-yr period over which 30 million 18-kip ESAL repetitions are applied to a standard pavement structure. The research team found that these two indexes meet general expectations with respect to the effects of mixture factors (e.g., aggregate gradation, binder content, RAP content, binder grade, type of binder modifier, compaction density, and aging) on mixture performance. The main strength of these indexes over other indexes is that the test results generated to determine the S_{app} and RSI values for a given mixture can be used in FlexPAVE for LTPP predictions (e.g., for pavement design or PRS).

In addition to these material-level advancements, the research team developed FlexMAT version 2.1 during this project. The various improvements and capabilities that the team added to FlexMAT Cracking include the 2S2P1D model for the dynamic modulus, hierarchical input levels for the CTC and aging properties, data quality indicators, and the DPSE calculation. The major improvement that the team made to FlexMAT Rutting is the calculation of the RSI value using the National Aeronautics and Space Administration Modern-Era Retrospective Analysis for Research and Applications, Version 2 (MERRA-2) temperature database.[89] In addition to these improvements and added capabilities, FlexMAT version 2.1 allows the use of either metric or imperial units of measure, generates output files that can be used in FlexPAVE versions 1.1 and 2.0, and uses a universal input data structure for AMPTs from different manufacturers. The

S_{app} and RSI values are calculated using FlexMAT, thus making FlexMAT an important element in index-based BMD and index-based PRS protocols.

Another pavement-level advancement is the development of preliminary transfer functions for FlexPAVE version 1.1. The research team predicted the pavement performance of 39 pavement sections at the National Center for Asphalt Technology test track, MnROAD project, Manitoba project, and Korea Expressway Corporation project using FlexPAVE version 1.1 and the measured properties of the original asphalt mixtures used in the construction. (See references 69, 90–92.) In general, the research team found good agreement between the observed and predicted performance. This comparison resulted in preliminary transfer functions for fatigue cracking and rutting. These transfer functions are preliminary because the amount of data used in the development of these functions was limited.

One of the major developments for pavement-level analysis is FlexPAVE version 2.0. FlexPAVE version 2.0 uses three-dimensional full finite element analysis instead of the layered analysis in version 1.1 and includes the National Cooperative Highway Research Program (NCHRP) 09-54 aging models, thermal cracking model, S-VECD model for fatigue cracking, and permanent strain shift model.[12,77,93] Seasonal effects of unbound materials also are implemented in version 2.0. The climatic data are determined using the EICM and MERRA-2 databases with altitude correction.[22,89] Finally, the GUI of FlexPAVE version 2.0 has been greatly simplified using Microsoft Excel. In short, FlexPAVE version 2.0 simulates asphalt pavement performance under moving loads and realistic climatic conditions and has a simple GUI that makes the software easy for pavement engineers to use.

The research team undertook several methodological developments in this project. First, the team established characterization methods for the PVR and IVR. The PVRs and IVRs are based on the four corners concept with two volumetric properties, i.e., in-place voids in mineral aggregate (VMA_{IP}) and in-place voids filled with asphalt (VFA_{IP}). The four corners approach is based on the finding that the performance of an asphalt mixture at any volumetric condition can be predicted if the performance of the mixture at the four corners is measured. This study used several mixtures, both laboratory mixed and plant produced, to characterize and verify the PVRs and IVRs. The major benefits of the PVR and IVR are that they allow engineers to continue to use current test methods and equipment for QA purposes, bridge the gap between the volumetric properties and performance of asphalt mixtures, and allow engineering judgment in mixture design and QA processes to be based on performance.

The successful development and verification of the PVR and IVR allowed the research team to use those relationships in BMD. In addition, the ability of the PVR and IVR to predict the performance of a mixture at various gradations, binder contents, and air void contents enabled the resultant BMD to optimize the mixture for both aggregate gradation and binder content for a given set of aggregate stockpiles and binder. The research team developed three tiers of BMD based on the AMPT suite of performance tests. Tiers 1 and 2 use the S_{app} and RSI parameters, whereas tier 3 uses the pavement life predicted by FlexPAVE. In tier 1, the S_{app} and RSI values of the design mix are measured and compared against the threshold values for the given traffic to determine pass or fail. Tier 2 BMD is similar to that of tier 3 predictive BMD. The main difference is that tier 2 uses the IVR concept and all the tests and analyses are performed at a fixed design air void content (e.g., 4 percent), thus requiring the AMPT tests to be performed at

two points rather than at four corners. Tier 3 uses the PVRs that are characterized using the pavement life predicted from FlexPAVE at the four corners volumetric conditions. Although the required mixture characterization efforts in tier 3 BMD are much greater than those in tier 2, the data generated in tier 3 provide information about the changes in mixture performance that occur as the air void content changes. Therefore, the data generated for tier 3 BMD can be readily used for developing payment provisions in PRS.

To account for the uncertain nature of mechanistic models, the research team evaluated known uncertainties as they pertain to model characterization and the propagation of those uncertainties into LTPP simulations. Specifically, the research team used the Bayesian inference-based MCMC method to investigate ways that the uncertainties of the S-VECD and rutting shift model input parameters propagate to pavement performance simulation errors.[12,52] The research team performed thousands of FlexPAVE simulations using different levels of material property variability, climate, loading, and structural conditions. Analysis of the material variations led to simplified and predictable relationships that can account for the uncertainty in long-term performance predictions. The predictive models can predict the propagation of the testing variability to %Cracking variations at any desired level of reliability with more than 98 percent accuracy (less than 2 percent error). For rutting, the error in material variation was found to propagate at a rate of approximately 1.5 to 3.5 times that of the variation in viscoplastic strain observed in AASHTO TP 134 experiments.[16]

In this research, the team developed a Microsoft Excel-based program, PASSFlex, to combine FlexMAT and FlexPAVE into a PRS framework and to support the user (e.g., agencies, contractors, researchers) in the different steps of a PRS-based project. PASSFlex was designed to offer the user five main tools:

- Development of a local database of mixtures based on AMPT testing.
- Development of PRS using a choice of protocol.
- Approval of the mixture that is based on an index or on performance.
- Evaluation (QA) by measured AQC and calibrated volumetric relationships.

Creation of a toolbox that contains FlexMAT and FlexPAVE in a single environment.

This report takes one of the three protocols developed under the auspices of the TFRS-01 project, *Quality Assurance (QA) Aspects of Performance Related Specifications (PRS)*, and uses it to describe the various elements of PASSFlex and how they work together to develop tables for payment provisions, which constitute the most critical element in successful PRS.[94]

Finally, the research team undertook three shadow projects in concert with the WFLHD, MaineDOT, and MoDOT, respectively, to introduce the AMPT suite of performance tests and PRS models to State departments of transportation. The research team used samples from actual construction projects to develop PVRs and to evaluate the PVRs' accuracy as a function of mixture volumetrics and in-place density values. The analysis results for the shadow project data clearly demonstrate the importance of in-place density on a pavement's cracking and rutting performance. Much less variation was found for binder content and aggregate gradation. The PVRs and IVRs that the team generated using the construction samples from the shadow projects were verified using the AMPT test results obtained from an independent set of construction samples.

FUTURE WORK

The following items would enhance the products the research team already has developed:

- A ruggedness and interlaboratory study of AASHTO TP 134.[16]
- The NCHRP 1-53 permanent deformation model of unbound materials incorporated into FlexPAVE version 2.0 once AASHTO has fully vetted FlexPAVE version 2.0.[95]
- A reflective cracking model based on the S-VECD model and the developed model incorporated into FlexPAVE version 2.0.[12]
- Transfer functions for FlexPAVE version 2.0 using a wide range of pavement sections with available original paving materials and reliable performance data.
- PVR and IVR verifications that the research team developed using laboratory-mixed, laboratory-compacted mixtures.
- Different PRS protocols incorporated into PASSFlex.

REFERENCES

1. West, R., C. Rodezno, F. Leiva, and F. Yin. 2018. *Development of a Framework for Balanced Mix Design*. NCHRP Report No. 20-07. Washington, DC: National Cooperative Highway Research Program.

2. Marasteanu, M., A. Zofka, M. Turos, X. Li, R. Velasquez, W. Buttlar, G. Paulino, A. Braham, E. Dave, J. Ojo, H. Bahia, C. Williams, J. Bausano, A. Gallistel, and J. McGraw. 2007. *Investigation of Low Temperature Cracking in Asphalt Pavements-Phase II National Pooled Fund Study 776 Phase I*. Report No. MN/RC 2012-23. St. Paul, MN: Minnesota Department of Transportation Research Services.

3. Zhou, F., H. Sheng, and T. Scullion. 2013. *Balanced RAP/RAS Mix Design and Performance Evaluation System for Project-specific Service Conditions*. Publication No. FHWA/TX-13/0-609203. Austin, TX: Texas Department of Transportation.

4. Robbin, M. M., C. Rodezno, N. Tran, and D. Timm. 2017. *Pavement ME Design - A Summary of Local Calibration Efforts for Flexible Pavements*. Report No. 17-07. Auburn, AL: National Center for Asphalt Technology.

5. Lanotte, M. A., M. E. Kutay, S. W. Haider, and K. G. Musunuru. 2018. "Improving Pavement ME Thermal Cracking Prediction Using Mix-Specific Calibration Coefficients for Michigan." Presented at the *97th Annual Meeting of the Transportation Research Board*. Washington, DC: Transportation Research Board.

6. Yuan, X., and I. Nemtsov. 2018. "Local Calibration of the MEPDG Distress and Performance Models for Ontario's Flexible Roads: Overview, Impacts, and Reflection." *Transportation Research Record* 2672, no. 40: 207–216. https://doi.org/10.1177/0361198118759013, last accessed September 6, 2023.

7. Kim, Y. R., J. Lee, and Y. D. Wang. 2010. *MEPDG Inputs for Warm-Mix Asphalt*. Report No. FHWA/NC/2012-01. Raleigh, NC: North Carolina Department of Transportation.

8. AASHTO. 2008. *Mechanistic-Empirical Pavement Design Guide, a Manual of Practice*. Publication No. MEPDG-1. Washington, DC: American Association of State Highway and Transportation Officials.

9. Christensen, D. W., and R. Bonaquist. 2015. "Improved Hirsch Model for Estimating the Modulus of Hot Mix Asphalt." *Road Materials and Pavement Design* 16, no. 2: 254–274. https://doi.org/10.1080/14680629.2015.1077635, last accessed June 6, 2023.

10. Kaloush, K., and M. W. Witczak. 2000. "Development of Permanent to Elastic Strain Ratio Model for Asphalt Mixtures." In *Development of the 2002 Guide for the Design of New and Rehabilitated Pavement Structure*. NCHRP 1-37 A. College Park, MD: University of Maryland,

11. Bonaquist, R., B. Paye, and C. Johnson. 2017. "Application of Intermediate Temperature Semi-Circular Bending Test Results to Design Mixtures with Improved Load-Associated Cracking Resistance." *Road Materials and Pavement Design* 18: 2–29. https://doi.org/10.1080/14680629.2017.1389069, last accessed September 6, 2023.

12. Underwood, B. S., C. Baek, and Y. R. Kim. 2012. "Simplified Viscoelastic Continuum Damage Model as Platform for Asphalt Concrete Fatigue Analysis." *Transportation Research Record* 2296, no. 1: 35–45.

13. Underwood, B. S., Y. R. Kim, and M. Guddati. 2010. "Improved Calculation Method of Damage Parameter in Viscoelastic Continuum Damage Model." *International Journal of Pavement Engineering* 11, no. 6: 459–476.

14. Ghanbari, A., B. S. Underwood, and Y. R. Kim. 2020. "Development of a Rutting Index Parameter Based on the Stress Sweep Rutting Test and Permanent Deformation Shift Model." *International Journal of Pavement Engineering* 23, no. 2: 1–13. https://doi.org/10.1080/10298436.2020.1748190, last accessed June 6, 2023.

15. AASHTO. 2023. *Standard Method of Test for Determining the Damage Characteristic Curve and Failure Criterion Using Small Specimens in the Asphalt Mixture Performance Tester (AMPT) Cyclic Fatigue Test*. T 411. Washington, DC: AASHTO.

16. AASHTO. 2023. *Standard Method of Test for Stress Sweep Rutting (SSR) Test Using Asphalt Mixture Performance Tester (AMPT)*. TP 134. Washington, DC: AASHTO.

17. FHWA. n.d. *FlexPAVE™* (software). Version 2.0.

18. Kim, Y. R., B. S. Underwood, M. N. Guddati, A. Ghanbari, B. Keshavarzi, Y. D. Wang, J. Jeong, D. Mocelin, F. D. C. Pivetta, and N. A. H. Saleh. n.d. *Development of Balanced Mixture Design Index Parameters and the Flex Suite of Performance Analysis Tools for Asphalt Pavements—Volume I*. Washington, DC: Federal Highway Administration. (Forthcoming.)

19. Wang, Y. D., A. Ghanbari, B. S. Underwood, and Y. R. Kim. 2019. "Development of a Performance-Volumetric Relationship for Asphalt Mixtures." *Transportation Research Record* 2674, no. 6: 416–430. https://doi.org/10.1177/0361198119845364, last accessed June 6, 2023.

20. Mun, S., G. R. Chehab, and Y. R. Kim. 2007. "Determination of Time-Domain Viscoelastic Functions Using Optimized Interconversion Techniques." *Road Materials and Pavement Design* 8, no. 2: 351–365.

21. Kim, D., and Y. R. Kim. 2017. "Development of Stress Sweep Rutting (SSR) Test for Permanent Deformation Characterization of Asphalt Mixture." *Construction and Building Materials* 154: 373–383.

22. Houston, W. N., and C. E. Zapata. 2008. *Calibration and Validation of the Enhanced Integrated Climatic Model for Pavement Design*. NCHRP Report No. 602. Washington, DC: Transportation Research Board.

23. Jeong, J., Y. D. Wang, A. Ghanbari, C. Nash, D. Nener-Plante, B. S. Underwood, and Y. R. Kim. 2020. "Pavement Performance Predictions Using Performance-Volumetric Relationship and Evaluation of Construction Variability: Example of MaineDOT Shadow Project for the Development of Performance-Related Specifications." *Construction and Building Materials* 263: 120150.

24. Lee, J., and N. Gibson. 2015. "Use of Mechanistic Models to Investigate Fatigue Performance of Asphalt Mixtures - Effects of Asphalt Mix Design Targets and Compaction." *Transportation Research Record* 2507: 108–119.

25. Vavrik, W. R., G. Huber, W. J. Pine, and S. H. Carpenter. 2002. "Bailey Method for Gradation Selection in Hot-Mix Asphalt Mixture Design." *Transportation Research Circular* E-C044. Washington, DC: Transportation Research Board. http://onlinepubs.trb.org/onlinepubs/circulars/ec044.pdf, last accessed January 14, 2014.

26. Wang, Y., A. Ghanbari, B. S. Underwood, and Y. R. Kim. 2020. "Development of Framework of the Predictive Performance-Engineered Mix Design Procedure for Asphalt Mixtures." *International Journal of Pavement Engineering* 23, no. 12: 4190–4205. https://doi.org/10.1080/10298436.2021.1938044, last accessed September 6, 2023.

27. North Carolina State University. "NC State University" (web page). https://www.ncsu.edu/, last accessed September 6, 2023.

28. Montgomery, D. C. 2008. *Design and Analysis of Experiments, 7th Edition*. New York, NY: John Wiley & Sons, Inc. https://www.wiley.com/en-us/Design+and+Analysis+of+Experiments%2C+10th+Edition-p-9781119492443, last accessed September 6, 2023.

29. Jeong, J., B. S. Underwood, and Y. R. Kim. 2021. "Rutting Performance Prediction Using Index-Volumetrics Relationships with Stress Sweep Rutting Test and Hamburg Wheel-Track Test." *Construction and Building Materials* 295: 123664.

30. AASHTO. 2019. *Standard Method of Test for Determining the Dynamic Modulus for Asphalt Mixtures Using Small Specimens in the Asphalt Mixture Performance Tester (AMPT)*. TP 132. Washington, DC: AASHTO.

31. Jeong, J., B. S. Underwood, and Y. R. Kim. 2021. "Cracking Performance Prediction Using Index-Volumetrics Relationships with Direct Tension Cyclic Fatigue Test and Illinois Flexibility Index Test (I-FIT)." *Construction and Building Materials* 315: 125631.

32. Microsoft®. 2023. *Microsoft Excel®* (software).

33. Kennedy, T. W., and R. J. Cominsky. 1990. *The SHRP Asphalt Research Program: 1990 Strategic Planning Document*. Report No. l SHRP-A/UWP-90-O07. Washington, DC: Strategic Highway Research Program National Research Council.

34. FHWA. 2010. *Superpave Mix Design and Gyratory Compaction Levels*. Publication No. FHWA-HIF-11-031. Washington, DC: FHWA Office of Pavement Technology. https://www.fhwa.dot.gov/pavement/materials/pubs/hif11031/hif11031.pdf, last accessed September 6. 2023.

35. McDaniel, R. S., R. B. Leahy, G. Huber, J. S. Moulthrop, and T. Ferragut. 2012. *The Superpave Mix Design System: Anatomy of a Research Program*. NCHRP Web-Only Document 186. Washington, DC: National Academies of Sciences. http://dx.doi.org/10.17226/22812, last accessed September 6, 2023.

36. Prowell, B. D., and E. R. Brown. 2007. *Superpave Mix Design: Verifying Gyration Levels in the Ndesign Table*. NCHRP Report No. 573. Washington, DC: Transportation Research Board.

37. West, R., and M. Marasteanu. 2013. *Improved Mix Deign, Evaluation, and Materials Management Practices for Hot Mix Asphalt with High Reclaimed Asphalt Pavement Content*. NCHRP Report No. 752. Washington, DC: Transportation Research Board.

38. Montoya, M. A., M. R. Pouranian, and J. E. Haddock. 2018. "Increasing Asphalt Pavement Density Through Mixture Design: A Field Project." *Journal of Association of Asphalt Paving Technologists* 87. Lino Lakes, MN: Association of Asphalt Paving Technologists.

39. Hekmatfar, A., A. Shah, G. Huber, R. McDaniel, and J. E. Haddock. 2015. "Modifying Laboratory Mixture Design to Improve Field Compaction." *Road Material and Pavement Design* 16: 149-167. Abingdon, UK: Taylor & Francis. https://trid.trb.org/view/1377701, last accessed September 6, 2023.

40. Roque, R., W. G. Buttlar, B. E. Ruth, M. Tia, W. Dickison, and B. Reid. 1997. *Evaluation of SHRP Indirect Tension Tester to Mitigate Cracking in Asphalt Concrete Pavements and Overlays*. Report no. WPI 0510755. Gainesville, FL: University of Florida.

41. Zhou, F., S. Hu, D. H. Chen, and T. Scullion. 2007. "Overlay Tester: Simple Performance Test for Fatigue Cracking." *Transportation Research Record* 2001, no. 1: 1–8.

42. Cao, W., L. N. Mohammad, M. Elseifi, S. B. Cooper, and S. Saadeh. 2018. "Fatigue Performance Prediction of Asphalt Pavement Based on Semicircular Bending Test at Intermediate Temperature." *Journal of Materials in Civil Engineering* 30, no. 9.

43. Zhou, F., S. Im, L. Sun, and T. Scullion. 2017. "Development of an IDEAL Cracking Test for Asphalt Mix Design and QC/QA." *Road Materials and Pavement*

Design 18: 405–427. https://doi.org/10.1080/14680629.2017.1389082, last accessed September 6, 2023.

44. Buttlar, W.G., L. Urra-Contreras, B. Jahangiri, P. Rath, and H. Majidifard. 2020. *Support for Balanced Asphalt Mixture Design Specification Development in Missouri*. Report No. cmr 20-010. Jefferson City, MO: Missouri Department of Transportation.

45. Newcomb, D., and F. Zhou. 2018. *Balanced Design of Asphalt Mixtures*. Report No. MN/RC 2018-22. St. Paul, MN: Minnesota Department of Transportation.

46. Cooper III, S.B., W. B. King, and M. S. Kabir. 2016. *Testing and Analysis of LWT and SCT Properties of Asphalt Concrete Mixtures*. Report No. FHWA/LA/536. Baton Rouge, LA: Louisiana Department of Transportation and Development.

47. Mensching, D. J., M. D. Elwardany, and V. Veginati. 2022. "Evaluating the Sensitivity of Intermediate Temperature Performance Tests to Multiple Loose Mixture Aging Temperatures Using the FHWA Accelerated Loading Facility's RAP/RAS Experiment." Presented at the *101st Annual Meeting of the Transportation Research Board*. Washington, DC: Transportation Research Board.

48. AASHTO. 2022. *Standard Practice for Preparation of Cylindrical Performance Test Specimens Using the Superpave Gyratory Compactor (SGC)*. R 83. Washington, DC: AASHTO.

49. NCDOT. 2019. *NCDOT Pavement Design Procedure AASHTO 1993 Method*. Raleigh, NC: North Carolina Department of Transportation. https://connect.ncdot.gov/resources/Materials/MaterialsResources/Pavement%20Design%20Manual.pdf, last accessed September 6, 2023.

50. AASHTO. 2022. *Standard Method of Test for Resistance of Compacted Asphalt Mixtures to Moisture-Induced Damage*. T 283. Washington, DC:AASHTO.

51. ASTM. 2005. *Standard Practice for Effect of Water on Bituminous-Coated Aggregate Using Boiling Water*. D3625-96. West Conshohocken, PA: ASTM International.

52. Dilip, D. M., and G. L. Sivakumar Babu. 2013. "Methodology for Pavement Design Reliability and Back Analysis Using Markov Chain Monte Carlo Simulation." *Journal of Transportation Engineering* 139 no. 1: 65–74.

53. Ullidtz, P., J. Harvey, I. Basheer, D. Jones, R. Wu, J. Lea, and Q. Lu. 2010. "CalME, a Mechanistic-Empirical Program to Analyze And Design Flexible Pavement Rehabilitation." *Transportation Research Record* 2153, no. 1: 143–152.

54. Mohammad, L. N., M. Elseifi, S. B. Cooper III, and A. Raghavendra. 2013. "Levels of Variability in Volumetric and Mechanical Properties of Asphalt Mixtures." *Journal of Materials in Civil Engineering* 25, no. 10: 1424–1431.

55. Caro, S., D. Castillo, and M. Sánchez-Silva. 2014. "Methodology for Modeling the Uncertainty of Material Properties in Asphalt Pavements." *Journal of Materials in Civil Engineering* 26, no. 3: 440–448.

56. Liu, J., S. Zhao, P. Li, and S. Saboundjian. 2017. "Variability of Composition, Volumetric, and Mechanic Properties of Hot Mix Asphalt for Quality Assurance." *Journal of Materials in Civil Engineering* 29, no. 3: D4015004.

57. Kassem, H., G. Chehab, and S. Najjar. 2019. "Development of Probabilistic Viscoelastic Continuum Damage Model for Asphalt Concrete." *Transportation Research Record* 2673, no. 5: 285–298.

58. Mehrez, L., E. Kassem, E. Masad, and D. Little. 2015. "Stochastic identification of Linear-Viscoelastic Models of Aged and Unaged Asphalt Mixtures." *Journal of Materials in Civil Engineering* 27, no. 4: 04014149.

59. Kim, Y. R., M. Guddati, M. Y. Choi, D. Kim, A. Norouzi, Y. D. Wang, B. Keshavarzi, M. Ashouri, A. Ghanbari, and A. Wargo. n.d. *Development of Asphalt Mixture Performance-Related Specifications. Final Report for FHWA Project DTFH61 08 H 00005*. Washington, DC: Federal Highway Administration. (Forthcoming.)

60. Kassem, H., G. Chehab, and S. Najjar. 2020. "Effect of Asphalt Mixture Components on the Uncertainty in Dynamic Modulus Mastercurves." *Transportation Research Record* 2674, no. 5: 135–148. https://doi.org/10.1177/0361198120914292, last accessed September 6, 2023.

61. Gudipudi, P. P., and B. S. Underwood. 2016. "Reliability Analysis of Fatigue Life Prediction from the Viscoelastic Continuum Damage Model." *Transportation Research Record* 2576, no. 1: 91–99.

62. Rema, A., and A. K. Swamy. 2018. "Quantification of Uncertainty in the Master Curves of Viscoelastic Properties of Asphalt Concrete." *Journal of ASTM International* 7, no. 2: 149–162.

63. Ding, J., Y. D. Wang, S. Gulzar, Y. R. Kim, and B. S. Underwood. 2020. "Uncertainty Quantification of Simplified Viscoelastic Continuum Damage Fatigue Model using the Bayesian Inference-Based Markov Chain Monte Carlo Method." *Transportation Research Record* 2674, no. 4: 247–260.

64. AASHTO. 1986. *AASHTO Guide for Design of Pavement Structures*. Washington, DC: AASHTO.

65. Alsherri, A., and K. P. George. 1988. "Reliability Model for Pavement Performance." *Journal of Transportation Engineering* 114, no. 3: 294–306.

66. FHWA. 2023. "LTPP InfoPave™" (web page). https://infopave.fhwa.dot.gov/, last accessed March 7, 2024.

67. Thyagarajan, S., B. Muhunthan, N. Sivaneswaran, and K. Petros. 2011. "Efficient Simulation Techniques for Reliability Analysis of Flexible Pavements Using the Mechanistic-Empirical Pavement Design Guide." *Journal of Transportation Engineering* 137, no. 11: 796–804.

68. Timm, D. H., D. E. Newcomb, and T. V. Galambos. 2000. "Incorporation of Reliability Into Mechanistic-Empirical Pavement Design." *Transportation Research Record* 1730, no. 1: 73–80.

69. Minnesota Department of Transportation. 2023. "MnROAD: Minnesota's Cold Weather Pavement Testing Facility" (web page). http://www.dot.state.mn.us/mnroad/, last accessed April 19, 2023.

70. Hall, K. D., D. X. Xiao, E. A. Pohl, and K. C. Wang. 2012. "Reliability-Based Mechanistic-Empirical Pavement Design with Statistical Methods." *Transportation Research Record* 2305, no. 1: 121–130.

71. National Technology and Engineering Solutions of Sandia, LLC. 2023. *Dakota* (software). https://dakota.sandia.gov/, last accessed September 6, 2023.

72. Khazanovich, L., S. F. Wojtkiewicz, and R. Velasquez. 2008. "MEPDG-RED: Framework for Reliability Analysis with Mechanistic-Empirical Pavement Design Procedure." Publication No. 08-3142. Presented at the *87th Annual Meeting of the Transportation Research Board*. Washington, DC: Transportation Research Board.

73. Wang, Y. D., A. Ghanbari, B. S. Underwood, and Y. R. Kim. 2021. "Development of Preliminary Transfer Functions for FlexPAVE™." *Construction and Building Materials* 266, Part B: 121182. https://doi.org/10.1016/j.conbuildmat.2020.121182, last accessed June 6, 2023.

74. MathWorks®. 2022. *MathWorks MATLAB® Nonlinear Curve Fitting Toolbox™* (software).

75. Choi, Y. T., V. Subramanian, M. N. Guddati, and Y. R. Kim. 2012. "Incremental Model for Prediction of Permanent Deformation of Asphalt Concrete in Compression." *Transportation Research Record* 2296, no. 1: 24–35.

76. Choi, Y. T., and Y. R. Kim. 2014. "Implementation and Verification of a Mechanistic Permanent Deformation Model (Shift Model) to Predict Rut Depths of Asphalt Pavement." *Road Materials and Pavement Design* 15, sup. 1: 195–218.

77. Olidis, C., and D. Hein. 2003. *Guide for Mechanistic-Empirical Design of New and Rehabilitated Pavement Structure Appendix HH: Field Calibration of Thermal Cracking Model*. Report No. NCHRP 1-37A. Washington DC: National Cooperative Highway Research Program.

78. Microsoft. 2023. *Microsoft Visual Basic for Applications®* (software).

79. Cominsky, R. J., G. A. Hubert, T. W. Kennedy, and M. Anderson. 1994. *The Superpave Mix Manual for new Construction and Overlays*. Report No. SHRP-A-407. Washington, DC: National Academy of Sciences.

80. AASHTO. 2019. *Standard Practice for Preparation of Small Cylindrical Performance Test Specimens Using the Superpave Gyratory Compactor (SGC) or Field Cores*. PP 99. Washington, DC: AASHTO.

81. Wang, Y. D., B. Keshavarzi, and Y. R. Kim. 2018. "Fatigue Performance Prediction of Asphalt Pavements with FlexPAVE™, the S-VECD Model, and DR Failure Criterion." *Transportation Research Record* 2672, no. 40: 217–227.

82. AASHTO. 2003. *Standard Method of Test for Sampling Bituminous Paving Mixtures*. T 168. Washington, DC: AASHTO.

83. Deschutes County. 2010. *Doc 608 Project Agreement Between Deschutes County, the City of Bend, and the Federal Highway Administration for the Skyliners Road Project*. Document No. 2010-608. Bend, OR: Deschutes County Board of Commissioners. https://weblink.deschutes.org/Public/DocView.aspx?id=82217&dbid=0&repo=LFPUB&cr=1, last accessed September 6, 2023.

84. FHWA. 2014. *The Standard Specifications for the Construction of Roads and Bridges on Federal Highway Projects (FP-14)*. Washington, DC: Federal Highway Administration. https://highways.dot.gov/federal-lands/specs, last accessed September 6, 2023.

85. Rahbar-Rastegar, R., E. V. Dave, and J. S. Daniel. 2018. "Fatigue and Thermal Cracking Analysis of Asphalt Mixtures Using Continuum-Damage and Cohesive-Zone Models." *Journal of Transportation Engineering, Part B: Pavements* 144, no. 4: 1–11.

86. AASHTO. 2017. *Standard Method of Test for Determining the Dynamic Modulus and Flow Number for Asphalt Mixtures Using the Asphalt Mixture Performance Tester (AMPT)*. T 378. Washington, DC: AASHTO.

87. Castorena C., B. S. Underwood, Y. R. Kim, K. Lee, N. Tran, and A. Taylor. *Ruggedness and Interlaboratory Studies for Asphalt Mixture Performance Tester (AMPT) Cyclic Fatigue Test: Phase I Report*. Report No. FHWA-HRT-21-057. Washington, DC: Federal Highway Administration. https://www.fhwa.dot.gov/publications/research/infrastructure/pavements/21057/index.cfm, last accessed September 6, 2023.

88. MoDOT. 2016. "2016 Missouri Standard Specifications for Highway Construction" (web page). https://www.modot.org/2016-missouri-standard-specifications-highway-construction, last accessed September 6, 2023.

89. NASA. 2022. "Modern-Era Retrospective Analysis for Research and Applications, Version 2" (web page). https://gmao.gsfc.nasa.gov/reanalysis/MERRA-2/, last accessed April 19, 2023.

90. Auburn University. n.d. “About the Test Track” (web page). https://www.eng.auburn.edu/research/centers/ncat/testtrack/index.html, last accessed April 19, 2023.

91. Manitoba. n.d. “Transportation and Infrastructure” (web page). https://www.gov.mb.ca/mit/index.html, last accessed April 19, 2023.

92. Seo, Y., S. M. Kim, and J. H. Lee. 2013. “Operation of the First Full Scale Road Test Facility in Korea and Lessons Learned from 8 Years of Experience.” *KSCE Journal of Civil Engineering* 17: 1023–1029.

93. Transportation Research Board. 2022. “NCHRP 09-54 [Completed] Long-Term Aging of Asphalt Mixtures for Performance Testing and Prediction” (web page). https://apps.trb.org/cmsfeed/TRBNetProjectDisplay.asp?ProjectID=3400, last accessed April 19, 2023.

94. Transportation Research Board. 2023. “TFRS 01 [Completed] Quality Assurance (QA) Aspects of Performance Related Specifications (PRS)” (web page). https://apps.trb.org/cmsfeed/TRBNetProjectDisplay.asp?ProjectID=4875, last accessed April 19, 2023.

95. Transportation Research Board. 2022. “NCHRP 01-53 [Completed] Proposed Enhancements to Pavement ME Design: Improved Consideration of the Influence of Subgrade and Unbound Layers on Pavement Performance” (web page). https://apps.trb.org/cmsfeed/TRBNetProjectDisplay.asp?ProjectID=3625, last accessed September 6, 2023.

Recycled
Recyclable

Recommended citation: Federal Highway Administration,
Development of Balanced Mixture Design Index Parameters and the Flex Suite of Performance Analysis Tools for Asphalt Pavements—Volume II
(Washington, DC: 2024) https://doi.org/10.21949/1521559

HRDI-20/07-24(WEB)E